Development of enzyme-specific chemical probes for high-throughput substrate profiling of histone deacetylases

Dissertation

der Mathematisch-Naturwissenschaftlichen Fakultät
der Eberhard Karls Universität Tübingen
zur Erlangung des Grads eines
Doktors der Naturwissenschaften
(Dr. rer. nat.)

vorgelegt von
Julian Seidel
aus Stuttgart-Hedelfingen

Tübingen
2021

Gedruckt mit Genehmigung der Mathematisch-Naturwissenschaftlichen Fakultät der Eberhard Karls Universität Tübingen.

Tag der mündlichen Qualifikation:	29.03.2022
Dekan:	Prof. Dr. Thilo Stehle
1. Berichterstatter:	Prof. Dr. Dirk Schwarzer
2. Berichterstatter:	Prof. Dr. Thorsten Stafforst

Erklärung

Ich erkläre hiermit, dass ich die zur Promotion eingereichte Arbeit mit dem Titel: „Development of enzyme-specific chemical probes for high-throughput substrate profiling of histone deacetylases“ selbständig verfasst, nur die angegebenen Quellen und Hilfsmittel benutzt und wörtlich oder inhaltlich übernommene Stellen als solche gekennzeichnet habe. Ich erkläre, dass die Richtlinien zur Sicherung guter wissenschaftlicher Praxis der Universität Tübingen (Beschluss des Senats vom 25.5.2000) beachtet wurden. Ich versichere an Eides statt, dass diese Angaben wahr sind und dass ich nichts verschwiegen habe. Mir ist bekannt, dass die falsche Abgabe einer Versicherung an Eides statt mit Freiheitsstrafe bis zu drei Jahren oder mit Geldstrafe bestraft wird.

Tübingen, den 10.11.2021

Julian Seidel

Abstract

Histone deacetylases (HDACs) are responsible for the deacetylation of *N*ε-acetyllysine residues of histones and non-histone proteins via zinc-dependent *Lewis*-acid catalysis. By modulating the acetylation status of chromatin, HDACs regulate diverse cellular functions on the level of transcriptional control. Aberrant HDAC activiy is associated with a variety of diseases such as cancer and neurodegenerative disorders. Consequently, HDAC inhibitors have been developed in order to treat these diseases. However, advancements in inhibitor specificity require detailed knowledge about HDAC substrate selectivity. Substrate selectivity of endogenous HDAC complexes can be investigated with affinity probes that contain an inhibitory moiety embedded into synthetic peptides derived from known acetylation sites.

In this work, strategies to create new, enzyme-specific peptide-based affinity probes for HDACs were developed. To this end, the influence of different zinc-binding functional groups and peptide sequence contexts on the recruitment of HDACs was investigated.

Based on the structure of hydroxamic acid-, 2-aminophenylamide- and ketone-type HDAC inhibitors, synthetic routes for protected amino acid building blocks that contain these moieties as zinc-binding groups were devised. Incorporation of the respective building blocks into peptide probes with minimal sequence context furnished new tools to capture endogenous HDACs from cellular lysates. Applied in pulldown assays, the 2-aminophenylamide probe showed a distinct selectivity for class I HDACs 1, 2 and 3, when compared to control probes containing either the broad-specificity hydroxamic acid or an unmodified lysine residue. Compared to the hydroxamic acid probe, the ketone-based probe was able to enrich class I HDAC1 more efficiently over the lysine control than class II HDAC6. The experiments were then extended to a proteome-wide level by analyzing the interactomes of selected probes. Compared to the hydroxamic acid control, components of the HDAC3 NCoR / SMRT complex were significantly enriched on the 2-aminophenylamide probe, demonstrating the ability of peptide-based affinity probes to address specific HDAC complexes.

The design of HDAC affinity probes was then optimized with regard to high-throughput approaches, which are required to investigate HDAC substrate selectivity on a proteome-wide scale. To this end, a high-throughput assay based on the format of 96-well plates was developed. A probe design was devised that uses an N-terminal thiol anchoring moiety to selectively capture full-length probes from crude product mixtures, bypassing time-consuming peptide purification. The new 96-well assay was then applied to assess the influence of peptide sequence contexts on HDAC selectivity by screening potential substrate sites of HDAC6 identified in cells with impaired HDAC6 activity. A majority of the tested sequences were able to enrich HDAC6 on hydroxamic acid-containing probes over the lysine controls, while HDAC1 was unspecifically or only weakly recruited. Selected sequence context probes were analyzed in-depth by MS-based proteomics, uncovering a distinct interaction profile of each sequence context with potential HDAC6 binding partners from diverse biological pathways, such as transcription factors, cytoskeletal proteins or components of the ubiquitin-proteasome system. Finally, a MALDI-MS-based kinetic assay with acetyllysine substrates revealed subtle differences in HDAC6-catalyzed deacetylation velocities depending on the individual peptide sequence.

Zusammenfassung

Histondeacetylasen (HDACs) sind verantwortlich für die Deacetylierung von *N*ε-Acetyllysinresten von Histonen und Nicht-Histonproteinen mittels zinkabhängiger *Lewis*-Säurekatalyse. Indem sie den Acetylierungsstatus des Chromatins beeinflussen, regulieren HDACs eine Vielzahl zellulärer Funktionen auf der Ebene der Transkriptionskontrolle. Veränderungen der HDAC-Aktivität werden mit Krebs und neurodegenerativen Erkrankungen in Verbindung gebracht. Um diese Krankheiten zu behandeln wurden HDAC-Inhibitoren entwickelt. Für eine Verbesserung der Spezifität von HDAC-Inhibitoren ist jedoch ein detailliertes Verständnis der Substratselektivität von HDACs erforderlich. Die Substratselektivität endogener HDAC-Komplexe kann mit Affinitätssonden untersucht werden, die eine Inhibitoreinheit enthalten, welche in synthetische Peptide engebettet ist, die sich von bekannten Acetylierungsstellen von Substratproteinen ableiten.

In dieser Arbeit wurden Strategien entwickelt um neue und spezifische peptidbasierte Affinitätssonden für HDACs zu etablieren. Zu diesem Zweck wurde der Einfluss verschiedener zinkbindender funktioneller Gruppen und Peptidsequenzkontexte auf die Rekrutierung von HDACs untersucht.

Basierend auf Hydroxamsäure-, 2-Aminophenylamid- und Keton-HDAC-Inhibitoren wurden Syntheserouten für geschützte Aminosäurebausteine entworfen, die diese Strukturelemente als zinkbindende Gruppen enthalten. Durch das Einbetten der jeweiligen Bausteine in Peptidsonden mit einem minimalen Sequenzkontext wurden neue Werkzeuge geschaffen um endogene HDACs aus zellulären Lysaten zu isolieren. Verglichen mit Kontrollsonden, die entweder eine Hydroxamsäure mit breiter Spezifität oder unmodifiziertes Lysin enthielten, zeigte die 2-Aminophenylamid-Sonde in Pulldown-Experimenten eine ausgeprägte Selektivität für die Klasse-I-HDACs 1, 2 und 3. Die Keton-Sonde konnte im Vergleich zur Hydroxamsäure-Sonde HDAC1 der Klasse I effektiver gegenüber der Lysin-Kontrolle anreichern als HDAC6 der Klasse II. Die Untersuchungen wurden dann auf eine proteomweite Ebene ausgedehnt und die Interaktome ausgewählter Sonden bestimmt. Gegenüber der Hydroxamsäure-Kontrolle konnte dabei der HDAC3-NCoR / SMRT-Komplex an der 2-Aminopheylamid-Sonde signifikant angereichert werden, was die Fähigkeit peptidbasierter Affinitätssonden aufzeigt HDAC-Komplexe spezifisch adressieren zu können.

Das Design der HDAC-Affinitätssonden wurde anschließend im Hinblick auf Hochdurchsatzverfahren optimiert, die notwendig sind, um die Substratspezifität von HDACs in einem proteomweiten Umfang zu untersuchen. Zu diesem Zweck wurde ein Hochdurchsatz-Assay entwickelt, der auf dem Format von 96-Well-Platten basiert. Ein Sondendesign wurde entworfen, das es ermöglicht vollständig synthetisierte Peptide selektiv aus einem rohen Produktgemisch mittels eines N-terminalen Thiol-Ankers zu isolieren und somit eine zeitaufwendige Reinigung zu umgehen. Der neu entwickelte 96-Well-Assay wurde dann angewendet, um den Einfluss von Peptidsequenzkontexten auf die Selektivität von HDACs zu bewerten. Dazu wurden potentielle Substrate von HDAC6 untersucht, die in Zellen mit verminderter HDAC6-Aktivität identifiziert wurden. Die Mehrheit der getesteten Sequenzen war dabei in der Lage HDAC6 an den entsprechenden Hydroxamsäure-Sonden gegenüber den Lysin-Kontrollen anzureichern, während HDAC1 unspezifisch oder nur schwach rekrutiert wurde. Ausgewählte Sequenzkontextsonden wurden im Detail mittels MS-gestützter Proteomik charakterisiert,

was es ermöglichte spezifische Interaktionsprofile der jeweiligen Sonden mit potentiellen HDAC6-Bindingspartnern zu ermitteln, die an vielfältigen biologischen Prozessen beteiligt sind, wie Transkriptionsfaktoren, Proteine des Cytoskeletts oder Komponenten des Ubiquitin-Proteasom-Systems. Abschließend konnte mittels eines MALDI-MS-basierten, kinetischen Assays und Acetyllysin-Substraten gezeigt werden, dass der jeweilige Peptidsequenzkontext einen fein abgestuften Einfluss auf die Geschwindigkeit der durch HDAC6 katalysierten Deacetylierungsreaktion ausübt.

Contents

List of Figures

List of Tables

List of Abbreviations

9-BBN	9-Borabicyclo[3.3.1]nonane
ABC	Ammonium bicarbonate
Ac	Acetyl
ADP	Adenosine diphosphate
AGC	Automatic gain control
Ahx	6-Aminohexanoic acid
Ala, A	Alanine
Alloc	Allyloxycarbonyl
Aoda	2-Amino-8-oxodecanoic acid
Aoe	2-Amino-8-oxo-9,10-epoxydecanoic acid
Apa	(2-Aminophenyl)amide
Apm	α-Aminopimelic acid
ApmHd	α-Aminopimelic acid ω-hydroxamate
APS	Ammonium peroxodisulfate
Arg, R	Arginine
Asn, N	Asparagine
Asp, D	Aspartic acid
Asu	α-Aminosuberic acid
AsuApa	2-Amino-8-((2-aminophenyl)amino)-8-oxooctanoic acid
AsuHd	α-Aminosuberic acid ω-hydroxamate
Atona	2-Amino-9,9,9-trifluoro-8-oxononanoic acid
ATP	Adenosine triphosphate
BCA	Bicinchoninic acid

Bn	Benzyl
Boc	*tert*-Butyloxycarbonyl
br	broad
BSA	*N*,*O*-Bis(trimethylsilyl)acetamide or bovine serum albumin
Bu	Butyl
CHCA	α-Cyano-4-hydroxycinnamic acid
COSY	Correlation spectroscopy
CuAAC	Copper(I)-catalyzed azide-alkyne cycloaddition
Cys, C	Cysteine
d	Doublet
DCM	Dichloromethane
DEPT	Distortionless enhancement by polarization transfer
DHB	2,5-Dihydroxybenzoic acid
DIC	*N*,*N*′-Diisopropylcarbodiimide
Dioxane	1,4-Dioxane
DIPEA	*N*,*N*-Diisopropylethylamine
DMB	2,4-Dimethoxybenzyl
DMF	*N*,*N*-Dimethylformamide
DMSO	Dimethylsulfoxide
Dns	Danysl, 5-(Dimethylamino)naphthalene-1-sulfonyl chloride
DTT	Dithiothreitol
EDC	1-Ethyl-3-(3-dimethylaminopropyl)carbodiimide
EDT	Ethane-1,2-dithiol
EDTA	Ethylenediaminetetraacetic acid
eq	Equivalent
ESI	Electrospray ionization
Et	Ethyl

FASP Filter-aided sample preparation

Faz *p*-Azidophenylalanine

FDR False discovery rate

Fmoc 9-Flourenylmethoxycarbonyl

Gln, Q Glutamine

Glu, E Glutamic acid

Gly, G Glycine

HAT Histone acetyltransferase

HATU *N*,*N*,*N*′,*N*′-Tetramethyl-*O*-(7-azabenzotriazol-1-yl)uronium hexafluorphosphate

HBTU 2-(1*H*-Benzotriazol-1-yl)-1,1,3,3-tetramethyluronium hexafluorophosphate

HCD Higher-energy collisional dissociation

HDAC Histone deacetylase

HDACi HDAC inhibitor

HEPES 2-(4-(2-Hydroxyethyl)piperazin-1-yl)ethanesulfonic acid

His, H Histidine

HMBC Heteronuclear multiple bond correlation

HMT Histone methyltransferase

HPLC High-performance liquid chromatography

HRP Horseradish peroxidase

HSQC Heteronuclear single quantum coherence

IC_{50} Half maximal inhibitory concentration

Ig Immunoglobulin

Ile, I Isoleucine

LC-MS Liquid chromatography-mass spectrometry

Leu, L Leucine

LFQ Label-free quantification

Lys, K Lysine

Lys8	$^{13}C_6$,$^{15}N_2$-Lysine
MALDI	Matrix-assisted laser desorption / ionization
Me	Methyl
Met, M	Methionine
MIC	Multi ion count
Mpa	3-Mercaptopropionic acid
Mpe	3-Methylpent-3-yl
MS	Mass spectrometry
NAD	Nicotinamide adenine dinucleotide
NES	Nuclear export signal
Nle	Norleucine
NLS	Nuclear localization signal
NMM	*N*-Methylmorpholine
NMP	*N*-Methylpyrrolidine-2-one
NMR	Nuclear magnetic resonance
ODT	Octane-1,8-dithiol
Oxyma	Ethyl 2-cyano-2-(hydroxyimino)acetate
PAGE	Polyacrylamide gel electrophoresis
Pbf	2,2,4,6,7-Pentamethyldihydrobenzofuran-5-sulfonyl
PDB	Protein data bank
PEG	Polyethylene glycol
PEG_2	8-Amino-3,6-dioxaoctanoic acid
PEG_3	12-Amino-4,7,10-trioxadodecanoic acid
Ph	Phenyl
Phe, F	Phenylalanine
PMB	*para*-Methoxybenzyl
Pra	Propargylglycine

Pro, P	Proline
PTM	Post-translational modification
PVDF	Polyvinylidene difluoride
q	Quartet
RP	Reverse-phase
RT	Room temperature
s	Singulet
SAHA	Syberoylanilide hydroxamic acid
SCX	Strong cation exchange
SDB	Styrenedivenylbenzene copolymer
SDS	Sodium dodecyl sulfate
Ser, S	Serine
SILAC	Stable isotope labeling by amino acids in cell culture
sp.	Species
SPE	Solid-phase extraction
SPPS	Solid-phase peptide synthesis
Su	Succinimide
SUMO	Small ubiquitin-related modifyer
t	Triplet
TBS	Tris-buffered saline
TBST	Tris-buffered saline with Tween 20
TEMED	*N*,*N*,*N*′,*N*′-Tetramethylethylenediamine
TFA	Trifluoroacetic acid
TFMK	Trifluoromethyl ketone
TFMSA	Trifluoromethanesulfonic acid
THF	Tetrahydrofuran
Thr, T	Threonine

TIPS	Triisopropylsilylamine
TLC	Thin layer chromatography
TMS	Trimethylsilyl
TOF	Time-of-flight
Tris	Tris(hydroxymethyl)aminomethane
Trp, W	Tryptophan
Trt	Trityl, Triphenylmethyl
TSA	Trichostatin A
Tyr, Y	Tyrosine
Val, V	Valine
Z	Benzyloxycarbonyl
ZBG	Zinc-binding group

1 Introduction

During evolution, eukaryotic organisms have developed an efficient mechanism for compacting their genetic material to fit within the limited space of the cellular nucleus. This is achieved by condensation of DNA with specialized scaffold proteins, resulting in the highly dense structure of chromatin.

1.1 Chromatin and histone proteins

The basic structural unit of chromatin is the nucleosome that comprises an octamer of the four histone proteins H2A, H2B, H3 and H4, forming the nucleosomal core. This octamer consists of a H3 / H4 heterotetramer and two copies of a H2A / H2B heterodimer, around which 146 base pairs of left-handed DNA superhelix are wrapped (Figure 1 A).[1,2] These structural units are separated by 20–90 base pairs of linker DNA, which makes them reminiscent of "beads on a string" (Figure 1 B). Through addition of the linker histone H1, that binds to the surface of the nucleosomal core at the DNA entry end exit sites, this structure can be condensed into the "30 nm-fiber". Finally, the 30 nm-fiber is further compacted with additional non-histone scaffold proteins to form densely packaged mitotic chromosomes.[3]

Based on the level of condensation, chromosomal regions can be classified as either heterochromatin or euchromatin. While the latter is the more loosely packed site of transcriptionally active genes, the dense heterochromatin comprises mostly transcriptionally silent genes.[4] The transition between these two states is crucial for the regulation of gene expression as well as DNA replication and is modulated by the presence of post-translational modifications (PTMs) on the histone proteins.[5] Both the histone cores and the N-terminal tails, which protrude from the nucleosomes into the nucleus, were shown to be extensively modified by PTMs *in vivo* (Figure 2). The N-terminal tails are highly conserved among eukaryotes and comprise, depending on the method of definition, approximately 10–40 amino acid residues. In addition, histones H2A and H2B possess short C-terminal tails.[6,7]

Acetylation of lysine, methylation of lysine and arginine, and phosphorylation of serine and threonine (and to a lower extent tyrosine and histidine) constitute the most abundant modifications of the histone tails. More recently, additional PTMs have been identified, including deimination of arginine to citrulline, lysine ubiquitinylation, SUMOylation and ADP-ribosylation, as well as a multitude of other lysine acylations including formylation, propionylation, crotonylation, malonylation and succinylation.[8,9] In order to explain the influence of PTMs and thus chromatin structure on transcriptional control, two theories have emerged.

The electrostatic model assumes that interaction of the positively charged lysine and arginine residues on the histone tails with the negatively charged phosphodiester backbone of the DNA further compacts chromatin structure and renders it inaccessible for the protein

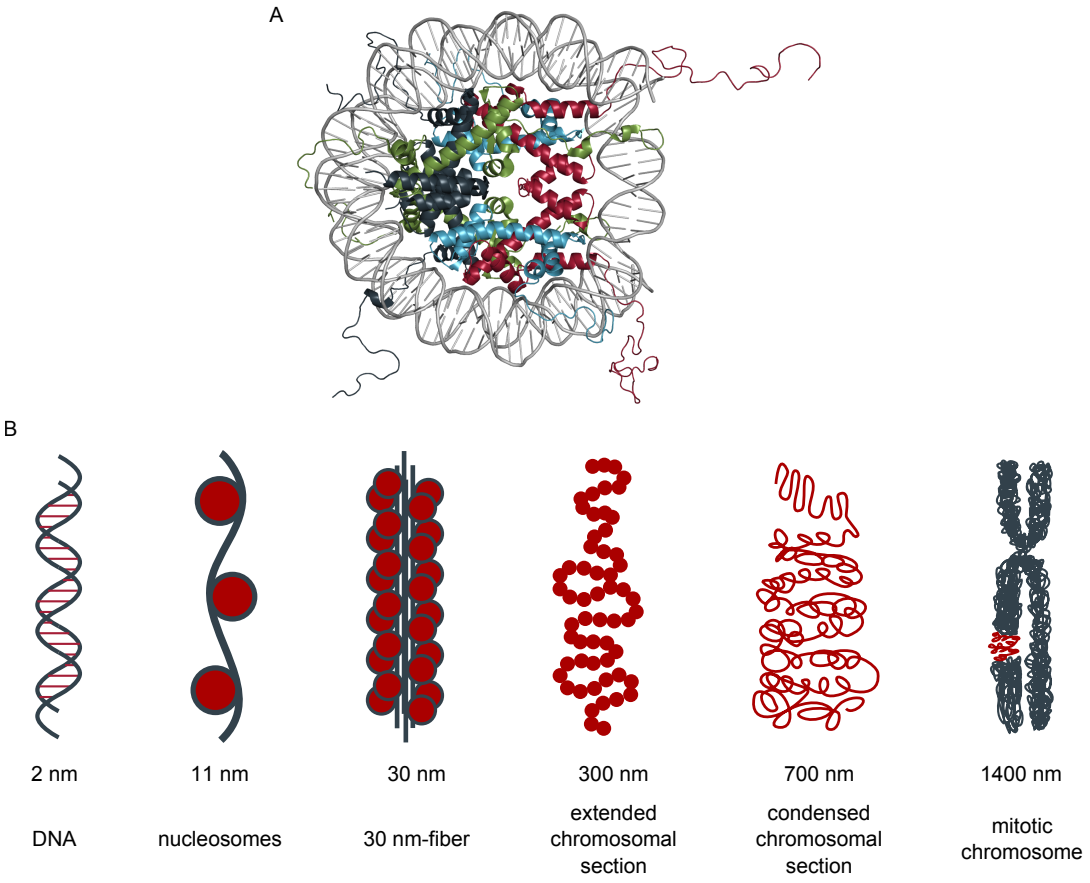

Figure 1: (A) Crystal structure of a nucleosome from *Xenopus laevis* (PDB ID: 1KX5).[16] Histone H3 is depicted in red, H4 in blue, H2A in green, and H2B in gray. (B) Structural units of chromatin with their approximate size, increasing from left to right.

machinery of gene transcription.[10] In addition, the tail of histone H4 is known to interact with a negatively charged surface region of the nucleosomal core formed by several conserved amino acid residues of histone H2A and H2B, which further contracts chromatin structure.[11] Post-translational acetylation of the lysine residues neutralizes their positive charge, thus loosening chromatin packing and increasing DNA accessibility.[12,13] Consequently, hyper-acetylation of histone tails is associated with gene activation, while hypoacetylation is thought to correlate with gene silencing.[14,15]

However, the electrostatic model does not explain the function and observed effects of post-translational modifications other than acetylation. To account for these effects, the histone code hypothesis has emerged, which assumes that different patterns of PTMs on the histone tails are able to recruit different effector proteins. The effectors or “readers” interact with PTMs in a site-specific manner and associate with additional proteins like chromatin remodelers or transcription factors, which in turn regulate chromatin structure and gene activity.[17] The identification of numerous types of conserved domains shared by effector proteins further supports the histone code theory.[18]

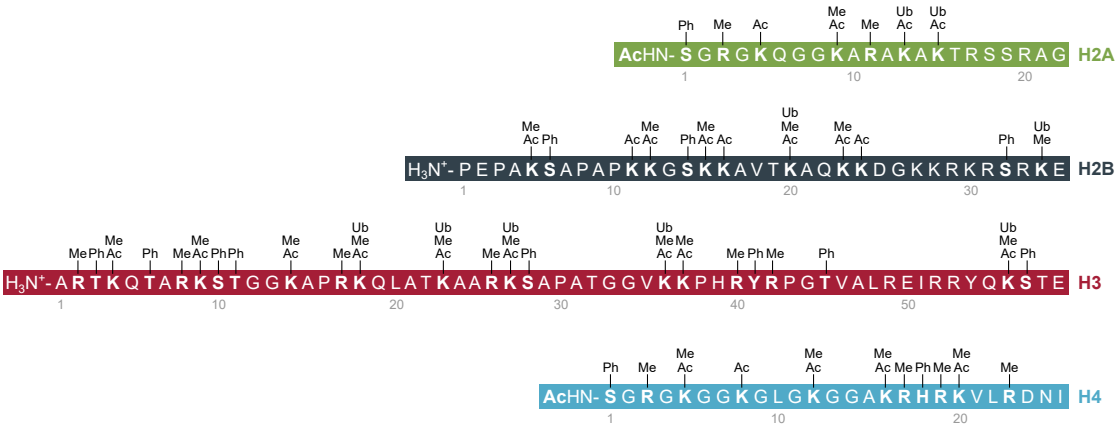

Figure 2: Post-translational modifications on the N-terminal tails of histone proteins including the non-globular fold extensions that are in contact with the DNA.[20] Tails are color coded according to the representation of histones in Figure 1 A. Ac: Acetylation, Me: Methylation, Ph: Phosphorylation, Ub: Ubiquitinylation.

Methylation marks on arginine and lysine are recognized by chromo-, tudor- and MBT domains, as well as PHD fingers and WD40 repeats. Binding to phosphorylated serine and threonine is mediated by 14-3-3 proteins and BRCT domains. Acetylated lysine residues are recognized by bromodomains, which are found in many chromatin remodeling complexes and histone-modifying enzymes.[5] Acetylation of H3K14, for example, is detected by the bromodomain-containing protein Swi2 / Snf2, which recruits the SWI / SNF remodeling complex to this site, thereby increasing chromatin accessibility.[19]

Importantly, the histone code theory implies a significant cross-talk between different post-translational modifications within the same or on two separate histone tails, between individual nucleosomes as well as between nucleosomes and modified (e.g. methylated) DNA.[9,21] One modification might prevent or promote the binding of a specific reader domain to another modification or modifications might act cooperatively to recruit effector proteins. A competitive action of different histone-modifying enzymes targeting the same modification site is also conceivable, especially for lysine. Furthermore, PTM marks are thought to be interdependent, since modification of one specific site may be required for subsequent targeting of an adjacent site by another histone modifying enzyme or the modification of the first site might prevent modification of the second site.[5] For example, it was shown that recognition of trimethylated H3K9 by the protein HP1 (heterochromatin protein 1) is associated with repressive heterochromatin formation, while binding of HP1 to H3K9Me_3 during mitosis is disrupted by phosphorylation of H3S10 (compare Figure 2).[22] Methylation of the adjacent H3K4, in turn, was found to be dependent on ubiquitinylation of H2BK123.[23]

The presence of post-translational modifications on histone tails is a dynamic process regulated by histone-modifying enzymes. Within the context of the histone code theory, enzymes introducing PTMs to histone tails are designated “writers” and enzymes removing modification marks are referred to as “erasers”. Methylation of arginine and lysine is catalyzed by histone methyltransferases (HMTs) using *S*-adenosyl methionine as co-factor, while the reverse reaction is facilitated by histone demethylases. Phosporylation of serine, threonine and tyrosine is introduced by kinases using ATP and removed by phosphatases. The prevalence

of lysine acetylation is regulated by histone acetyltransferases (HATs) and histone deacetylases (HDACs).[24] The balanced action of both “writer” and “eraser” enzymes consequently enables eukaryotes to carefully adjust cellular functions on the level of transcriptional control, exploiting the multiple levels of complexity within the histone code.

1.2 Histone deacetylases

Lysine acetylation constitutes one of the best studied post-translational modification of histone proteins and is introduced by histone acetyltransferases (HATs) utilizing acetyl coenzyme A (Figure 3). The reverse reaction, lysine deacetylation, is catalyzed by histone deacetylases (HDACs).[24] Although lysine acetylation was initially discovered on histone proteins,[25] in the past decades an even greater amount of other nuclear, cytosolic and mitochondrial proteins was shown to be modified by this PTM.[26] Consequently, in addition to targeting acetyl histone substrates, a role for HDACs emerged in deacetylating non-histone substrates as well, thereby regulating their activity and function.[27]

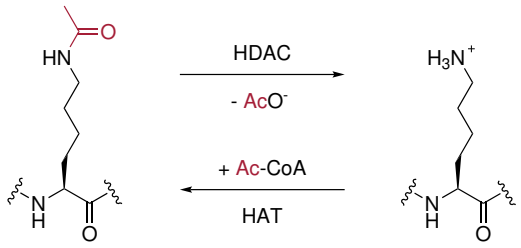

Figure 3: Regulation of lysine acetylation by histone acetyltransferases (HATs) and histone deacetylases (HDACs). While HATs transfer an acetyl group from acetyl coenzyme A (Ac-CoA) to the side chain of lysine residues, HDACs remove the acetyl group in histone and non-histone substrates by hydrolysis.

The family of histone deacetylases can be divided into two large subgroups. Based on their catalytic mechanism, zinc-dependent “classical” HDACs are distinct from the subfamily of sirtuins, which employ NAD^+ as co-substrate (Figure 4). To date, 18 human HDACs have been identified, that are further grouped into four classes according to sequence similarity with their respective yeast homologs. This classification is primarily based on the conserved catalytic domains. Class I comprises HDAC1, 2, 3 and 8 which show homology to the deacetylase Rpd3 from *S. cerevisiae*. Class II HDACs display homology to the yeast enzyme Hda1 and can be further divided into two subclasses, IIa with HDAC4, 5, 7 and 9, and IIb with HDAC6 and 10. Class III comprises the sirtuins (SIRT1–7), which are homologs to the transcriptional repressor Sir2 in yeast. HDAC11 shows homology to both class I and class II HDACs and is therefore grouped into a separate class IV.[28,29]

HDACs of class I are regarded as ubiquitously expressed in all cell types, while HDACs of class II show a more tissue-specific distribution. HDAC4, 5 and 9 are preferentially expressed in heart, skeletal muscle and brain, whereas HDAC7 shows highest expression in heart and lung tissue. HDAC6 and HDAC10 are most strongly expressed in liver, spleen, kidney and testis.[30,31]

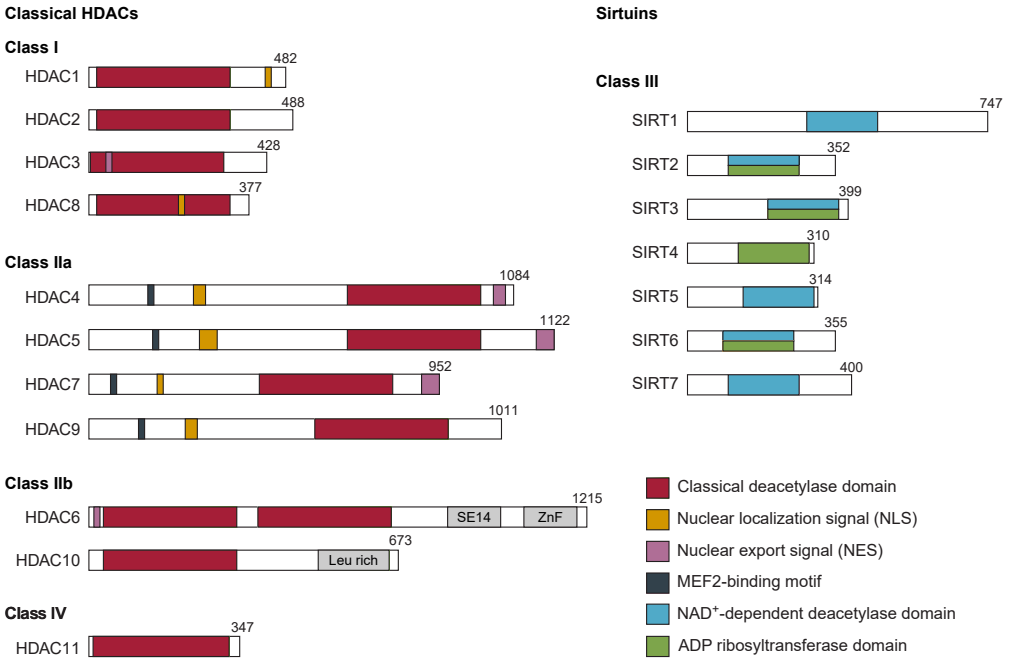

Figure 4: Classification and domain organization of zinc-dependent HDACs and sirtuins. The total number of amino acid residues is shown to the right of each protein. The second, partial catalytic domain of HDAC10 is designated "Leu rich". SE14: Ser-Glu-containing tetradecapeptide repeats. ZnF: Zinc finger ubiquitin binding (ZnF-UBP) domain. Modified from [29, 30, 32, 33].

1.2.1 Class I

HDAC1 and HDAC2 are closely related proteins with a sequence identity of 82 %. Both enzymes share a conserved N-terminal catalytic domain and while only HDAC1 possesses a C-terminal nuclear localization signal (NLS), both HDAC1 and HDAC2 primarily reside in the nucleus due to the lack of a nuclear export signal (NES).[30] HDAC1 and HDAC2 are only active within large multi-protein complexes that mediate their catalytic activity and selectivity for histone substrates (see Chapter 1.2.5). With the complex components steering recruitment to chromatin, HDAC1 and 2 regulate gene activity by deacetylation of all four core histones, however, with a distinct preference for the respective acetylation site.[29] In addition to complex formation, activity of HDAC1 and HDAC2 is regulated and fine-tuned by post-translational modifications such as phosphorylation. While increased phosphorylation stimulates deacetylase activity and simultaneously decreases the ability to associate with other complex components, hypophosphorylation facilitates complex formation, which is in turn required for enzymatic activity.[34]

A well established non-histone substrate of HDAC1 is the tumor suppressor protein p53, which is an important regulator of cell cycle progression and apoptosis. Upon DNA damage, p53 induces cell cycle arrest, subsequently initiating either DNA repair or programmed cell death. In unstressed cells the levels of p53 are kept low through continuous ubiquitinylation and proteasomal degradation. Ubiquitinylation of p53, in turn, is enabled by HDAC-mediated deacetylation.[35]

HDAC3 shares the highest homology with HDAC8 (34 % sequence identity) and possesses an overall domain structure similar to other class I HDACs.[30] HDAC3 is thought to be a primarily nuclear enzyme, but due to an NES it may also localize to the cytoplasm, depending on the cell type and other conditions affecting the cell.[36,37] HDAC3 forms different multi-protein complexes than HDAC1 and HDAC2 and is able to interact with HDACs 4, 5 and 7 via the NCoR or SMRT components of these complexes.[38]

Like HDAC1 and HDAC2, HDAC3 is recruited to chromatin e.g. by transcription factors and acts as transcriptional repressor via deacetylation of histones.[29] A well characterized non-histone substrate of HDAC3 is the p65 subunit (RELA) of the transcription factor complex NF-κB, with the acetylation status of NF-κB subunit influencing protein-protein interactions as well as nuclear import and export.[39]

HDAC8 is evolutionarily most closely related to HDAC3 and posesses an NLS within its catalytic domain.[30] However, it is thought to be located both in the nucleus and the cytosol.[37] In addition to its catalytic domain, HDAC8 only comprises a short C-terminal extension. While the longer C-terminal part of other class I HDACs enables multi-protein complex formation, which is necessary for enzymatic activity, HDAC8 is the only class I HDAC that is an active deacetylase *in vivo* and *in vitro* in the absence of complex partners. Nevertheless, HDAC8 was found to associate with a variety of proteins that may steer its cellular functions that are regarded as distinct from other class I HDACs.[40] As opposed to HDAC1 and HDAC2, phosporylation of HDAC8 inhibits rather than stimulates its enzymatic activity.[29]

Many non-histone substrates have been identified for HDAC8 with high confidence with SMC3 being the most well established. SMC3 is a component of cohesin, a complex necessary for chromosome cohesion in the cell cycle. During anaphase, dissociation of the complex from chromatin is achieved by HDAC8-catayzed deacetylation of SMC3.[39,41]

1.2.2 Class II

Class IIa

Within class IIa, HDAC4 and HDAC5 are most closely related with a similarity of 70 %, followed by HDAC7 with around 58 % similarity to both other HDACs. In contrast to class I HDACs, HDAC4, 5 and 7 possess a C-terminal catalytic domain and a long N-terminal extension containing the NLS sequence.[30] Since HDAC4, 5 and 7 also comprise a C-terminal NES, they are able to shuttle between nucleus and cytosol.[31,42] This process is regulated by phosphorylation of the HDACs at several conserved, serine-rich sites at the N-terminal extensions. Binding of 14-3-3 proteins to phosphorylated HDAC4, 5 and 7 induces their export from the nucleus and at the same time causes their retention in the cytoplasm by masking the NLS. Dephosphorylation and subsequent release of 14-3-3 proteins enables HDAC4, 5 and 7 to re-enter the nucleus.[29,32] All three HDACs further share an N-terminal binding site for the DNA-binding transcription factor MEF2.[31] MEF2 plays an important role in muscle cell differentiation and class IIa HDACs are thought to be involved in the regulation of this process. When HDAC4, 5 and 7 are located in the nucleus, MEF2-binding inhibits its activity as a transcription factor, thus blocking cell differentiation. Upon phosphorylation of HDAC4, 5 and 7, MEF2 is released again and the respective HDAC is exported from the nucleus via the aforementioned mechanism.[30]

HDAC9 separated early in evolution from HDAC4, 5 and 7 and represents its own subcluster within class IIa HDACs, including multiple splice variants. HDAC9 shares the same domain structure as the other class IIa HDACs, but lacks an NES.[30] Although HDAC9 represses gene activity when recruited to a promotor through histone deacetylation, this deacetylase activity might stem from association with HDAC3 complexes.[29,43] One of the HDAC9 splice variants, HDAC9c (also called myocyte enhancer-binding factor 2-interacting transcriptional repressor (MITR) or HDAC-related protein (HDRP)), does not possess a catalytic domain but still functions as transcriptional regulator through interaction with MEF2 and HDAC3. Consequently, the alternative splice variants of HDAC9 may contribute to fine-tuning its activity, possibly also depending on the cell type.[30,44]

The catalytic domains of all HDACs of class IIa display only very weak intrinsic deacetylase activity.[45] This is caused by a substitution of a tyrosine residue in the active site, which acts as a transition state stabilizer and is conserved in other HDACs, by histidine (see Chapter 1.2.6).[29] Consequently, HDACs of class IIa are thought to function as regulatory binding domains of acetylated lysine rather than deacetylases.[46]

Class IIb

HDAC6 shares the highest homology with HDAC10 (55 % sequence identity) and both enzymes possess a unique domain structure within the group of zinc-dependent HDACs.[29] HDAC6 is a predominantly cytosolic enzyme due to an NES at the N-terminus and a C-terminal SE14 (Ser-Glu-containing tetradecapeptide repeats) motif which serves in anchoring HDAC6 to the cytoplasm. In addition, HDAC6 posesses a C-terminal zinc finger ubiquitin binding (ZnF-UBP) domain which is also found in ubiquitin-specific proteases and enables binding of mono- and poly-ubiquitin chains.[47] HDAC6 is the only HDAC that contains two functional catalytic domains, designated CD1 and CD2, which are thought to act either independently or in tandem, depending on the substrate. While only CD2 shows deacetylase activity for acetyllysine within peptide sequences *in vitro*, CD1 is able to efficiently deacetylate C-terminal acetyllysines. However, α-tubulin, a physiological substrate of HDAC6, is most efficiently deacetylated with both domains intact. This may assign CD1 a further role in the binding of α-tubulin and other target proteins.[47,48]

Due to its localization, HDAC6 primarily deacetylates cytosolic non-histone substrates and is thought to fulfill regulatory purposes at several intersecting cellular pathways unrelated to histone modification. By deacetylation of α-tubulin, HDAC6 regulates the dynamics of microtubule stability and by deacetylation of cortactin, it exerts an influence on F-actin polymerization. Both mechanisms are thought to be involved in a variety of cellular processes that require re-organization of the cytoskeleton, such as cell adhesion and migration or immune synapse formation.[49,50] HDAC6-mediated deacetylation may also be crucial for the stability and function of various cellular proteins through its influence on chaperone signaling. Deacetylation of the chaperone HSP90 by HDAC6 is required for association with the co-chaperone p23 and the glucocorticoid receptor (GR), which in turn enables activation and hormone binding of the GR.[51,52] Through its ZnF-UBP domain, HDAC6 is involved in the clearance of misfolded proteins from the cytosol by providing a link to the molecular motors of the microtubule cytoskeleton, the ubiquitin-proteasome system and the autophagic machinery.[47,53,54]

HDAC10, the most recently identified member of class II HDACs, is most closely related to HDAC6 and comprises an active N-terminal catalytic domain and a second partial and inactive C-terminal catalytic domain.[30,55] The second domain is rich in leucine residues and important for enrichment of HDAC10 in the cytoplasm.[56] However, HDAC10 is able to reside both in the cytoplasm as well as the nucleus and is found to associate with several other HDACs of class I and II except HDAC6.[30] When recruited to chromatin, HDAC10 acts as a transcriptional repressor, possibly by a deacetylase-independent mechanism.[57]

Recently, polyamine deacetylase activity was reported for HDAC10 with a strong preference for N^8-acetylspermidine as substrate. Consequently, HDAC10 might be involved in the regulation of polyamine metabolism and thereby also play a role in autophagy, which is promoted by the accumulation of spermidine. Notably, HDAC10 seems to be the closest relative to the family of arginases which adopt the same three-dimensional fold as HDACs and are responsible for the generation of ornithine from arginine, with ornithine being the starting material for polyamine biosynthesis.[58]

1.2.3 Class III

Class III HDACs, or sirtuins, are distinct from zinc-dependent HDACs in both their structure and reaction mechanism. Although originally identified as lysine deacetylases, many sirtuins are able to catalyze the removal of other acyl groups from lysine residues with NAD^+ as co-substrate, generating 2′-*O*-acyl ADP ribose.[29,59]

While SIRT1 is predominantly nuclear, SIRT2 is found both in the nucleus and the cytoplasm, and SIRT3 is a mitochondrial enzyme.[60] All three enzymes possess lysine deacetylase activity. SIRT1 is regarded as a transcriptional regulator acting on acetylated histones as well as on transcription factors like NF-κB. A well known non-histone substrate of SIRT1 is the tumor suppressor protein p53. Deacetylation of p53 by SIRT1 decreases its ability to transcriptionally activate the cell cycle inhibitor p21, which in turn delays apoptosis and enables the cell to re-enter the cell cycle after DNA damage and repair. SIRT2 deacetylates histone as well as non-histone substrates. Like HDAC6, SIRT2 is able to catalyze the deacetylation of α-tubulin and is thereby involved in the regulation of cell motility.[29,60,61] SIRT2 and HDAC6 were also found to interact with each other.[50,61] Due to its localization, SIRT3 is not likely to act on histone substrates and is instead the major deacetylase of mitochondrial proteins.[60,61] SIRT3 was also shown to possess weak lysine decrotonylase activity.[59]

SIRT4, 5, 6 and 7 possess no or only very weak deacetylase activity *in vitro*.[27,61] SIRT4 and SIRT5 are exclusively mitochondrial enzymes, while SIRT6 and SIRT7 are located in the nucleus.[60] SIRT4 is able to catalyze the removal of lipoyl groups from lysine residues of pyruvate dehydrogenase which leads to its inhibition. Since lipoyl modifications are present on a variety of enzymes that catalyze the oxidative decarboxylation of α-keto acids such as pyruvate and α-ketoglutarate, SIRT4 might exert an influence on the output of the citric acid cycle in mitochondria.[59] SIRT5 was shown to remove acyl groups derived from dicarboxylic acids from lysine residues with a strong preference for lysine demalonylation, desuccinylation and deglutarylation. Through its desuccinylase activity, SIRT5 is thought to regulate various metabolic enzymes in the mitochondrion, which were shown to be modified by succinylation.[27,59,62] SIRT6 was found to remove several long-chain fatty acyl groups

from lysine residues *in vitro* and to regulate the secretion of the cytokine TNF-α through lysine demyristoylation *in vivo*.[63] SIRT7 might act on histone substrates by deacetylation, debutyrylation and desuccinylation.[64]

Several sirtuins were also reported to possess ADP ribosyl transferase activity, although the physiological relevance of this reaction is not clear.[59] However, the usage of NAD^+ as co-substrate of sirtuins has been considered to link metabolism and gene expression by coupling transcriptional repression to the redox state of the cell.[65]

1.2.4 Class IV

HDAC11 shares sequence homology with both class I and class II HDACs, but is most closely related to HDAC3 and HDAC8.[30] It is the least studied zinc-dependent HDAC and was found to reside primarily in the nucleus, although it also co-immunoprecipitates with HDAC6.[66] HDAC11 was initially reported to possess histone deacetylase activity, however, the observed effects could not be directly attributed to its catalytic domain. HDAC11 is thought to regulate stability of the DNA replication factor CDT1 and the expression of interleukin 10.[29] Recent investigations demonstrated a lack of activity for acetyllysine substrates *in vitro*, but proficient fatty-acid deacylase activity, allowing the preferred removal of caprinyl, lauryl and myristoyl groups from lysine residues, which is reminiscent of SIRT6.[67]

1.2.5 HDAC complexes

Despite their function in regulating histone acetylation levels, HDACs do not directly bind to chromatin, but are often part of large multi-protein complexes, that steer recruitment to specific genomic loci and mediate catalytic activity.[29,68] Especially class I HDACs, except HDAC8, associate with other proteins to form four well defined complexes, that contain binding proteins for histone modifications and additional histone modifying enzymes (Figure 5). HDAC1 and HDAC2 are both part of the CoREST (co-repressor of RE1-silencing transcription factor), Sin3 (switch-independent 3) and NuRD (nucleosome remodeling deacetylase) complexes, that are required for proficient enzymatic activity.[69] HDAC3 forms the NCoR / SMRT (nuclear receptor corepressor / silencing mediator for retinois and thyroid hormone receptors) complex, which was shown to significantly increase its deacetylase activity.[70] Besides their ability to deacetylate lysine residues, HDAC complexes harbor further activities, such as DNA helicase (NuRD) or lysine demethylase (CoREST) activity.[32]

Through combination of the many different isoforms of HDAC complex components, several distinct versions of complexes containing the same HDAC might exist within a cell. This may be a way of fine-tuning HDAC activity, since complex composition was found to be cell-type-specific. In T-cells, for example, the Sin3 complex preferentially contains HDAC1 but not HDAC2. Additionally, the dimeric CoREST and Sin3 / NuRD complexes might contain both HDAC1 and HDAC2, and this redundancy seems especially tackling in the development of specific HDAC inhibitors.[68,71]

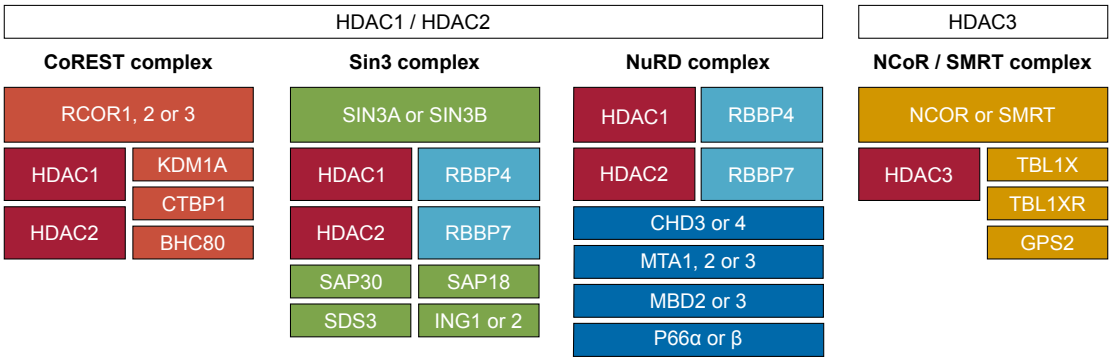

Figure 5: Schematic overview of class I HDAC complexes. HDAC1 and HDAC2 are part of the CoREST, Sin3 and NuRD complexes, while HDAC3 forms the NCoR / SMRT complex.[32,68,71,72]

CoREST

In addition to HDAC1 or HDAC2, the CoREST complex contains the co-repressor RCOR1, 2 or 3, which acts as central adaptor, recruiting both HDAC1 / 2 and the histone demethylase KDM1A via its ELM2-SANT domain. Depending on the method of isolation, this core complex was observed to interact with further proteins. Although RCOR is proposed to interact directly with DNA through a second SANT domain, binding of the PHD finger protein BHC80 to CoREST might also mediate chromatin binding. The co-repressor CtBP1 was also shown to associate with CoREST.[32,72] The effect of combined demethylase / deacetylase activity of CoREST was demonstrated for H3K4Me$_2$. While this modification is a signal for increased gene expression, demethylation by CoREST synergizes with deacetylation of the H3 tail to repress transcription.[68] Unlike other class I HDAC complexes, CoREST does not form a dimer.[71]

Sin3

HDAC1 or HDAC2 are recruited to the Sin3 complex via co-repressors Sin3A or Sin3B, which, however, do not contain an ELM2-SANT domain. Instead HDAC1 / 2 is bound by a third protein, SDS3, forming a ternary core complex.[32,68] Sin3 complexes are thought to elicit distinct functions depending on the Sin3 isoform present.[72] The Sin3 complex further contains the protein SAP30, which is able to bind to DNA via its zinc finger domain and targets Sin3A to the nucleolus, and SAP18, which enhances transcriptional repression and contains an ubiquitin fold.[32,73] Components ING1 / 2 possess a PHD finger domain and ING1 interacts with the tumor suppressor p53.[74] ING2 is able to bind methylated H3K4 and steers the Sin3A complex towards deacetylation of nucleosomes in a methylation-dependent manner.[32] With the NuRD complex, the Sin3 complex shares histone binding proteins RBBP4 and RBBP7, which contain WD40 repeat motifs. The Sin3 complex forms dimers by association of the SDS3 components.[71]

NuRD

In the NuRD complex, both HDAC1 or HDAC2 and RBBP4 or RBBP7 are bound to the protein MTA1, 2 or 3 through its SANT domain and C-terminus, respectively, forming a dimeric core complex.[68,71] Additional components include the methylated DNA binding proteins MBD2 or MBD3, the chromodomain-containing ATP-dependent DNA helicases CHD3 or CHD4, and the transcriptional repressors p66α or p66β.[32,75] The NuRD complex may also associate with the histone demethylase KDM1A.[72]

NCoR / SMRT

The NCoR / SMRT complex contains the homologous, non-redundant co-repressors NCoR or SMRT, which bind to HDAC3 through their SANT domains. Further components are the WD40 repeat proteins TBL1X and TBL1XR1, and the protein GPS2, that are involved in transcriptional activation.[76] Through the TBL1 components, the NCoR / SMRT complex is able to dimerize.[71] In contrast to the SMRT complex, NCoR is able to interact with the histone demethylases KDM4A and KDM5C.[72] The NCoR / SMRT complex was also found to associate with class II HDACs 4, 5, 7 and 9.[46]

1.2.6 Catalytic mechanism

The active site of classical, zinc-dependent HDACs (hereafter referred to as HDACs) comprises a tube-like binding pocket to accommodate the acetyllysine residue, a divalent zinc ion, which is coordinated by two aspartate and one histidine residue, two histidine-aspartate charge relay systems, that are reminiscent of metalloproteases, and, except for class IIb HDACs, a conserved tyrosine residue (Figure 6). A reaction mechanism for the deacetylation of *N*ε-acetyllysine residues was proposed on the basis of crystal structures of an HDAC homologue from the thermophilic bacterium *Aquifex aeolicus* and from human HDAC8.[77] This mechanism is similar to other zinc-dependent metalloenzymes like thermolysin or carboxypeptidase A.[78,79]

Deacetylation of the lysine residue is thought to be achieved via *Lewis*-acid catalyzed hydrolysis by a water molecule that is bound to the active site zinc ion. Upon binding of the acetyllysine residue to the active site, the side chain acetyl group is polarized by coordination of the carbonyl oxygen to the zinc ion and hydrogen bonding via the conserved tyrosine residue. In the native HDAC, as well as in the substrate bound state, the coordination geometry of the zinc ion is thought to be five-coordinate square pyramidal. In addition, the amide nitrogen of the acetyl group interacts with the carbonyl of a glycine residue adjacent to the active site via hydrogen bonding, which presumably helps to orient the amide group for the subsequent reaction.[77,80] Nucleophilic attack of the water molecule on the carbonyl group is then facilitated by abstraction of a proton through one of the His-Asp charge relay systems.

The emerging tetrahedral oxyanion intermediate is stabilized through coordination to zinc as well as hydrogen bonding with the conserved tyrosine residue and one of the histidines. Collapse of the tetrahedral intermediate is caused via protonation of its nitrogen atom by one of the His-Asp charge relay systems. While initially the mode of binding of the tetrahedral intermediate was inferred from crystal structures of HDAC8 bound to buffer molecules,[81]

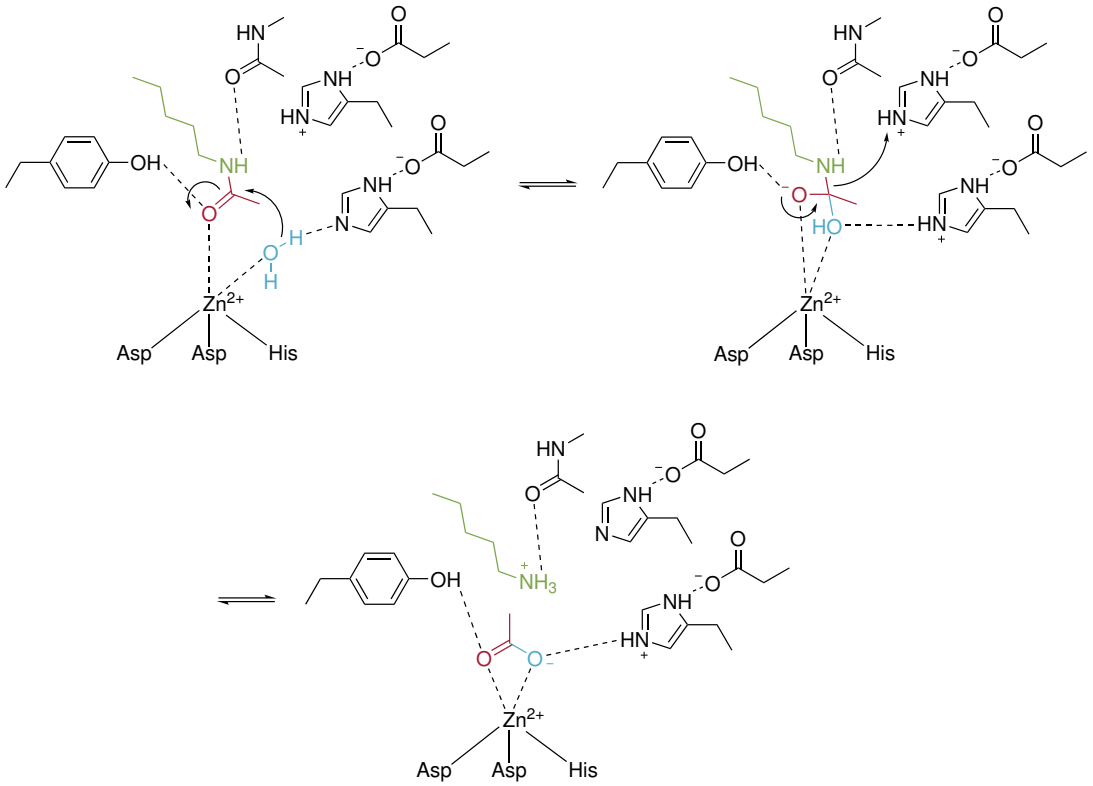

Figure 6: Proposed catalytic mechanism of zinc-dependent HDACs. The active site water molecule hydrolyzing the amide bond is depicted in blue, the acetyl group in red and the lysine residue in green. Modified from [24, 77, 80].

an acetyllysine peptide substrate could be captured in the crystal structure of an HDAC6 CD2 mutant from zebra fish.[48] In this mutant, the histidine residue, that acts as general acid protonating the tetrahedral intermediate, was substituted by an alanine, which consequently blocked the reaction progress and locked the tetrahedral intermediate in place.

After protonation and collapse of the tetrahedral intermediate, a second proton transfer yields the free lysine residue and acetate as products. Crystal structures of HDACs bound to acetate suggest that the acetate molecule remains initially coordinated to the active site zinc ion in a bidentate fashion, and may subsequently exit the enzyme.[48,80]

Nucleophilic attack of the water molecule on the side chain carbonyl is believed to be the rate determining step of the deacetylation reaction catalyzed by HDAC8, because hydrolytic activity was found to be enhanced by substrates with increased electrophilicity containing trifuoroacetyllysine.[82] Notably, HDACs of class IIa, which are catalytically inactive towards acetyllysine due to a Tyr to His mutation, are able to efficiently remove the trifluoroacetyl group from trifluoroacetyllysine substrates. This also highlights the importance of the conserved tyrosine residue as a transition state stabilizer. Consequently, back-mutation of His to Tyr was found to restore catalytic activity towards acetyl substrates for class IIa HDACs.[83]

1.3 HDAC inhibitors

Altered levels of HDAC activity, especially overexpression, are associated with a variety of diseases. For example, deacetylation-mediated silencing of genes that are responsible for cell cycle regulation or apoptosis may lead to tumor genesis. Acute promyelocytic leukaemia (APL) was one of the first forms of cancer in which the role of HDACs was elucidated in detail. For therapeutic treatment it is therefore desirable to identify molecules that are able to inhibit HDAC activity.[84,85] Suberoylanilide hydroxamic acid (SAHA) represents the first HDAC inhibitor (HDACi) for cancer therapy that was authorized by the American Food and Drug Administration, and several other inhibitors are either approved for treatment or under clinical investigation.[86,87]

Based on elucidation of the structure-activity relationship of HDACi and especially aided through crystal structures of HDACs, a common model for the pharmacophore of HDAC inhibitors was devised.[88–90] This pharmacophore is exemplified in Figure 7 A by the structure of SAHA and consists of three relevant parts. A zinc-binding group (ZBG), which is able to chelate the active site zinc ion, is essential to almost all known HDACi and makes a significant contribution to the overall binding of the inhibitor. The zinc-binding group is connected to a commonly non-polar linker, that reaches into the tubular substrate channel joining the active site with the surface of the enzyme, and interacts with its hydrophobic residues through *van der Waals* contacts. A “cap” moiety at the end of the linker interacts with the amino acids at the rim of the tubular binding pocket of HDACs and with the enzyme surface, mimicking the amino acid residues of native protein substrates. Often aromatic rings or cyclic tetrapeptides serve as cap groups.

HDACs exert diverse cellular functions and not all of the eleven human enzymes might be involved in the pathogenesis of a certain disease to the same degree. Consequently, the development of selective HDAC inhibitors is crucial, and these inhibitors can in turn be used as tools to dissect the cellular functions of individual HDACs.[91] Although the pharmacophore model of HDACi is valid for a wide variety of compounds, and selectivity can be influenced by all of the three constituents (ZBG, cap and linker), selective HDAC inhibitors have been reported that lack either a zinc-binding group or a cap moiety.[92,93]

Known HDAC inhibitors can be classified according to their zinc-chelating functional group into four main categories: Short-chain fatty acids, hydroxamic acids, benzamides and ketones. Ketones are often found in cyclic peptide natural products and various cyclic peptide inhibitors exist that exploit other functional groups, which are, however, less thoroughly characterized (Figure 7 B).[24]

1.3.1 Short-chain fatty acids

Initially identified HDAC inhibitors were short-chain fatty acids or their salts, respectively, such as sodium butyrate (**I**) or the synthetic valproic acid and 4-phenylbutyric acid, which are used as clinically approved drugs.[90,97] These compounds were characterized as relatively weak binders of HDACs with IC_{50} values in the micromolar to millimolar range.[98] Short-chain fatty acids were reported to possess limited selectivity for class I over class IIb HDACs, although the reasons for this are not clear.[91] Crystal structures of HDACs bound to acetate, the

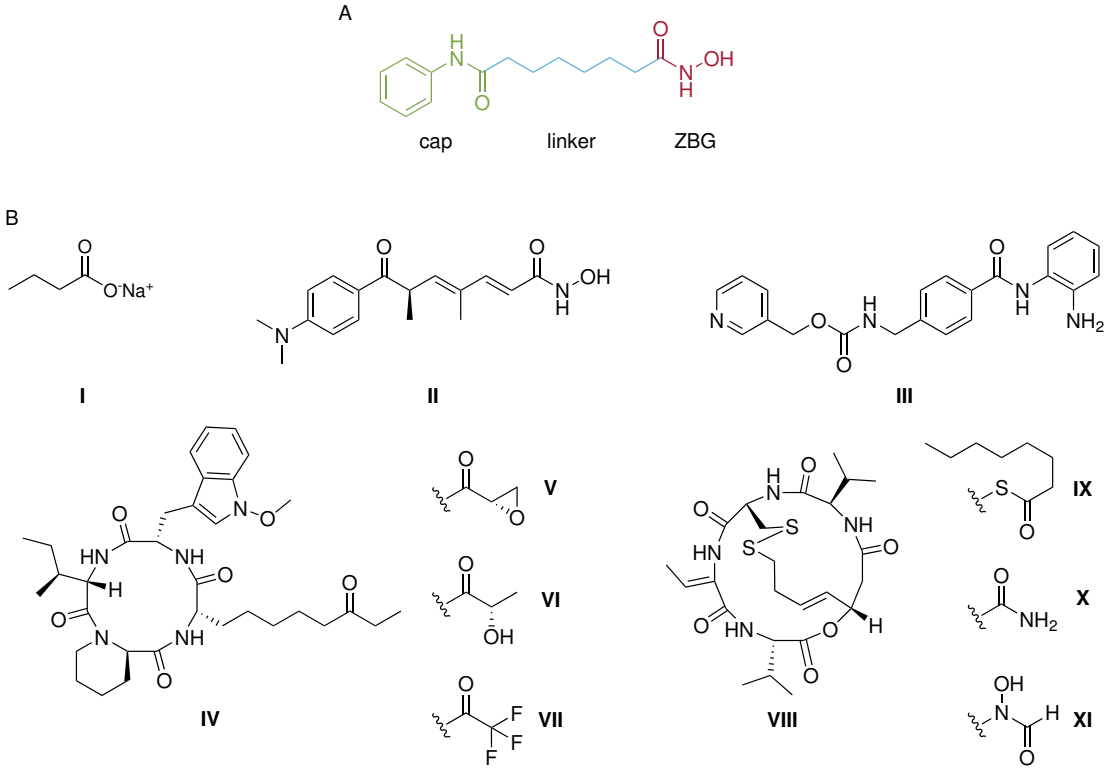

Figure 7: (A) General design of HDAC inhibitors with zinc-binding group (ZBG, red), linker (blue) and cap (green). (B) Examples of HDAC inhibitors and zinc-binding groups: Carboxylic acid (**I**, sodium butyrate), hydroxamic acid (**II**, trichostatin A), benzamide (**III**, MS-275), ethyl ketone (**IV**, apicidin), α,β-epoxy ketone (**V**; trapoxin, HC-toxin, chlamydocin), α-hydroxy ketone (**VI**, FR235222), trifluoromethyl ketone (**VII**), disulfide (**VIII**, romidepsin), thioester (**IX**, largazole), carboxamide (**X**; azumamide A, B, D), *N*-formylhydroxylamine (**XI**).

product of the deacetylation reaction, suggest that short-chain fatty acids chelate the active site zinc ion through bidentate coordination by their carboxyl group. However, they were also reported to show a non-competitive behavior, which hints to another site for binding.[48,90]

1.3.2 Hydroxamic acids

The first hydroxamic acid inhibitor of HDACs was found with the natural product trichostatin A (TSA, **II**), which was isolated from the bacterium *Streptomyces hygroscopicus* .[99] IC_{50} values in a low nanomolar range indicated that hydroxamic acids are potent inhibitors of HDAC activity.[100] Most aliphatic hydroxamic acids like TSA or SAHA are reported as pan-specific, inhibiting both class I and class II HDACs to a comparable extent. This can be explained by the fact that they mainly interact with structural features that are conserved among HDAC classes.[89,90]

However, selectivity of hydroxamic acid inhibitors can be steered towards distinct HDACs or HDAC classes by modification of the cap and linker moiety, or by addition of further substituents to the pharmacophore that exploit distinct structural features of individual HDACs. In the HDAC6-selective inhibitor tubacin, the phenyl moiety of SAHA was replaced by a

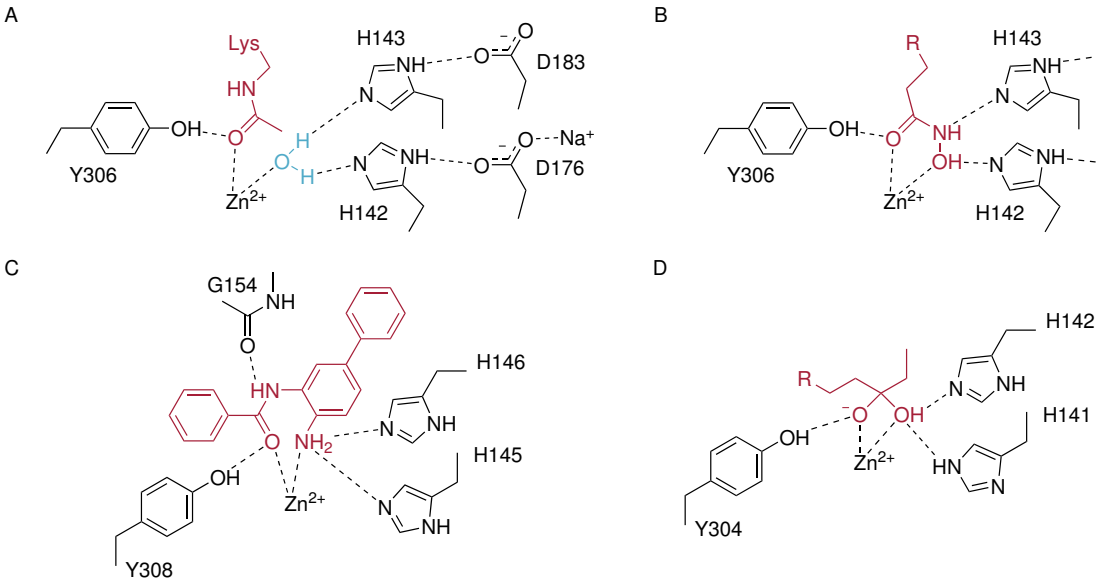

Figure 8: Schematic representations of HDAC inhibitors bound to the active site of HDACs based on crystal structures. (A) Proposed mode of binding of acetyllysine (red) and the active site water molecule (blue) to HDAC8.[94] (B) Scheme of hydroxamic acid inhibitor (red) bound to the active site of HDAC8.[94] (C) Scheme of benzamide inhibitor (red) bound to the active site of HDAC2.[95] (D) Scheme of ketone inhibitor (red) bound to the active site of HDAC2.[96]

sterically very demanding cap group including multiple aromatic substituents, that specifically addresses the structure of the binding pocket rim, which is wider and more shallow in HDAC6 when compared to other HDACs.[101] Additional substitution of the aliphatic linker by an aromatic phenylene moiety in the benzhydroxamic acid derivative tubastatin A, further increased the selectivity for HDAC6.[102] Even the “cap-less”, simple benzhydroxamic acid shows selectivity towards HDAC6 by exploiting contacts with distinct phenylalanine residues in the tubular cavity.[92] HDACs of class IIa possess an additional cavity at the end of the substrate binding channel termed the “lower pocket”, which can accommodate aromatic substituents attached to the linker moiety close to the hydroxamate group, while the “side pocket” that is found in the HDAC8 variant of some species, can be addressed by additional moieties connected to the linker at the distal end.[90]

Crystal structures of HDAC8 co-crystalized with hydroxamic acid inhibitors such as TSA show that hydroxamic acids closely mimic the acetylated lysine substrate of HDACs, for which a similar mode of binding is proposed (Figure 8 A). The hydroxamic acid chelates the active site zinc ion in a bidentate fashion through the carbonyl and the hydroxy group, forming a five-membered ring (Figure 7 B). The hydroxy group consequently also replaces the active site water molecule bound to the zinc ion and interacts with the nearby histidine residue, while the carbonyl group forms a hydrogen bond with the conserved tyrosine residue. The overall hydrogen bonding interaction network with hydroxamic acids is therefore also similar to the one formed upon native substrate binding.[94]

1.3.3 Benzamides

Synthetic benzamides were found to possess HDAC inhibitory activity through a screening effort, in which MS-275 (**III**) was identified as the most promising compound.[103,104] Although generally termed benzamides, because initial members of this class of inhibitors contained an *N*-(2-aminophenyl)benzamide structure, the crucial part for HDAC inhibition is the *o*-aminoanilide or 2-aminophenylamide (Apa) moiety, and inhibitors exist, that are not based on the benzoic acid scaffold.[90,105] Benzamides are reported as less potent than hydroxamic acids with IC_{50} values in a medium nanomolar or low micromolar range. However, benzamides show a distinct selectivity profile, being inactive towards class II HDACs and HDAC8, but effectively inhibiting class I HDAC1, 2 and 3.[89,90] This is explained by the fact that the phenylene ring of the Apa moiety can accommodate the entrance of the so-called “foot pocket” in HDAC1, 2 and 3, a cavity at the bottom of the active site perpendicular to the tubular substrate binding tunnel, which is blocked or missing in HDAC8 and class II HDACs. Selectivity of benzamide inhibitors can be further influenced towards HDAC1 and HDAC2 by introduction of bulky substituents attached at the phenylene ring in *para*-position to the amino group, and this selectivity is thought to be caused by the more narrow and less flexible foot pocket of HDAC3.[90,106,107]

Co-crystallization of HDAC2 with a 5-substituted *N*-(2-aminophenyl)benzamide revealed that the 2-aminophenylamide moiety binds to the active site zinc ion of HDACs in a bidentate fashion through its amino and carbonyl function forming a seven-membered ring (Figure 7 C). Binding is further stabilized by hydrogen bonding of the two conserved histidine residues to the amino group, the tyrosine residue to the carbonyl function, and a glycine residue to the amide nitrogen of the inhibitor. The additional phenyl ring at the 5-position of the phenylamide moiety can reach into the foot pocket, thereby achieving HDAC class selectivity.[95]

1.3.4 Ketones and cyclic peptides

Ketones are found in many structurally related natural product HDAC inhibitors that bear a hydrophobic cyclic tetrapeptide as cap moiety. Apicidin (**IV**) and its several derivatives, which were isolated from the fungal plant pathogen *Fusarium pallidoroseum*, contain the keto amino acid 2-amino-8-oxodecanoic acid (Aoda), with the ethyl ketone at the side chain of Aoda serving as zinc-binding group.[90,108,109] An α,β-epoxy ketone moiety (**V**) is found in the fungal metabolites trapoxin from *Helicoma ambiens*[110], HC-toxin from the maize pathogen *Cochliobolus / Helminthosporium carbonum*,[111] or chlamydocin from *Diheterospora chlamydosporia*,[112] which are all cyclic tetrapeptides containing 2-amino-8-oxo-9,10-epoxydecanoic acid (Aoe). Importantly, an immobilized version of trapoxin B was used as a tool for isolation and identification of the first human HDAC, HDAC1.[113] Further identified ketone inhibitors comprise, among others, α-hydroxy ketones (**VI**), as in the cyclic tetrapeptide FR235222 from *Acremonium* sp.,[114,115] and synthetic trifluoromethyl ketones (TFMKs, **VII**).

Apicidins exhibit strong activity against protozoan parasites of the subphylum Apicomplexa, which cause diseases such as malaria, and inhibit their respective histone deacetylase in the low nanomolar range.[116]. Trapoxin and chlamydocin were even shown to possess

picomolar potency against human HDACs.[90] While in general, ketone-type inhibitors were found to be selective for class I HDACs, the reasons for this are not entirely clear and may depend on the specific compound. When replacing the epoxy ketone moiety of trapoxins with a hydroxamic acid, inhibitory potency is preserved, but class selectivity is diminished.[117] Based on the observation that trapoxins inhibit class II HDACs only weakly and reversibly, but class I HDACs irreversibly, it was initially reasoned that the latter are covalently modified at the active site by the epoxide moiety. However, crystal structures of trapoxin A with HDAC8 and HC-toxin with HDAC6 indicate, that inhibitors containing Aoe bind non-covalently to HDACs of both classes. Instead, the orientation of the epoxide moiety within the active site seems to be crucial for class selectivity, and interactions with the active site residues are less favorable in class II HDACs.[48,118] In other ketone-type inhibitors, like α-hydroxy ketones and the Aoda-containing apicidins, class selectivity might in part be mediated by different modes of coordination to the active site zinc ion.[48,96,119] Despite these findings, efficient and selective HDAC inhibitors were reported based on apicidin-derived cyclic tetrapeptide structures that lack a zinc-binding keto group, which indicates that selectivity is also mediated by the amino acid residues of the peptide cap.[92] While synthetic trifluoromethyl ketones (TFMKs) also inhibit class I HDACs,[90,120] they were found to be superior inhibitors of class IIa HDACs when compared to hydroxamic acids.[121,122]

In a crystal structure of HDAC2 co-crystallized with apicidin, the Aoda ethyl ketone assumes the conventional mode of binding observed for ketone-type inhibitors (Figure 8 D).[96] Upon binding to the active site of HDACs, ketone-type inhibitors are activated and undergo hydration by the zinc-bound water molecule, forming the geminal diol or diolate, respectively. The *gem*-diol(ate) coordinates to the zinc ion in a bidentate fashion forming a four-membered ring, with one of the oxygen atoms interacting with the two histidine residues. The other oxygen atom interacts with the conserved tyrosine residue, which stabilizes the tetrahedral oxyanion intermediate in the native deacetylation reaction. Hence, ketone-type inhibitors act as analogues of the tetrahedral reaction intermediate and its flanking transition state rather than being substrate analogues. Notably, in crystal structures of HDACs with ketones displaying bidentate zinc coordination, one of the zinc-oxygen bonds is commonly shorter than the other, supporting the proposed binding as a diolate and underpinning the role of the tyrosine residue in its stabilization.[48,90]

1.3.5 Other cyclic peptides and functional groups

Besides ketone derivatives, other natural product cyclic peptide inhibitors of HDACs are known. Romidepsin (**VIII**), which is now a clinically approved anticancer drug, is a disulfide-containing depsipeptide isolated from *Chromobacterium violaceum*, and shows selectivity for class I HDACs with low nanomolar IC_{50} values.[90,123,124] The related largazole form the marine cyanobacterium *Symploca* sp. contains a thioester moiety (**IX**) and inhibits HDAC1, 2 and 3 in the picomolar range.[90,125] Both romidepsin and largazole are pro-drugs, that are transformed *in vivo* by reduction of the disulfide or hydrolysis of the thioester to form the active compound containing 3-hydroxy-7-mercaptohept-4-enoic acid. The thiol at the side chain of this β-hydroxy acid is then able to coordinate to the active site zinc ion, which thereby assumes a nearly perfect tetrahedral coordination geometry.[90,126]

Cyclic tetrapeptides azumamides A–E, which were isolated from the marine sponge *Mycale izuensis*, contain the unique β-amino acid 3-amino-2-methylnon-5-enedioic acid or its corresponding amide (**X**) at the side chain. Azumamides were reported as selective for class I HDACs, for which they show nanomolar IC_{50} values. The mode of coordination of azumamides to the active site of HDACs is unknown, although it is assumed that both the acid and carboxamide derivatives bind in a bidentate fashion via the carbonyl and hydroxy group or the amide nitrogen, respectively.[90,127,128]

A further group of synthetic inhibitors comprise *N*-acylhydroxylamines, also referred to as "retro hydroxamates". While a cyclic tetrapeptide-based *N*-formylhydroxylamine (**XI**) was reported as a pan-specific HDAC inhibitor with nanomolar potency, an *N*-acetylhydroxylamine containing peptide showed moderate selectivity for HDAC1, 2 and 6.[129,130] It was demonstrated that retro hydroxamates coordinate to the active site zinc ion of HDACs in an inverted manner compared to hydroxamic acids.[90]

1.4 Determination of the HDAC-dependent acetylome and interactome

Changes in the abundance of proteins within a cell upon various stimuli, such as drug or inhibitor treatment, can be investigated with techniques summarized as proteomics. While early approaches relied on the separation of protein mixtures via gel electrophoresis followed by individual analysis of resolved proteins, advances in mass spectrometry coupled with high-performance liquid chromatography made it possible to determine the entirety of cellular proteins (the proteome) within one single experiment and in complex biological mixtures.[131,132] Importantly, these techniques also enable to map the post-translational modifications of identified proteins, and the understanding of lysine acetylation and HDAC activity in a proteome-wide context has greatly improved by MS-based proteomics.[27] While the sum of all acetylation sites on proteins in a cell is referred to as the acetylome and changes in the abundance of these sites are investigated by MS-based acetylomics, approaches focusing on protein-protein interactions or interactions of proteins with other molecules are designated interactomics.[133,134]

Mass spectrometry-based proteomics can be conducted following two general strategies. "Top-down" approaches rely on whole, intact proteins, that are ionized, partially fragmented and sequenced by MS / MS analysis, including the identification of post-translational modifications.[131] However, due to the sensitivity of proteins in handling, low ionization efficiencies, complexity of the obtained MS spectra and the need for extensive sample purification limit top-down proteomics to simple, defined questions and problems. In contrast, "bottom-up" or "shotgun" proteomics approaches can be applied to complex biological mixtures extracted from cells or whole tissues, because all proteins are measured in parallel and are then "re-constituted" from their peptide fragments by computational analysis.[27,135]

A typical workflow for "bottom-up" proteomics is depicted in Figure 9. Proteins are first extracted from whole tissues or cells and then digested by proteases, most commonly trypsin, to yield a large set of peptide fragments. Peptides are subsequently separated by nano-HPLC and their sequences, including the presence of post-translational modifications, is determined

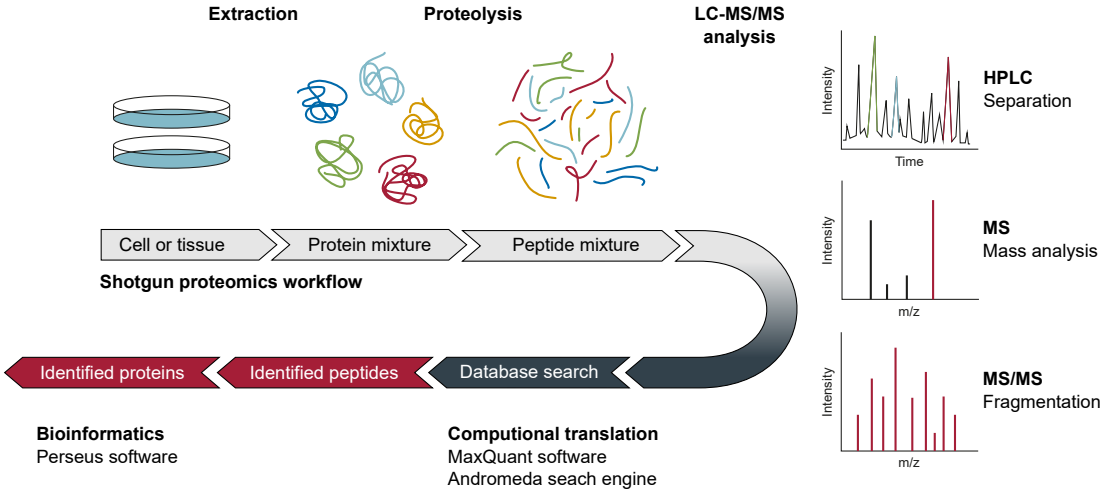

Figure 9: Workflow of MS-based bottom-up or shotgun proteomics. Proteins extracted from cells or tissues are digested by proteases and, depending on the application, peptides are optionally enriched and pre-fractionated. After separation by reverse-phase HPLC and ionization by ESI-MS, peptides of interest are fragmented and sequenced by MS / MS. Computional analysis and database searches are performed to identify peptides and their associated proteins. Modified from [135, 136].

via MS / MS analysis. Sequenced peptides are quantified and matched to the respective proteins via computational data processing and protein database searches.[27,131,135]

In case of acetylome investigations, additional steps have to be implemented on the peptide level. Since the stoichiometry of post-translational modifications is commonly low compared to the fraction of unmodified proteins within a cell, enrichment of acetylated peptides with panspecific anti-acetyllysine antibodies is crucial before MS / MS analysis. In order to increase the dynamic range of intensities that can by measured, and consequently the amount of proteins and modifications that can be identified, sample complexity can be further reduced by peptide fractionation, for example using microscale strong cation exchange chromatography (micro-SCX) or isoelectric focusing.[27,132]

By comparing the intensities of acetylated peptides between two samples, acetylation sites can be identified that are regulated under specific conditions, e.g. upon inhibitor treatment.[27] Relative quantification regarding the abundance of post-translational modifications and affected proteins is achieved by either labeling of different samples with stable isotopes or direct comparison of peptide intensities.[137] Isotopic labeling can be conducted metabolically through techniques such as SILAC (stable isotope labeling by amino acids in cell culture),[138] or chemically by specific reagents. In case of acetylomics, metabolic labeling relies on incorporation of isotopically labeled lysine and arginine during protein biosynthesis, resulting in labeled peptides covering the respective acetylation sites after tryptic digest. This method introduces the least bias to MS-based quantification, because two samples with different treatment (one labeled, one unlabeled) can be pooled at the cell extract level, which minimizes subsequent errors by different handling of samples. A further advantage is that differential isotopic labeling allows mixing and relatively quantifying two samples in a single MS analysis. Chemical labeling is most commonly performed on the protein or peptide level, for example by isotopomeric dimethyl tags obtained by reductive amination of formaldehyde with the

free primary amines on proteins.[139] Accuracy of chemical labeling is intermediate, because samples can be combined at an early stage, but the varying availability of reactive groups on different proteins and unwanted side reactions may introduce some bias. Combining samples only at the data level, label-free quantification (LFQ) methods are the least accurate. They directly compare the intensities of acetylated peptides between two samples measured in two separate MS runs. Although more time consuming, no special treatment of cells or samples is necessary. However, through advancements in computational algorithms normalizing peptide intensities between different runs, the accuracy of LFQ methods has greatly improved.[27,140]

Interactomics to dissect protein-protein interactions or identify the composition of multi-protein complexes can be performed in a similar fashion, but the enrichment step for post-translational modifications is replaced by an affinity purification step specific for the proteins or protein complexes of interest. This might include enrichment by a specific antibody for one of the proteins involved, or using a recombinantly expressed affinity tag, e.g. a streptavidin-binding peptide, which can be captured by immobilized streptavidin. Interaction partners can also be enriched by "pulldown" from cellular lysates, if one of them is expressed recombinantly and immobilized as bait.[133] Regarding the composition of HDAC complexes and profiling of their selectivity, affinity enrichment was achieved by pulldown with immobilized HDAC inhibitors.[136,141,142] Quantification in MS-based interactomics is enabled by comparison of a specifically enriched sample versus a background control by the same methods as described for acetylomics, and interaction partners are identified by introduction of cut-off values for their enrichment.[133,134]

A global analysis of lysine acetylation by this sort of bottom-up proteomics approach revealed 3600 acetylation sites on 1750 proteins, which are known to exert diverse cellular functions, such as chromatin remodeling, cell cycle control, splicing, nuclear transport, and actin nucleation. Conducting the same experiment with samples containing the inhibitors suberoylanilide hydroxamic acid (SAHA) and the benzamide MS-275, together effectively inhibiting class I, II and IV HDACs, increased the abundance of about ten percent of all acetylation sites at least by a factor of two, indicating that these sites are likely regulated by HDAC activity.[26] In a related experiment by *J. Sindlinger* with HDAC6 knockdown HeLa cells over 1200 acetylation sites were identified. Upon HDAC6 knockdown, 147 of these sites were upregulated, rendering them potential substrate sites of HDAC6.[136]

It appears plausible that specificity of HDAC6 for this high number of potential substrates is mediated by binding proteins and other interaction partners. Consequently, the associated proteins are promising candidates to be investigated in greater detail using chemical approaches. However, since not all of the discovered acetylation sites might be regulated by HDAC6 through direct deacetylation, devising strategies to confirm substrates on a biochemical level is necessary.

1.5 Concept of peptide-based HDAC affinity probes

Exploiting the strong binding of hydroxamic acid inhibitors, it was shown that, by incorporation into suitable chemical probes, hydroxamic acids can be used to selectively capture HDACs and HDAC complexes from cellular lysates for further biochemical characterization.[143]

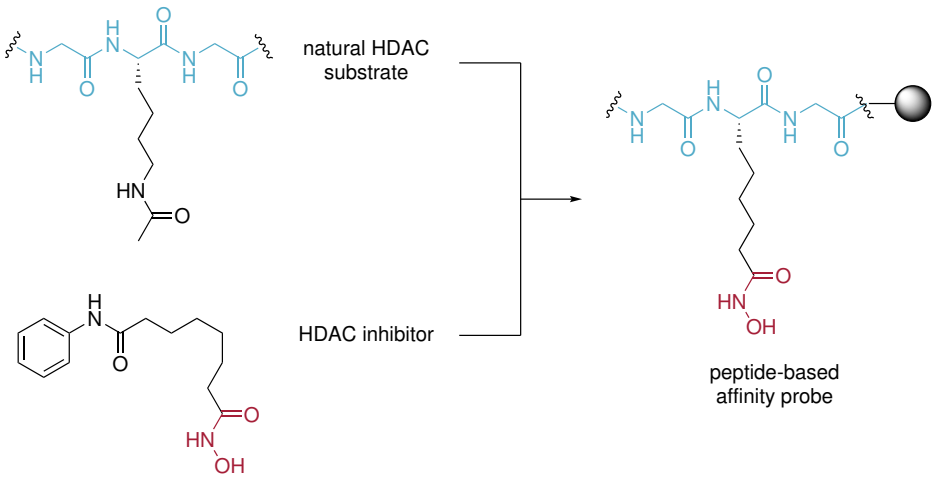

Figure 10: Concept of peptide-based HDAC affinity probes combining natural peptide substrates (blue) and HDAC inhibitory moieties (red).

The concept of these probes relies on combination of the natural substrate of HDACs, a polypeptide chain containing an acetylated lysine residue, with an HDAC inhibitory moiety (Figure 10). To achieve this, the acetylated lysine in the peptide is replaced by an amino acid bearing the inhibitory moiety, i.e. the hydroxamic acid function, at the side chain. The resulting peptide-based HDAC affinity probe can then be immobilized onto solid-support for easy handling in pulldown assays and is able to recruit endogenous HDACs by chelation of the active site zinc ion and interaction of the linear peptide with the surface of the enzyme, thereby serving as cap moiety. Peptide-based HDAC affinity probes are readily accessible via solid-phase peptide synthesis (SPPS) and the central, so-called HDAC-trapping amino acid, which contains the inhibitory moiety, is incorporated as a suitable protected building block.

The utility of these probes as tools to uncover the substrate specificity of HDACs was demonstrated when applying α-aminosuberic acid ω-hydroxamate (AsuHd) as HDAC-trapping amino acid together with peptide sequence contexts derived from acetylation sites of the proteins p53 and α-tubulin, that are known to be regulated by HDAC activity. Combination of these experiments with MS-based proteomics enabled to further uncover the composition and selectivity of HDAC complexes.[136,142]

1.6 Aim of study

The aim of the present work was to improve the versatility and selectivity of peptide-based affinity probes as tools to study histone deacetylases and the complexes embedding them. Furthermore, the concept of peptide-based HDAC affinity probes should be adapted to high-throughput formats, enabling the biochemical validation of data provided by large-scale acetylomic experiments.

Inspired by the pharmacophore model of HDAC inhibitors, in a first part of this work, the influence of different zinc-binding functional groups on HDAC class selectivity should be

investigated. To do so, a set of novel HDAC-trapping amino acid building blocks had to be created and synthetic routes had to be devised, providing suitable protection schemes for incorporation of these amino acids into peptid-based probes via solid-phase peptide synthesis (SPPS). Besides pan-specific hydroxamic acids, 2-aminophenylamide (Apa) and ketone moieties should be tested, and the respective building blocks should be designed with respect to the distinct requirements of parallel SPPS and subsequent high-throughput experimental approaches.

A second objective was to analyze the influence of the peptide sequence context of HDAC affinity probes on their ability to recruit individual HDACs. As a tangible example, this should be done by investigating the substrate and sequence selectivity of HDAC6, for which large sets of acetylomic data are available. In order to further validate these data and the high number of acetylation sites that are potentially regulated by HDAC6, a new high-throughput HDAC binding assay had to be developed. A probe design should be established which would circumvent the time-consuming need for peptide purification and enable selective capture of pure, full-length probes from a crude product mixture. Together with the optimized hydroxamic acid building block the new peptide design should enable to synthesize a large set of HDAC probes within a limited amount of time, making it possible to rapidly screen the proteomics-derived acetylation sites for HDAC-binding.

In a third part, the most promising substrate sites that efficiently and selectively recruited HDAC6 in the high-throughput binding assays should be investigated in detail. This should include an analysis of potential binding partners of HDAC6 by MS-based proteomics, as well as conducting kinetic studies to assess the influence of the substrate site sequence context on HDAC catalysis.

In summary the aim of this work was to optimize the selectivity of peptide-based HDAC affinity probes and to adapt them to high-throughput formats in three sub-projects:

1. Establishing hydroxamate, 2-aminopheylamide and ketone containing amino acid building blocks, ideally compatible with massive parallel SPPS, and assessing their individual HDAC-trapping abilities;

2. Developing a high-throughput HDAC binding assay to screen for acetylation sites potentially regulated by HDAC6, and a corresponding probe design that bypasses the need for time-consuming peptide purification; and

3. In-depth analysis of selected HDAC6 substrate sites regarding the influence of the amino acid sequence context on HDAC binding partners and catalysis.

2 Results

The current knowledge about histone deacetylases was acquired in large part through the aid of chemical and often peptide-based probes. Playing a key role in the initial discovery of HDACs, peptide-based probes were proven to be useful tools to investigate the cellular function of these enzymes and to elucidate the composition of their diverse complexes.[113,141,144]

Proteomics approaches enabled the determination of HDAC-dependent acetylomes, uncovering hundreds of acetylation sites potentially regulated by HDACs.[26,132,145] In order to keep up with the rapidly increasing number of these sites that require validation, chemical probes for HDACs need to be adjusted to high-throughput formats and improved with regard to their ability to adapt to different experimental conditions and questions.

Further insights could be gained by controlling the selectivity of HDAC probes, with the ultimate goal of synthesizing fully flexible probes in a mix-and-match type of fashion to address all eleven human HDACs individually. Following the design of known HDAC inhibitors, this selectivity can be fine-tuned by three main factors:[24,85] Exchange of the functional group chelating the active site zinc ion, modulation of the length of the linker region, and choice of a suitable cap group or peptidic sequence context, derived from a known acetylation site.

2.1 Functional groups

Both, low- and high-throughput methods, using chemical HDAC-affinity probes rely on the zinc-chelating ability of the employed functional groups. However, these functional groups may possess an inherent specificity for individual HDACs e.g. due to their sterical or electronic properties. Into peptide-based probes they are most conveniently introduced attached to the side-chain of modified amino acids. It is therefore desirable to synthesize a broad set of so-called HDAC-trapping amino acids suitable for solid-phase peptide synthesis (SPPS), in order to target specific HDACs or HDAC complexes optimally.

In a first part of this work, new building blocks were introduced and synthesis routes were established that allow an easy installation of hydroxamic acids, 2-aminophenylamides and ketones in peptide-based HDAC affinity probes, and that – in case of the first two moieties – are fully compatible with massive parallel SPPS necessary for high-throughput assays.

2.1.1 Hydroxamic acids

Hydroxamic acids range among the most versatile HDAC-trapping moieties due to their broad specificity, being able to capture all HDACs of class I and IIb, and – to a lesser extent – some HDACs of class IIa.[142,145,146] They are suitable for applications where a low bias caused by the zinc-chelating group is necessary, e.g. for the comparison of different peptide sequence contexts across HDAC classes.

It was previously demonstrated that an ideal building block for introduction of the hydroxamic acid moiety into peptide probes is based on α-aminosuberic acid ω-hydroxamate (AsuHd), because its total chain length of eight carbon atoms resembles that of the potent HDAC inhibitor suberoylanilide hydroxamic acid (SAHA).[142,143] However, examples of protected AsuHd building blocks suitable for fully automated solid-phase peptide synthesis are sparse in literature. Available *N*α-protecting groups comprise Boc,[147] Alloc[142] and Fmoc,[148–150] and published side-chain protecting groups for the hydroxamate moiety are benzyl,[147] *para*-methoxybenzyl (PMB)[148] and *tert*-butyl.[142,149,150] Only the combination of Fmoc and PMB or *t*Bu can be applied in the standard form of Fmoc / *t*Bu-based SPPS used today in an automated fashion. Unfortunately, slow and incomplete deprotection of *O*-*tert*-butyl hydroxamates often requires time-consuming purification of the respective peptides, thereby strongly hampering high-throughput assay approaches.[151]

In order to solve this problem and to create an Fmoc-protected AsuHd building block suitable for miniaturized parallel peptide synthesis, the established *t*Bu group for hydroxamate protection was replaced by the more acid-labile trityl (triphenylmethyl, Trt) group.[152] Although there are many examples of *O*-Trt hydroxamates found in literature, up to now no Trt-protected AsuHd building block for SPPS was reported.

2.1.1.1 Hydroxamate building block synthesis

Starting from commercially available DL-α-aminosuberic acid (**1**), the trityl-protected hydroxamate moiety had to be selectively installed to the side chain of **1**, followed by introduction of the Fmoc group (Figure 11).

In order to achieve this the α-amino and -carboxy group needed to be orthogonally protected, preferentially in one single step. A feasible solution was found in 1,3,2-oxazaborolidin-5-ones, or boroxazolidinones, which were initially described in 1963 by *Lang et al.*[153] As a protection agent 9-borabicyclo[3.3.1]nonane (9-BBN), which is a versatile and widely applied reagent in organic synthesis, seemed especially suitable. Oxazaborolidinones derived from 9-BBN and amino acids were first prepared by *H. C. Brown* in the nineteen-eighties,[154] and their remarkable stability in reactions targeting the amino acid side chain was demonstrated in depth by *Dent et al.* in 2002.[155] The cyclooctane-1,5-diyl moiety of 9-BBN further provides the advantage of increasing the solubility of protected amino acids in organic solvents. Consequently, H-Asu-OH (**1**) was reacted with 9-BBN in refluxing methanol, which gave a full conversion of reactants into the desired oxazaborolidinone (**2**), typically within two hours. After purification via preparative HPLC Asu-BBN (**2**) was obtained with a yield of 91 %.

In a second step the hydroxamate moiety could then be coupled to the side chain of the amino acid. Previous attempts to do this by amide-forming reagents of the carbodiimide- and uronium-type, using the sterically demanding *O*-trityl hydroxylamine and an oxazolidinone-protected Asu precursor, failed due to very low conversions and side reactions involving the oxazolidinone. The high stability of the 9-BBN protecting group could now be exploited in order to use more potent methods of carbonyl activation requiring harsher reaction conditions. Asu-BBN (**2**) was reacted with stoichiometric[156] amounts of thionyl chloride and pyridine to form the acid chloride at the side chain. Subsequently, the freshly formed acid chloride of **2** was coupled with *O*-trityl hydroxylamine – with an excess of DIPEA as base neutralizing

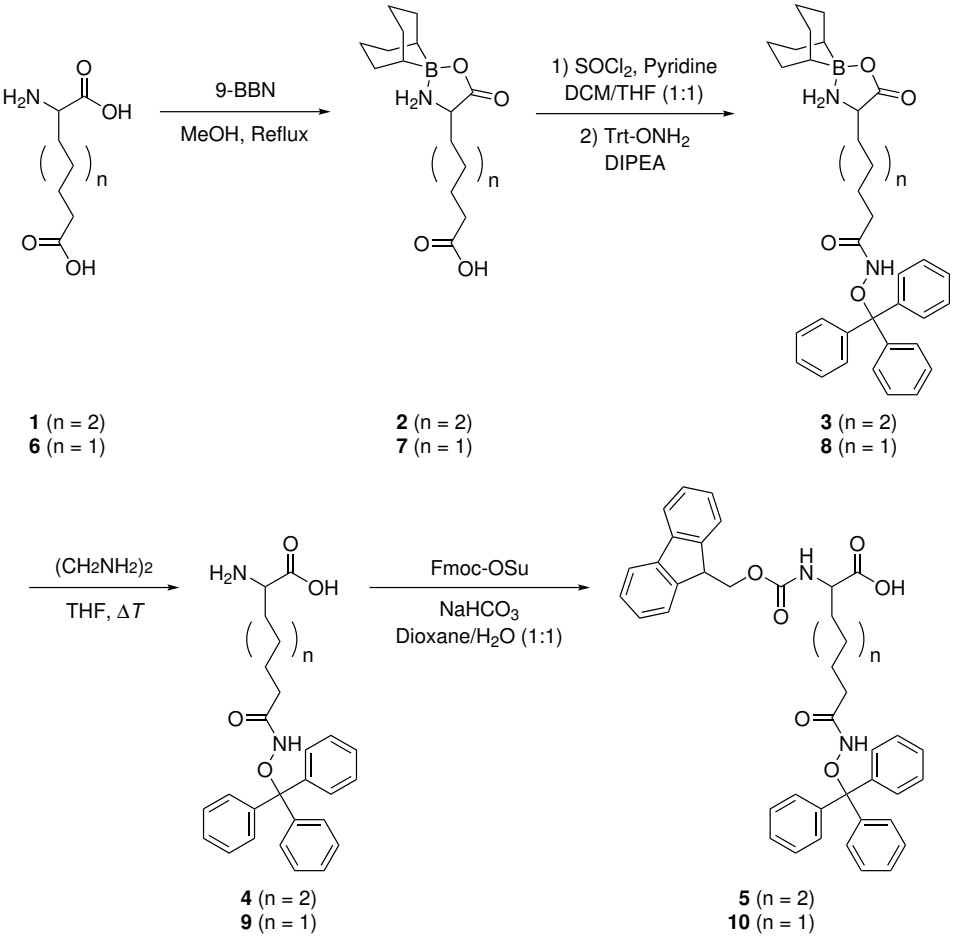

1 (n = 2)
6 (n = 1)

2 (n = 2)
7 (n = 1)

3 (n = 2)
8 (n = 1)

4 (n = 2)
9 (n = 1)

5 (n = 2)
10 (n = 1)

Figure 11: Synthesis of Fmoc-AsuHd(OTrt)-OH (**5**) and Fmoc-ApmHd(OTrt)-OH (**10**).

the liberated HCl, preventing unwanted trityl deprotection. The success of this approach was conformed by LC-MS analysis of the reaction mixture, indicating a high conversion of reactants into products. However, purification of the formed AsuHd(OTrt)-BBN (**3**) was not feasible without significant losses and therefore omitted.

In the next step, the 9-BBN moiety needed to be removed. Due to the high acid lability of the side chain Trt group, hydrolysis of the oxazaborolidinone with strong acids as described in early reports, most commonly with gaseous hydrogen chloride[157] or aqueous HCl,[158] was not possible. A milder way of 9-BBN deprotection was found in the oxidative cleavage with methanolic chloroform.[159,160] Initial attempts were made with this method, however, reaction times exceeded one day and a strong formation of unidentified side products was observable. Exploiting the higher stability of diazaborolidines as compared to oxazaborolidinones, the 9-BBN group can also be rapidly cleaved by diamines, such as ethylendiamine.[155] To this end, crude AsuHd(OTrt)-BBN (**3**) was heated with an excess of ethylenediamine in THF, leading to almost complete deprotection within a few minutes. Crude **4** was then purified by preparative HPLC to remove the residual ethylenediamine, which would otherwise have

complicated Fmoc-protection of the α-amino group in the last step. H-AsuHd(OTrt)-OH (**4**) was obtained with a yield of 61 % with respect to **2** over two steps.

Finally, H-AsuHd(OTrt)-OH (**4**) was reacted with Fmoc hydroxysuccinimide ester (Fmoc-OSu) and sodium bicarbonate as base in dioxane / water in the last step. In order to prevent Fmoc-β-alanine formation by basic cleavage of excess Fmoc-OSu, as could be observed in initial experiments, Fmoc-OSu was added in small portions until full conversion of **4** into the final building block Fmoc-AsuHd(OTrt)-OH (**5**) was indicated by LC-MS analysis. The usual acidic workup after this reaction was omitted because of the acid-lability of the *O*-trityl hydroxamate. Direct extraction from the reaction mixture afforded the desired product **5** with sufficient purity for its application in SPPS and with a yield of 79 %. The overall yield with respect to H-Asu-OH (**1**) was 48 % over four steps.

In order to compare the HDAC-trapping abilities of this building block to a version with a shorter spacer between amino acid backbone and hydroxamate moiety, the synthesis outlined for α-aminosuberic acid (**1**) was repeated with racemic α-aminopimelic acid (**6**, Apm), comprising seven carbon atoms (Figure 11). This furnished the final building block Fmoc-ApmHd(OTrt)-OH (**10**) with comparable yields to Fmoc-AsuHd(OTrt)-OH (**5**) and without the need for further optimization.

LC-MS data of the products of all four reaction steps in the synthesis of Fmoc-AsuHd(OTrt)-OH (**5**) and Fmoc-ApmHd(OTrt)-OH (**10**), and NMR spectra of **2**, **4**, **7** and **9** can be found in the appendix (Chapter 7).

The AsuHd building block **5** was then used in the synthesis of peptide-based HDAC affinity probes for comparison with other HDAC-trapping functional groups of the 2-aminophenylamide- (Chapter 2.1.2) and ketone-type (Chapter 2.1.3). The full potential of this building block, as well as its Apm version **10**, was further demonstrated in miniaturized, parallel SPPS of 96 individual peptides for a newly developed, high-throughput HDAC assay (Chapter 2.2.1).

2.1.2 2-Aminophenylamides

Peptide-based HDAC affinity probes containing α-aminosuberic acid ω-hydroxamate (AsuHd) were already characterized regarding their ability to recruit HDACs from cellular lysates in previous reports. They proved to be useful tools to investigate the composition of endogenous HDAC complexes.[136,142,143] However, the use of different HDAC-trapping amino acids instead of AsuHd seems desirable, offering the possibility to influence class- or even enzyme-selectivity by making use of the rich body of known HDAC inhibitors.

After short-chain fatty acids and naturally occurring hydroxamic acids, synthetic benzamides were a third group of HDAC inhibitors considered for clinical trials, with derivative MS-275 (compare Figure 7) as most promising compound.[103,104] Benzamide inhibitors were reported to be selective for class I HDACs, with the exception of HDAC8.[29,145,146] The part of these inhibitors responsible for chelating the HDAC active site zinc ion is the 2-aminoanilide or 2-aminophenylamide (Apa) moiety.[95] Consequently, grafting the Apa moiety onto the side-chain of α-aminosuberic acid represented a promising approach for establishing a new HDAC-trapping amino acid.

2.1.2.1 Apa building block synthesis

The AsuApa building block was synthesized following the same approach that already proved to be useful for the trityl-protected AsuHd building block (Figure 12).

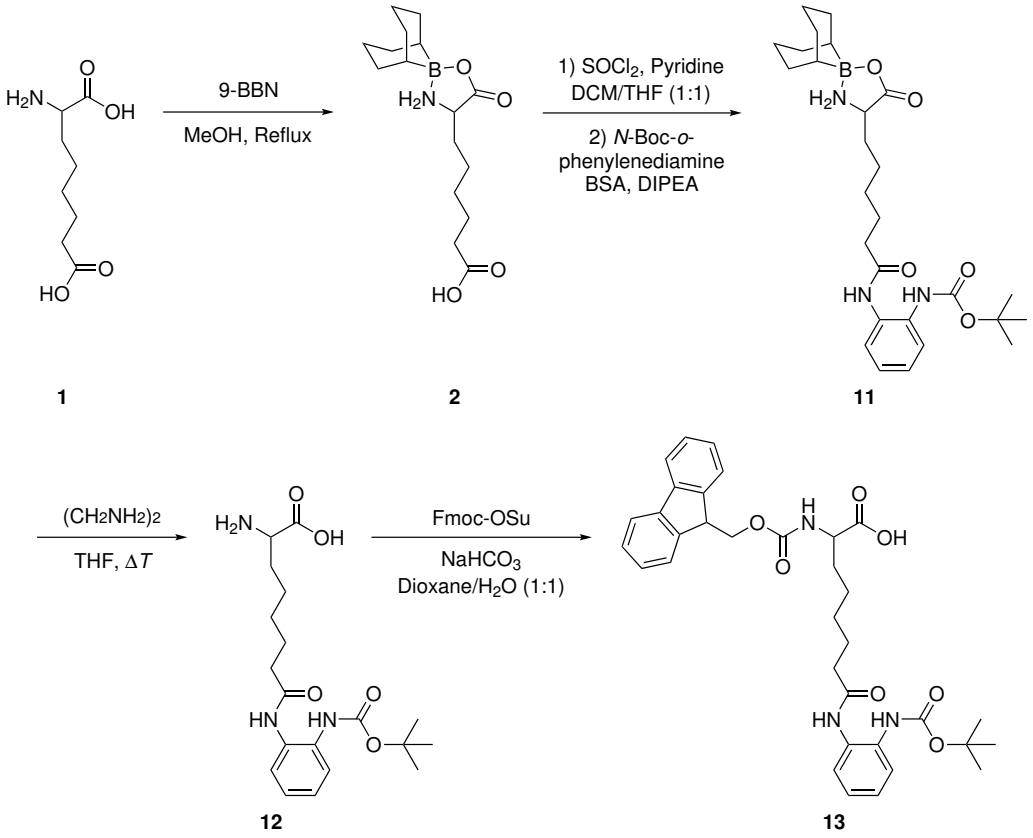

Figure 12: Synthesis of Fmoc-AsuApa(Boc)-OH (**13**).

Starting from DL-α-aminosuberic acid (**1**), the α-amino and -carboxy group were protected with 9-BBN in the first step, furnishing Asu-BBN (**2**). After activation of the side-chain carbonyl group using thionyl chloride, the resulting acid chloride of **2** was coupled with *N*-Boc-*o*-phenylenediamine, which itself was previously activated by silylation with bis(trimethylsilyl)acetamide (BSA), yielding AsuApa(Boc)-BBN (**11**). Crude **11** was then 9-BBN-deprotected by heating with an excess of ehtylenediamine. After HPLC purification, H-AsuApa(Boc)-OH (**12**) was obtained with a yield of 21 % with respect to Asu-BBN (**2**) over two steps. H-AsuApa(Boc)-OH (**12**) was Fmoc-protected in the last step using Fmoc hydroxysuccinimide ester (Fmoc-OSu) and sodium bicarbonate as base in dioxane / water. Purification by flash chromatography afforded the final building block Fmoc-AsuApa(Boc)-OH (**13**) with a yield of 59 % and high purity. The overall yield with respect to the starting material H-Asu-OH (**1**) was 12 %.

LC-MS data for all steps up to the final building block Fmoc-AsuApa(Boc)-OH (**13**) can be found in the appendix (Chapter 7), as well as NMR spectra of **12** and **13**.

2.1.2.2 Peptide synthesis and design of HDAC affinity probes

Having synthesized new amino acid building blocks containing 2-aminopheylamide as well as hydroxamic acid functionalities, they were incorporated into peptide-based affinity probes for capturing HDACs from native cell lysates (Figure 13).

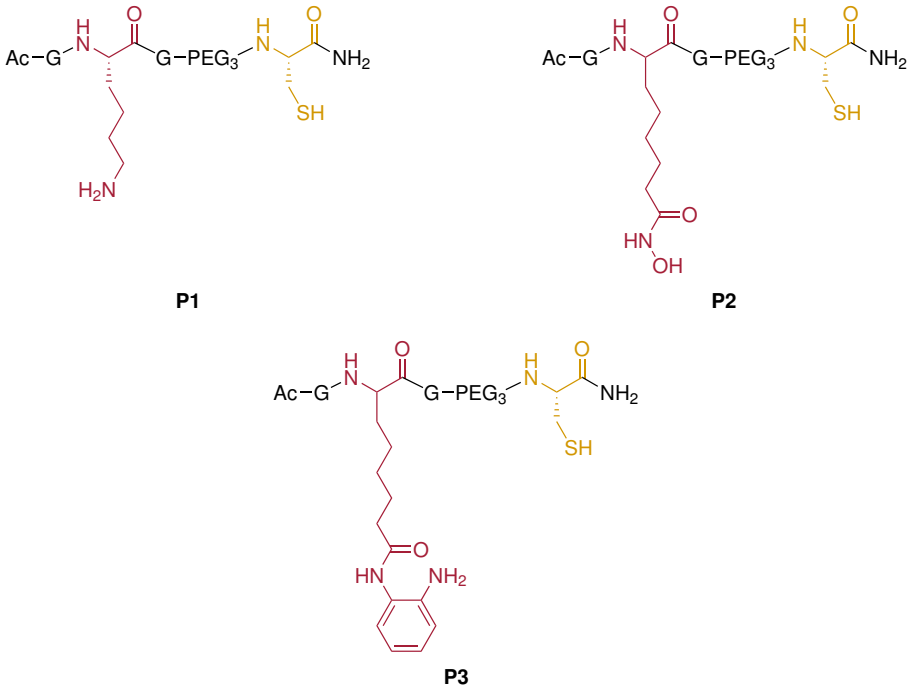

Figure 13: Mini-probes mini-Lys (**P1**), mini-AsuHd (**P2**) and mini-AsuApa (**P3**). The central lysine residue or the respective HDAC-trapping amino acids AsuHd and AsuApa are depicted in red and the C-terminal cysteine residue for immobilization is shown in yellow.

The general design of these probes comprises a central HDAC-trapping amino acid embedded into a peptidic sequence context of variable length, which can be derived from a known HDAC substrate.[142] The HDAC-trapping amino acid therefore replaces the acetylated lysine residue naturally present in this sequence. Hence, the binding part of the affinity probe recruits HDACs via two distinct interactions: Firstly, the inhibitory moiety grafted onto the central amino acid reaches into the binding pocket, chelating the active site zinc ion, and secondly, the peptide sequence reinforces binding to the enzyme surface. With the sequence reduced to a minimal context of two flanking glycine residues in the so-called mini-probes **P1**–**P3**, binding mainly relies on zinc-chelation, rendering them ideal tools to evaluate different inhibitory moieties and linker lengths. A C-terminal cysteine residue enables immobilization of the affinity probes on solid-support with its thiol group. The cysteine residue and the binding part of the probes are connected by a polyethylene glycol-based spacer that further increases solubility in aqueous media. In order to improve their stability in cellular lysates against aminopeptidases, the N-termini of the probes are acetylated.

Peptide probes **P1**–**P3** were synthesized manually by solid-phase peptide synthesis applying the Fmoc strategy with acid labile side-chain protecting groups. Building blocks Fmoc-AsuHd(OTrt)-OH (**5**) and Fmoc-AsuApa(Boc)-OH (**13**) for the probes mini-AsuHd (**P2**) and mini-AsuApa (**P3**), respectively, were fully compatible with SPPS conditions. The probe mini-Lys (**P1**) with a central lysine residue, which does not recruit HDACs in a specific manner, was synthesized as a control.

Peptides **P1**–**P3** were purified by preparative HPLC and then immobilized onto iodoacetyl-modified agarose for testing their abilities to recruit endogenous HDACs in pulldown experiments with cellular lysates. LC-MS data for **P1**–**P3** can be found in the appendix (Chapter 7).

2.1.2.3 Pulldown assays with mini-probes

Pulldown assays with the probes mini-Lys (**P1**), mini-AsuHd (**P2**) and mini-AsuApa (**P3**) were performed by incubating the immobilized peptides with equal amounts of native lysate from HeLa cells (200 µg total protein). The agarose beads were washed to remove unspecific binders and the desired proteins were eluted under denaturating conditions with SDS containing buffer at high temperature. Protein samples were then separated by SDS-PAGE and analyzed by western blotting. The blots were incubated with primary antibodies against all HDACs of class I (HDAC1, 2, 3, 8) and IIb (HDAC6, 10), and against HDAC4 as a representative meber of class IIa. Secondary antibody-horse radish peroxidase (HRP) conjugates were used for detection. After addition of an HRP substrate, chemiluminescent images were recorded (Figure 14). Experiments were performed in cooperation with *T. Meisinger*.[161]

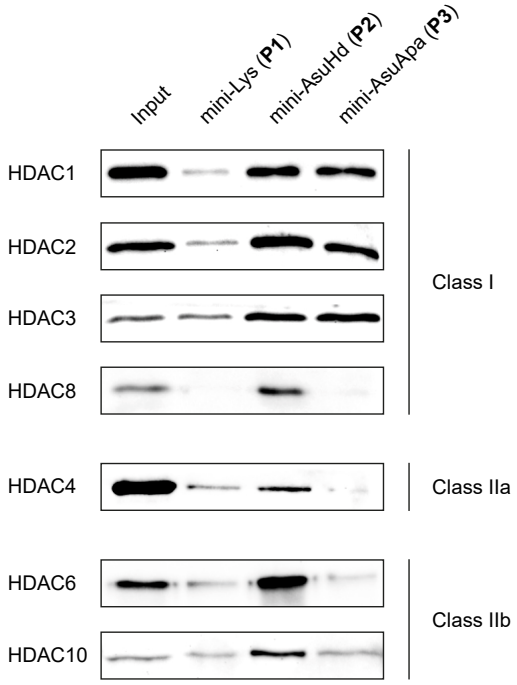

Figure 14: Representative chemiluminescent images of western blots from pulldown experiments with mini-Lys (**P1**), mini-AsuHd (**P2**) and mini-AsuApa (**P3**) using HeLa lysate (1 mg mL^{-1}, 200 µg total protein). Input samples: 16 µg.

All HDACs of class I and class IIb could be enriched on mini-AsuHd (**P2**), when compared to the lysine control **P1**, consistent with previous reports. Recruitment of the class IIa HDAC4 was weaker, but still detectable. These findings seem to reflect the broad specificity of hydroxamic acid-based HDAC inhibitors.

In contrast, mini-AsuApa (**P3**) showed a distinct binding profile. **P3** did not enrich HDACs of class IIb, HDAC4 or HDAC8 over the lysine control **P1**. However, class I HDACs 1, 2 and 3 were efficiently recruited to mini-AsuApa (**P3**). This indicates that the HDAC-specificity of small molecule inhibitor MS-275 could be preserved in the HDAC-trapping amino acid AsuApa,[162] paving the way for enzyme-selective peptide-based probes.

2.1.2.4 Interactomes of mini-probes

Having investigated the HDAC class-selectivity of mini-AsuApa (**P3**) qualitatively, a chemical proteomics approach was chosen in order to obtain quantitative and more detailed information about the composition of recruited HDAC complexes. LC-MS / MS measurements, data processing and quantification were performed in cooperation with the group of *I. Finkemeier* (Westfälische Wilhelms-Universität Münster).[163]

Pulldown experiments with mini-Lys (**P1**), mini-AsuHd (**P2**) and mini-AsuApa (**P3**) using HeLa lysate were conducted in triplicate as described before (Chapter 2.1.2.3), but eluted protein samples were alkylated at thiol groups, digested with trypsin and lysyl endopeptidase (Lys-C), pre-fractionated, and then identified and relatively quantified by lable-free LC-MS / MS analysis. Statistical analysis was performed with proteins identified in each of three biological replicates with different batches of cell lysate. Results were then visualized using volcano plots (Figure 15). The $\log_2$-fold enrichment ratios of mini-AsuHd (**P2**) and mini-AsuApa (**P3**) in comparison to the lysine control **P1** were plotted against the negative $\log_{10} p$ value of the statistical analysis. With cut-off values set at $p \leq 0.05$ ($-\log_{10} p > 1.3$) and $\log_2$-fold enrichment ≥ 0.6, proteins significantly enriched more than 1.5-fold on the respective probe versus the control are located in the upper right-hand section of the plots.

HDACs that could be identified in all three replicates of the experiment include HDAC1, 2, 3 and 6. Consistent with western blot analysis, all of these HDACs were significantly enriched on mini-AsuHd (**P2**) over the lysine control **P1**, with HDAC6 showing the strongest enrichment of all detected proteins (Figure 15 A). Components of known complexes containing HDAC1 and HDAC2 were also enriched on mini-AsuHd (**P2**). These include RCOR3 and KDM1A of the CoREST complex, SIN3B of the Sin3 complex, and p66 and RBBP7 of the NuRD complex. Among all HDAC complex proteins components of CoREST showed the strongest enrichment. Components of the HDAC3-containing NCoR / SMRT complex were also enriched on mini-AsuHd (**P2**), but to a lesser extent than complex proteins of HDAC1 and HDAC2, consistent with the fact that HDAC3 itself showed a lesser enrichment than HDAC1, 2 and 6.

The volcano plot of mini-AsuApa (**P3**) versus mini-Lys (**P1**) further supports the results from western blot analysis (Figure 15 B). Class II HDAC6 was only marginally enriched on mini-AsuApa (**P3**), while class I HDACs 1, 2 and 3 showed stronger recruitment. HDAC complex proteins co-enriched on this probe again include components of the CoREST, Sin3 and NuRD complexes, underlining the capacity of **3** as probe for HDAC1 and HDAC2. Moreover, proteins of the NCoR / SMRT complex of HDAC3 were strongly recruited to this probe, with

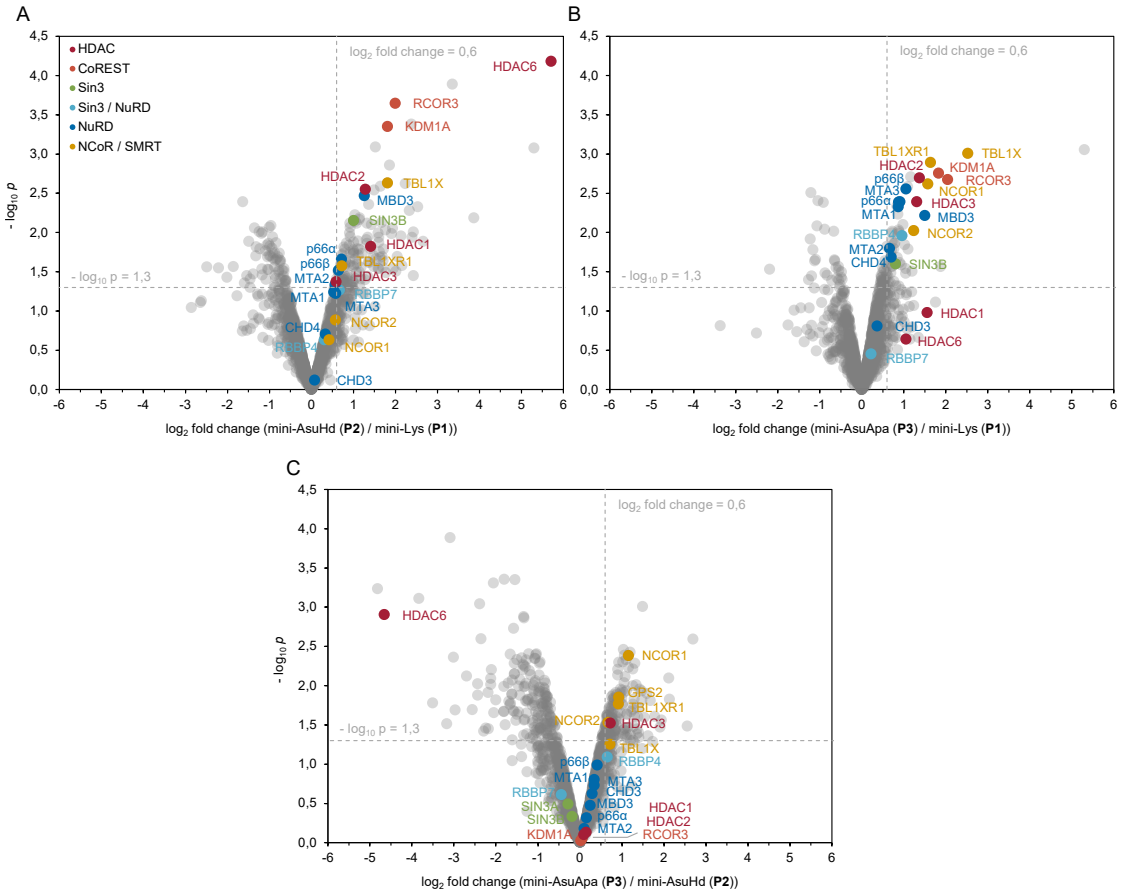

Figure 15: Volcano plots of proteomic pulldown experiments of (A) mini-AsuHd (**P2**) versus mini-Lys (**P1**), (B) mini-AsuApa (**P3**) versus mini-Lys (**P1**), and (C) mini-AsuApa (**P3**) versus mini-AsuHd (**P2**). Mean $\log_2$-fold enrichment ratios of the respective probes are plotted against the negative $\log_{10} p$ value of statistical analysis. Cut-off values indicating significantly enriched proteins were set at $p \leq 0.05$ ($-\log_{10} p > 1.3$) and $\log_2$-fold enrichment ≥ 0.6. Experiments were performed as biological triplicates using HeLa lysate (1 mg mL^{-1}, 200 µg total protein).

TBL1X and NCOR1 ranking among the most highly enriched proteins on mini-AsuApa (**P3**). This behavior seemed more pronounced as for mini-AsuHd (**P2**).

A more direct comparison of the binding properties of both probes was possible by visualizing the enrichment ratio of mini-AsuApa (**P3**) versus mini-AsuHd (**P2**) (Figure 15 C). In this plot, proteins enriched on mini-AsuApa (**P3**) are located in the upper right-hand part, whereas proteins enriched on mini-AsuHd (**P2**) are shown in the upper left-hand part. Proteins enriched on both probes to the same extent are confined to the center of the plot. HDAC6 is located in the upper left-hand section, further supporting the observed lack of ability of mini-AsuApa (**P3**) to recruit HDACs of class II. HDAC1 and HDAC2, as well as components of the CoREST, Sin3 and NuRD complexes, are found in the center of the volcano plot, indicating that both mini-AsuHd (**P2**) and mini-AsuApa (**P3**) are capable of recruiting these HDAC complexes with comparable efficiency. HDAC3 and further proteins of the NCoR / SMRT complex are almost exclusively found in the upper right-hand section of the plot, confirming the notion that mini-AsuApa (**P3**) is a superior probe in recruiting this

complex. Identified proteins of the NCoR / SMRT complex together with their enrichment values are summarized in Table 1.

Table 1: Identified proteins of the NCoR / SMRT complex on mini-AsuApa (**P3**) as compared to mini-AsuHd (**P2**). Protein names are listed together with their UniProt ID, gene name and $\log_2$-fold enrichment ratio. Bold numbers indicate statistical significance of $p \leq 0.05$.

UniProt ID	Protein	Gene	$\log_2$ fold change
O15379-2	Histone deacetylase 3	HDAC3	**0.72**
O75376-2	Nuclear receptor corepressor 1	NCOR1	**1.15**
C9JE98	Nuclear receptor corepressor 2	NCOR2	**0.67**
O60907-2	F-box-like/WD repeat-containing protein TBL1X	TBL1X	0.72
A0A0D9SF63	F-box-like/WD repeat-containing protein TBL1XR1	TBL1XR1	**0.92**
I3L4X7	G protein pathway suppressor 2	GPS2	**0.92**

2.1.3 Electrophilic ketones

Besides naturally occurring as well as synthetic hydroxamic acids and synthetic 2-aminophenylamides, a large number of known HDAC inhibitors are cyclic tetrapeptides produced by a multitude of microorganisms. Among these, the group of apicidins produced by the fungus *Fusarium pallidoroseum* contain the unusual keto amino acid 2-amino-8-oxodecanoic acid (Aoda).[108,109] The parent compound apicidin is reported to be selective for class I HDACs.[141] With the electrophilic ketone at the side chain serving as zinc-binding group and mimicking the acetylated lysine residue in HDAC substrates, Aoda seemed to be an ideal candidate to be introduced into peptide-based probes and evaluated as HDAC-trapping amino acid.

There are several synthetic procedures found in literature for the preparation of apicidin and numerous protected building blocks for the introduction of the Aoda residue, with most of them intended for cyclization of the peptide at the amino group of Aoda in solution. Reported *N*α-protecting groups therefore comprise Z[164,165] and Boc,[166,167] but also Fmoc[167] derivatives are known.

In this work a new approach was chosen to synthesize a suitable building block of Aoda, making use of the newly established and versatile 9-BBN-protected α-aminosuberic acid precursor Asu-BBN (**2**) employed in the synthesis of Fmoc-AsuHd(OTrt)-OH (**5**) and Fmoc-AsuApa(Boc)-OH (**13**).

2.1.3.1 Ketone building block synthesis

The desired Aoda building block was synthesized from α-aminosuberic acid (Asu) through elongation of its side chain by two carbon atoms as outlined in Figure 16.

In the first step, DL-α-aminosuberic acid (**1**) was protected with 9-BBN as oxazaborolidinone to form Asu-BBN (**2**). In the second step, Asu-BBN (**2**) was converted to its acid chloride at the side chain using thionyl chloride and pyridine. Subsequently, the acid chloride of **2** was reacted with *N,O*-dimethylhydroxylamine hydrochloride in order to obtain the corresponding *Weinreb* amide **14**.[168] Crude Asu(NMe-OMe)-BBN (**14**) was then subjected to a *Grignard* reaction with ethylmagnesium bromide in the third step, forming the ethyl ketone moiety

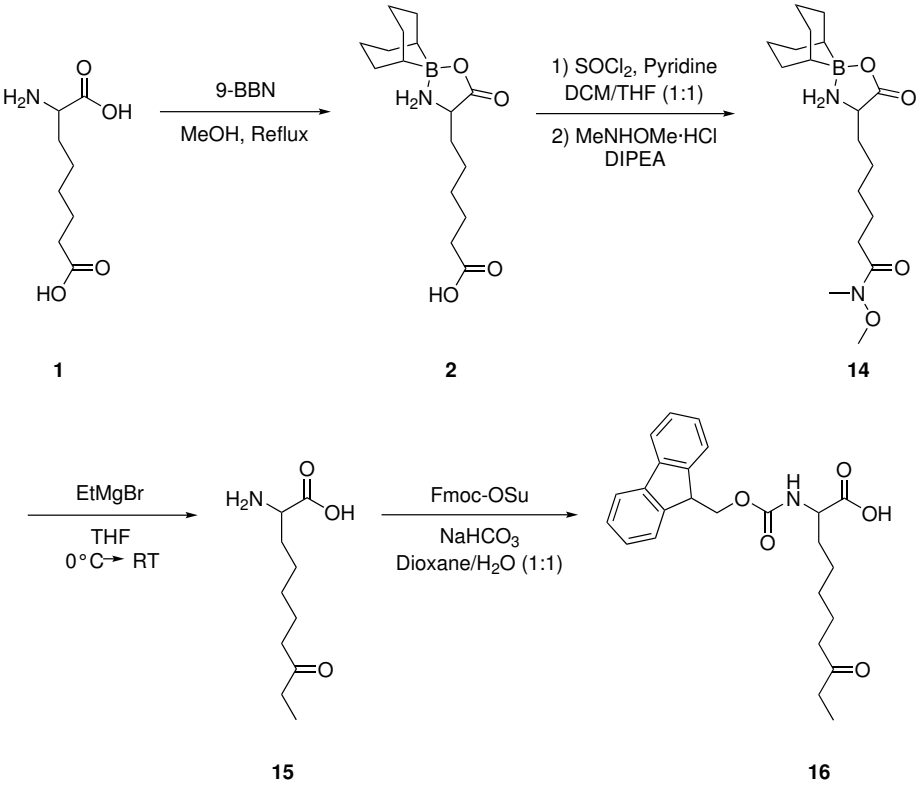

Figure 16: Synthesis of Fmoc-Aoda-OH (**16**).

at the side chain. Initial attempts to do so with only one equivalent of ethylmagnesium bromide resulted in incomplete conversion of the *Weinreb* amide **14** to the corresponding ketone. Most of the EtMgBr seemed to be consumed by deprotecting the 9-BBN group, giving a mixture of 9-BBN-deprotected **14** and H-Aoda-OH (**15**). However, the instability of the 9-BBN group towards *Grignard* reaction conditions was of no disadvantage, because it would have been necessary to remove the 9-BBN protection in the next reaction step at any rate. Eventually, conducting the reaction with a total of three equivalents ethylmagnesium bromide led to full conversion of **14** into the desired H-Aoda-OH (**15**). In the fourth and last reaction step H-Aoda-OH (**15**) was *N*α-protected using Fmoc-OSu and sodium bicarbonate as base. After purification by flash chromatography, the final building block Fmoc-Aoda-OH (**16**) was obtained with a yield of 21 % with respect to Asu-BBN (**2**) and sufficient purity for its application in solid-phase peptide synthesis.

LC-MS data of Asu(NMe-OMe)-BBN (**14**), H-Aoda-OH (**15**) and Fmoc-Aoda-OH (**16**), as well as NMR spectra of **16** can be found in the appendix (Chapter 7).

2.1.3.2 Peptide synthesis and optimization of the click reaction

With the building block Fmoc-Aoda-OH (**16**) in hand the HDAC-trapping ability and potential selectivity of the Aoda residue could be examined by incorporation into peptide-based probes following the same concept as applied for the hydroxamic acid and 2-aminophenylamide buliding blocks AsuHd and AsuApa, respectively.

However, initial attempts to use the established design of mini-probes with a C-terminal cysteine residue for immobilization failed. After synthesis and cleavage of a respective mini-Aoda peptide, HPLC purification did not yield sufficient amounts of product, presumably due to yet uncharaterized side reactions involving the ketone and thiol groups. This seems plausible because cleavage of the peptide off the solid phase with a cocktail containing ethane-1,2-dithiol (EDT) resulted in quantitative formation of the 1,3-dithiolane at the Aoda side chain (compare Figure 42).

Design of mini-click-probes

In order to circumvent this problem, a new peptide design and strategy for immobilization was devised, avoiding the presence of the Aoda and cysteine residue within the same peptide (Figure 17). Hence, the probe was divided into two parts: The C-terminal part containing the cysteine for immobilization onto the same iodoacetyl-functionalized solid support as used in previous assays, a short aliphatic spacer (6-aminohexanoic acid, Ahx), and a *p*-azidophenylalanine residue, resulting in the peptide mini-C (**P4**). And an N-terminal part

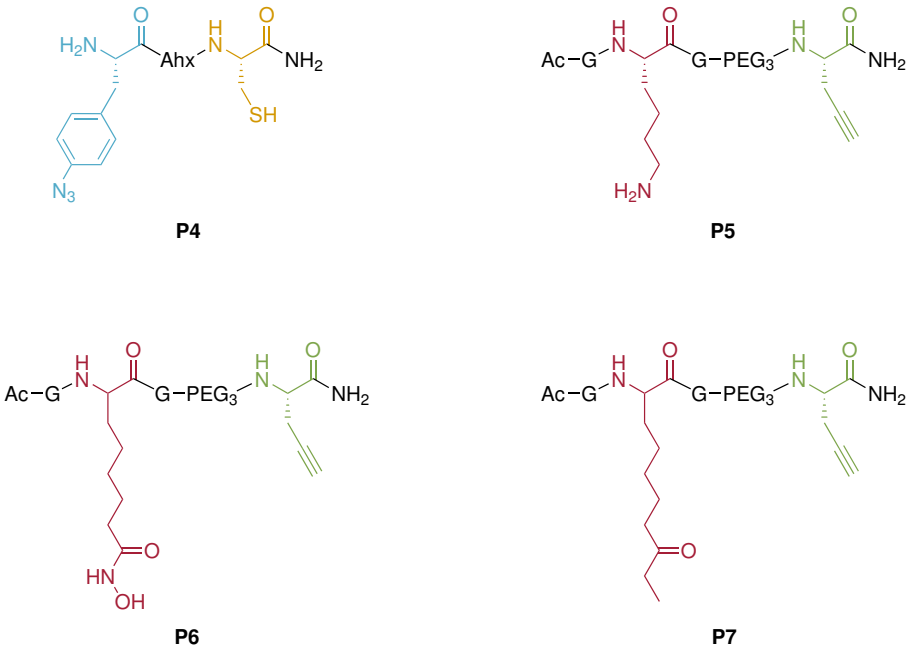

Figure 17: Precursors of mini-click-probes: Mini-C (**P4**), mini-Lys-N (**P5**), mini-AsuHd-N (**P6**) and mini-Aoda-N (**P7**). The cysteine residue in the C-terminal part of mini-click-probes is shown in yellow and the *p*-azidophenylalanine in blue. In the N-terminal parts the central lysine residue or the respective HDAC-trapping amino acids AsuHd and Aoda are depicted in red and the propargylglycine residue is shown in green.

identical to the established mini-probes **P1**–**P3**, but with a propargylglycine residue replacing the cysteine. Three versions of the N-terminal part were synthesized, with either unmodified lysine, AsuHd or Aoda as central amino acid, resulting in the mini-Lys-N (**P5**), mini-AsuHd-N (**P6**) and mini-Aoda-N (**P7**) peptides. In a first step the C-terminal part should then be immobilized via its cysteine residue, with the N-terminal part being connected in a second step using the azide and alkyne functionalities in an on-resin *Huisgen* cycloaddition or "click" reaction[169,170] to create the final, immobilized mini-click-probes.

Synthesis of peptides **P4**–**P7** via SPPS as well as purification by preparative HPLC was feasible without further complications. Solely the cleavage conditions for the mini-Aoda-N probe had to be optimized, since cleavage with the standard cocktail containing triisopropylsilane (TIPS) as scavenger led to reduction of the Aoda ketone to the corresponding secondary alcohol. Omitting TIPS from the cleavage cocktail for mini-Aoda-N (**P7**) solved this issue and did not interfere with peptide yield or purity, since **P7** did not contain any side chain protecting groups to be scavenged.

LC-MS data of purified peptides **P4**–**P7** can be found in the appendix (Chapter 7).

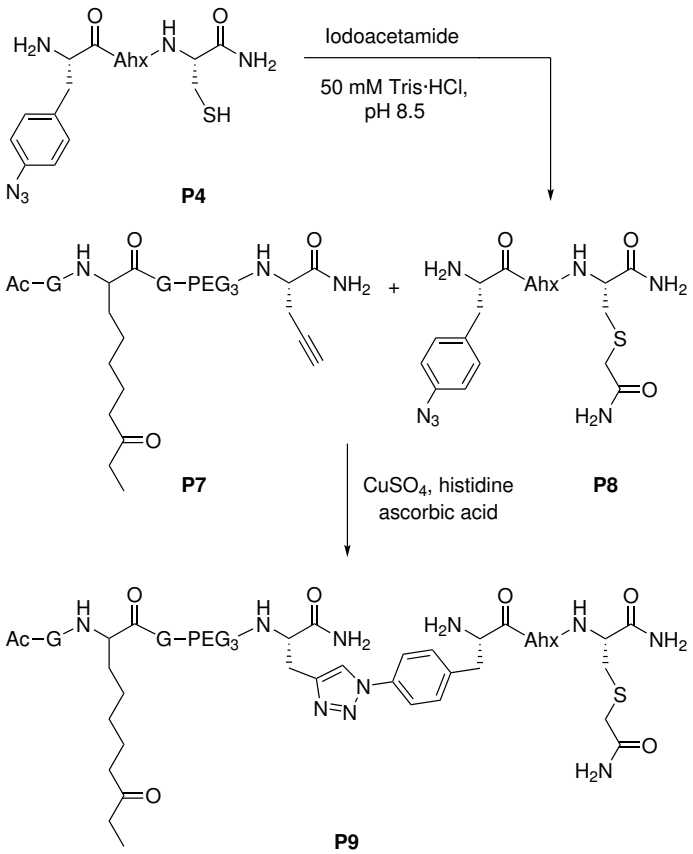

Figure 18: Reaction scheme for testing the click reaction of mini-C (**P4**) with mini-Aoda-N (**P7**) in solution. Carbamidomethylation of mini-C (**P4**) is carried out first, yielding peptide **P8**, which is then connected to mini-Aoda-N (**P7**) via a copper-catalyzed cycloaddition (*click* reaction) in the second step forming the click product **P9**.

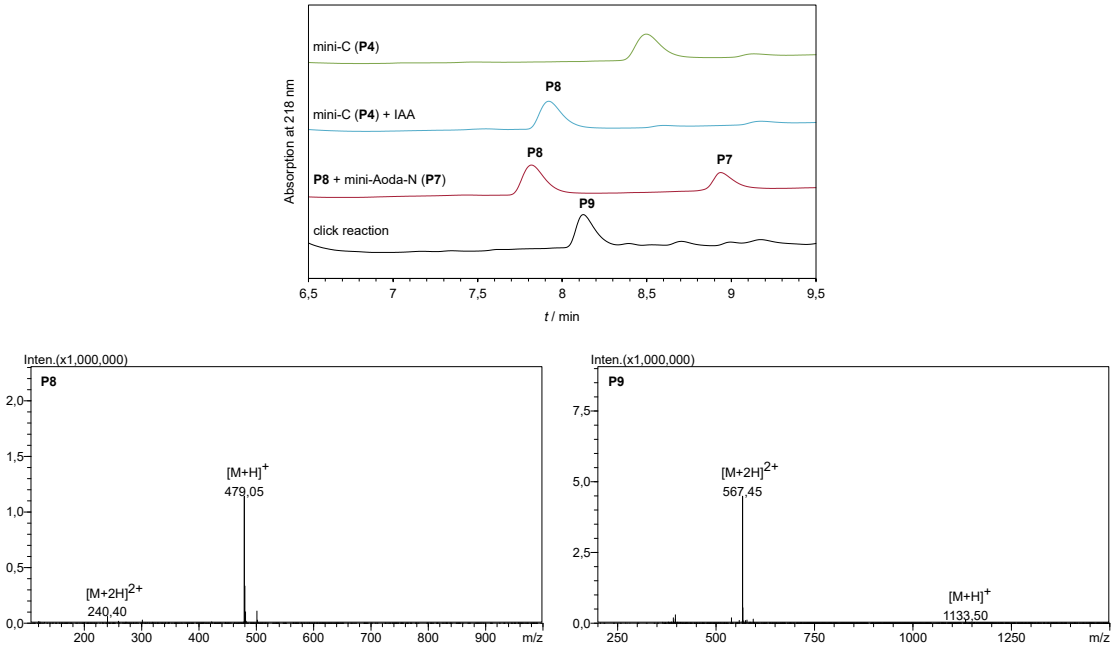

Figure 19: LC-MS analysis of the click reaction of mini-C (**P4**) with mini-Aoda-N (**P7**) in solution. Chromatograms of different stages of the reaction are depicted in the upper part. The UV trace at the top (green) shows the starting material **P4** for reference. The second UV trace (blue) together with the mass specrum to the left confirm quantitative formation of the carbamidomethylated product **P8** after addition of iodoacetamide (IAA). The third UV trace (red) shows the reaction mixture after addition of a stiochiometric amount of mini-Aoda-N (**P7**), while the bottom trace (black) together with the mass spectrum to the right confirm formation of the desired click product **P9** after addition of the copper catalyst and overnight incubation.

Click reaction in solution

Having synthesized a set of suitable peptides for investigating the binding properties of Aoda in pulldown assays, the new two-step concept of immobilization could be tested (Figure 18).

In order to confirm the identity of the intended product of the click reaction, the reaction was performed in solution and each step was analyzed by LC-MS (Figure 19). Firstly, mini-C (**P4**) was dissolved in Tris buffer and then carbamidomethylated with iodoacetamide to block the thiol group of cysteine, yielding peptide **P8**. In this step, carbamidomethylation was intended to mimic immobilization on the iodoacetyl-functionalized solid-support. LC-MS analysis confirmed that the reaction was completed within 15 min and that only one single species was formed (blue UV trace in Figure 19).

Secondly, the N-terminal probe part mini-Aoda-N (**P7**) was added in a stoichiometric amount to the formed **P8**, resulting in two peaks detectable by LC-MS (red UV trace in Figure 19). The click reaction was started by addition of copper(II) sulfate and ascorbic acid, producing the catalytically active copper(I) species *in situ*, with histidine[171] serving as water-soluble ligand. The reaction was allowed to proceed overnight and then again analyzed by LC-MS, indicating full conversion of reactants into the desired triazole-containing product **P9**, thus confirming the feasibility of the approach (black UV trace in Figure 19).

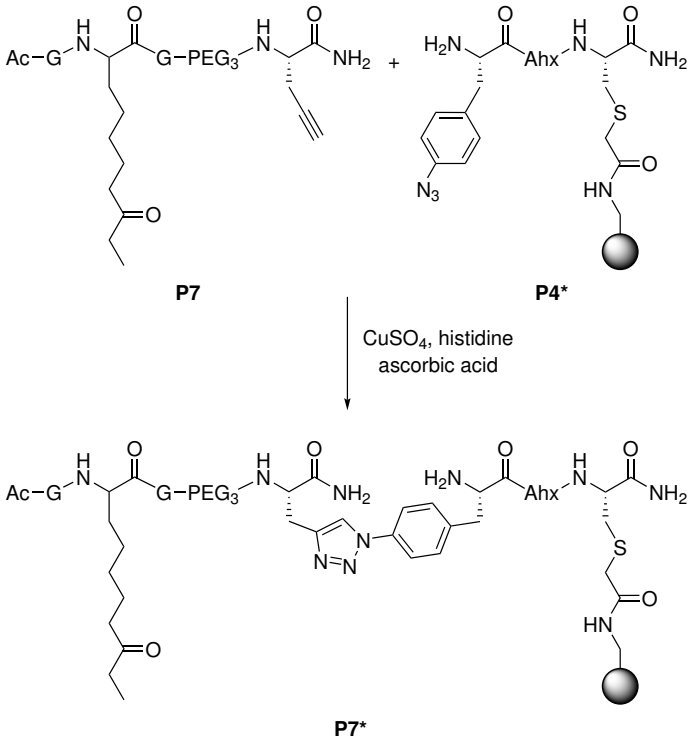

Figure 20: Reaction scheme for the on-resin click reaction of immobilized mini-C (**P4**) with mini-Aoda-N (**P7**), yielding mini-click-Aoda (**P7***).

On-resin click reaction

In the next step, the click reaction between mini-C (**P4**) and mini-Aoda-N (**P7**) was performed on the solid-phase intended for subsequent HDAC pulldown assays. First, mini-C (**P4**) was immobilized onto the solid support, followed by connection of the N-terminal part mini-Aoda-N (**P7**) via click reaction, resulting in the immobilized mini-click-Aoda probe (**P7***) (Figure 20). Although product formation of both reactions could not be monitored by LC-MS in a direct fashion, reaction progress could be followed indirectly by analysis of reactants remaining in the supernatant after separation from the solid-phase.

To this end, mini-C (**P4**) was immobilized onto iodoacetyl-functionalized agarose beads via its cysteine residue according to the established protocol previously used for conventional mini-probes **P1**–**P3**. Figure 21 shows the mass chromatograms of samples taken before and one hour after incubation of mini-C (**P4**) with the agarose beads, indicating that **P4** is completely captured from the reaction mixture. After blocking unreacted iodoacetyl groups of the resin with β-mercaptoethanol and extensive washing steps, a solution of a stoichiometric amount of mini-Aoda-N (**P7**), containing copper(II) sulfate, ascorbic acid and histidine, was added. Samples of this solution were taken before addition to the resin and one hour after that, and analyzed by LC-MS. With mass chromatograms indicating only incomplete immobilization, the pH of the reaction mixture was checked and re-adjusted from approximately 1–2 to 7 with aqueous NaOH. Additional equivalents of copper were added and the reaction was

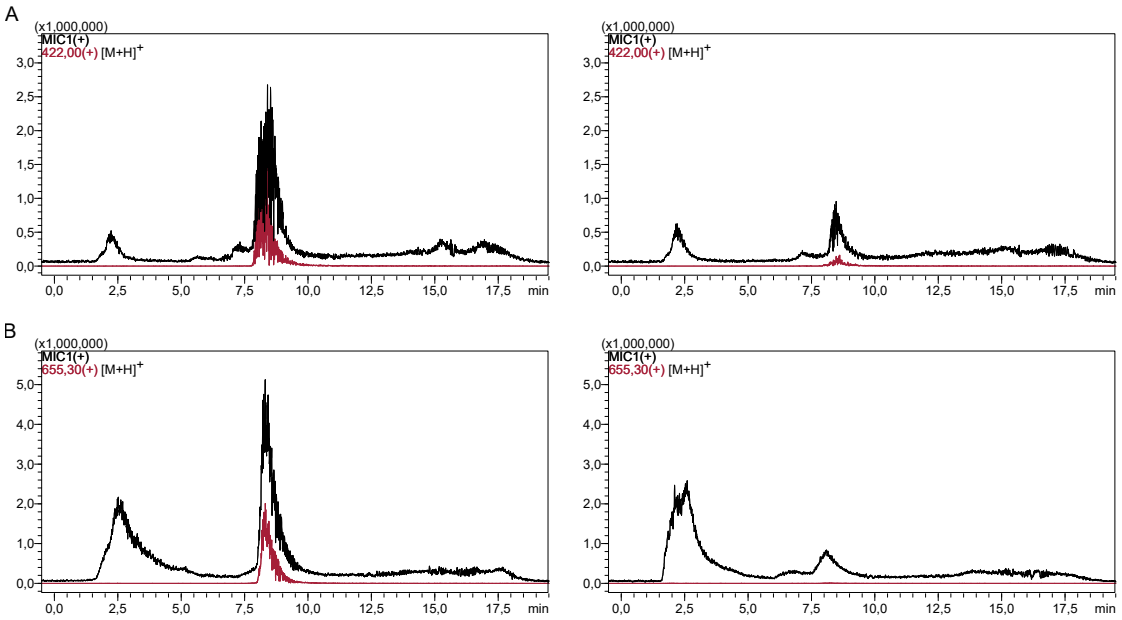

Figure 21: LC-MS analysis of the immobilization of (A) mini-C (**P4**) and (B) mini-Aoda-N (**P7**) via click reaction. Mass chromatograms of samples from the solutions of the respective peptides before incubation with the solid support are shown to the left, with mass chromatograms after incubation shown to the right. The residual signal for mini-C (**P4**) after incubation stems from a small fraction of **P4** oxidized to the respective disulfide, which is not immobilized. MIC: Multi ion count (m / z = 200–2000).

allowed to proceed overnight with solid-phase-bound mini-C (**P4**). Figure 21 shows the mass chromatograms of samples before the click reaction and after overnight incubation, with mini-Aoda-N (**P7**) being immobilized completely under the modified conditions.

Consequently, the click reaction could also be successfully applied on solid support, providing a new method for generation of an immobilized peptide-based probe containing the Aoda moiety, mini-click-Aoda (**P7***). Mini-Lys-N (**P5**) and mini-AsuHd-N (**P6**) were immobilized in the same way, leading to the probes mini-click-Lys (**P5***) and mini-click-AsuHd (**P6***).

2.1.3.3 Pulldown assays with mini-click-probes

Having successfully synthesized an immobilized, peptide-based probe containing Aoda as HDAC-trapping amino acid and suitable controls with unmodified lysine or AsuHd, the ability of Aoda to recruit endogenous HDACs from cellular lysates could be examined.

Pulldown assays with the probes mini-click-Lys (**P5***), mini-click-AsuHd (**P6***) and mini-click-Aoda (**P7***) were performed in the same way as described for conventional mini-probes **P1**–**P3** (Chapter 2.1.2.3) with equal amounts of native lysate from HeLa cells (200 µg total protein). Unspecific binders were removed by extensive washing and desired proteins were eluted with SDS sample buffer at high temperature. Proteins were then separated by SDS-PAGE and analyzed by western blotting. The blots were incubated with primary antibodies against HDAC1 and HDAC6, and secondary antibody-horse radish peroxidase (HRP) conjugates. After addition of an HRP substrate, chemiluminescent images were recorded (Figure 22).

Experiments were conducted in cooperation with *A. Lodek*.[172]

Analysis was performed for HDAC1 and HDAC6 as representative members of class I and class IIb deacetylases, respectively. Mini-click-AsuHd (**P6***) was able to enrich both HDACs when compared to the lysine control **P5***, which is in agreement with the results obtained with mini-AsuHd (**P2**) previously. Mini-click-Aoda (**P7***) showed only weak recruitment of HDAC1 and HDAC6 when compared to its hydroxamic acid congener **P6***. However, when comparing the signal intensities of mini-click-Lys (**P5***) with mini-click-Aoda (**P7***), the Aoda-containing probe was able to enrich HDAC6 approximately 1.5-fold over the lysine control and HDAC1 even 5-fold. Although these numbers can only be regarded as a rough estimate rather than a quantitative measure, and cellular abundance of the respective HDACs also plays a key role in their enrichment and resulting western blot signal intensities, these results seem to reflect the HDAC preference of the class-I-specific inhibitor apicidin, from which the Aoda moiety was derived.

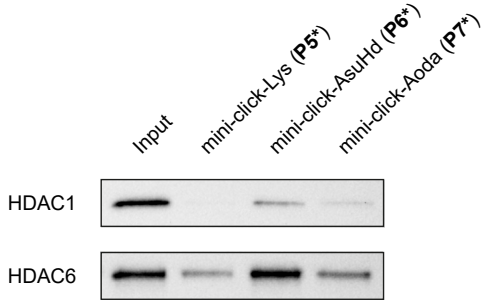

Figure 22: Representative chemiluminescent images of western blots from pulldown experiments with mini-click-Lys (**P5***), mini-click-AsuHd (**P6***) and mini-click-Aoda (**P7***) using HeLa lysate (1 mg mL^{-1}, 200 µg total protein). Input samples: 16 µg.

Despite the weaker recruitment of HDACs to the ketone-containing Aoda when compared to hydroxamic acids, with the building block Fmoc-Aoda-OH (**16**) and the mini-click-Aoda probe (**P7***) promising and versatile tools were developed to further adjust the selectivity of HDAC probes. A slightly reduced interaction with the HDAC-trapping amino acid seems especially desirable when peptidic sequence context is added to HDAC probes, enabling to compare the influence of different sequences on HDAC binding with less bias introduced by the HDAC-trapping amino acid.[143]

2.2 Sequence context

Besides the identity of the zinc-binding functional group, another key factor governing the HDAC-selectivity of chemical probes and HDAC inhibitors is the nature of the cap moiety, which is connected to the zinc-binding group most commonly by an aliphatic linker. The cap moiety interacts with residues at the surface of the HDAC enzyme, mimicking the natural HDAC substrate, the polypeptide chain of an acetylated protein.[24,85] It is therefore advantageous to embed the zinc-binding moiety as HDAC-trapping amino acid into a synthetic peptide sequence derived from a natural HDAC substrate. On the one hand, this peptidic sequence context can be used to fine-tune the enzyme-selectivity of the respective HDAC

probe or inhibitor, and on the other hand, it can also be exploited as a tool for studying the substrate selectivity of HDACs and to uncover previously unknown substrate proteins and interactions partners of these enzymes, thus elucidating their diverse physiological functions.

Peptide-based probes with central hydroxamic acid residues and sequence context derived from acetylation sites of known HDAC substrate proteins have successfully been applied for investigating the substrate selectivity and composition of endogenous HDAC complexes.[136,142]

In addition, the understanding of protein acetylation and HDAC activity is in large part aided by advancements in MS / MS-based proteomics, which uncovered thousands of acetylation sites within the human proteome. Acetylome profiling in presence of HDAC inhibitors showed increased abundances of hundreds of the identified sites, indicating that they are likely regulated by the targeted HDACs.[145] Although powerful and versatile tools for gaining detailed insights into HDAC selectivity, the established peptide-based HDAC affinity probes can only be used in order to validate and further examine a small number of acetylation sites on selected proteins identified in proteomics experiments.

Therefore, in a second part of this work, new concepts for the synthesis, peptide design, immobilization and assay strategy applying HDAC affinity probes were developed, adapting them to the high-throughput approaches necessary for validating large proteomic data sets.

2.2.1 High-throughput screening of HDAC6 substrate sequences

In a recent approach to determine the acetylome of HDAC6 knockdown HeLa cells over 1200 acetylation sites were identified. In total 147 acetylation sites were upregulated upon HDAC6 knockdown, rendering these potential substrate sites of HDAC6.[136] Due to the high number and diversity of these sites it appears plausible that HDAC binding proteins are involved by mediating substrate specificity of the HDAC. As opposed to HDACs of class I, which form several known complexes, little is known about the binding partners of HDAC6. Hence, the HDAC6-dependent acetylome seemed an ideal resource for development of a new method for high-throughput screening of HDAC binding to the identified substrate sites.

Table 2 lists a selected number of upregulated acetylation sites on proteins identified in two different proteomics experiments, the aforementioned HDAC6 knockdown acetylome[136] and a data set recorded with the HDAC6-selective inhibitor tubacin.[145] The list further comprises the acetylation sites K382 of p53, a known substrate of HDAC1, K40 of α-tubulin, a known substrate of HDAC6, as well as four other sites on proteins that were identified in knockdown acetylomes of HDAC1, 2, 3 and 10, respectively.[136] Together with a minimal sequence context site with only two flanking glycine residues (mini), these sequences should serve as controls in subsequent pulldown assays.

For each sequence three peptide-based HDAC affinity probes were synthesized with either, unmodified lysine, or the hydroxamate-containing ApmHd or AsuHd replacing the acetylated lysine residue, resulting in 96 peptides (**6P1**–**6P96**).

Table 2: Potential substrate proteins of HDAC6 identified by acetylome analysis. For each protein the ID of the canonical sequence according to UniProt, the corresponding gene name, the position of the acetylation site, and a sequence window of 14 amino acids embedding the acetylated lysine are given. Experimental sources comprise HDAC6 knockdown (kd) acetylomes[136] or acetylomes recorded using the HDAC6-selective inhibitor tubacin.[145] The last four entries (PPL, JADE3, RSF1, MATR3) and p53 (TP53) represent potential substrate proteins of HDAC1, HDAC2, HDAC3, and HDAC10, respectively. In addition, for each sequence the abbreviations of the corresponding peptide probes (**6Px**, **x** = 1–96) are listed, with either Lys, ApmHd, or AsuHd replacing the acetylated lysine.

UniProt ID	Protein	Gene	Sequence	Position	Experiment	Lys	ApmHd	AsuHd
-	mini-probe	-	GKacG	-	-	**6P1**	**6P2**	**6P3**
P04637	Cellular tumor antigen p53	TP53	QSTSRHKKacLMFKTEG	382	-	**6P4**	**6P5**	**6P6**
Q71U36	Tubulin alpha-1A chain	TUBA1A	DGQMPSDKacTIGGGDD	40	-	**6P7**	**6P8**	**6P9**
Q6UUV7-1	CREB-regulated transcription co-activator 3	CRTC3	LHRRSGDKacPGRQFDG	113	HDAC6 kd	**6P10**	**6P11**	**6P12**
Q15369	Elongin-C	ELOC	DGHEFIVKacREHALTS	32	HDAC6 kd	**6P13**	**6P14**	**6P15**
P14618-1	Pyruvate kinase PKM	PKM	ETLKEMIKacSGMNVAR	66	HDAC6 kd	**6P16**	**6P17**	**6P18**
P06744	Glucose-6-phosphate isomerase	GPI	ERMFNGEKacINYTEGR	89	HDAC6 kd	**6P19**	**6P20**	**6P21**
P04406-1	Glyceraldehyde-3-phosphate dehydrogenase	GAPDH	AHLQGGAKacRVIISAP	117	HDAC6 kd	**6P22**	**6P23**	**6P24**
P07900-1	Heat shock protein HSP 90-alpha	HSP90AA1	TKVILHLKacEDQTEYL	191	HDAC6 kd	**6P25**	**6P26**	**6P27**
P27824-1	Calnexin	CANX	KTGIYEEKacHAKRPDA	217	HDAC6 kd	**6P28**	**6P29**	**6P30**
P48643	T-complex protein 1 subunit epsilon	CCT5	LMGLEALKacSHIMAAK	35	HDAC6 kd	**6P31**	**6P32**	**6P33**
P78371	T-complex protein 1 subunit beta	CCT2	LGPKGMDKacILLSSGR	50	HDAC6 kd	**6P34**	**6P35**	**6P36**
P62937	Peptidyl-prolyl cis-trans isomerase A	PPIA	SFELFADKacVPKTAEN	28	HDAC6 kd	**6P37**	**6P38**	**6P39**
Q8N8S7-1	Protein enabled homolog	ENAH	RRRRIAEKacGSTIETE	461	HDAC6 kd	**6P40**	**6P41**	**6P42**
Q13162	Peroxiredoxin-4	PRDX4	DHSLHLSKacAKISKPA	78	HDAC6 kd	**6P43**	**6P44**	**6P45**
Q14247	Src substrate cortactin	CTTN	ASHGYGGKacFGVEQDR	87	Tubacin	**6P46**	**6P47**	**6P48**
Q14247	Src substrate cortactin	CTTN	SVRGFGGKacFGVQMDR	124	Tubacin	**6P49**	**6P50**	**6P51**
O60684	Importin subunit alpha-7	KPNA6	ETMASPGKacDNYRMKS	9	Tubacin	**6P52**	**6P53**	**6P54**
P23588	Eukaryotic translation initiation factor 4B	EIF4B	PEENPASKacFSSASKY	586	Tubacin	**6P55**	**6P56**	**6P57**
P50542	Peroxisomal targeting signal 1 receptor	PEX5	AGHFTQDKacALRQEGL	28	Tubacin	**6P58**	**6P59**	**6P60**
Q09666	Neuroblast differentiation-associated protein AHNAK	AHNAK	SLEGPEGKacLKGPKFK	1177	Tubacin	**6P61**	**6P62**	**6P63**
P49792	E3 SUMO-protein ligase RanBP2	RANBP2	NFSEKASKacFGNTEQG	1851	Tubacin	**6P64**	**6P65**	**6P66**
Q15942	Zyxin	ZYX	KFTPVASKacFSPGAPG	279	Tubacin	**6P67**	**6P68**	**6P69**
Q13153-1	Serine/threonine-protein kinase PAK 1	PAK1	RSILPGDKacTNKKKEK	63	Tubacin	**6P70**	**6P71**	**6P72**
P35658-1	Nuclear pore complex protein Nup214	NUP214	LQPAVAEKacQGHQWKD	691	Tubacin	**6P73**	**6P74**	**6P75**
Q14258	E3 ubiquitin/ISG15 ligase TRIM25	TRIM25	PVPALPSKacLPTFGAP	402	Tubacin	**6P76**	**6P77**	**6P78**
Q92793	CREB-binding protein	CREBBP	KNNKKTNKacNKSSISR	1595	Tubacin	**6P79**	**6P80**	**6P81**
P35579-2	Myosin-9	MYH9	QEQGTHPKacFQKPKQL	419	HDAC6 kd	**6P82**	**6P83**	**6P84**
O60437	Periplakin	PPL	FRKRNKGKacYSPTVQT	12	HDAC1 kd	**6P85**	**6P86**	**6P87**
Q92613	Protein Jade-3	JADE3	SKIPNEHKacKPAEVFR	38	HDAC2 kd	**6P88**	**6P89**	**6P90**
Q96T23-1	Remodeling and spacing factor 1	RSF1	GGGVGRGKacDISTITG	1061	HDAC3 kd	**6P91**	**6P92**	**6P93**
P43243	Matrin-3	MATR3	VRVHLSQKacYKRIKKP	473	HDAC10 kd	**6P94**	**6P95**	**6P96**

2.2.1.1 Assay design

The generation of large peptide libraries and high-throughput screenings thereof, e.g. for enzyme or antibody binding, can be achieved using the SPOT method, where peptides are synthesized in nanomol scale on cellulose membranes, which may then be spotted as peptide-cellulose conjugates onto glass slides producing a large number of copies of the respective library.[173,174] However, due to the cellulose conjugation and the small amounts of peptide, the drawback of this method is that peptides can hardly be characterized, analyzed for purity and quantified routinely, potentially introducing errors into followup assays.

The workflow for generation of peptide arrays for HDAC pulldown experiments introduced in this work is therefore based on the format of 96-well plates, creating a link between traditional approaches focusing on single HDAC substrates and array technologies. The 96-well approach fully retains all possibilities of peptide analysis and quantification established for traditional peptide synthesis. The key step for successful portation of the previously used HDAC assay principle to the high-throughput format was to eliminate the need for time-consuming purification of peptides by preparative HPLC. To do so, a probe design was developed which enables selective capture of pure, full-length peptides from the crude product mixtures by immobilization.

Immobilization strategy

Established peptide-based probes are immobilized onto iodoacetyl functionalized agarose beads as solid-support for HDAC binding assays via their cysteine thiol, which reacts with the resin-bound iodoacetyl groups under formation of a thioether bond (Figure 23 A). However, since these probes are immobilized via a C-terminal cysteine residue, purification prior to use in biochemical experiments is mandatory, because truncation products that form during peptide synthesis will also contain the C-terminal cysteine.

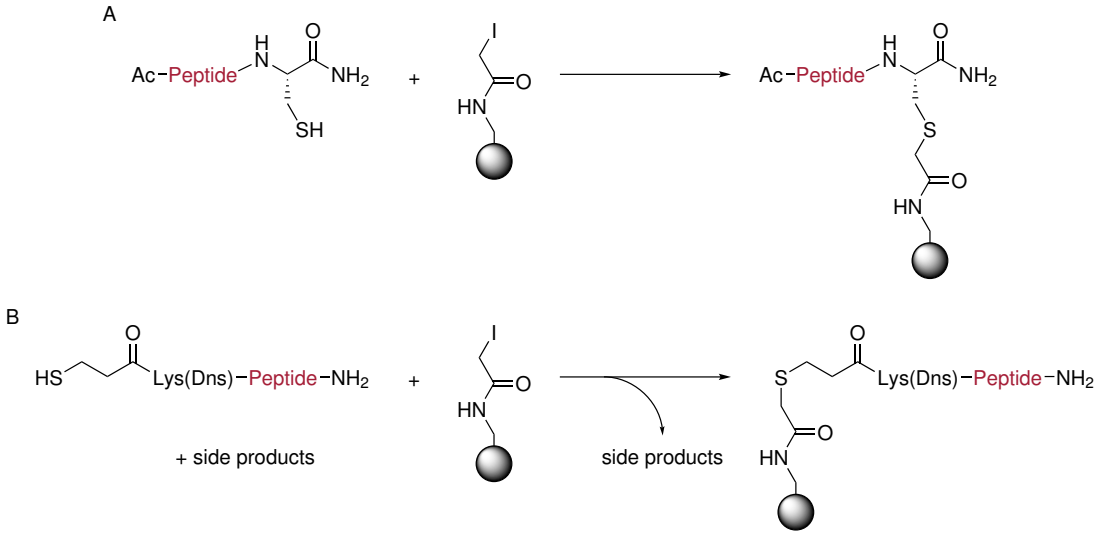

Figure 23: Scheme of peptide immobilization on solid-support with (A) the established design of HDAC affinity probes through a C-terminal cysteine residue and (B) peptide design introduced in this work with immobilization through an N-terminal thiol-containing anchoring moiety.

In the new probe design for 96-well application, the thiol for immobilization is positioned at the N-terminus of the peptides and truncation products are capped by acetylation after each amino acid coupling during SPPS. In this way, only one single species with a thiol group should be present in the crude mixture, which can then be selectively captured from a solution of the crude product (Figure 23 B). An N-terminal fluorophore (dansyl, Dns) is further attached for simplifying quantification and HPLC analysis.

Peptide probe design

The general design of newly developed HDAC affinity probes (**6P1**–**6P96**) for 96-well application is shown in Figure 24.

A D-proline amide and a short, polyethylene glycol-based spacer were installed at the C-terminus in order to improve stability of the peptides in cellular lysates used for HDAC binding assays. These lysates often exhibit residual metallocarboxypeptidase activity, because stringent inhibition of metalloenzymes is not possible without interfering with HDAC activity.[142,175] The core of the probe comprises a sequence window of seven amino acids both N- and C-terminal to one of the identified acetylation sites potentially regulated by HDAC6 (Table 2). Into this sequence context the hydroxamate-containing ApmHd or AsuHd were embedded as central HDAC-trapping amino acid. A version of the probe with unmodified lysine served as control. A further PEG spacer connects the peptide core with the N-terminal anchoring moiety. This anchoring moiety comprises a thiol group, facilitating immobilization on solid-support, and a dansyl moiety attached to the side chain of a lysine residue, enabling quantification of full-lenght probe peptides. In order to ensure that only full-lenght peptides contain the N-terminal anchor, it should be introduced as a single building block, *N*α-(3-mercaptopropionyl)-*N*ε-dansyllysine (Chapter 2.2.1.2).

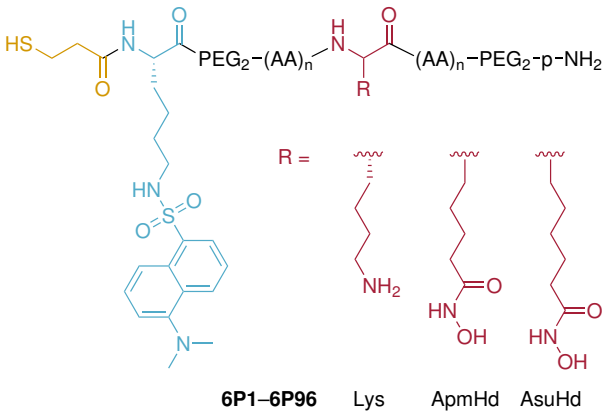

Figure 24: Peptide-based affinity probes based on HDAC6 susbtrate sites for 96-well assay format. The central lysine residue, or the respective HDAC-trapping amino acids ApmHd and AsuHd, are shown in red. The *N*ε-dansyllysine used for quantification is shown in blue and the N-terminal 3-mercaptopropionic acid used for immobilization is depicted in yellow. n = 1 for mini-probes (**6P1**–**6P3**) and n = 7 for probes with sequence context (**6P4**–**6P96**).

Assay workflow

Although methods for the synthesis of peptides in 96-well or microtiter plates exist,[176–180] suitable procedures for parallel cleavage from the solid-phase, peptide quantification, probe immobilization, conducting the HDAC binding assay, and analysis of the large number of pulldown samples had to be established. In Figure 25 the intended workflow for the new assay format in 96-well plates is depicted from synthesis to final analysis.

In the first step, peptides are synthesized on an automated peptide synthesizer equipped for the synthesis in 96-well format in one single plate, using the building blocks Fmoc-ApmHd(OTrt)-OH (**10**) and Fmoc-AsuHd(OTrt)-OH (**5**). These building blocks were designed with regard to massive parallel SPPS, requiring *N*α-protecting groups that can be removed in

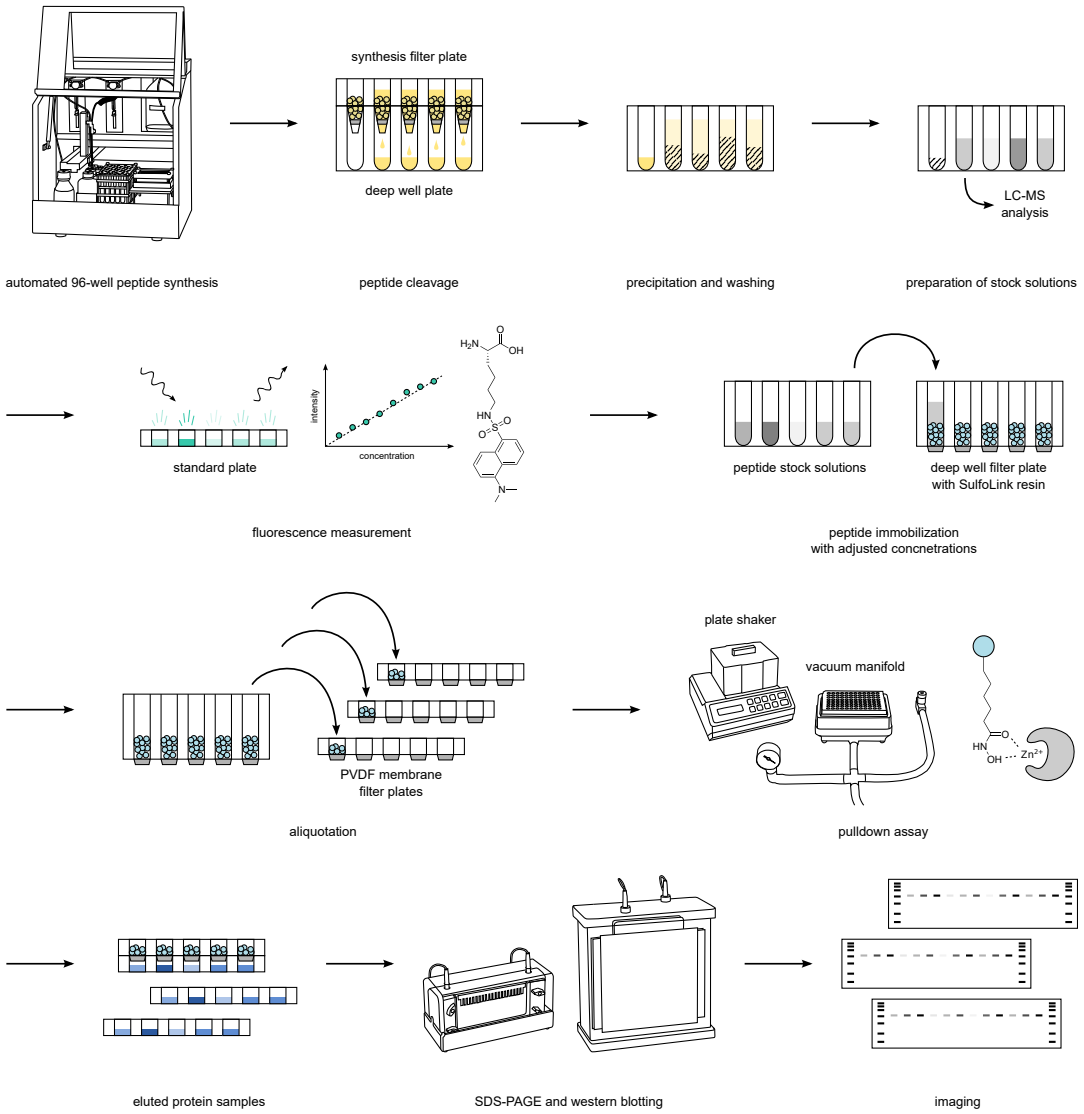

Figure 25: Workflow of the 96-well HDAC pulldown assay.

an automated fashion and and side chain protecting groups that are easily deprotected by common cleavage cocktails. Peptides are cleaved in parallel using an optimized cleavage cocktail, precipitated and washed in suitable deep well plates. Stock solutions are then prepared and analyzed by LC-MS in order to assess the identity and purity of each individual peptide.

In the next step, samples of these stock solutions are measured by fluorescence readout using the dansyl fluorophore of the N-terminal anchoring moiety. The fluorescence signal is calibrated with a suitable reference compound in order to estimate peptide yields and adjust differences in peptide concentrations. Immobilization of the peptide probes onto iodoacetyl-functionalized agarose beads can then be carried out in the next step using the adjusted concentrations of sock solutions, ensuring immobilization of the same amount of peptide in each well of the plate. To this end, a filter-bottom deep well plate is used, enabling the simultaneous immobilization of all 96 peptides. Washing steps are carried out using a dedicated 96-well plate shaker and vacuum manifold. The agarose-bound probe peptides can then be aliquoted into smaller filter-bottom plates suitable for subsequent pulldown assays. From one round of immobilization, several ready-to-use 96-well assay plates are generated, sealed and stored at –20 °C until further usage, allowing multiple replicates of the assay.

The actual HDAC pulldown assay can be conducted following the same protocol as used for the established low-throughput version, ensuring high comparability with previous experiments. During the assay, plates are again handled using the 96-well plate shaker and vacuum manifold. After elution of bound proteins with SDS containing buffer from the filter-bottom into 96-well collection plates, samples are separated using large-scale SDS-PAGE. The 96 samples of one plate are transferred to five gels of suitable size, which are all blotted in one run onto PVDF membranes with a large-scale wet tank blotting system. Detection of bound HDACs with suitable antibodies and imaging can be conducted as described before.

2.2.1.2 Synthesis of a fluorophore building block

Having synthesized the hydroxamate building blocks Fmoc-ApmHd(OTrt)-OH (**5**) and Fmoc-ApmHd(OTrt)-OH (**10**) (Chapter 2.1.1.1), which were already designed to fit the needs of high-throughput formats, a suitable synthesis route for the N-terminal anchoring moiety, *N*α-(3-mercaptopropionyl)-*N*ε-dansyllysine, had to be devised. To this end, the 9-BBN protection method for selective modification of the side chain of amino acids, previously applied in the synthesis of the hydroxamates, as well as the AsuApa and Aoda building blocks, could be exploited, again demonstrating the versatility of this method under a wide variety of conditions (Figure 26).

In a first step, L-lysine monohydrochloride (**17**) was *N*α- and carboxy-protected with 9-BBN in refluxing methanol, resulting in Lys-BBN (**18**). To introduce the fluorophore, crude Lys-BBN (**18**) was then reacted with 5-(dimethylamino)naphthalene-1-sulfonyl chloride (dansyl chloride) and DIPEA as base in anhydrous THF, yielding the respective sulfonamide **19** at the side chain. The oxazaborolidinone protection of Lys(Dns)-BBN (**19**) was hydrolized in the third step by heating crude **19** in trifluoroacetic acid for several hours, until full conversion into 9-BBN-deprotected H-Lys(Dns)-OH (**20**) was observed by LC-MS analysis. In the fourth and final step the amide at the α-amino group of **20** with a suitably protected 3-mercaptopropionic

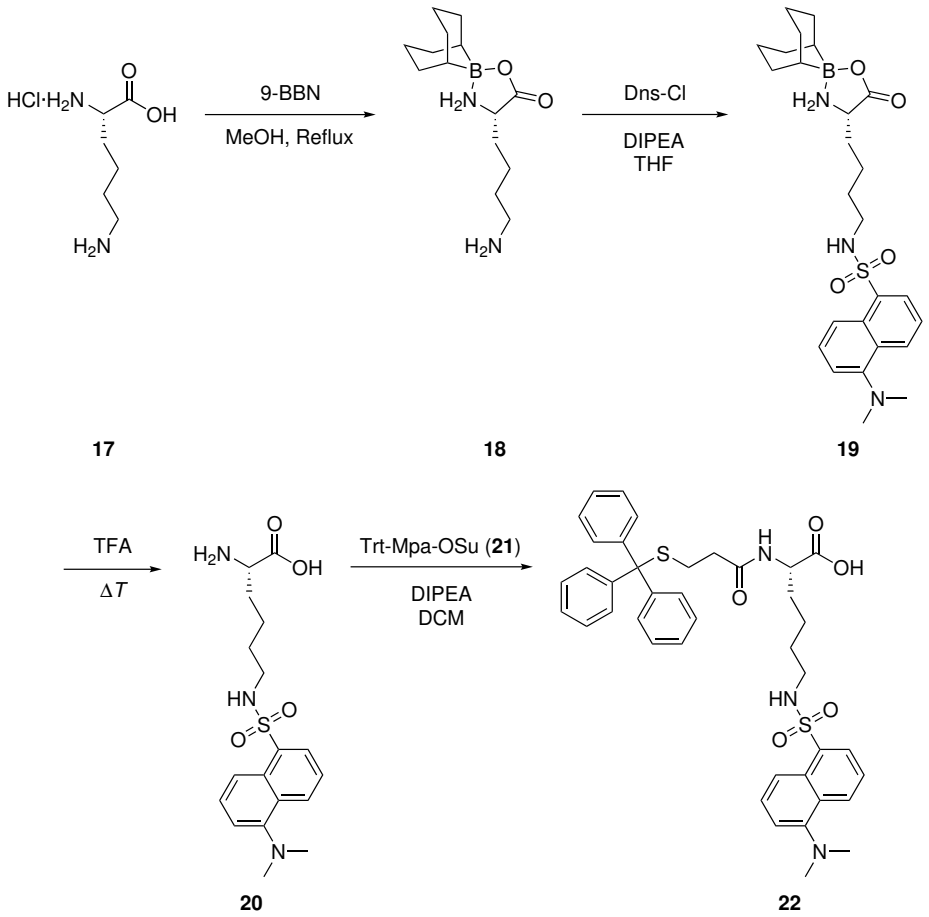

Figure 26: Synthesis of Trt-Mpa-Lys(Dns)-OH (**22**).

acid had to be formed. Initial attempts to do so using *S*-trityl-3-mercaptopropiocic acid (Trt-Mpa) and a methyl ester protected version of **20** were of limited success. Coupling with the uronium-based reagent HATU was impractical due to the desired product of the reaction and the formed tetramethylurea being inseparable by column chromatography. Use of the carbodiimide-based coupling reagent EDC, which creates a water soluble urea by-product, as well as reaction of the mehtyl ester of **20** with the *in situ* generated acid chloride of Trt-Mpa, led only to incomplete conversion.

However, a suitable form of activation was found in the *N*-hydroxysuccinimide (OSu) ester of Trt-Mpa. Trt-Mpa-OSu (**21**) was synthesized from Trt-Mpa-OSu and *N*-hydroxysuccinimide using EDC as activating reagent and DIPEA as base in a mixture of DCM and THF. After extraction, Trt-Mpa-OSu (**21**) was obtained with high purity and coupled to H-Lys(Dns)-OH (**20**) under basic conditions. H-Lys(Dns)-OH (**20**) was applied in excess with respect to Trt-Mpa-OSu (**21**) in order to ensure full conversion of the OSu ester. Excess 3-mercaptopropionic acid in preparations of the final building block would likely have interfered with peptide quantification of the high-throughput assay approach, because peptides could have been

immobilized that lack the dansyl fluorophore. After purification by column chromatography, the final N-terminal anchoring building block Trt-Mpa-Lys(Dns)-OH (**22**) was obtained with a yield of 82 % with respect to Trt-Mpa and high purity.

LC-MS data for all steps up to the final building block **22** as well as NMR spectra of **18**, **20** and **22** can be found in the appendix (Chapter 7).

2.2.1.3 96-well peptide synthesis

With suitable building blocks in hand for introduction of the HDAC-trapping hyroxamates ApmHd and AsuHd, and the N-terminal anchoring moiety, probe peptides for the 96-well HDAC pulldown assay could be synthesized via SPPS. Synthesis was carried out applying the Fmoc strategy with acid labile side chain protecting groups on an automated synthesizer equipped for use with 96-well filter-bottom plates and in a 2 µmol scale per peptide. Couplings of the respective amino acids were performed twice with HATU as activator and *N*-mehthylmorpholine as base, and a capping step with acetic anhydride was implemented after each cycle.

In order to test the synthesis protocol and the newly established building blocks, in a first round only minimal sequence context probes **6P1**–**6P3** were synthesized. Test cleavage of the resulting peptides from a small amount of resin and subsequent LC-MS analysis suggested the general feasibility of the approach, however, it also revealed a side product with double incorporation of the respective hydroxamates ApmHd and AsuHd. Analysis of the stock solutions of ApmHd and AsuHd that were prepared in *N*-methylpyrrolidin-2-one (NMP) via LC-MS indicated partial deprotection of the Fmoc group of the two building blocks (data not shown). The pH of these solutions was approximately 9, while pure NMP or stock solutions of commercial Fmoc amino acids in NMP showed a pH of 7. It therefore seemed plausible that residual base in preparations of the hydroxamate building blocks caused the Fmoc cleavage in the stock solutions over time, since they had not been purified by chromatography but only separated by extraction. To circumvent this problem, stock solutions of ApmHd and AsuHd were adjusted to pH 7 prior to synthesis by addition of formic acid, which did not couple to free amino groups under the SPPS conditions chosen.

Subsequently, all 96 peptides could be successfully synthesized in parallel in one single run. After correct peptide assembly was confirmed by LC-MS analysis, all peptides were cleaved off the solid-phase. Tests were conducted with selected peptides **6P7**–**6P9** (α-tubulin probes) using the cleavage cocktail (Reagent R[181]) previously employed in the

Table 3: Cleavage cocktails applied in 96-well peptide synthesis.

	Reagent R	Reagent K	Octanedithiol	Dithiothreitol
TFA	85 %	82.5 %	81.5 %	81.5 %
H_2O	5 %	5 %	5 %	5 %
PhOH	5 %	5 %	5 %	5 %
PhSMe	-	5 %	5 %	5 %
TIPS	5 %	-	1 %	1 %
EDT	-	2.5 %	-	-
ODT	-	-	2.5 %	-
DTT	-	-	-	2.5 %

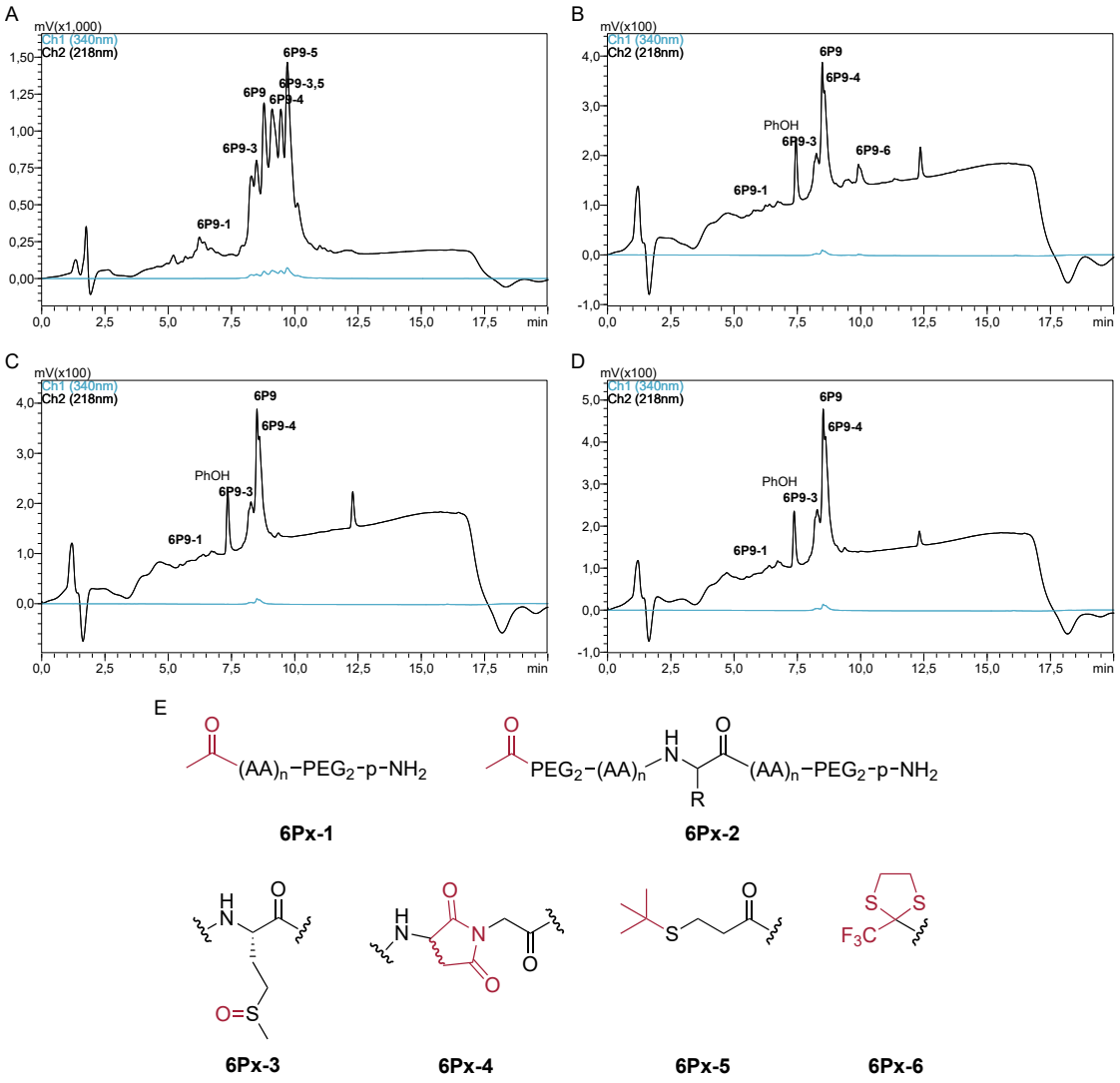

Figure 27: Cleavage of TUBA1A-AsuHd (**6P9**) in a 96-well plate. UV chromatograms from LC-MS analysis of cleavage with (A) Reagent R (B) Reagent K, (C) ODT and (D) DTT are shown. (E) Structure of side products observed with 96-well peptides. n = 1 for mini-probes (**6P1**–**6P3**) and n = 7 for probes with sequence context (**6P4**–**6P96**). R = Lys, ApmHd, AsuHd and **x** = 1–96 depending on the respective probe.

synthesis of mini-probes and mini-click-probes. This cocktail contained TFA, water, phenol and triisopropylsilane (TIPS), and was applied in small portions to the wells of the peptide synthesis plate over the course of several hours (Table 3). After precipitation from the collected cleavage solutions and washing with cold diethyl ether, solvation in water / acetonitrile and lyophilization, crude peptides were analyzed by LC-MS.

As representative example, the UV chromatogram of TUBA1A-AsuHd (**6P9**) is shown in Figure 27 A. Use of the cleavage cocktail Reagent R resulted in impure peptides. Major side products that could be identified are depicted in Figure 27 E. As expected, capped truncation products from incomplete couplings of amino acids were detectable. Capping at the site

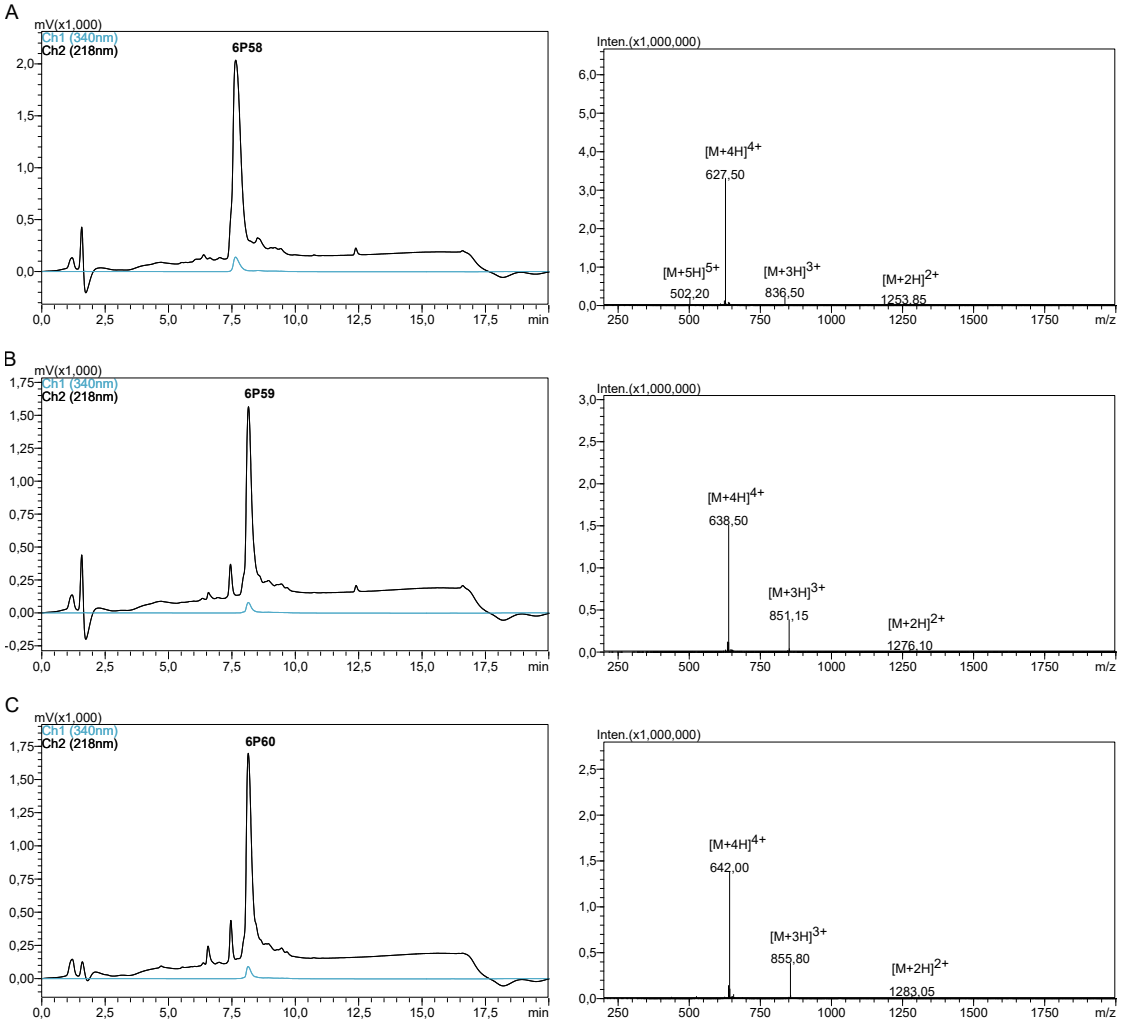

Figure 28: LC-MS analysis of crude (A) PEX5-Lys (**6P58**), (B) PEX5-ApmHd (**6P59**) and (C) PEX5-AsuHd (**6P60**) cleaved with DTT-containing, modified Reagent K.

of the hydroxamate building blocks, resulting in products **6Px-1**, occurred for all respective peptides, but to a relatively low extent. The capping product without the N-terminal anchor **6Px-2** only occurred for peptides with lysine in place of the hydroxamates (data not shown), since with the latter, the soichiometry of free amino groups was reduced in the end of the synthesis by previous capping steps, ensuring complete coupling of Trt-Mpa-Lys(Dns)-OH (**22**). Further detectable modifications included methionine oxidation (**6Px-3**) and succinimide formation from an aspartate N-terminal to glycine (**6Px-4**). The most prominent impurity was, however, caused by *tert*-butylation of the peptide, which is possible, for example, at the N-terminal thiol (**6Px-5**). This could be confirmed by immobilization of a crude sample of the peptide, with species **6Px-5** remaining in the reaction solution. *tert*-Butylation was also detectable together with methionine oxidation, resulting in **6Px-3,5**. Other combinations of these modifications or further side products stemming from the succinimide (**P6x-4**) seem

likely within the bulk of peaks caused by various species in the UV chromatogram. It could be inferred from these results, that the amount and potency of scavengers in Reagent R was too low in proportion to the peptide resin when applied in the small volumes necessary for cleavage in 96-well plates. Especially excess *tert*-butyl cations liberated from amino acid side chains or *tert*-butyl trifluoroacetate, respectively, seemed to be a problem.

A possible solution to address the side reactions during peptide cleavage was found in the cleavage cocktail Reagent K, which was introduced in 1990 by *King et al.*[182] Besides water and phenol, this cocktail uses thioanisole and ethane-1,2-dithiol (EDT) as scavengers to minimize methionine oxidation and modification of the peptide by liberated side chain protecting groups, respectively (Table 3). The UV chromatogram of a sample of TUBA1A-AsuHd (**6P9**) cleaved with this cocktail and analyzed by LC-MS is shown in Figure 27 B. Although methionine oxidation could not be fully prevented, *tert*-butylation was completely suppressed, demonstrating the potency of the EDT scavenger and the suitability of Reagent K for the 96-well approach. However, as compared to the standard cleavage cocktail, the formation of a new side product **6P9-6** was observed. According to its mass difference it was assigned to be a 2-trifluoromethyl-1,3-dithiolane adduct of the peptide (**6Px-6**). This modification was previously discovered on tryptophan residues of peptides and likely arises by electrophilic addition of the dithioacetal cation formed by TFA and EDT at high temperatures.[183] Although it seems plausible that the dansyl moiety is modified in peptide **6P9** due to the lack of other aromatic residues in its sequence, TFA-EDT-modified **6P9** could not be immobilized from solutions of the crude peptide. This hints at the N-terminal thiol as site of attachment, which is supported by a finding of *Coffen*, who, in 1967, refluxed TFA with EDT, obtaining a stable orthothioester, which consists of two 2-trifluoromethyl-1,3-dithiolan-2-yl groups bridged by EDT.[184] It therefore seems likely that **6P9** is modified in the form of a 2-alkylthio-2-trifluoromethyl-1,3-dithiolane at the N-terminus (see Chapter 3).

In order to eliminate formation of the TFA-EDT adduct, which would interfere with peptide quantification during immobilization in the same way as *tert*-butylation, modifications of Reagent K are suggested in literature.[183] Besides conducting the cleavage at lower temperatures, EDT can be replaced by other thiol scavengers, which disfavor the formation of the respective dithioacetal. To this end, samples of **6P9** were cleaved with two versions of Reagent K, where either octane-1,8-dithiol (ODT) or dithiothreitol (DTT) replaced the EDT (Table 3). In addition, 1 % of TIPS was included in both cocktails. The UV chromatograms from LC-MS analysis are shown in Figure 27 C and D, respectively. Both cleavage cocktails showed similar results with no observable *tert*-butylation (**6Px-5**) or dithioacetal adduct formation (**6Px-6**). Methionine oxidation (**6Px-3**) remained minimized as compared to Reagent R (Figure 27 A), leaving succinimide formation (**6Px-4**) the most prominent side reaction.

These optimization steps appeared sufficient for the envisioned high-throughput screening approach, and the DTT-containing version of Reagent K was chosen for final cleavage of all 96 HDAC6 probe peptides. Peptides were precipitated from cleavage solutions in a deep well plate and washed with additional ether to remove most of the residual phenol. After lyophilization, all 96 peptides were analyzed by LC-MS, indicating reasonable to good purity depending on the sequence. As representative example, UV chromatograms and MS spectra of PEX5-Lys (**6P58**), PEX5-ApmHd (**6P59**) and PEX5-AsuHd (**6P60**) are depicted in Figure 28.

2.2.1.4 96-well peptide immobilization

After the library of 96 probe peptides derived from potential HDAC6 substrate sites had been successfully synthesized, peptides were immobilized onto iodoacetyl-modified agarose beads applying the established protocol. However, since the HDAC6 affinity probes were not purified by preparative HPLC, quantification of full-length peptides by fluorescence readout using the dansyl moiety of the N-terminal anchor was mandatory, thereby ensuring immobilization of the same amount of peptide for each sequence. To do so, the fluorescence signal of **6P1**–**6P96** was referenced to the signal of HPLC-purified amino acid building block H-Lys(Dns)-OH (**20**) as fluorescence standard.

Optimal wavelengths for measurement were determined by recording the excitation-emission-spectrum of **20** in the coupling buffer used for immobilization (Figure 29 A). Excitation was maximal at 333 nm while the emission maximum was observed at 568 nm. Using these values, a calibration curve was recorded, ranging from concentrations of 0 to 2 mM (Figure 29 B).

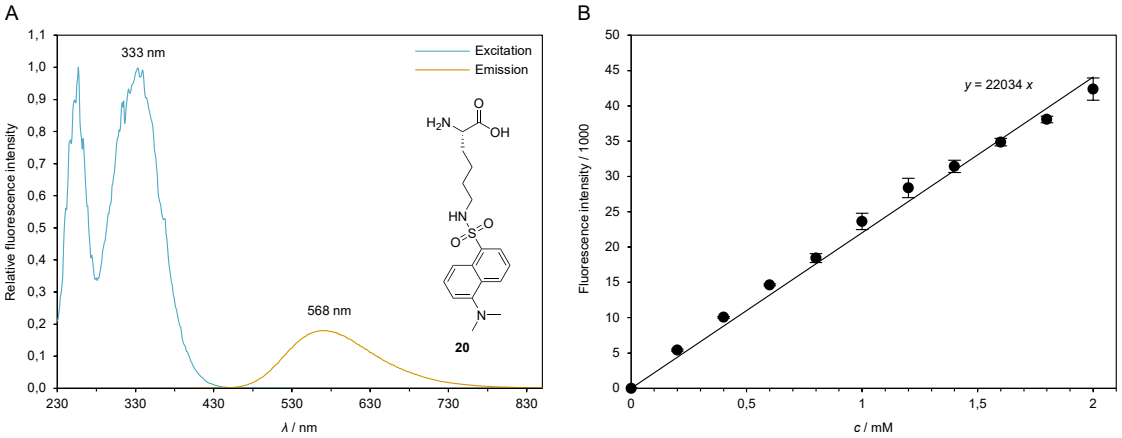

Figure 29: Calibration of fluorescence for 96-well peptide immobilization. (A) Excitation-emission spectrum of reference compound H-Lys(Dns)-OH (**20**). (B) Calibration curve with concentrations of H-Lys(Dns)-OH (**20**) ranging from 0 to 2 mM.

Stock solutions of **6P1**–**6P96** were then prepared in water / acetonitrile with an approximate concentration of 10 mM, by assuming a quantitative yield of 2 µmol per peptide. Samples of these solutions were diluted sufficiently with coupling buffer in order to neutralize the varying amounts of residual TFA in the crude peptides, providing constant pH conditions for fluorescence measurement. Although the average concentration of the 96 peptide stock solutions was determined to be approximately 20 mM and thus, higher than possible with a quantitative yield, correction factors for adjusting the concentration of all peptides could be calculated from the fluorescence signal. Possible influences affecting the calibration are further discussed in Chapter 3.

Stock solutions were then diluted to 1 mM for immobilization taking the correction factor of each individual peptide into account. Immobilization was carried out in a filter-bottom deep well plate, which was handled using a 96-well plate shaker and a vacuum manifold for draining. Before and after addition of the peptide stock solutions to the iodoacetyl-functionalized agarose beads, samples were taken of all 96 peptides and analyzed by LC-MS.

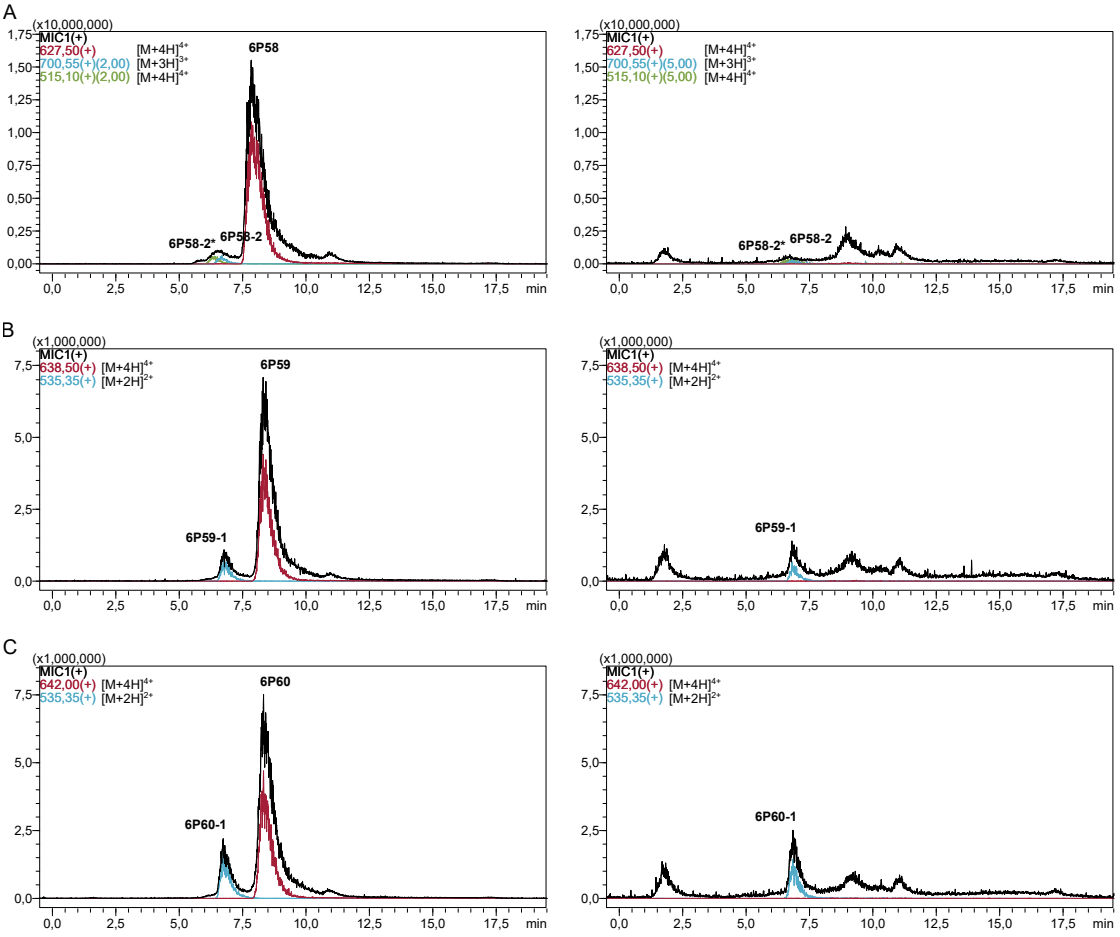

Figure 30: LC-MS analysis of 96-well peptide immobilization with (A) PEX5-Lys (**6P58**), (B) PEX5-ApmHd (**6P59**) and (C) PEX5-AsuHd (**6P60**). Mass chromatograms to the left show samples of peptide solutions before incubation with iodoacetyl-modified agarose beads, whereas chromatograms on the right side show samples of the same solutions after incubation. **6P58-2** is the capping product of **6P58** without the N-terminal anchor, while **6P58-2*** is the non-acetylated version. **6P59-1** and **6P60-1** are identical and are the capping product of **6P59** and **6P59** without the respective hydroxamic acid building blocks. MIC: Multi ion count (m / z = 200–2000).

A representative example showing MS chromatograms of solutions of PEX5-Lys (**6P58**), PEX5-ApmHd (**6P59**) and PEX5-AsuHd (**6P60**) before and after immobilization is depicted in Figure 30. For all three versions of the probe, only the full-length peptide was captured from the coupling solution, indicating the success of the combined immobilization and purification strategy developed for the 96-well HDAC assay. Fragments without the N-terminal anchoring moiety, which are **6P58-2** and **6P58-2*** (**6P58-2** without acetylation) for PEX5-Lys (**6P58**), and **6P59-1** / **6P60-1** for PEX5-ApmHd (**6P59**) and PEX5-AsuHd (**6P60**), were not immobilized and remained in solution (see also Figure 27 E for reference).

Agarose beads from the filter-bottom deep well plate were then transferred to several standard-sized filter-bottom plates, which were sealed and stored in the cold for later use, enabling multiple replicates of the 96-well HDAC pulldown assay.

2.2.1.5 96-well pulldown assay

With a library of 96 peptide-based affinity probes derived from potential HDAC6 substrate sites at hand, pulldown assays could be performed. To this end, native lysate from HeLa cells was added to the wells of filter-bottom plates containing agarose-bound **6P1**–**6P96**. A fixed concentration of 1 mg mL^{-1} (200 µg total protein) was used for all peptides, except for the TP53-probes (p53), where the input concentration was reduced to 0.5 mg mL^{-1} (100 µg total protein). After incubation with the cell lysate agarose beads were washed to remove unspecific binders using a 96-well plate shaker and vacuum manifold.

Compared to the low-throughput version of HDAC pulldown assays, the procedure for elution of proteins from the peptide probes had to be slightly adjusted. Since the 96-well filter-bottom plates used for the assay could not be fully sealed during elution, a larger volume of SDS sample buffer was applied, accounting for additional evaporation while heating. Also, plates could not be heated above 70 °C due to material instability, which made it necessary to increase the elution time. However, through a series of initial tests varying both parameters, buffer volume and elution time, similar signal intensities and thus similar amounts of eluted protein could be achieved as compared to the conventional assay (data not shown).

Eluted protein samples were then centrifuged into 96-well collection plates and separated by SDS-PAGE. Samples of one plate corresponding to one replicate of the pulldown were loaded onto five polyacrylamide gels of suitable size. These five gels were then blotted in parallel onto PVDF membranes using a large-scale wet tank blotting apparatus. Membranes were cut at appropriate sites and incubated with primary antibodies against HDAC6 or HDAC1, respectively. After incubation with secondary antibody-horse radish peroxidase (HRP) conjugates and addition of an HRP substrate, chemiluminescent images were recorded. Figure 31 shows a representative example of the 96-well pulldown with peptides **6P1**-**6P96**.

Peptides **6P7**–**6P96** represent known and potential substrates of HDAC6 identified in two different proteomics experiments determining the HDAC6-dependent actylome, and are shown in the first four sections of Figure 31. The bottom section shows the peptides intended as controls: Minimal sequence context probes **6P1**–**6P3** and TP53-probes **6P4**–**6P6** derived from the known HDAC1 substrate p53. Other control peptides are potential substrates of the respective HDACs from additional knockdown acetylomes: Peptides **6P85**–**6P87** of HDAC1, **6P88**–**6P90** of HDAC2, **6P91**–**6P93** of HDAC3 and **6P94**–**6P96** of HDAC10. In general, most probes were able to enrich HDAC6 over the respective lysine control, with enrichment on AsuHd higher than on ApmHd. HDAC1, which was included in the western blot analysis for comparison, also bound to some of the sequences, but with a different binding pattern.

In agreement with previous results, the α-tubulin-derived TUBA1A-probe **6P9** incorporating AsuHd could efficiently enrich HDAC6 when compared to the lysine control. In contrast, HDAC1 bound evenly weak to all three probes of this sequence, indicating a repulsive influence of the α-tubulin sequence context on this HDAC. This pattern was also observed for the CRTC3-probes **6P10**–**6P12**.

Probes **6P13**–**6P24** were able to enrich both HDAC6 and HDAC1 over the lysine controls. Peptides **6P25**–**6P27**, derived from the heat shock protein 90 α (HSP90AA1), however, only efficiently recruited HDAC6. This seems plausible, since the chaperone HSP90 is a known target of HDAC6.[50]

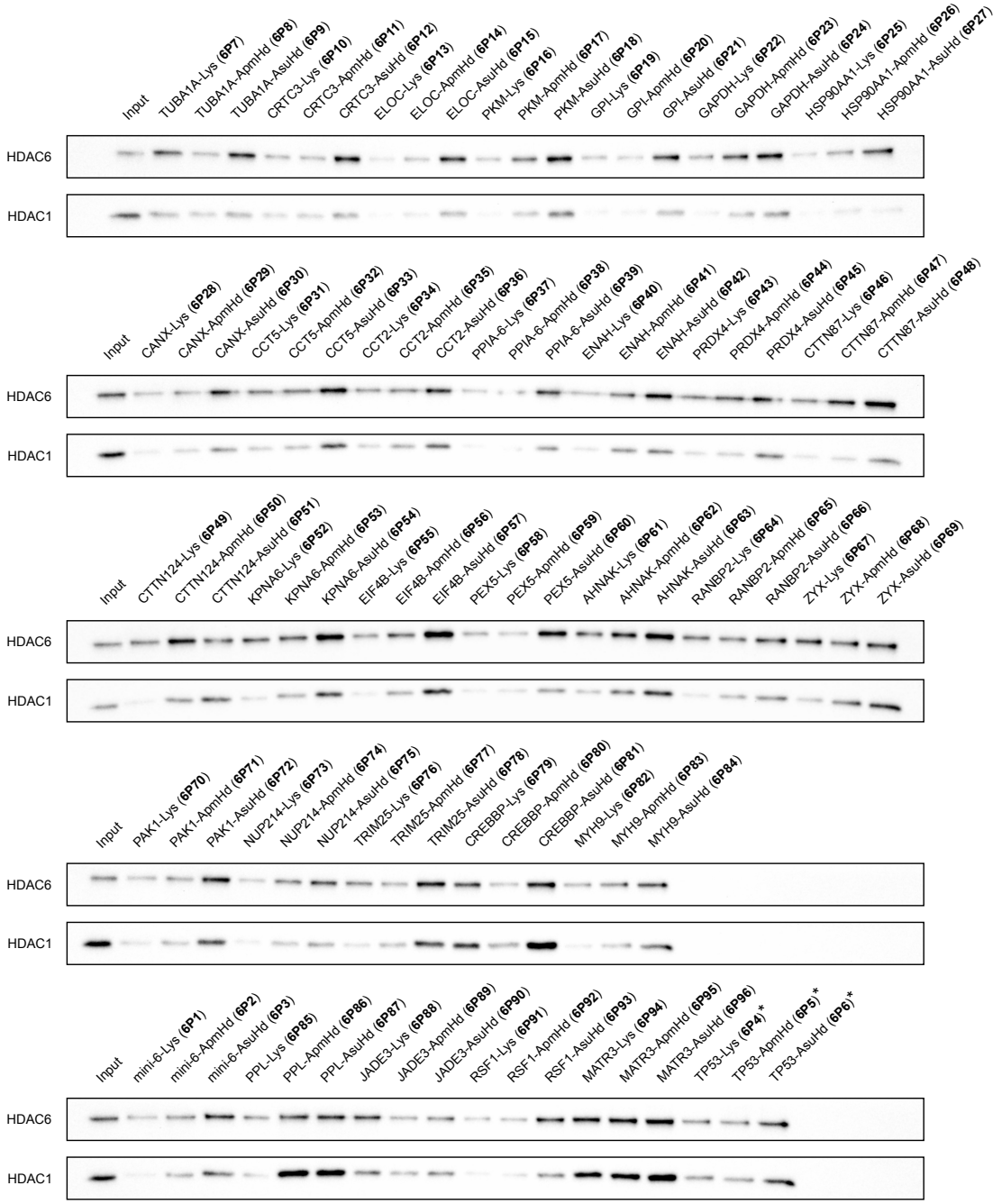

Figure 31: Representative chemiluminescent images of western blots from 96-well pulldown assay with peptide probes **6P1**–**6P96** based on HDAC6 substrate sites and HeLa lysate (1 mg mL^{-1}, 200 µg total protein; *0.5 mg mL^{-1}, 100 µg total protein). Input samples: 16 µg.

Furthermore, HDAC6 and HDAC1 were both enriched by probes **6P28**–**6P45**, but HDAC6 to a lesser extent on the CCT2 (**6P34**–**6P36**) and PRDX4 (**6P43**–**6P45**) sequence, when compared to the other probes. With probes CTTN87 and CTTN124, two different acetylation

sites of the known HDAC6 substrate cortactin, which is a component of the actin cytoskeleton, were tested.[50] When compared to the lysine control HDAC6 showed a stronger preference for CTTN87 (**6P46**–**6P48**) than for CTTN124 (**6P49**–**6P51**).

Probes **6P52**–**6P63** again enriched both HDAC6 and HDAC1, but with an apparently stronger preference of HDAC6 for the PEX5 sequence **6P58**–**6P60** as compared to HDAC1. The RANBP2- (**6P64**–**6P66**) and ZYX-probes (**6P67**–**6P69**) seemed to recruit HDAC6 in an unspecific fashion. Among probes **6P70**–**6P84**, enrichment was comparable between HDAC6 and HDAC1, with only weak recruitment to the NUP124-probes (**6P73**–**6P75**).

As expected, the minimal sequence context probes **6P1**–**6P3** did not differentiate in their recruitment of both of the tested HDACs. The PPL-probes **6P85**–**6P87**, which were derived from the HDAC1 knockdown acetylome, very strongly enriched HDAC1 when compared to the lysine version, but not HDAC6, which was only marginally enriched. Probes of potential substrate JADE3 of HDAC2 (**6P88**–**6P90**) were not able to enrich both HDAC6 and HDAC1. RSF1-probes derived from the knockdown acetylome of HDAC3, however, efficiently recruited both of the tested HDACs. Binding to the potential HDAC10 substrate probes **6P94**–**6P96** was unspecific and strong for both HDAC6 and HDAC1. Known HDAC1 substrate p53 derived probes **6P4**–**6P6** did not differentiate in their ability to recruit HDAC6 or HDAC1 at the input concentration of cell lysate chosen for the assay. According to previous experiments, differentiation would probably have been observable at even lower concentrations.[142]

To conclude, these findings indicated the feasibility of the newly established 96-well HDAC pulldown assay, showing distinct interaction patterns for HDAC6 and HDAC1. The success of the underlying high-throughput approach was enabled in large part by the special probe design, circumventing peptide purification, and by an optimized synthesis and assay workflow. Analysis of the 33 different peptide sequences and resulting 96 HDAC probes individually by traditional approaches would have been difficult and much more laborious.

2.2.2 Selected HDAC6 substrates

After the library of potential substrate sites derived from HDAC6-dependent acetylomes was successfully screened by a newly established 96-well-plate-based high-throughput version of HDAC binding assay, four sequences were chosen from the library (compare Table 2) to be examined in more detail in follow-up experiments. These experiments should elucidate the influence of the substrate site sequence context on HDAC binding partners and on catalysis. To this end, established low-throughput pulldown assays were conducted on a proteome-wide scale in order to investigate the interacting proteins possibly mediating binding between the HDAC and its substrates. In addition, deacetylation assays with recombinant HDAC6 were performed based on MALDI mass spectrometry which should provide further insights into the role of the substrate site sequence context for enzymatic activity.

Besides α-tubulin (**6P7**–**6P9**), the CRTC3 (**6P10**–**6P12**) and HSP90 (**6P25**–**6P27**) sequences seemed to be promising candidates regarding their selectivity for HDAC6. The PPIA (**6P37**–**6P39**) sequence was chosen in addition (Table 4).

Table 4: Selected known and potential substrate proteins of HDAC6. For each protein the ID of the canonical sequence according to UniProt, the corresponding gene name, the position of the acetylation site, and a sequence window of 16 amino acids embedding the acetylated lysine are given. In addition, for each sequence the abbreviations of the corresponding peptide probes are listed, with either Lys or L-AsuHd replacing the acetylated lysine.

UniProt ID	Protein	Gene	Sequence	Position	Lys	L-AsuHd
Q71U36	Tubulin alpha-1A chain	TUBA1A	PDGQMPSDKacTIGGGDDS	40	**P10**	**P11**
Q6UUV7-1	CREB-regulated transcription coactivator 3	CRTC3	PLHRRSGDKacPGRQFDGS	113	**P12**	**P13**
P07900-1	Heat shock protein HSP 90-alpha	HSP90AA1	GTKVILHLKacEDQTEYLE	191	**P14**	**P15**
P62937	Peptidyl-prolyl cis-trans isomerase A	PPIA	VSFELFADKacVPKTAENF	28	**P16**	**P17**

2.2.2.1 Pulldown assays with selected HDAC6 substrate peptides

In order to validate the observations of the 96-well assay and to achieve consistency with previous experiments, new probe peptides were synthesized for each of the chosen substrate sites, following the design of previously published peptide-based HDAC affinity probes (Figure 32).[136,142] To this end, the sequence context was extended to 8 amino acids N- and C-terminal to the acetylation site, with either unmodified lysine or L-AsuHd replacing the acetylated lysine residue. The design further comprises the conventional C-terminal cysteine residue for immobilization, which is connected to the substrate site part of the probe by a 6-aminohexanoic acid (Ahx) spacer. The N-terminus remained unmodified.

In total, this resulted in eight peptide probes (**P10**–**P17**, Table 4), which were supplemented for HDAC pulldown assays by established minimal sequence context probes mini-Lys (**P1**) and the enantiomerically pure version of **P2**, mini-L-AsuHd (**P2***). Peptides were synthesized via automated SPPS and immobilized on iodoacetyl-functionalized agarose beads. LC-MS data of purified peptides **P10**–**P17** can be found in the appendix (Chapter 7).

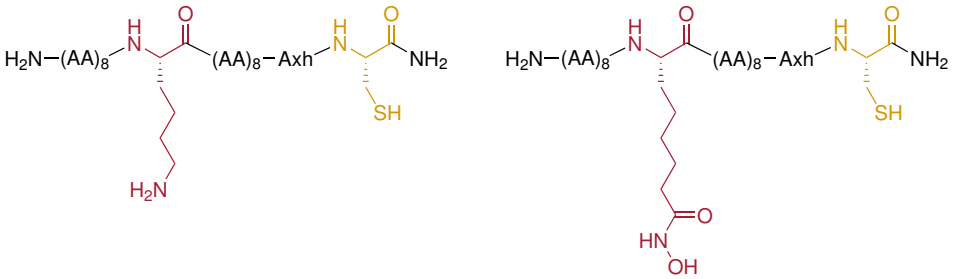

P10, **P12**, **P14**, **P16** **P11**, **P13**, **P14**, **P17**

Figure 32: Peptide-based affinity probes **P10**–**P17** based on selected HDAC6 susbtrate sites. The central lysine residue or the respective HDAC-trapping amino acid L-AsuHd are depicted in red and the C-terminal cysteine residue is shown in yellow.

Pulldown assays were then conducted as described before for conventional mini-probes (Chapter 2.1.2.3) with the immobilized HDAC substrate peptides and HeLa lysate (1 mg mL^{-1}, 200 µg total protein). Chemiluminescent images for HDAC6 and HDAC1 from western blot analysis are shown in Figure 33.

As observed in the 96-well pulldown assay, HDAC6 could be enriched on all of the chosen L-AsuHd-containing probes when compared to the respective lysine controls. Consistent with previous experiments, the mini-AsuHd probe did recruit both HDAC6 and HDAC1 to a similar extent with respect to the input. The AsuHd-containing HSP90-, CRTC- and PPIA-probe also efficiently recruited HDAC1, which was unexpected when compared to the results of the 96-well assay, where recruitment was much less pronounced. This could probably be explained by the fact that differences in the recruitment of HDACs on different peptide sequences were only observable in previous experiments at input concentrations well below 1 mg mL^{-1}.[136,142] However, in relation to the input signal (set to 8 % of the theoretical maximum signal intensity for 200 µg total protein), HDAC6 was more strongly enriched on the CRTC- (25 % signal intensity) and PPIA-probe (20 % signal intensity) than HDAC1 (5 % and 10 % signal intensity, respectively). Interestingly, recruitment to the control HSP90-Lys (**P12**) was high for both HDACs when compared to the other lysine controls, hinting at a strong reinforcement of binding by the sequence context of the HSP90-probes.

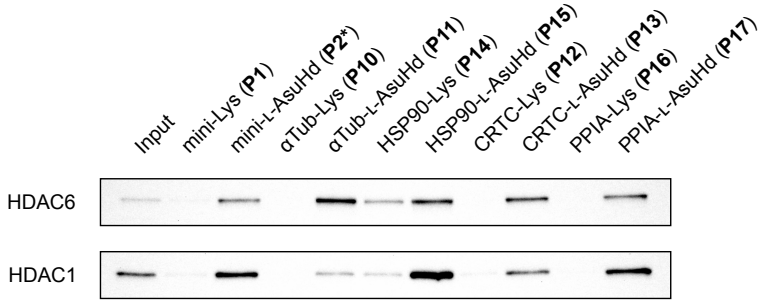

Figure 33: Pulldown with selected HDAC6 substrate peptides **P10**–**P17** and HeLa lysate (1 mg mL^{-1}, 200 µg total protein). Input samples: 16 µg.

Results for the α-tubulin-probes (**P10**, **P11**), however, were fully consistent with the 96-well assay and with previous results, showing strong enrichment of HDAC6 but only very slight enrichment of HDAC1 when compared to the lysine control, confirming the repulsive nature of the tubulin sequence context on other HDACs than HDAC6.[136]

2.2.2.2 Interactomes of selected HDAC6 substrate peptides

In order to evaluate the influence of the substrate site sequence context on the recruitment of HDAC6 binding partners on a proteome-wide level, samples from pulldown assays with selected HDAC6 substrate peptides **P10**–**P17** and mini-probes **P1** and **P2*** were also analyzed by LC-MS / MS, again in cooperation with the group of *I. Finkemeier* (Westfälische Wilhelms-Universität Münster).

Sample preparation using the FASP protocol and downstream data analysis were performed in the same way as described for mini-probes **P1**–**P3** (Chapter 2.1.2.4). Statistical

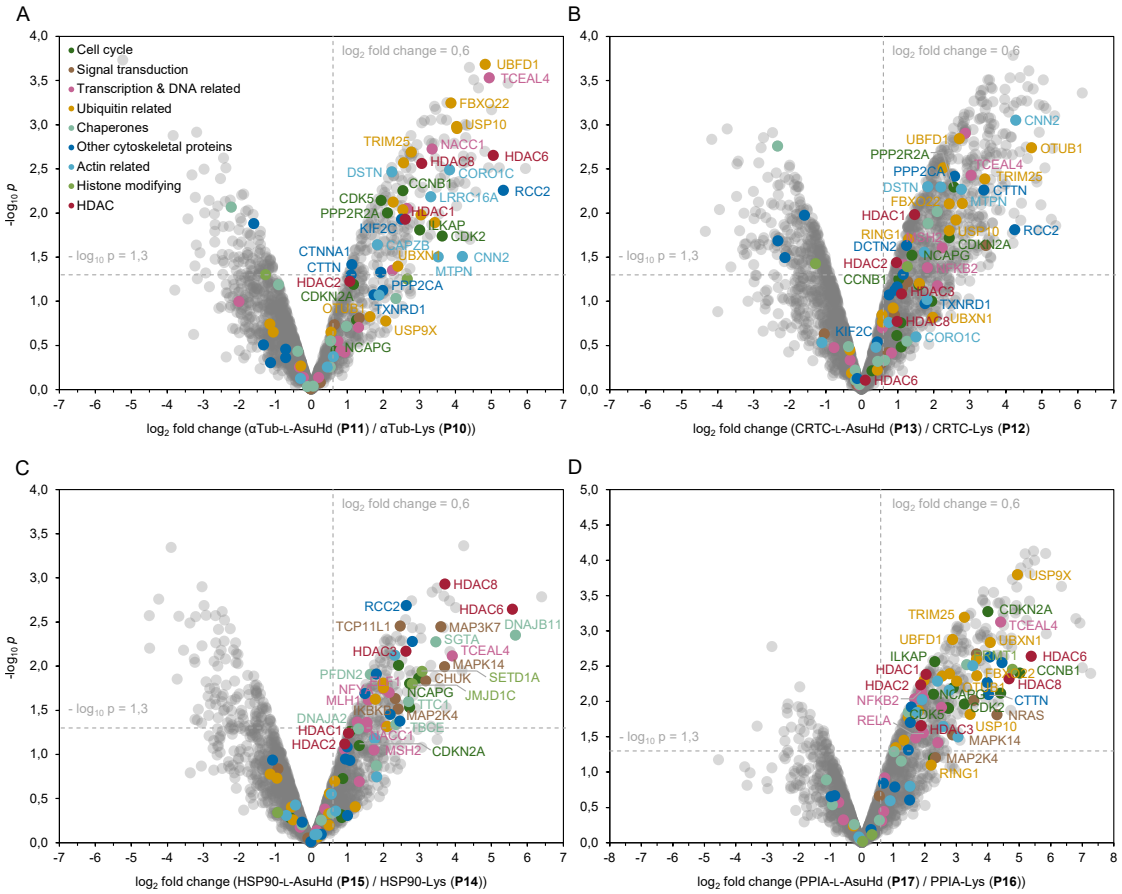

Figure 34: Volcano plots of proteomic pulldown experiments of (A) αTub-L-AsuHd (**P11**) versus αTub-Lys (**P10**), (B) CRTC-L-AsuHd (**P13**) versus CRTC-Lys (**P12**), (C) HSP90-L-AsuHd (**P15**) versus HSP90-Lys (**P14**), and (D) PPIA-L-AsuHd (**P17**) versus PPIA-Lys (**P16**). Mean $\log_2$-fold enrichment ratios of the respective probes are plotted against the negative $\log_{10} p$ value of statistical analysis. Cut-off values indicating significantly enriched proteins were set at $p \leq 0.05$ ($-\log_{10} p > 1.3$) and $\log_2$-fold enrichment ≥ 0.6. Experiments were performed as biological triplicates using HeLa lysate (0.5 mg mL^{-1}, 100 µg total protein).

analysis was performed with proteins identified in each of three biological replicates with different batches of cell lysate and results were visualized by volcano plots (Figure 34). The $\log_2$-fold enrichment ratios of αTub-L-AsuHd (**P11**), CRTC-L-AsuHd (**P13**), HSP90-L-AsuHd (**P15**) and PPIA-L-AsuHd (**P17**) in comparison to their respective lysine controls were plotted against the negative $\log_{10} p$ value of the statistical analysis. With cut-off values set at $p \leq 0.05$ ($-\log_{10} p > 1.3$) and $\log_2$-fold enrichment ≥ 0.6, proteins significantly enriched more than 1.5-fold on the respective AsuHd-containing probe versus the control are located in the upper right-hand section of the plots. The volcano plot of mini-L-AsuHd (**P2***) versus mini-Lys (**P1**) can be found in the appendix (Chapter 7). In addition to HDACs, selected proteins identified on at least one of the four probes were grouped into eight categories according to their cellular function. A further subselection of these proteins is labeled with their gene names in Figure 34 and listed in Table 5 together with their enrichment ratios between AsuHd and Lys for better comparison among the different probes.

Table 5: Selected proteins identified in the interactomes of αTub-L-AsuHd (**P11**), CRTC-L-AsuHd (**P13**), HSP90-L-AsuHd (**P15**) and PPIA-L-AsuHd (**P17**) in relation to the respective lysine controls. Protein names are listed together with their UniProt ID, gene name and $\log_2$-fold enrichment ratios. Bold numbers indicate statistical significance of $p \leq 0.05$.

UniProt ID	Protein	Gene	$\log_2$ fold change			
HDAC			αTub	CRTC	HSP90	PPIA
Q13547	Histone deacetylase 1	HDAC1	**2.62**	**1.47**	1.03	**2.04**
Q92769	Histone deacetylase 2	HDAC2	1.07	**0.97**	0.93	**1.88**
O15379	Histone deacetylase 3	HDAC3	-	1.12	**2.63**	**1.88**
Q9UBN7	Histone deacetylase 6	HDAC6	**5.05**	0.10	**5.59**	**5.38**
Q9BY41	Histone deacetylase 8	HDAC8	**3.07**	0.99	**3.71**	**4.68**
Histone modifying						
Q15652	Probable JmjC domain-containing histone demethylation protein 2C	JMJD1C	-	-	**2.80**	0.03
Q99873	Protein arginine N-methyltransferase 1	PRMT1	2.66	**1.27**	–0.94	**4.79**
O15047	Histone-lysine N-methyltransferase SETD1A	SETD1A	–1.27	–1.27	**3.07**	0.32
Actin related						
P47756	F-actin-capping protein subunit beta	CAPZB	**1.84**	0.40	0.15	0.91
Q99439	Calponin-2	CNN2	**4.20**	**4.28**	**2.32**	**2.40**
Q9ULV4	Coronin-1C	CORO1C	**3.85**	1.51	1.81	**1.91**
P60981	Destrin	DSTN	**2.24**	**1.84**	–0.69	**3.06**
Q5VZK9	F-actin-uncapping protein LRRC16A	LRRC16A	**3.32**	–1.10	0.10	1.53
P58546	Myotrophin	MTPN	**3.52**	**2.78**	1.76	**3.52**
Other cytoskeletal proteins						
P35221	Catenin alpha-1	CTNNA1	**1.13**	–0.12	0.99	0.69
Q14247	Src substrate cortactin	CTTN	1.11	**3.40**	–0.02	**4.03**
Q13561	Dynactin subunit 2	DCTN2	**–1.60**	**1.25**	–0.25	0.30
Q99661	Kinesin-like protein KIF2C	KIF2C	**2.51**	0.44	0.95	**1.55**
P67775	Serine/threonine-protein phosphatase 2A catalytic subunit alpha isoform	PPP2CA	1.99	**2.59**	**1.49**	**3.98**
Q9P258	Protein RCC2	RCC2	**5.34**	**4.26**	**2.64**	**4.45**
Q16881	Thioredoxin reductase 1, cytoplasmic	TXNRD1	1.74	1.77	1.07	**4.07**
Chaperones						
O60884	DnaJ homolog subfamily A member 2	DNAJA2	0.53	–0.06	1.31	1.03
Q9UBS4	DnaJ homolog subfamily B member 11	DNAJB11	-	–0.16	**5.67**	-
Q9UHV9	Prefoldin subunit 2	PFDN2	2.35	**2.10**	**1.64**	**3.33**
O43765	Small glutamine-rich tetratricopeptide repeat-containing protein alpha	SGTA	**–2.22**	0.64	**3.46**	–0.24
Q15813	Tubulin-specific chaperone E	TBCE	0.98	0.45	**2.35**	0.56
Q99614	Tetratricopeptide repeat protein 1	TTC1	–0.10	**1.85**	**2.71**	1.26
Ubiquitin related						
Q8NEZ5	F-box only protein 22	FBXO22	**3.88**	**2.44**	-	**3.65**
Q96FW1	Ubiquitin thioesterase OTUB1	OTUB1	1.63	**4.72**	0.49	**3.02**
Q06587	E3 ubiquitin-protein ligase RING1	RING1	-	**1.31**	**2.10**	2.21
Q14258	E3 ubiquitin/ISG15 ligase TRIM25	TRIM25	**2.78**	**3.43**	0.50	**3.25**
O14562	Ubiquitin domain-containing protein UBFD1	UBFD1	**4.83**	**2.71**	-	**2.88**
Q04323	UBX domain-containing protein 1	UBXN1	**2.41**	1.98	-	**4.08**
Q14694	Ubiquitin carboxyl-terminal hydrolase 10	USP10	**4.04**	**2.44**	1.22	**3.44**
Q93008	Probable ubiquitin carboxyl-terminal hydrolase FAF-X	USP9X	2.07	–0.33	0.18	**4.94**
Transcription & DNA related						
P32519	ETS-related transcription factor Elf-1	ELF1	-	-	**2.16**	-
P40692	DNA mismatch repair protein Mlh1	MLH1	–0.33	–0.19	**1.58**	0.73
P43246	DNA mismatch repair protein Msh2	MSH2	**2.66**	**2.24**	1.74	**1.71**
Q96RE7	Nucleus accumbens-associated protein 1	NACC1	**3.36**	**1.16**	**1.55**	**1.96**
Q00653	Nuclear factor NF-kappa-B p100 subunit	NFKB2	1.32	**1.83**	–0.31	**1.89**
P23511	Nuclear transcription factor Y subunit alpha	NFYA	-	-	**2.01**	-
Q96EI5	Transcription elongation factor A protein-like 4	TCEAL4	**4.95**	**3.04**	**3.92**	**4.41**
Q04206	Transcription factor p65	RELA	0.78	–0.20	-	**1.96**
Signal transduction						
O15111	Inhibitor of nuclear factor kappa-B kinase subunit alpha	CHUK	-	–0.16	**3.18**	-
O14920	Inhibitor of nuclear factor kappa-B kinase subunit beta	IKBKB	-	–1.04	**2.33**	-
P45985	Dual specificity mitogen-activated protein kinase kinase 4	MAP2K4	–0.02	1.14	**2.41**	2.35
O43318	Mitogen-activated protein kinase kinase kinase 7	MAP3K7	-	0.55	**3.60**	-
Q16539	Mitogen-activated protein kinase 14	MAPK14	-	0.91	**3.70**	**2.89**
P01111	GTPase NRas	NRAS	0.25	–0.13	–0.93	**4.30**
Q9NUJ3	T-complex protein 11-like protein 1	TCP11L1	-	1.28	**2.47**	0.56
Cell cycle						
P14635	G2/mitotic-specific cyclin-B1	CCNB1	**2.54**	1.04	0.84	**5.01**
P24941	Cyclin-dependent kinase 2	CDK2	**3.64**	1.59	0.88	**3.26**
Q00535	Cyclin-dependent-like kinase 5	CDK5	**1.94**	0.30	0.84	**2.76**
P42771	Cyclin-dependent kinase inhibitor 2A	CDKN2A	1.18	**2.44**	1.33	**4.01**
Q9H0C8	Integrin-linked kinase-associated serine/threonine phosphatase 2C	ILKAP	**3.02**	-	–0.58	**2.33**
Q9BPX3	Condensin complex subunit 3	NCAPG	0.69	**1.40**	**2.73**	**2.28**
P63151	Serine/threonine-protein phosphatase 2A 55 kDa regulatory subunit B alpha isoform	PPP2R2A	**2.12**	**2.57**	**2.73**	**2.90**

The interactome of αTub-L-AsuHd (**P11**) versus the lysine control (Figure 34 A) shows a strong enrichment of HDAC6 (marked red), ranging among the most highly enriched proteins on this probe. In addition, HDAC1, HDAC2 and HDAC8 were recruited, but with HDAC2 being only marginally enriched and without statistical significance. The comparably strong enrichment of HDAC1 and HDAC8 could probably be explained by the previous observation that the sequence context probes αTub-AsuHd as well as p53-AsuHd are only able to differentiate efficiently between different HDACs at strongly reduced input concentrations.[136,142]

Two major functional categories of proteins identified on the αTub-L-AsuHd (**P11**) probe are actin related (marked light blue) and other cytoskeletal proteins (marked dark blue). Since HDAC6 is known to be involved in the regulation of microtubule polymerization by direct deacetylation of α-tubulin,[49] is appears plausible, that it may also be able to exert indirect influence on cytoskeleton organization through interaction with other regulatory proteins. RCC2, the third most strongly enriched protein in the interactome of **P11**, is a regulatory protein involved in organization of the microtubule cytoskeleton during interphase and required for correct assembly of the mitotic spindle.[185] Kinesin-like protein KIF2C plays a key role in micotubule depolymerization and chromosome segregation during mitosis.[186] Catenin alpha-1 (CTNNA1) is a component of adherens junctions of epithelial cells, which connect the actin cytosekleton to the plasma membrane, resulting in adhesive contacts between cells.[187] Strongly enriched calponin-2 (CNN2) is able to bind to actin, calmodulin and tropomyosin, and is involved in the modulation of smooth muscle contraction.[188] F-actin-capping protein subunit beta (CAPZB) regulates actin filament growth by blocking the exchange of subunits at the fast growing end of the filaments.[189] Myotrophin (MTPN) on the other hand inhibits the F-actin-capping protein complex formed by CAPZB and CAPZA1.[190] Destrin (DSTN) binds to actin monomers and depolymerizes F-actin.[191]

A third major category of proteins identified on αTub-L-AsuHd (**P11**) is related to cell cycle control (marked dark green). Cyclin-dependent kinases 2 (CDK2) and 5 (CDK5) are important serine / threonine protein kinases, with the first being required for normal progression through the cell cycle from the G1 (gap 1) phase to the S (synthesis) phase, and the latter being responsible for cell cycle arrest in neuronal cells.[192,193] G2 / mitotic-specific cyclin-B1 (CCNB1) forms a complex with the protein kinase CDK1, which is essential for transition of the cell from the G2 (gap 2) phase into mitosis.[194] Serine / threonine-protein phosphatase 2A, of which the 55 kDa regulatory subunit B alpha (PPP2R2A) is found in the interactome of **P11**, also mediates the G2-mitosis transition through dephosphorylation of its substrate protein.[195] Integrin-linked kinase-associated serine / threonine phosphatase 2C (ILKAP) is another protein phosphatase involved in cell cycle control, which in addition modulates cell adhesion and growth factor signaling by association with integrin linked kinase (ILK).[196]

By using its C-terminal zinc finger (ZnF) ubiquitin binding domain, HDAC6 is thought to be involved in the proteasome-independent clearance of misfolded, ubiquitinylated proteins from the cytosol.[50] It is thus not surprising that another large fraction of strongly enriched proteins on the αTub-L-AsuHd (**P11**) probe is constituted by ubiquitin related proteins (marked yellow), like ligases or hydrolases, or ubiquitin domain containing proteins.

In the interactome of CRTC-L-AsuHd (**P13**) (Figure 34 B) HDAC1, HDAC2, HDAC3 and HDAC8 were all enriched to a comparable extent, but only HDAC1 and HDAC2 with statistical significance. HDAC6 was not enriched on either CRTC-L-AsuHd (**P13**) or its control CRTC-Lys (**P12**), indicating even binding to both probes, which could stem from interaction of the HDAC primarily with the amino acid sequence context of the probe rather than the hydroxamic acid moiety. This is, however, contradictory to the western blot results of pulldown assays with **P12** and **P13** (Chapter 2.2.2.1).

Compared to αTub-L-AsuHd (**P11**), the interactome of CRTC-L-AsuHd (**P13**) versus the lysine control does not show preferential enrichment of one or more of the eight designated functional categories of proteins. Instead, several proteins of each category are found to interact with this probe. Most notably, among cytoskeletal proteins, the known HDAC6 substrate cortactin (CTTN) is strongly enriched with high significance. By deacetylation of cortactin, which is able to bind to F-actin and promotes its branching in the periphery of the cell, HDAC6 modulates cell motility.[197] With dynactin subunit 2 (DCTN2) a component of the dynein-dynactin microtubule motor complex was found to interact with **P13**. HDAC6 is known to bind to subunit 1 (DCTN1) of dynactin, which acts as linking protein between microtubules, dyneins and their cargos, thus enabling transport of vesicles and organelles along microtubules.[49,198]

With nuclear factor NF-kappa-B p100 (NFKB2) a subunit of the important transcription factor NF-κB was found in the interactome of **P13**. NF-κB is the target of a multitude of signaling pathways, ultimately regulating many biological processes like inflammation, immune response or apoptosis by promoting or repressing transcription of the respective genes.[199]

The interactome of HSP90-L-AsuHd (**P15**) versus the lysine control (Figure 34 C) shows again strong enrichment of HDAC6 and HDAC8, and medium enrichment of HDAC3. HDAC1 and HDAC2 were only weakly enriched and without statistical significance.

Regarding the function of other recruited proteins, HSP90-L-AsuHd (**P15**) exhibits a very different binding pattern when compared to αTub-L-AsuHd (**P11**) and CRTC-L-AsuHd (**P13**). While recruitment of ubiquitin related proteins is strongly reduced, the chaperone-derived HSP90 sequence context seems to preferentially enrich other chaperone proteins (marked light teal). A co-chaperone of HSPA5, which is responsible for correct protein folding in the lumen of the endoplasmatic reticulum (ER), DnaJ homolog subfamily B member 11 (DNAJB11) is the second most strongly enriched protein on **P15**.[200] Small glutamine-rich tetratricopeptide repeat-containing protein alpha (SGTA) is also a co-chaperone, that mediates transport of misfolded proteins to the ER or regulates their proteasomal degradation, if mediation fails.[201] Prefoldin subunit 2 (PFDN2) is responsible for the transfer of target proteins to cytosolic chaperonin (c-CPN) and also promotes folding of nascent polypeptide chains.[202] Most notably, with tubulin-specific chaperone E (TBCE) a chaperone was found to interact with HSP90-L-AsuHd (**P15**) which is specialized in the folding of tubulin and thus thought to be essential for correct organization of the microtubule cytoskeleton.[203] Interaction of TBCE with HDAC6 therefore seems plausible, since the latter is also involved in the regulation of microtubule stability and cell motility via tubulin deacetylation.

Another group of proteins enriched on HSP90-L-AsuHd (**P15**) is comprised of transcription factors and other DNA-related proteins (marked pink). Transcription elongation factor A protein-like 4 (TCEAL4) is a transcription factor highly enriched over the lysine control not only on **P15**, but on all of the four selected HDAC6 substrate sequences, while ETS-related transcription factor Elf-1 (ELF1) and nuclear transcription factor Y subunit alpha (NFYA) are found exclusively in the interactome of **P15**.[204–206] Nucleus accumbens-associated protein 1 (NACC1) is a transcriptional corepressor, which is thought to interact with HDAC3 and HDAC4 in neuronal cells.[207] With DNA mismatch repair protein Msh2 (MSH2) and DNA mismatch repair protein Mlh1 (MLH1) two components of the post-replicative DNA mismatch repair system were also enriched on **P15**.[208]

Moreover, a subset of proteins involved in signal transduction (marked brown) was identified in the interactome of HSP90-L-AsuHd (**P15**). Of the MAP kinase signal transduction pathway, mitogen-activated protein kinase 14 (MAPK14), dual specificity mitogen-activated protein kinase kinase 4 (MAP2K4) and mitogen-activated protein kinase kinase kinase 7 (MAP3K7), were enriched on **P15**. The MAP kinase signaling cascade is integral to the cellular response to diverse external stimuli, like environmental stress or signals related to cell proliferation, differentiation, inflammation and apoptosis.[209] Inhibitor of nuclear factor kappa-B kinase subunit alpha (CHUK) and inhibitor of nuclear factor kappa-B kinase subunit beta (IKBKB) are both part of the IKK (IκB kinase) complex involved in the canonical signaling pathway leading to NF-κB activation. The IKK complex phosphorylates inhibitors of NF-κB (IκB), which are subsequently ubiquitinylated and degraded by the proteasome.[199]

Other histone modifying enzymes (marked light green) found to interact with HSP90-L-AsuHd (**P15**) include strongly enriched histone-lysine N-methyltransferase SETD1A (SETD1A) as well as probable JmjC domain-containing histone demethylation protein 2C (JMJD1C).[210,211]

In the interactome of PPIA-L-AsuHd (**P17**) versus the lysine control, HDAC6 is again the most strongly enriched HDAC, followed by HDAC8. HDAC1, HDAC2 and HDAC3 are all enriched to a comparable and medium extent, but with statistical significance.

Although many cell cycle related proteins, transcription factors (such as the p65 (RELA) subunit of NF-κB) and cytoskeletal proteins are also efficiently recruited to **P17**, the most prominently enriched functional category seems to be the one of ubiquitin related proteins. Of all four selected HDAC6 substrate sequence probes, PPIA-AsuHd (**P17**) enriched the largest number of these proteins with statistical significance. Probable ubiquitin carboxyl-terminal hydrolase FAF-X (USP9X) and ubiquitin carboxyl-terminal hydrolase 10 (USP10) remove ubiquitin from substrate proteins, with the latter being known to target p53, thereby regulating its stability.[212,213] Ubiquitin domain-containing protein UBFD1 (UBFD1) as well as UBX domain-containing protein 1 (UBXN1) (with the UBX domain being structurally related to ubiquitin) are both thought to be involved in regulation of the NF-κB signaling pathway and may interact with the ubiquitin binding domain of HDAC6.[214,215] With F-box only protein 22 (FBXO22) the substrate-recognition component of an E3 ubiquitin ligase complex was enriched on **P17**, as well as the E3 ubiquitin/ISG15 ligase TRIM25 (TRIM25), which is involved in protein degradation and cellular signaling as a response to viral infections.[216,217] The E3 ubiquitin-protein ligase RING1 (RING1) on the other hand plays a role in epigenetic transcriptional repression through monoubiquitinylation of K199 of histone H2A.[218]

Other notable interactors with **P17** include the histone modifying protein arginine N-methyltransferase 1 (PRMT1) and the GTPase NRas (NRAS) of the Ras superfamily of small GTPases, involved in cell proliferation via the MAP kinase signal transduction pathway.[219,220]

In summary, analysis of pulldowns with selected HDAC6 substrate peptides **P10**–**P17** by LC-MS / MS uncovered a specific interaction profile for each of the employed peptide sequence contexts and further supports the notion, that substrate selectivity of HDACs is mediated by their interaction partners. With the biological roles of identified interacting proteins being consistent with the current knowledge about the cellular functions of HDAC6, the applied proteomics approach also helped to reveal many previously unknown potential binding partners of this HDAC.

2.2.2.3 Kinetic measurements with recombinant HDAC6

After high-throughput screening of potential substrate sequences for HDAC6 binding and further in-depth analysis of the interaction partners involved, it was of interest whether the observed binding pattern of the HDAC also translates into preferences regarding catalysis. To this end, acetylated lysine embedded into multiple sequence contexts should be deacetylated by recombinant HDAC6 and reaction velocities should be compared. A suitable method for monitoring the deacetylation reaction was found in a MALDI-MS-based assay originally

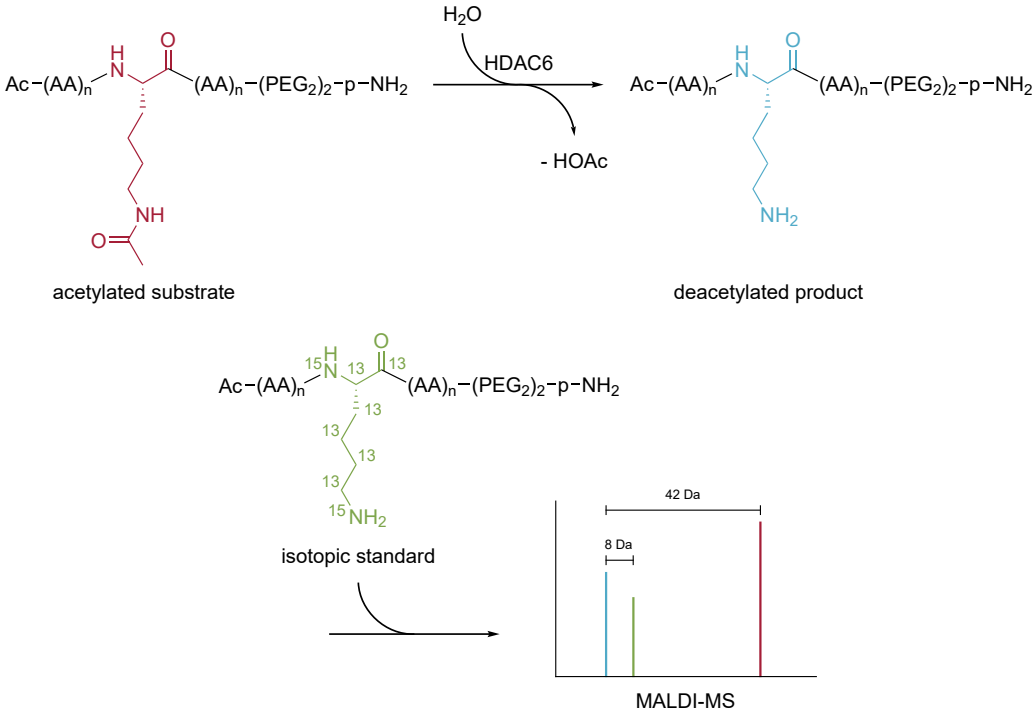

Figure 35: General principle of the MALDI-MS-based deacetylation assay. The substrate containing an acetylated lysine residue is marked in red, the deacetylated product is shown in blue, and the isotopically labeled standard is depicted in green. Respective signals in the MALDI-MS spectrum are coded with the same colors. Masses of the acetylated substrate and deacetylated product differ by 42 Da, whereas deacetylated product and isotopic standard differ by 8 Da.

established to measure activity of endogenous HDACs from cellular lysates.[175] This assay seemed ideal for complementing the previous high-throughput approach, since it allows the readout of many samples in a miniaturized format, requiring only picomol amounts of peptide and femtomol amounts of enzyme. Quantification is achieved by direct comparison of MS signal intensities of the deacetylation product with an isotopically labeled internal standard.

The general principle of the MALDI-MS-based deacetylation assay is outlined in Figure 35. In a first step, a substrate peptide incorporating an acetylated lysine residue is deacetylated by HDAC6 and the reaction is stopped at selected time points by addition of an HDAC inhibitor. However, the deacetylated product of the reaction cannot be quantified directly in comparison to the acetylated substrate using MALDI-MS, since both peptides could differ with respect to their ionization properties. To this end, a defined amount of isotopically labeled standard peptide is added to the sample in a second step. The standard peptide is chemically identical to the deacetylated product of the reaction and contains an isotopically labeled lysine residue (Lys8), which causes a mass shift of 8 Da. The reaction sample can then be measured by MALDI-MS and distinct signals of the acetylated substrate, deacetylated product and isotopic standard can be observed. In the last step, using the ratio of isotopically labeled standard and deacetylated product, MS signal intesities can be converted to molar concentrations.

In order to asses the influence of different substrate site sequence contexts on the HDAC6-catalyzed deacetylation, the MALDI peptides examined were based on the four previously selected sequences (α-tubulin, CRTC, HSP90, PPIA) originating from the 96-well pulldown screening (Table 6). These sites were again supplemented by a minimal sequence context version, employing only two flanking glycine residues. For each sequence, two peptides were synthesized via automated solid-phase peptide synthesis: One substrate peptide containing an acetylated lysine residue and one standard peptide instead containing isotopically labeled Lys8. Lys8 was introduced manually as *N*α-Fmoc- and *N*ε-Boc-protected building block Fmoc-Lys8(Boc)-OH, which was synthesized from $^{13}C_6$,$^{15}N_2$-L-lysine as reported previously.[175] Methionine in the α-tubulin peptides **P20** and **P21** was replaced by norleucine (Nle) in order to prevent oxidation during ionization, thereby simplifying analysis of the MS spectra.

Table 6: Potential substrate sites of HDAC6 examined with the MALDI-MS-based deacetylation assay. For each protein the ID of the canonical sequence according to UniProt, the corresponding gene name, the position of the acetylation site, and a sequence window of 16 amino acids embedding the acetylated lysine are given. In addition, for each sequence the abbreviations of the corresponding MALDI substrate or isotopic standard peptides are listed, containing either Lys(Ac) or Lys8.

UniProt ID	Protein	Gene	Sequence	Position	Lys(Ac)	Lys8
-	mini-probe	-	GKacG	-	**P18**	**P19**
Q71U36	Tubulin alpha-1A chain	TUBA1A	PDGQNlePSDKacTIGGGDDS	40	**P20**	**P21**
Q6UUV7-1	CREB-regulated transcription coactivator 3	CRTC3	PLHRRSGDKacPGRQFDGS	113	**P22**	**P23**
P07900-1	Heat shock protein HSP 90-alpha	HSP90AA1	GTKVILHLKacEDQTEYLE	191	**P24**	**P25**
P62937	Peptidyl-prolyl cis-trans isomerase A	PPIA	VSFELFADKacVPKTAENF	28	**P26**	**P27**

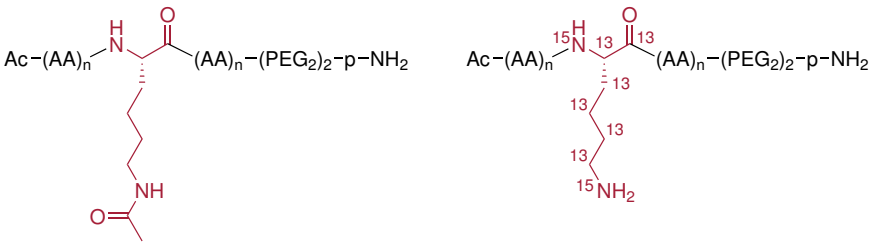

Figure 36: Substrate (**P18**, **P20**, **P22**, **P24**, **P26**) and isotopically labeled standard peptides (**P19**, **P21**, **P23**, **P25**, **P27**) for the MALDI-MS-based HDAC deacetylation assay. The acetylated lysine or the $^{13}C_6$,$^{15}N_2$-lysine (Lys8) residue is depicted in red. n = 1 for mini peptides (**P18** and **P19**) and n = 8 for peptides with extended sequence context (**P20**–**P27**).

The general design of MALDI peptides **P18**–**P27** is depicted in Figure 36. The acetylated lysine residue or $^{13}C_6$,$^{15}N_2$-lysine (Lys8) as central amino acids are embedded into a sequence context of eight residues N- and C-terminal to the acetylation site in peptides **P20**–**P27**. For mini peptides **P18** and **P19** the sequence context only comprises two flanking glycine residues. In analogy to the 96-well HDAC affinity probes, the original design of the MALDI peptides further comprises a C-terminal extension with a D-proline amide and a polyethylene glycol-based spacer to prevent degradation by carboxypeptidases in cellular lysates. Although in this work recombinant, purified enzyme was used, the established design was retained in order to increase solubility of the peptides through the PEG spacer and to preserve flexibility for multiple applications. The N-termini of peptides were acetylated to improve stability. LC-MS data of the HPLC-purified, final peptides **P18**–**P27** is included in the appendix (Chapter 7).

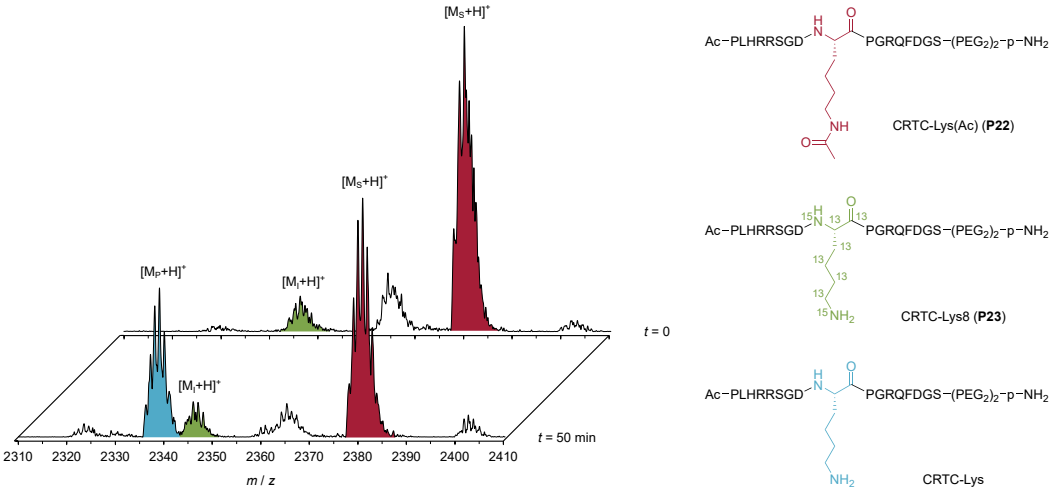

Figure 37: MALDI mass spectra of the deacetylation reaction with CRTC-Lys(Ac) (**P22**) and HDAC6 after 0 and 50 min. The proton signal of the acetylated substrate **P22** ($[M_S+H]^+$) is marked in red, the signal of the isotopic standard CRTC-Lys8 (**P23**) ($[M_I+H]^+$) is marked in green, and the signal of the deacetylated product CRTC-Lys ($[M_P+H]^+$) is marked in blue. Other peaks stem from sodium or potassium adducts, respectively. Spectra were normalized to the intensity of the $[M_I+H]^+$ peak of the isotopic standard.

The feasibility of the MALDI-MS-based deacetylation assay was then tested with recombinant, full-length human HDAC6 and the CRTC-Lys(Ac) (**P22**) peptide at a fixed substrate concentration of 100 µM. An enzyme concentration of 100 nM proved to be suitable for monitoring the reaction. After 50 min a sample of the reaction was stopped by addition of the HDAC inhibitor trichostatin A (TSA), sufficiently diluted, spotted onto a polished steel target, and measured by MALDI-MS. Figure 37 shows the corresponding mass spectrum in comparison to the mass spectrum of a sample recorded without enzyme, representing $t = 0$. For all three species, CRTC-Lys(Ac) (**P22**), CRTC-Lys8 (**P23**) and CRTC-Lys, distinct molecular ion peaks as proton adducts could be observed. The peak of the deacetylated product CRTC-Lys (labeled in blue) appears shifted by –42 Da from the peak of the substrate CRTC-Lys(Ac) (**P22**) (labeled in red). While the intensity of the isotopic standard (labeled in green), which is shifted from CRTC-Lys by +8 Da, remained constant in proportion to the other signals, intensity for the deacetylated product increased over time, indicating that the recombinant HDAC6 was active under the reaction conditions chosen and able to deacetylate the CRTC substrate.

Subsequently, in order to compare the influence of the substrate site sequence context on catalysis in a quantitative fashion, initial velocities were determined for the deacetylation of MALDI substrate peptides **P18**, **P20**, **P22**, **P24** and **P26** by HDAC6. Reactions were again performed with 100 µM of the substrates and an enzyme concentration of 100 nM. Samples were taken at time points between 0 and 25 min, stopped by addition of TSA, and spotted onto a MALDI target. After measurement and conversion into molar concentrations using the isotopic standard, data from three independent experiments were plotted against time and fitted by linear regression, resulting in Figure 38 A.

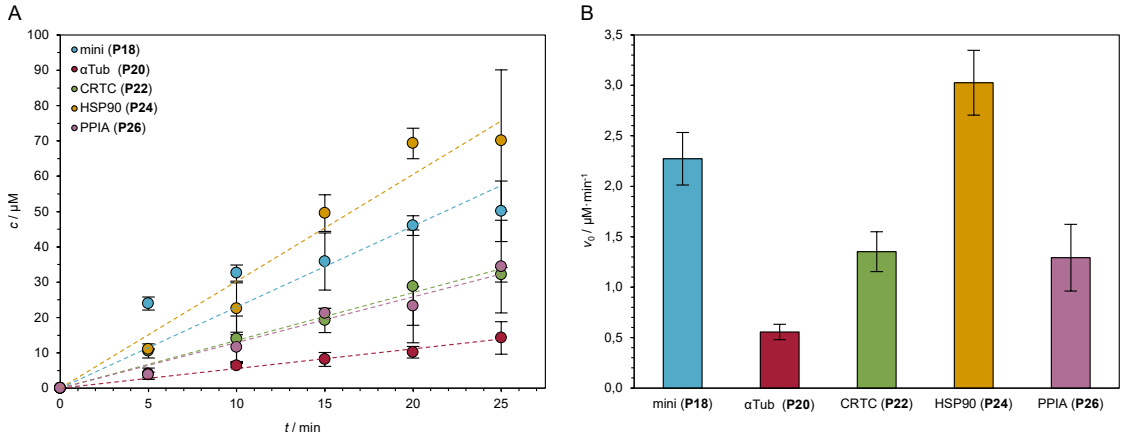

Figure 38: Results of the MALDI-MS-based deacetylation assay with HDAC6. (A) Concentration of deacetylated product plotted against the reaction time for substrates **P18**, **P20**, **P22**, **P24** and **P26**. (B) Activity profile of HDAC6 showing initial velocities v_0 for the deacetylation of substrates **P18**, **P20**, **P22**, **P24** and **P26**. Mean values and standard deviations were determined from three independent experiments.

In order to allow for a more direct comparison, mean initial velocities together with their standard deviations were visualized in Figure 38 B for each substrate. With a velocity of 3.0 µM min^{-1} deacetylation of HSP90-Lys(Ac) (**P24**) was fastest, followed by mini-Lys(Ac) (**P18**), which was deacetylated at a rate of 2.3 µM min^{-1}. CRTC-Lys(Ac) (**P22**) and

PPIA-Lys(Ac) (**P26**) showed comparable velocities for their deacetylation by HDAC6, with 1.4 µM min^{-1} and 1.3 µM min^{-1}, respectively. The αTub-Lys(Ac) peptide (**P20**) derived from the known HDAC6 substrate site K40 of α-tubulin, was deacetylated at the slowest rate of 0.6 µM min^{-1}. The reaction velocity for the substrate which was deacetylated fastest (**P24**) was approximately six-fold higher than for the substrate which was deacetylated slowest (**P20**).

To conclude, the MALDI-MS-based deacetylation assay with peptides derived from potential substrate sites of HDAC6 uncovered a distinct activity profile for the different sequence contexts, which could not have been anticipated from previous pulldown experiments (Chapter 2.2.1.5 and Chapter 2.2.2.1). In these experiments that only investigate binding affinity of the HDAC for the probe peptides, all of the five corresponding probes for mini, αTub, CRTC, HSP90, and PPIA enriched HDAC6 comparably well. The subtle differences exerted by the individual sequence contexts were likely overridden by the high-affinity hydroxamate moiety and diminished by the fact that the pulldown assay did not account for effects on enzymatic turnover.

3 Discussion

Histone deacetylases (HDACs) catalyze the deacetylation of *N*ε-acetyllysine residues, thereby regulating gene expression on an epigenetic level, as well as protein function and activity.[29] Since altered levels of HDAC activity are associated with a variety of diseases, HDACs represent potential drug targets for therapeutic treatment.[84,85] Understanding the substrate selectivity of these enzymes is therefore essential to the development of specific inhibitors. In turn, HDAC inhibitors can serve as valuable chemical tools for broadening the knowledge about the physiological function of HDACs.[91]

As part of larger multi-protein complexes that mediate catalytic activity and substrate binding, which applies especially to class I enzymes, zinc-dependent HDACs can hardly be investigated as recombinantly expressed proteins *in vitro*. Although procedures for the expression of HDACs and reconstitution of their complexes exist,[221,222] development of alternative methods for biochemical characterization of HDACs is desirable.

Peptide-based affinity probes bound to solid-support capture endogenous HDACs selectively from native cell lysates, retaining their physiologically associated binding partners, which can subsequently be analyzed.[142] These affinity probes are based on HDAC inhibitors and comprise an inhibitory, zinc-chelating moiety as well as a peptidic sequence context which is commonly derived from known HDAC substrate proteins, with both parts of the probe reinforcing binding to the enzyme.

The selectivity of an HDAC inhibitor is governed by three main structural features: The zinc-chelating functional group, a cap moiety, and the linker connecting both parts.[90] This model can also be applied to peptide-based affinity probes and different combinations of functional groups and peptide sequence contexts allow fine-tuning their selectivity. With the ultimate goal of addressing all human HDACs individually, flexible sets of affinity probes exploiting various functional groups and sequence contexts represent promising tools for profiling HDAC specificity and complex assembly. However, with advancements in MS / MS-based proteomics revealing hundreds of acetylation sites potentially regulated by HDAC activity,[26,27] HDAC affinity probes also need to be adapted to new high-throughput approaches of analysis.

3.1 HDAC selectivity mediated by functional groups

The first part of this work focused on influencing HDAC selectivity mediated by the zinc-chelating functional group of peptide-based affinity probes (Chapter 2.1). To this end, building blocks for solid-phase peptide synthesis were developed based on the scaffold of known HDAC inhibitors, that allow the incorporation of HDAC-trapping amino acids of the hydroxamate-, 2-aminophenylamide- and ketone-type into synthetic peptides, which were then applied in biochemical HDAC assays.

3.1.1 Synthesis of a Trt-protected hydroxamate building block

Resembling the carbon chain length of the potent, nanomolar HDAC inhibitor suberoylanilide hydroxamic acid (SAHA), α-aminosuberic acid ω-hydroxamate (AsuHd) emerged as an ideal building block for incorporating the hydroxamic acid moiety into peptide-based HDAC probes.

Shortly after the identification of SAHA as HDAC inhibitor, the potential of AsuHd was recognized as an amino acid analogue to be incorporated into synthetic peptides, e.g. into the cyclic inhibitor CHAP (cyclic hydroxamic-acid-containing peptide), which combines the aliphatic hydroxamic acid side chain with the cap moiety of trapoxin, another potent HDAC inhibitor.[117] However, in this approach AsuHd was installed using a precursor and converted into the hydroxamic acid after cyclization of the CHAP peptide upon cleavage off the solid-phase or in solution, thus limiting its synthetic application.

To this date, only a few protected AsuHd building blocks for peptide synthesis have been reported and only some of these are suitable for fully automated, Fmoc-based SPPS (Figure 39).

The *N*α-Boc-protected *O*-benzyl hydroxamate **23** was obtained from α-aminosuberic acid (Asu) by a four-step synthesis and incorporated into a cyclic peptidomimetic, with the Boc group intended for cleavage in solution prior to cyclization of the compound.[147] Together with the *N*α-Boc protection, necessity to cleave the Bn group by hydrogenolysis or with strong acids limits the utility of this building block with standard SPPS protocols.

*N*α-Fmoc-protected *O*-(*p*-methoxybenzyl) (PMB) hydroxamate **24** was synthesized through a five-step procedure also using Asu as starting material.[148] With Fmoc protection and the PMB group being removable by standard cleavage cocktails containing TFA, this building block can be used in automated SPPS without limitations. However, synthesis according to the published route is complicated by the fact that the reaction conditions used are not fully compatible with the Fmoc protecting group, which gets cleaved in one step and needs to be re-installed at a later stage.

*N*α-Alloc-protected *O*-*tert*-butyl hydroxamate **25**, which is accessible through a four-step synthesis in analogy to **23** and **24**, circumvents this problem by using the Alloc group for α-amino protection.[142,143] Although the *t*Bu hydroxamate is compatible with standard SPPS cleavage conditions, the Alloc group has to be removed manually, e.g. using palladium(0) complexes and suitable borane scavengers under exclusion of ambient atmosphere.[223] Hence, **25** can only be applied in semi-automated approaches with a limited numer of peptides, that allow pausing the synthesis for Alloc deprotection.

The *N*α-Fmoc-protected α-allyl ester of the solid-phase-bound hydroxamate **26** represents an on-resin strategy for installing the hydroxamate moiety to the side chain of Asu.[224] In a first step, a protected version of Asu is synthesized *de novo* by olefin cross-metathesis which is then coupled to a hydroxylamine resin in a second step. After coupling of a previously synthesized C-terminal peptide part and extension of the N-terminus by SPPS, standard acidic cleavage liberates the AsuHd-containing peptide. Despite the advantage of a *de novo* synthesis of Asu from cheap and readily available precursors, the overall approach can only be automatized in part and introduction of a large C-terminal peptide may be difficult.

Two synthetic procedures for the *N*α-Fmoc-protected *O*-*tert*-butyl hydroxamate **27** were reported recently. The first route achieves the asymmetric synthesis of AsuHd by alkylation

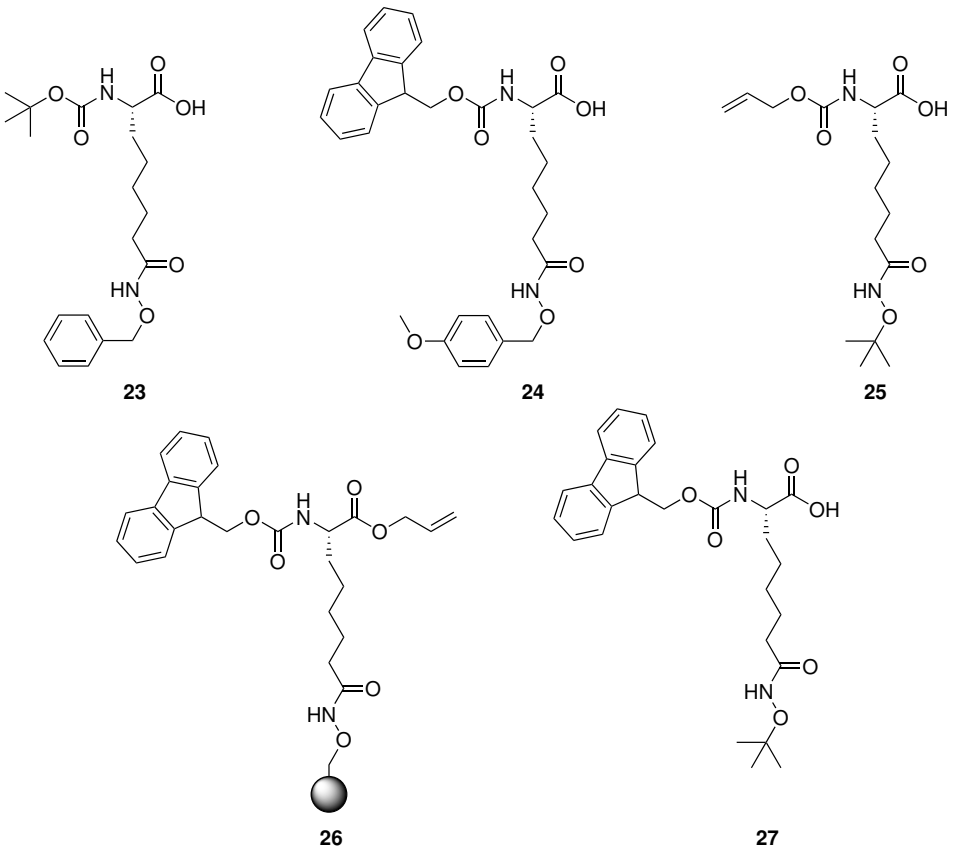

Figure 39: Examples of published AsuHd building blocks for peptide synthesis.

of a nickel complex of glycine,[149] while the second route relies on enzymatic resolution of an AsuHd derivative which is synthesized by alkylation of an acetamido malonate precursor.[150] A major advantage of **27** is the full compatibility with automated Fmoc-based SPPS.

However, the main drawback of the *t*Bu-protected building blocks is the slow reaction kinetics for the deprotection of *O*-*tert*-butyl hydroxamates, often requiring overnight incubation with SPPS cleavage cocktail. This leaves the peptide susceptible to oxidation and other side reactions, and may decrease peptide yields if only incomplete conversion is achieved.[151] In addition, incomplete deprotection complicates the use of *t*Bu hydroxamates in miniaturized synthesis and assay formats like SPOT synthesis on cellulose membranes, because SPOT peptides are not intended to be purified. Other high-throughput approaches are also strongly hampered by the demand of time for cleavage and necessity for purification.

Especially with respect to high-throughput screenings of HDAC substrate sites from proteomics experiments, it was desirable to replace the *t*Bu group for hydroxamate protection by the trityl (Trt) group, which is readily cleaved even by dilute acid (Chapter 2.1.1). However, previous attempts of installing a Trt hydroxamate to the side chain of Asu, following the same route that was used for **25**, failed.[225]

The synthetic procedure for the AsuHd building block **5** devised in this work allowed to install the Trt hydroxamate by reacting the sterically demanding *O*-tritylhydroxylamine with the acid chloride of the side chain carboxy group of Asu by using the versatile and stable precursor Asu-BBN (**2**) (Chapter 2.1.1.1). Protection of the α-amino and -carboxy group of Asu as oxazaborolidinone with 9-BBN, which tolerates a wide variety of reaction conditions, proved to be ideal for selectively modifying the side chain of the amino acid.

Methods for subsequent removal of the 9-BBN moiety of Asu-BBN (**2**) were extensively tested in a previous work.[226] Deprotection attempts with fluoride sources (Bu_4NF) or oxidation by peroxycarboxylic acids or with methanolic chloroform led to either no conversion at all, slow deprotection, or a very impure product. Cleavage with acid for AsuHd(OTrt)-BBN (**3**) was prohibited by presence of the Trt group. The most satisfactory results with **3** were obtained by "complexation" of 9-BBN with ethylenediamine as diazaborolidinone, achieving a high conversion within a few minutes. The only drawback of this method was the need for HPLC purification of the deprotected product H-AsuHd(OTrt)-OH (**4**) in order to remove excess ethylenediamine, which would otherwise react with Fmoc-OSu in the next step. It was also crucial to neutralize the HPLC fractions of **4**, due to concentration of resudual TFA from the eluents upon lyophilization, thus deprotecting the Trt group.

Fmoc protection of H-AsuHd(OTrt)-OH (**4**) had to be conducted step-wise. Reaction of the amino acid with one equivalent of Fmoc-OSu led to incomplete conversion into the desired Fmoc-AsuHd(OTrt)-OH (**5**) and to strong formation of a side product identified as Fmoc-β-alanine by LC-MS. Previous reports showed that Fmoc-OSu is converted into Fmoc-β-Ala under basic conditions and in the absence of any other suitable nucleophile by a *Lossen*-type rearrangement.[227] Although the amino group of **4** was the intended nucleophile in this reaction, the sterical demand of H-AsuHd(OTrt)-OH probably led to a slow conversion, with basic cleavage of Fmoc-OSu being the faster reaction. To circumvent this problem, only small portions of Fmoc-OSu were added to the reaction mixture at a time and the course of the reaction was followed by LC-MS. In this way, full conversion into the final building block Fmoc-AsuHd(OTrt)-OH (**5**) could be achieved without Fmoc-β-Ala formation.

HPLC purification of **5** with aqueous eluents was prohibited by its very hydrophobic nature caused by the Fmoc and Trt protecting groups. However, also flash chromatography with organic eluents on silica gel failed, because the building block **5** interacted too strongly with the stationary phase, presumably by its free α-carboxy group, and was not efficiently eluted. Addition of a small amount of formic acid to the eluent solved this problem, but also severed the Trt hydroxamate (data not shown).

Fortunately, due to its hydrophobicity, it was possible to extract Fmoc-AsuHd(OTrt)-OH (**5**) from the reaction mixture even at a near neutral pH without substantial loss in yield and sufficient purity for successful application in manual and automated SPPS.

Regarding high-throughput methods for the generation and screening of peptide libraries, the existing building block Fmoc-AsuHd(O*t*Bu)-OH (**27**) is only suitable for approaches that ensure full deprotection of the *t*Bu group, e.g for the *CelluSPOT* variant[174] of SPOT synthesis. In the *CelluSPOT* methodology cellulose-peptide conjugates are created by decomposing the cellulose membrane on which the peptides are synthesized with a cleavage cocktail containing the very strong trifluoromethanesulfonic acid (TFMSA). Although TFMSA also ensures efficient *t*Bu deprotection in this approach, it can neither be applied in standard

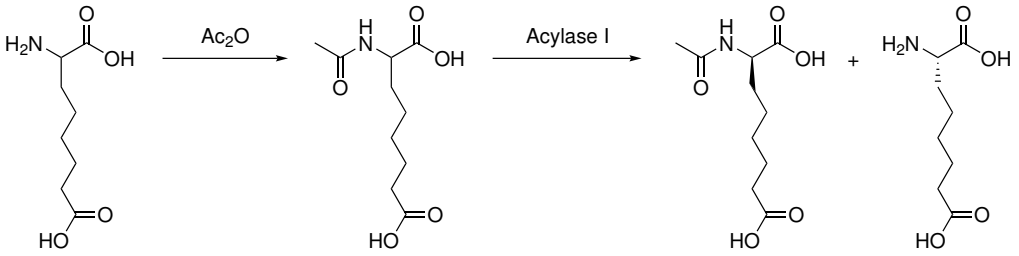

Figure 40: Scheme for the enzymatic resolution of α-aminosuberic acid adapted from *S. Kichgässner*.[228] In a firt step, H-DL-Asu-OH (**1**) could be acetylated e.g. with acetic anhydride yielding Ac-DL-Asu-OH (**28**). **28** could then be treated with readily available acylase I from porcine kidney or *Aspergillus* sp., which stereospecifically deacetylates the L-enantiomer of *N*α-acetyl amino acids. Subsequently, Ac-D-Asu-OH (**29**) and H-L-Asu-OH (**30**) could be separated and the latter used for further synthesis.

SPOT synthesis, where the membrane needs to remain intact, nor with polymeric SPPS resins, that decompose under these conditions.

The novel Fmoc-protected *O*-trityl hydroxamate Fmoc-AsuHd(OTrt)-OH (**5**) introduced in this work represents an ideal and versatile building block for introduction of the AsuHd residue into peptides by any means of Fmoc-based SPPS. With the readily cleavable Trt-group, it is especially suitable for high-throughput applications where peptide purification has to be omitted. The four-step synthetic procedure yields the final building block with a high overall yield and was easily adaptable for Fmoc-Apm(OTrt)-OH (**10**) with a shorter carbon chain.

Fmoc-AsuHd(OTrt)-OH was synthesized from racemic α-aminosuberic acid leading to the racemic building block **5**, as well as from its L-enantiomer, creating Fmoc-L-AsuHd(OTrt)-OH (**5***). For future applications the synthetic procedure of Fmoc-AsuHd(OTrt)-OH (**5**) and Fmoc-Apm(OTrt)-OH (**10**) could be further improved by including an enzymatic resolution step in analogy to the synthesis of **27** (Figure 40).[150] This would enable to synthesize Fmoc-L-AsuHd(OTrt)-OH (**5***) from racemic α-aminosuberic acid instead of using the expensive L-enantiomer.

3.1.2 Synthesis and application of a 2-aminophenylamide-based HDAC affinity probe

In order to create an HDAC-trapping amino acid with a different selectivity profile than hydroxamic acids with a broad specificity, the new synthetic route devised for Fmoc-AsuHd(OTrt)-OH (**5**) was exploited for introduction of the 2-aminophenylamide (Apa) moiety derived from benzamide-type HDAC inhibitors to the side chain of α-aminosuberic acid (Chapter 2.1.2). The resulting 2-amino-8-((2-aminophenyl)amino)-8-oxooctanoic acid or AsuApa was previously installed into a cyclic peptide HDAC inhibitor by an on-resin approach.[229] However, synthesizing a protected building block for standard SPPS seemed a more flexible strategy for the design of HDAC probes with a distinct selectivity profile.

The key step for successful synthesis of Fmoc-AsuApa(Boc)-OH (**13**) was coupling of *N*-Boc-*o*-phenylenediamine using the side chain acid chloride of Asu-BBN (**2**) (Chapter 2.1.2.1). With the aromatic amino group of the phenylenediamine derivative being less nucleophilic than

an aliphatic amine, the side chain carboxylic acid of Asu required a strong mode of activation. The stability of the oxazaborolidinone **2** enabled the comparably harsh reaction conditions necessary for a *Schotten-Baumann*-type amide synthesis. In addition, excess DIPEA served to neutralize the hydrochloric acid which is formed during this reaction, preventing hydrolysis of the 9-BBN group. The pheylenediamine derivative, on the other hand, was reacted with *N,O*-bis(trimethylsilyl)acetamide (BSA) prior to coupling with **2**, increasing its solubility in the reaction solvents and additionally activating the amino group by silylation.[230,231]

9-BBN deprotection and Fmoc protection to form the final Fmoc-AsuApa(Boc)-OH (**13**) could then be carried out in the same way as for Fmoc-AsuHd(OTrt)-OH (**5**). Importantly, in contrast to **5**, Fmoc-AsuApa(Boc)-OH (**13**) could be purified by flash chromatography without losing the side chain protecting group, yielding a cleaner product and enabling NMR analysis.

Bearing only protecting groups that are easily removed by standard SPPS cleavage cocktails, Fmoc-AsuApa(Boc)-OH (**13**) is well suited for application in parallel peptide synthesis necessary for high-throughput HDAC assays.

The ability of the zinc-chelating functional group of AsuApa to differentiate between HDAC enzymes in comparison to AsuHd was then tested after incorporation of **5** and **13** into established peptide-based HDAC affinity probes with minimal sequence context, resulting in mini-AsuHd (**P2**) and mini-AsuApa (**P3**) (Chapter 2.1.2.2). Pulldown assays for capturing endogenous HDACs were conducted with HeLa lysate and analyzed by Western blotting (Chapter 2.1.2.3). Compared to the control peptide mini-Lys (**P1**), mini-AsuHd (**P2**) enriched all HDACs of class I and IIb, and to a lesser extent HDAC4 (class IIa). Mini-AsuApa (**P3**), however, only efficiently recruited class I HDAC1, 2 and 3. HDAC8 was not enriched, which is in agreement with the reported selectivity of benzamide HDAC inhibitors.[162]

This selectivity can be explained by crystal structures of HDAC8 compared to HDAC2 co-crystallized with a series of 5-substituted *N*-(2-aminophenyl)benzamides (**31**) (Figure 41 A).[29,95] These structures show that HDAC2 possesses an additional cavity next to the active site, which can be occupied by the phenylene moiety of the 2-aminophenyl group and its substituents at the 5-position. While HDAC1 and HDAC3 also feature the so-called “foot pocket”, HDAC8 lacks this additional cavity, thus sterically excluding the Apa moiety of the inhibitor.

Having investigated the HDAC class selectivity of mini-AsuApa (**P3**), a chemical proteomics approach allowed to determine the composition of HDAC complexes recruited by this probe (Chapter 2.1.2.4). When compared to the lysine control **P1**, mini-AsuApa (**P3**) was able to enrich proteins of the CoREST, Sin3 and NuRD complexes containing both HDAC1 and HDAC2, and also components of the HDAC3 complex NCoR / SMRT. While the NCoR / SMRT complex components ranked among the most strongly enriched proteins on **P3**, class IIb HDAC6 was only weakly enriched, confirming the selectivity of this probe for class I HDACs observed by Western blot analysis. The interactome of mini-AsuApa (**P3**) in direct comparison to mini-AsuHd (**P2**) further elucidated the inherent HDAC complex selectivity of the Apa moiety in contrast to hydroxamic acids. While HDAC6 was strongly enriched on mini-AsuHd (**P2**), HDAC1, HDAC2 and proteins of their complexes (CoREST, Sin3, NuRD) were recruited to both **P2** and **P3** with comparable efficiency. Most strikingly, only HDAC3 and proteins of the NCoR / SMRT complex were significantly enriched on mini-AsuApa (**P3**) when compared to its hydroxamic acid congener, revealing a unique HDAC complex selectivity for this probe.

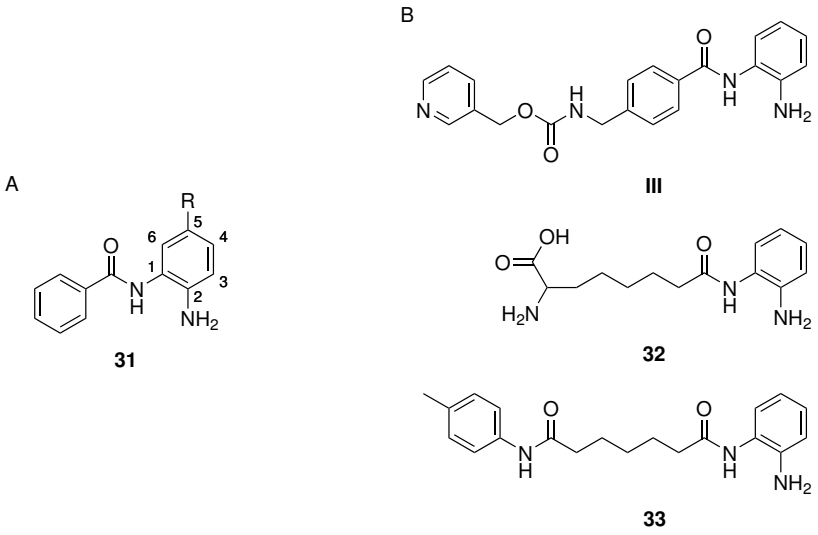

Figure 41: (A) Structure of *N*-(2-aminophenyl)benzamides (**31**) co-crystallized with HDAC2. R = H or a series of aromatic residues. (B) Comparison of MS-275 (**III**), AsuApa (**32**) and pimelic diphenylamide inhibitor 106 (**33**).

This selectivity differs from benzamide-type HDAC inhibitors like MS-275, which inhibits HDAC1 and HDAC3 with comparable efficiency.[162] While the crucial 2-aminophenyl moiety is linked to an aromatic benzamide derivative in MS-275 (**III**), it is attached to a long aliphatic carboxamide in AsuApa (**32**) (Figure 41 B). With this structural feature AsuApa resembles the pimelic diphenylamide inhibitor 106 (**33**).[105] **33** was reported to show HDAC binding properties similar to AsuApa and an activity-based probe derived from **33** interacted with HDAC3 most efficiently. This suggests that the aliphatic side chain of AsuApa is important in mediating its superior selectivity for the HDAC3 NCoR / SMRT complex.

To conclude, with the building block Fmoc-AsuApa(Boc)-OH (**13**) and the peptide-based probe mini-AsuApa (**P3**) versatile tools for the efficient capture of class I HDACs and especially the HDAC3 NCoR / SMRT complex could be developed.

Since the Apa moiety differs in size from the hydroxamate group, which most efficiently recruits HDACs when installed to the side chain of the eight-carbon Asu, future experiments could focus on optimization of the side chain length in Apa-containing probes, e.g. employing the seven-carbon α-aminopimelic acid (Apm) for building block synthesis.

3.1.3 Synthesis and application of a ketone-based HDAC affinity probe

As a third zinc-binding functional group for tuning the selectivity of peptide-based HDAC affinity probes, the ethyl ketone moiety of the natural cyclic peptide inhibitor apicidin was investigated in this work (Chapter 2.1.3). Apicidin inhibits all HDACs of class I with low nanomolar affinity, while HDACs of class II are not or only weakly inhibited.[232] This selectivity motivated an attempt to incorporate the keto amino acid Aoda of apicidin into the established minimal sequence context probe scaffold and to use this probe in HDAC binding assays.

To this end, a suitable protected Aoda building block for SPPS had to be synthesized. Due to a large and early interest in the structurally unique apicidin as a tool for epigenetic as well as clinical research, a considerable amount of synthetic routes for apicidin analogues and Aoda building blocks is available in literature. These building blocks are often obtained by chain homologation of existing amino acid precursors, with the α-carboxy group protected as methyl or allyl ester.

The first synthesis of an Aoda building block (Z-Aoda-OMe) was reported in 1985 and achieved by reaction of a suitable organocuprate containing the dioxolane-protected ketone with a halogen derivative of homoserine.[164] Z-Aoda-OMe was also obtained by *Michael* addition of a halogen derivative of Z-protected glutamic acid methyl ester with ethyl vinyl ketone under photolytic conditons with *n*-Bu_3SnH.[165]

In a total synthesis of apicidin, a precursor of Aoda (derived from serine) bearing a silyl ether function in place of the carbonyl group was introduced to the peptide first. After the peptide was cyclized, the silyl ether was deprotected and the resulting secondary alcohol oxidized to yield the ketone moiety.[233] For incorporation into a tetrapeptoid analogue of apicidin, Boc-Aoda-OH was synthesized from *Garner's* aldehyde in a six-step process. In this synthesis, a carboxylic acid precursor of the Aoda side chain was first connected to the aldehyde by a *Wittig* reaction, which was then converted to the Aoda ethyl ketone in a *Weinreb-Nahm* ketone synthesis.[166] Fmoc-Aoda-OAllyl was generated by a related approach, but using glutamic acid as the starting material, which was first transformed to the aldehyde at the side chain and then reacted with a suitable phosphonium salt containing the dioxolane-protected ketone.[167]

An enantioselective *de novo* synthesis of H-Aoda-OMe was achieved using the *Schöllkopf* method employing the bislactim ether derived from valine and glycine, which was alkylated with a dioxolane-protected side chain precursor.[234]

Unfortunately, none of these building blocks is suitable for standard Fmoc-based SPPS without further modifications, because most of them were intended for the solution synthesis of cyclic apicidine and apicidine analogues.

Recently the asymmetric synthesis of ready-to-use Fmoc-Aoda-OH for SPPS was achieved by alkylation of a nickel complex of glycine.[149] However, in this work, a new approach was chosen to obtain Fmoc-Aoda-OH (**16**), which represents a combination of the 9-BBN-aided route devised for the AsuHd (**5**) and AsuApa building blocks (**13**), and the *Weinreb-Nahm* ketone synthesis employed in the above-mentioned procedure for Boc-Aoda-OH (Chapter 2.1.3.1). In this way, all of the three building blocks Fmoc-AsuHd(OTrt)-OH (**5**), Fmoc-AsuApa(Boc)-OH (**13**) and Fmoc-Asu-OH (**16**) could be synthesized from the same versatile precursor Asu-BBN (**2**).

Key to the synthesis of Fmoc-Aoda-OH (**16**) was the transformation of Asu-BBN (**2**) to the *Weinreb* amide at the side chain via the acid chloride of **2**. This reaction proceeded very cleanly, which made chromatographic purification of the product Asu(NMe-OMe)-BBN (**14**) expendable. Although the 9-BBN group did not tolerate the reaction conditions of the *Grignard* reaction of **14** with ethylmagnesium bromide, the *Weinreb* amide could be successfully transformed to the Aoda ethyl ketone, at the same time conveniently liberating the α-amino and -carboxy group of H-Aoda-OH (**15**). Compared to the direct *Grignard* reaction of **2** or its acid chloride, the approach via *Weinreb* amide **14** further provided

Figure 42: Side reactions involving the Aoda ketone. (A) Formation of the 1,3-dithiolane by acidic peptide cleavage with a cocktail containing ethane-1,2-dithiol (EDT). (B) Reduction by TIPS forming the secondary alcohol.

the advantage of preventing over-addition to the side chain carbonyl, forming the tertiary alcohol.[168]

Subsequent Fmoc protection and purification by flash chromatography furnished the final building block Fmoc-Aoda-OH (**16**). With the synthetic procedure devised in this work, **16** could be obtained from α-aminosuberic acid in only four steps.

Fmoc-Aoda-OH (**16**) could then be incorporated into peptide-based HDAC affinity probes by standard SPPS (Chapter 2.1.3.2). However, the peptide design with a C-terminal cysteine residue for immobilization onto the agarose resin used in pulldown assays seemed to be incompatible with the unprotected Aoda ketone. Once a mini-peptide synthesized in analogy to **P1**-**P3** containing the Aoda residue was cleaved off the solid-phase and subjected to HPLC purification, the desired product was no longer detectable. Although no side product could be identified by LC-MS, quantitative formation of the 1,3-dithiolane of Aoda in the presence of ethane-1,2-dithiol (EDT) during peptide cleavage, hints at a side reaction involving both the ketone and cysteine thiol (Figure 42 A).

The new immobilization strategy based on the copper(I)-catalyzed azide-alkyne cycloaddition (referred to as CuAAC or “click” reaction)[235] developed in this work represents a simple but efficient solution to address this problem by splitting the probe into two parts. A C-terminal part, which contains the cysteine and a *p*-azidophenylalanine residue, and an N-terminal part incorporating the Aoda residue and a propargylglycine. The C-terminal part is first immobilized conventionally onto the iodoacetyl-functionalized agarose by its cysteine residue, followed by immobilization of the N-terminal part via click reaction.

This type of 1,3-dipolar *Huisgen* cycloaddition proceeds regioselectively, yielding the 1,4-disubsituted 1,2,3-triazole-linked products exclusively.[170] In addition to the very broad scope of applications and the wide variety of conditions tolerated by the CuAAC reaction, most commonly quantitative yields represent a further advantage for its use in immobilization approaches. Moreover, the generated triazole is inert towards cellular environments, which promotes its use in many biological applications and renders it an ideal linkage for HDAC affinity probes used in pulldown experiments with cellular lysates.[235]

After synthesis of the respective peptides, cleavage of the mini-Aoda-N (**P7**) probe part had to be slightly optimized by excluding the TIPS scavenger from the cleavage cocktail, which led to a reduction of the Aoda ketone to the secondary alcohol (Figure 42 B).

Proceeding quantitatively in solution, which was confirmed in an initial test by LC-MS analysis, the click reaction between the C-terminal peptide mini-C (**P4**) and the N-terminal mini-Aoda-N (**P7**) was then investigated on the agarose resin. CuAAC reactions with either the azide or the alkyne part immobilized to a solid-support are well characterized and many examples are found in literature.[235] They most commonly apply a copper(I) species or

copper(II) with a reducing agent (e.g. sodium ascorbate), a ligand which prevents (re-)oxidation of the copper, an optional base, and a polar solvent for both hydrophobic and hydrophilic resins. The conditions chosen in this work employed copper sulfate together with ascorbic acid, histidine as water-soluble ligand and an aqueous Tris buffer as solvent. This mixture was incubated with the immobilized, agarose-bound mini-C (**P4**) peptide and a stoichiometric amount of mini-Aoda-N (**P7**). At first, **P7** was immobilized only incompletely, but optimizations including additional equivalents of copper and adjusting the pH of the mixture from acidic to neutral, eventually led to quantitative capture of **P7** from the solution, furnishing the mini-click-Aoda (**P7***) probe. Consequently, for future applications, the click immobilization approach could be further optimized by directly including a base in the reaction mixture or by using sodium ascorbate instead of ascorbic acid.

Together with the respective mini-click-Lys (**P5***) and mini-click-AsuHd (**P6***) probes as controls, mini-click-Aoda (**P7***) was then tested for HDAC binding and selectivity (Chapter 2.1.3.3). Initial pulldown experiments were analyzed for recruitment of HDAC1 as representative member of class I HDACs and HDAC6 as member of class IIb enzymes. Mini-click-Aoda (**P7***) could enrich both HDACs over the lysine control **P5***, but binding was weaker as observed for the hydroxamate probe **P6***. Although the absolute western blot signal intensity was higher for HDAC6 than for HDAC1, the latter was enriched on **P7*** more strongly relative to **P5***.

This prompts the conclusion that the selectivity for class I HDACs of apicidin is preserved in the mini-click-Aoda (**P7***) probe. However, there are mixed reports in literature whether the Aoda ethyl ketone alone is sufficient for mediating this class selectivity.

Binding of ketone-type inhibitors to zinc-dependent hydrolases in general was first explained on the basis of a crystal structure of carboxypeptidase A and a trifluoromethyl ketone (TFMK).[236] Due to their high electrophilicity, trifluoromethyl ketones readily hydrate in aqueous media to form the geminal diol, which is then able to coordinate to the active site zinc ion in a bidentate fashion. This mode of binding could also be confirmed for HDACs by a crystal structure of class IIa HDAC4 with a TFMK derivative.[237]

Lacking the electronegative substituents, the ethyl ketone of Aoda is much less electrophilic than TFMKs. However, by the nature of their catalytic mechanism, zinc-dependent hydrolases are potentially able to activate any sterically suitable carbonyl compound for attack of a water molecule through zinc-chelation and the distinct hydrogen bonding network in their active sites. This means that upon enzyme binding hydration could be facilitated for all types of ketone inhibitors. In contrast to hydroxamic acids, which mimic the acetyllysine substrate, ketone-type inhibitors are therefore analogues of the tetrahedral transition state of the deacetylation reaction of HDACs.[48]

Within this context, the weaker interaction of the ketone-containing Aoda probe **P7*** compared to its hydroxamate congener with the tested HDACs as well as the selectivity of Aoda-containing inhibitors for class I HDACs in general can be rationalized on the basis of several findings: In molecular modeling studies, docking of an hydroxamic acid inhibitor into the active site of class IIb HDAC6 resulted in a bidentate coordination of the zinc ion, which is also observed in crystal structures of other HDACs co-crystallized with hydroxamic acids (Figure 43 A).

On the other hand, docking of an α-hydroxy ketone analogue resulted in a monodentate and thus presumably weaker coordination.[119] Although in the latter case the coordinating moiety

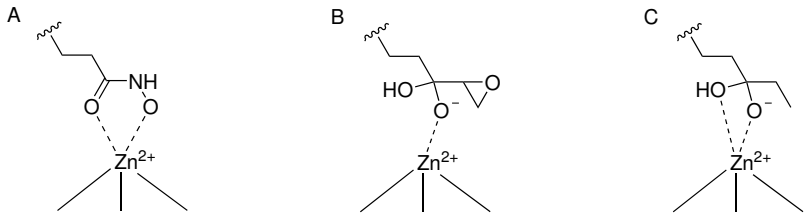

Figure 43: Schematic representation of different binding modes observed in crystal structures for HDAC inhibitors. (A) Bidentate coordination of hydroxamic acids to HDACs of class I and IIb.[48,94] (B) Monodentade coordination of (α,β-epoxy) ketone-type inhibitors to HDACs of class IIb.[48] (C) Bidentate coordination of (ethyl) ketone-type inhibitors to HDACs of class I.[96]

was the α-hydroxy group, which is not present in Aoda, these results were confirmed by a crystal structure of HDAC6 with the α,β-epoxy ketone-containing inhibitor HC toxin, where zinc-chelation was also monodentate through one of the *gem*-diols, but without participation of the epoxy group (Figure 43 B).[48]

Docking of the above α-hydroxy ketone analogue to the active site of HDAC1, in contrast, resulted in a bidentate, thus stronger coordination of the zinc ion.[119] This mode of binding to class I HDACs could recently be confirmed by a crystal structure of HDAC2 in complex with apicidin, that unambiguously shows bidentate coordination of the active site zinc ion by the *gem*-diol(ate) of Aoda (Figure 43 C).[96]

These observations suggest that the Aoda ethyl ketone possesses an inherent specificity for HDACs of class I which is based on its mode of coordination and the structure of the active site of the respective enzymes. However, there are also reports of efficient and class selective HDAC inhibitors lacking a zinc-binding group. By an optimization effort exchanging the Aoda side chain of apicidin for various alkyl groups and also modifying the other amino acids, low micromolar inhibitors for class I HDACs could be generated, that preserved selectivity over HDAC6.[92] Using a non-natural inhibitor scaffold, in which short alkyl chains replaced the zinc-binding group, even an inhibitor with nanomolar IC_{50} values for class I HDACs could be synthesized. Yet, simply removing the ketone carbonyl of apicidin resulted in a compound with significantly reduced activity in biochemical and cellular assays, suggesting that the zinc-chelating moiety is indispensable for this naturally evolved inhibitor.[96]

The conclusion which may be drawn from this is that an approach of generating a selective HDAC inhibitor or HDAC probe based on a certain functional group or cap moiety alone can be successful, although the most promising compounds can be obtained through a combination of both parts. Peptide-based HDAC affinity probes are well suited for this purpose, enabling the flexible combination of functional groups and sequence contexts as cap moieties in a mix-and-match type of fashion. With the building block Fmoc-Aoda-OH (**16**) and the click immobilization approach versatile tools could be created to use the Aoda ethyl ketone moiety in these probes.

In order to fully elucidate the HDAC selectivity of mini-click-Aoda (**P7***), additional pulldown experiments with other HDACs are necessary in a first step. In a second step, the selectivity could be fine-tuned by addition of a peptide sequence context. For future experiments, the scope of ketone-based HDAC affinity probes could also be extended to HDACs of class IIa by incorporating the TFMK building block Atona.[238]

3.2 HDAC selectivity mediated by peptide sequence contexts

In the second part of this work, the influence of peptide sequence contexts on HDAC selectivity was investigated (Chapter 2.2). To this end, a new high-throughput assay based on 96-well plate format was developed. The assay was applied in order to validate a proteomics data set of acetylation sites potentially regulated by HDAC6. Selected sequences were also investigated in greater detail regarding their influence on HDAC interaction partners and on catalysis.

Peptide-based HDAC affinity probes with sequence contexts derived from known acetylation sites of HDAC substrates have successfully been applied for uncovering the substrate selectivity and composition of endogenous HDAC complexes, with the sequence context mediating this selectivity.[136,142]

In the probe p53-AsuHd, derived from the regulatory acetylation site K382 of the tumor suppressor and transcription factor p53, the HDAC-trapping amino acid AsuHd replaced the acetylated lysine residue. This probe could enrich class I HDACs 1, 2 and 3 over the lysine control even at reduced input concentrations of cellular lysate, where the corresponding probe without sequence context, mini-AsuHd (**P2**), was not able to do so. In contrast, class I HDAC8 and HDACs of class II did not differentiate between the two probes, suggesting that binding with these HDACs mainly relies on zinc-chelation. This is consistent with HDAC1 being the known regulatory deacetylase of K382 of p53,[39] and the respective sequence context enforcing strong binding to the enzyme. Extending the investigations to a proteom-wide level provided further insight into the potential substrate selectivity of multi-protein complexes embedding HDAC1 and supported the notion that this selectivity is mediated by the respective interaction partners of the HDAC.[136,142]

The benefit of screening for HDAC substrates is thus two-fold: While on the one hand, uncovering the specificity and binding partners of HDACs further elucidates their biological role, the knowledge obtained can on the other hand also be used to increase the selectivity of peptide-based probes and HDAC inhibitors.

3.2.1 High-throughput screening for HDAC6 substrates

As a target for screening and validating HDAC substrates, a library of peptide sequences derived from acetylation sites potentially regulated by HDAC6 from two proteomics approaches was used (Chapter 2.2.1).[136,145] These sequences were further supplemented with controls including known and potential substrates of other HDACs, yielding 32 individual peptide sequences. For each sequence three peptide-based HDAC affinity probes were synthesized incorporating either unmodified lysine or the hydroxamate amino acids ApmHd or AsuHd, leading to a total library size of 96 peptides. Due to the demand of time to synthesize such an amount of peptides by conventional methods of SPPS including HPLC purification, alternative, high-throughput methods were established. In addition, the peptide design of HDAC affinity probes was adjusted accordingly.

3.2.1.1 Developing an assay strategy

Strategies for the parallel synthesis of large peptide libraries for high-throughput screenings emerged in the mid-nineteen-eighties. One of the first methods was the “pin” method, where peptides are synthesized on the amino-functionalized tips of polyethylene rods on a nanomol scale. These rods are attached to a suitable assembly by which they can be simultaneously immersed into the wells of a microtiter plate containing the coupling solutions.[239] After synthesis, the rod array is then directly used in biochemical assays, since the peptides cannot be cleaved from the support without further modifications. This also prevents their analysis regarding identity and purity.

In the “tea bag” method conventional peptide synthesis resins are used as the solid-support.[240] Each peptide is synthesized on a relatively large micromol scale on a portion of resin enclosed in a polypropylene mesh bag, which is labeled for identification. While the bags are sorted into different reaction vessels for coupling reactions depending on the respective amino acid, removal of the *N*α-protecting group can be conducted for all peptides in a single vessel. Although this method provides large amounts of peptide for extensive analysis, all steps have to be carried out manually, thus limiting the size of the generated peptide library.

By the early nineteen-nineties, advances in “split-and-mix”[241,242] and “one-bead-one-compound”[243] approaches allowed the synthesis of mixtures of more than one million of different peptides within a limited amount of time. These mixtures are then assayed on the solid-phase and beads containing a peptide of interest, identified by a suitable method, are isolated. After cleavage, peptides can be identified by MS / MS sequencing.

Together with the pin and tea bag method, all of these approaches are more suitable for the generation of randomized peptide libraries rather than screening for given protein sequences.

An early method for parallel synthesis of miniaturized peptide arrays with a defined sequence at fixed, individually addressable positions was published in 1991 by *Fodor et al.*[244] This procedure uses amino-functionalized glass slides as solid-support and amino acid building blocks with a photolabile *N*α-protecting group. Individual positions can be addressed with photolithographic masks by irradiation of the photo-protected peptides at a suitable wavelength, enabling coupling reactions only at irradiated areas.

The SPOT synthesis published in 1992 by *R. Frank*, however, is an approach more compatible with standard SPPS building blocks and conditions.[173] If automated, and depending on the size of the spots and the cellulose membranes that are used as solid-support, thousands of defined peptides can be synthesized with this method in a spatially addressable manner on a nanomol scale. Biochemical assays are conducted directly on the membranes or on glass slides, onto which cellulose-peptide conjugates can be spotted.[174] Although analysis of peptides is possible for selected controls by introduction of an acid-labile linker between membrane and peptide, due to the small synthesis scale and number of samples SPOT peptides cannot be routinely assessed for purity and identity. This lack in confirming uniform peptide quality is in part accounted for by the large number of copies which can be created from one array, allowing a large number of experimental replicates. However, systematic errors during peptide synthesis, i.e. inherent to the sequences, can hardly be addressed. Especially applications investigating protein binding and affinity are complicated by the fact

that the amount of full-length peptide may vary between different sequences and spots. The high density of peptides on the membrane surface is also prone to interfere with protein binding.[245]

Intermediate between massive SPOT arrays and more traditional approaches regarding sample capacity, synthesis and screening methods based on the format of 96-well plates combine the advantages of high-throughput handling with the possibility of individual analysis and characterization for each peptide. A first synthesizer enabling fully automated parallel synthesis of 96 peptides in microtiter plates on a low micromol scale was introduced in 1989 by *Schnorrenberg* and *Gerhardt*.[176] While most approaches of 96-well synthesis use filter-bottom plates combined with resins as solid-support, also a variant was developed in which the peptides are synthesized directly on a polylysine-functionalized plate surface.[178] Although these plates can be conveniently used in biochemical assays, the covalent linkage with the plate prohibits analysis of peptides synthesized by this method. In order to increase coupling efficiency and peptide purity, manual peptide synthesis in 96-well plates was also combined with microwave irradiation.[179] In a promising approach by *Pipkorn et al.* 96-well peptide synthesis was first carried out on an automated synthesizer, followed by purification of the peptides by reverse-phase solid-phase extraction (RP-SPE). With SPE being conducted in suitable 96-well plates, also the peptide purification step was successfully adapted to the high-throughput format.

Although the SPOT method represents one of the best suited approaches for the initial screening of very large sets of peptide sequences, for the library of acetylome-derived HDAC6 substrate sites investigated in this work a more precise method was developed by adapting the established peptide-based HDAC affinity probes to the high-throughput format of 96-well plates. While 96-well plates were both used for peptide synthesis and HDAC binding assays, thus facilitating these steps, key to successfully establishing this approach was a fast and easy method for peptide purification without relying on time-consuming RP-HPLC (Chapter 2.2.1.1).

In order to achieve this, the design of peptide-based HDAC affinity probes was changed by substituting the C-terminal cysteine for immobilization by an N-terminal, thiol-containing building block (N-terminal anchor). After each synthesis cycle, a capping step was implemented, preventing elongation of deletion sequences. Since the N-terminal anchoring moiety was introduced as the last building block of each peptide, only full-length peptides contained the thiol for immobilization. Subsequent incubation of the crude peptide mixture with the iodoacetyl-functionalized solid-support used in HDAC assays resulted in exclusive immobilization of full-length peptides, while truncation products remained in solution and could be separated.

This method of purification by N-terminal immobilization can be classified as a mix of solid-phase extraction and affinity purification and its concept is closely related to strategies developed by *Zitterbart* and *Seitz*.[246] In the “catch-and-release” approach peptides are synthesized by standard SPPS and deletion sequences are capped after each cycle. A linker is introduced at the N-terminus of full-length peptides exclusively and peptides are cleaved off the solid-phase. The linker contains an *O*-alkyl hydroxylamine by which target peptides can then be immobilized onto aldehyde-functionalized agarose beads through oxime formation and truncation products can easily be separated since they remain in solution. After washing,

the target peptide is released by basic cleavage of a sulfonylethoxycarbonyl moiety of the linker, releasing the peptide with a free N-terminus.[247]

The concept of affinity purification by an N-terminal thiol, however, was first described in 1976 by *Krieger* and *Merrifield*.[248] In their approach, a Cys-Met dipeptide is introduced to the N-terminus of full-length peptides which can be immobilized onto organomercury-functionalized agarose. After separation of capping products, the target compound is released by cleavage of the peptide bond C-terminal to methionine by bromo cyanide.[249]

The drawback of these methods as well as the one developed in this work is, that the N-terminus of the peptides cannot be modified, because its derivatization is required for affinity purification. In addition, if the functional group used for immobilization is a thiol, no (unprotected) cysteine residues can be present in the peptide sequence. Since hardly any substrate sites from the HDAC6-dependent acetylomes investigated in this work contained a cysteine residue and none of the chosen sequences (Table 2), this limitation was not an obstacle for the newly developed 96-well HDAC assay. Although the peptides remained bound to the agarose beads after affinity purification and could not be used otherwise, the N-terminal immobilization approach devised in this work represented an ideal strategy to enable a high-throughput version of HDAC pulldown assay in 96-well plates.

3.2.1.2 Optimization of 96-well peptide synthesis

Peptid probes **6P1**–**6P96** for the 96-well HDAC pulldown assay were synthesized in filter-bottom plates on a scale of 2 µmol using an automated synthesizer (Chapter 2.2.1.3). To ensure a maximum coupling efficiency amino acids were coupled twice and with a high stoichiometry in relation to the resin. Bearing the Fmoc protecting group, hydroxamate building blocks Fmoc-AsuHd(OTrt)-OH (**5**) and Fmoc-ApmHd(OTrt)-OH (**10**) were easily integrated into the automated workflow. In addition, the Trt-group on both building blocks, which was readily deprotected under peptide cleavage conditions, ensured the exclusive immobilization of free, unprotected hydroxamic acid-containing peptides for the subsequent HDAC assay. This represented a major advantage over established *tert*-butyl hydroxamate building blocks, because they are only slowly and often incompletely deprotected. It would not have been possible to separate the resulting *tert*-Bu hydroxamate-containing peptides by the N-terminal immobilization approach, thus prohibiting any quantitative analysis of HDAC pulldown assays. The Trt hydroxamate building blocks therefore aided both the effectiveness of the affinity purification and the interpretation of assay results. Although in this work **5** and **10** were synthesized from inexpensive racemic amino acid precursors, the presumably more effective L-enantiomers of **5** and **10** could be used for future assays by implementing an enzymatic resolution step (compare Figure 40).

After synthesis, test cleavages were conducted and analyzed by LC-MS. For most of the HDAC6 substrate peptides **6P1**-**6P96** synthesis proceeded very cleanly, yielding only a small fraction of truncated peptides as by-products. These were caused by incomplete couplings of the hydroxamates as well as the N-terminal anchoring building block, since they were used with a lower stoichiometry compared to the commercial amino acids.

The major problem for the miniaturized 96-well synthesis and assay approach emanated from the final peptide cleavage. Only a maximum of 200 µL of cleavage cocktail could be

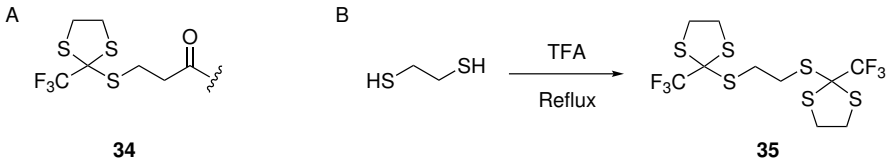

Figure 44: (A) Possible 2-alkylthio-2-trifluoromethyl-1,3-dithiolane modification (**34**) generated from EDT, TFA and the N-terminal 3-mercaptopropionic acid of HDAC6 substrate peptides **6P1**-**6P96**. (B) Synthesis of the orthothioester **35**.

added to a well of the synthesis plate at a time, with the capacity of available deep-well collection plates (∼1–2 mL) also limiting the overall volume that could be used. The small volume of cleavage cocktail in proportion to the resin and thus low amount of scavengers led to impure crude peptides when cleavage was tested with Reagent R, the cocktail used for all other peptides in this work. These impurities were not observed during the test cleavages with Reagent R after synthesis, because the volume of cleavage cocktail was large in proportion to the amount of resin used in these cleavages.

The most prominent side reaction in the course of peptide cleavage was *tert*-butylation through *t*Bu cations or *t*Bu trifluoroacetate generated by side-chain deprotection. Although for this modification various sites of attachment are possible, due to its nucleophilicity, the N-terminal thiol seemed especially susceptible and modified peptides could not be immobilized. Other notable side-reactions were methionine oxidation yielding methionine sulfoxide and aspartimide formation from the sequence Asp-Gly.

A solution to address some of these side-reactions was found in Reagent K, a cleavage cocktail containing scavengers with increased potency compared to Reagent R. Besides TFA, water and phenol (scavenging the Pbf group from Arg, preventing Trp modification), this cocktail contains thioanisole (suppressing Met oxidation) and ethane-1,2-dithiol (scavenging *t*Bu / *t*Bu trifluoroacetate and Trt cations). Cleavage with Reagent K resulted in a greatly improved purity of the respective peptides, preventing *tert*-butylation completely and decreasing the extent of methionine oxidation.

However, with Reagent K a further side-product was observed that could also not be immobilized by the N-terminal thiol. According to LC-MS analysis the side-product was assigned as a peptide containing a 2-trifluoromethyl-1,3-dithiolane moiety, which was initially discovered on Trp residues.[183] This modification is thought to be caused by electrophilic addition of a dithioacetal cation formed by TFA and EDT at high temperatures. Since 96-well peptide cleavage was conducted at elevated ambient temperatures (≥30 °C) and cleavage solutions were concentrated by evaporation for prolonged time, these conditions likely favored the reaction. However, the inability of the peptide to be immobilized hinted at the N-terminal thiol as site of attachment of this modification rather than on an aromatic residue. Consequently, the peptide would be modified as the 2-alkylthio-2-trifluoromethyl-1,3-dithiolane **34** (Figure 44 A). A structure related to **34**, the unusual orthothioester **35**, where two 2-trifluoromethyl-1,3-dithiolan-2-yl groups are bridged by EDT, was reported in 1967.[184] **35** was discovered during attempts to protect carbonyl compounds as dithiolanes and obtained when EDT was refluxed in neat TFA. Although the conditions during peptide cleavage were less harsh, this finding renders modification **34** likely.

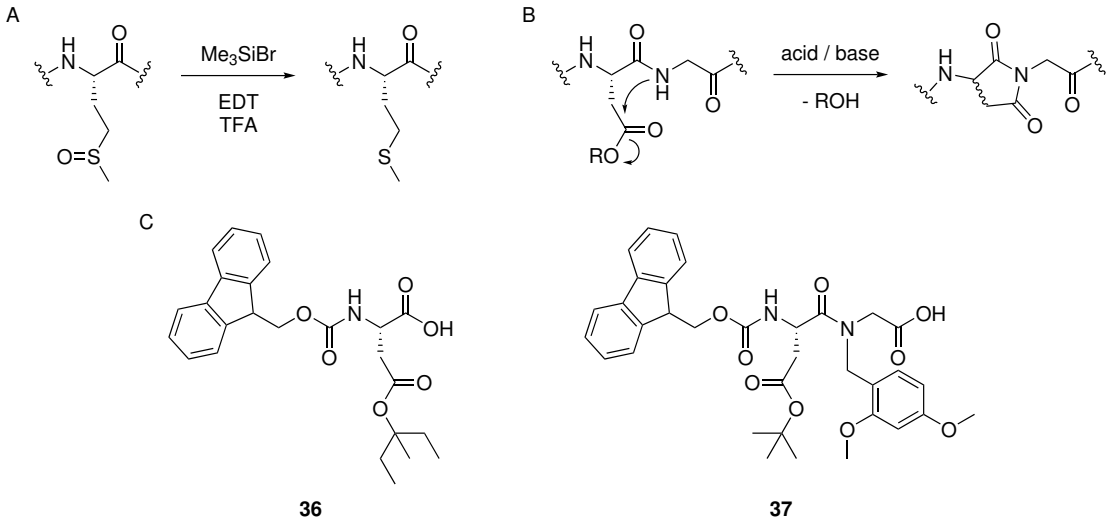

Figure 45: Strategies for optimization of 96-well peptide synthesis and cleavage. (A) Reduction of methionine sulfoxides with TMS bromide and ethane-1,2-dithiol in TFA. (B) Acid- or base-catalyzed mechanism of aspartimide formation. (C) Building blocks Fmoc-Asp(OMpe)-OH (**36**) and Fmoc-Asp(O*t*Bu)-(Dmb)Gly-OH (**37**) for suppression of aspartimide formation.

In order to prevent formation of **34**, EDT was substituted for either octane-1,8-dithiol (ODT) or dithiothreitol (DTT) as suggested in literature.[183] These alternative thiol scavengers disfavor formation of the respective cyclic dithioacetals by unfavorable ring sizes (ODT) or ring strain (DTT). In addition, TIPS was included as additional scavenger (for Trt) yielding two modified versions of Reagent K. Both versions could successfully suppress modifications in the form of **34** and gave almost identical results. Being less odorous, the DTT-modified Reagent K was then used for final cleavage of all 96 peptides.

However, also with the modified Reagent K methionine sulfoxide formation could not be fully eliminated. Although methionine oxidation occurs *in vivo* and can contribute to protein structure and function,[250] the degree of oxidation of the HDAC6 substrate sequences selected in this work is unknown under physiological conditions. In order to achieve a uniform oxidation state of the peptide library in future experiments using the 96-well HDAC assay, an additional reduction step could be introduced after peptide cleavage, which is only applied to Met-containing peptides. A procedure well adaptable for the miniaturized format of 96-well plates uses trimethylsilyl (TMS) bromide in TFA as reducing agent (Figure 45 A).[251] The bromine that is created upon the reaction is in turn scavenged and reduced by EDT. Due to the reagents used in this procedure, TMS bromide could also be conveniently included directly into the Reagent K cleavage cocktail. In addition, instead of slow concentration of cleavage solutions by evaporation under ambient conditions prior to precipitation, which leaves the peptides susceptible to oxidation, a suitable vacuum centrifuge with a cooling trap could be used.

Aspartimide formation remained the most prominent side-reaction with the modified versions of Reagent K. Although not as severe for the 96-well assay as *tert*-butylation, this acid- or base-catalyzed reaction can lead to racemization of the Asp residue, conversion to isoaspartyl-β-peptides or – if piperidine is used for Fmoc cleavage – formation of piperidides

of Asp. Since the reaction is initiated by attack of an adjacent backbone nitrogen on the Asp side chain, Asp-Gly sequences are especially prone to this modification, with Gly being the least sterically hindered amino acid (Figure 45 B).[252] In order to further minimize or even completely suppress this reaction in future 96-well synthesis approaches, optimized building blocks instead of the standard Fmoc-Asp(O*t*Bu)-OH could be used (Figure 45 C). Due to the steric bulk of the 3-methylpent-3-yl (Mpe) protecting group, the derivative Fmoc-Asp(OMpe)-OH (**36**) is less prone to a nucleophilic attack of the backbone nitrogen.[253] For introduction of the Asp-Gly sequence, backbone-protected dipeptide building blocks as the derivative Fmoc-Asp(O*t*Bu)-(Dmb)Gly-OH (**37**) are especially suitable, with the Dmb (2,4-dimethoxybenzyl) group effectively blocking backbone amide attack.[252]

3.2.1.3 Establishing a 96-well HDAC pulldown assay

Having successfully synthesized a library of peptide-based affinity probes derived from known and potential HDAC6 substrates, a suitable high-throughput pulldown assay for analysis of HDAC binding was established.

More than 6800 substrate sites from general human acetylomic data have been previously screened using SPOT-based peptide micro arrays and recombinant constructs of HDAC6.[254] In this approach, as opposed to standard SPOT or *CelluSpot* techniques, some control over the amount of peptides used was achieved by first cleaving them from the cellulose support, followed by exhaustive immobilization on functionalized glass slides by a special tag within spots of defined size. However, with regard to the scope of this approach, quality control of peptides is hardy possible.

Although the 96-well-based assay developed in this work is only suitable for a much smaller set of substrate sites, assessment of purity and identity of peptides is easily possible by LC-MS analysis, thus increasing the reliability of the results. Due to this increased precision the 96-well approach seemed appropriate for analysis of the limited set of HDAC6-specific acetylomic data. The ability to analyze endogenous HDACs in cellular lysates represents a further advantage of this assay.

Both the purification of peptide probes **6P1**-**6P96** by N-terminal immobilization and precise quantification of the amount of peptide to be immobilized were enabled by the building block Trt-Mpa-Lys(Dns)-OH (**22**) for introducing the N-terminal anchoring moiety (Chapter 2.2.1.2). Trt-Mpa-Lys(Dns)-OH (**22**) was conveniently synthesized from lysine exploiting the 9-BBN protection strategy that already worked well for the synthesis of HDAC-trapping amino acids. The dansyl (Dns) group attached to the side chain of lysine allowed fast quantification by fluorescence readout. Due to this feature, differences in peptide yield by varying amounts of resin during synthesis, non-uniform coupling efficiency and different precipitation characteristics could be compensated by adjusting peptide concentration prior to immobilization. Importantly, **22** was introduced as a dipeptide instead of using two separate building blocks to ensure that every thiol-containing peptide that is immobilized also contains a fluorophore and is quantifiable.

In order to estimate peptide yields, fluorescence was calibrated using HPLC-purified H-Lys(Dns)-OH (**20**) as reference (Chapter 2.2.1.4). Unfortunately, results obtained for stock solutions generated from the 96 peptides were approximately two-fold higher than

possible by assuming quantitative yield. Although a suitable buffer was used to dissolve the peptides, providing uniform pH conditions and rendering pH effects a less likely explanation of this discrepancy, other components and side-products in the crude peptide mixture could have modified fluorescence compared to reference samples. However, since fluorescence intensities were higher than expected it seemed more plausible that the concentrations of stock solutions were also higher than intended. Despite the polar PEG-spacers that were included in the peptide design, most of the peptides **6P1**-**6P96** were hydrophobic and required a buffer containing up to 50 % acetonitrile to be dissolved. Handling this buffer in the open 96-well plates likely led to evaporation of acetonitrile, thus concentrating the samples. Consequently, the method for quantification in 96-well immobilizations could be further improved by increasing the solubility of peptides, e.g. through introduction of several D-lysine or D-arginine residues as a protease-stable solubility tag.[255]

Although absolute quantification was not possible, peptides could be quantified relatively and concentrations were adjusted for subsequent, uniform immobilization on iodoacetyl-functionalized agarose. LC-MS analysis of samples from peptide solutions before and after immobilization demonstrated the success of the N-terminal affinity purification strategy. While only full-length peptides were immobilized, truncation products lacking the HDAC-trapping amino acids remained in solution. In spite of successful adjustment of peptide concentrations for immobilization, a minor error could have been introduced when the agarose-bound peptide probes were manually aliquoted into the plates used for the pulldown assay. However, this could be accounted for by performing multiple replicates of the pulldown experiments.

The subsequent HDAC assay with native HeLa lysates could be greatly accelerated by use of the 96-well plate techniques compared to the established protocol using micro centrifuge tubes with a filter insert (Chapter 2.2.1.5). Filter bottom-plates in combination with a vacuum manifold for draining of solutions allowed to rapidly conduct washing and elution steps for all 96 samples in parallel. Ensuring a maximum of comparability, most steps of the 96-well assay protocol could be conducted in the same way as in the established low-throughput protocol. Only elution of bound proteins had to be modified in order to compensate for increased evaporation of sample buffer caused by the open 96-well format. Since the plates could only be heated up to 70 °C due to material instability, elution time was prolonged and the sample buffer volume increased.

Chemiluminescent images from large-scale Western blotting showed that most of the AsuHd-containing probes were able to enrich HDAC6 over the lysine control. Recruitment of HDAC6 to ApmHd-containing probes was weaker and observed less often, reflecting the optimal length of the side chain of AsuHd to reach into the active site of HDACs. While HDAC1 was not enriched on various hydroxamate-containing peptides over the lysine control e.g. for the TUBA1A sequence (**6P7**–**6P9**), other HDAC6 substrate sequences also efficiently recruited HDAC1 (e.g. EIF4B, **6P55**–**6P57**). Some sequences recruited HDAC6 and HDAC1 unspecifically with comparable enrichment on Lys- and hydroxamate-containing probes (RANBP2, **6P64**–**6P66** and ZYX, **6P67**–**6P69**). Most of the controls that were derived from proposed substrate sites of other HDACs than HDAC6 enriched HDAC6 unspecifically. However, probes **6P4**–**6P6** derived from the known HDAC1 substrate p53 did not differentiate in their recruitment of HDAC6 or HDAC1, which was efficient for both HDACs, as opposed to previous reports.[142] This can be explained by the high input concentration of 1 mg mL^{-1}

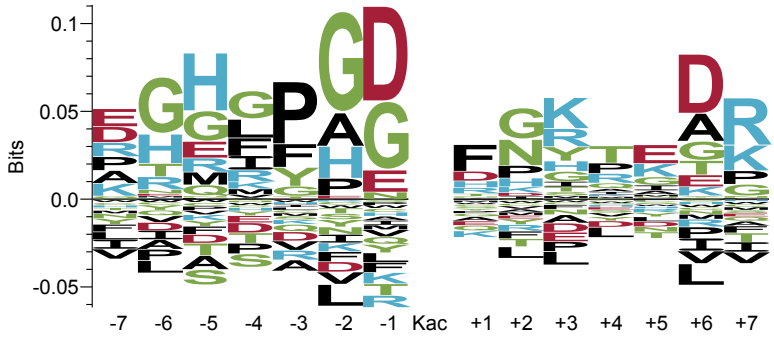

Figure 46: Probability weighted *Kullback-Leibler* sequence logo generated using the *Seq2Logo 2.0* tool (Technical University of Denmark), which accounts for small sample sizes.[256] Parameters were set as default. The logo shows amino acids enriched or depleted at the respective positions relative to the acetylated lysine among sequences favoring HDAC6 recruitment in high-throughput pulldown assays (Table 2 without TP53, CCT2, PRDX4, CTTN124, RANBP2, ZYX, NUP214, PPL, JADE3 and MATR3). The height of each amino acid corresponds to its probability at the respective position times its log-odds score calculated by the *Seq2Logo* algorithm. Large stacks of letters represent conserved positions, whereas small stacks represent more flexible positions. Color coding: Acidic residues (red); basic residues (blue); neutral, polar residues (green); hydrophobic residues (black).

used for the 96-well assay, with the input concentration used in previous experiments being much lower. The efficiency of HDAC recruitment to the peptide probes is both determined by their cellular abundance and their affinity. Low-abundance HDACs might be driven off the probes by high-abundance HDACs, especially when a pan-specific zinc-chelating moiety is used. Consequently, future experiments with the 96-well assay could also investigate the influence of reduced input concentrations on HDAC binding.

In order to visualize the influence of the substrate site sequence context on HDAC6 recruitment in a compact manner, a sequence logo was generated from sequences favoring binding of HDAC6 in the 96-well pulldown assay (Figure 46). The logo shows possible consensus sequences of these substrates, with the likeliness of a certain amino acid residue at the respective position indicated by its size on the y-coordinate. While large stacks of residues represent conserved positions, small stacks indicate a less conserved position in the sequence. Residues depleted at the respective positions within the sequences favoring HDAC6 binding are shown on the negative y-coordinate.

In general, residues N-terminal to the acetylation site seem to be more conserved than C-terminal residues, with the –1 and –2 positions being most crucial. At both of these positions, glycine (G) was strongly favored, which is in agreement with the results of the SPOT screening approach for HDAC6.[254] However, in these screenings also arginine (R) residues were frequently observed at positions –1 to –3, and acidic glutamate (E) residues were strongly disfavored. This is in contrast to the results obtained with the 96-well assay, where preferred binding to sequences containing an aspartic (D) or glutamic (E) acid residue at the –1 position was detected. This divergence could be related to the small sample size of the 96-well assay as compared to the several thousand sequences of the SPOT approach. However, it should be noted that the confirmed substrate site K40 of α-tubulin contains an Asp (D) residue at the –1 position. Disfavor of valine (V) at position –2 and the conserved phenylalanine (F) residue at the +1 position were again in agreement with the SPOT study.

3.2.2 In-depth analysis of selected HDAC6 substrates

In the next step, four promising hits for substrate sites (TUBA1A, CRTC3, HSP90AA1, PPIA) from the 96-well assay, which were able to efficiently recruit HDAC6 but not HDAC1, were investigated in detail (Chapter 2.2.2).

α-Tubulin (TUBA1A) is a cytoskeletal protein that, as a heterodimer together with β-tubulin, polymerizes to form microtubuli. Microtubuli are responsible for the separation of chromatides during mitosis, involved in cellular transport as attachment sites for motor proteins, and play a role in cell motility.[257] Through deacetylation of K40 of α-tubulin, HDAC6 is known to regulate cell motility by influencing tubulin polymerization.[49] CREB-regulated transcription coactivator 3 (CRTC3) is a coactivator of the transcription factor CREB1, which is involved, for example, in regulation of hepatic gluconeogenesis.[258] CRTC has not yet been reported as HDAC6 substrate. Heat shock protein HSP 90 α (HSP90AA1) is a high-abundance molecular chaperone which promotes folding and activation of its target proteins. HDAC6 was shown to activate HSP90 by deacetylation in several studies.[51,52,259] Peptidyl-prolyl cis-trans isomerase A (PPIA) catalyzes the cis-trans isomerization of proline peptide bonds. Also known as cyclophilin A, PPIA plays a role in inflammation, protein folding and modulation of protein activity.[260] It is yet unknown to be deacetylated by HDAC6.

3.2.2.1 Validation of the 96-well pulldown assay

In order to further examine the acetylation sites of the aforementioned proteins, new probe peptides were synthesized following the design of established sequence context HDAC probes with a C-terminal cysteine for immobilization.[142] In the resulting αTub-, CRTC-, HSP90- and PPIA-probes (**P10**–**P17**) either lysine or L-AsuHd were incorporated at the acetylation site. To validate the binding pattern observed for HDAC6 in the 96-well assay, pulldown assays were repeated with **P10**–**P17** using the established low-throughput protocol (Chapter 2.2.2.1). Enrichment of HDAC6 could be confirmed for all substrates. However, only the αTub-probe differentiated in its recruitment between HDAC6 and HDAC1, demonstrating the repulsive nature of the αTub sequence context on HDAC1. As opposed to the results of the 96-well assay the CRTC-, HSP90- and PPIA-probe efficiently recruited HDAC1 as well. This could probably be explained by substitution of racemic AsuHd by its L-enantiomer in probes **P10**–**P17**, with the larger fraction hydroxamate-bound HDAC in combination with a high input of cellular lysate possibly overriding the influence of the sequence context. Furthermore, the efficiency of HDAC enrichment does not depend on probe affinity alone, but also on HDAC abundance. In future experiments with these probes the input concentration should therefore be reduced or they could be re-synthesized with the lower-affinity L-ApmHd. Interestingly, the low-throughput pulldown assays revealed a comparably strong interaction of HDAC6 with the control peptide HSP90-Lys (**12**). This suggests that the sequence around K191 of HSP90 reinforces binding of HDAC6 especially strongly.

3.2.2.2 Analysis of interacting proteins

In the following, the interactomes of the αTub-, CRTC-, HSP90- and PPIA-L-AsuHd-probes compared to their respective lysine controls in HeLa lysate were determined by tandem mass spectrometry-based proteomics (Chapter 2.2.2.2). This approach aimed at identifying new potential interaction partners of HDAC6 which might be directly or indirectly involved in targeting of specific substrates and regulation of cellular pathways by this enzyme. Proteins identified in these experiments were grouped into different categories according to their cellular function.

The αTub-probe seemed to preferentially enrich proteins related to the actin cytoskeleton and a variety of other cytoskeletal proteins involved in functions such as microtubule organization or cell adhesion. In addition, cell cycle and ubiquitin related proteins were found to be recruited. The interactome of the CRTC-probe versus its control did not show a clear preference for enrichment of a specific functional group of proteins. Instead, proteins of several groups were recruited to a comparable extent. Interestingly, in contrast to the other three probe pairs, most of the identified ubiquitin related proteins were not enriched on the HSP90 sequence. However, the HSP90-probe displayed a strong preference for chaperones, transcription factors and signal transducers. The PPIA-probe, in contrast, showed significant interaction with the largest number of ubiquitin related proteins among the four probes.

Although selected HDAC6 substrate peptides **P10**–**P17** were not able to differentiate between class I HDACs and HDAC6 by means of sequence context alone in these sensitive, MS-based experiments, and the experimental design does not imply a direct interaction relationship of identified proteins with HDAC6, a connection between several of the preferentially enriched functional categories of proteins and the cellular role of HDAC6 can be established.

Especially the high number of significantly enriched ubiquitin related, cytoskeletal and chaperone proteins is consistent with the fact that HDAC6 is thought to participate in autophagic clearance of misfolded proteins at intersecting pathways of protein degradation, transport and chaperone-mediated signaling as a response to cellular stress (Figure 47).[47,50]

Through its C-terminal zinc finger (ZnF) ubiquitin binding domain HDAC6 is able to bind to mono- and polyubiquitinylated protein aggregates, thereby delaying their degradation by the proteasome.[54] The chaperone VCP, which is a known interaction partner of HDAC6, is able to separate HDAC6 from protein aggregates and consequently a fine-tuned equilibrium between VCP and HDAC6 may be essential to the regulation of ubiquitinylated protein processing. When proteasomal degradation is impaired and misfolded proteins accumulate within the cell, HDAC6 can act as an adaptor protein between ubiquitinylated aggregates and dynein motors, which are responsible for cellular transport along microtubules.[47] These motors bind to HDAC6 in the linker region between its two catalytic domains[48] and it is thus not surprising that dynactin subunit 2 (DCTN2), a component of the dynein-dynactin motor complex, was significantly enriched in the interactome of the CRTC-probe. By this mechanism, HDAC6 is able to mediate the transport of misfolded proteins along microtubule tracks to structures called aggresomes, which are formed as a protective response to accumulation of cytotoxic protein aggregates and subsequently cleared by autophagy.[53,261] The tubulin deacetylase activity of HDAC6 might also contribute to the regulation of this pathway as well as cellular transport of cargo in general, because the acetylation status of microtubules was shown to

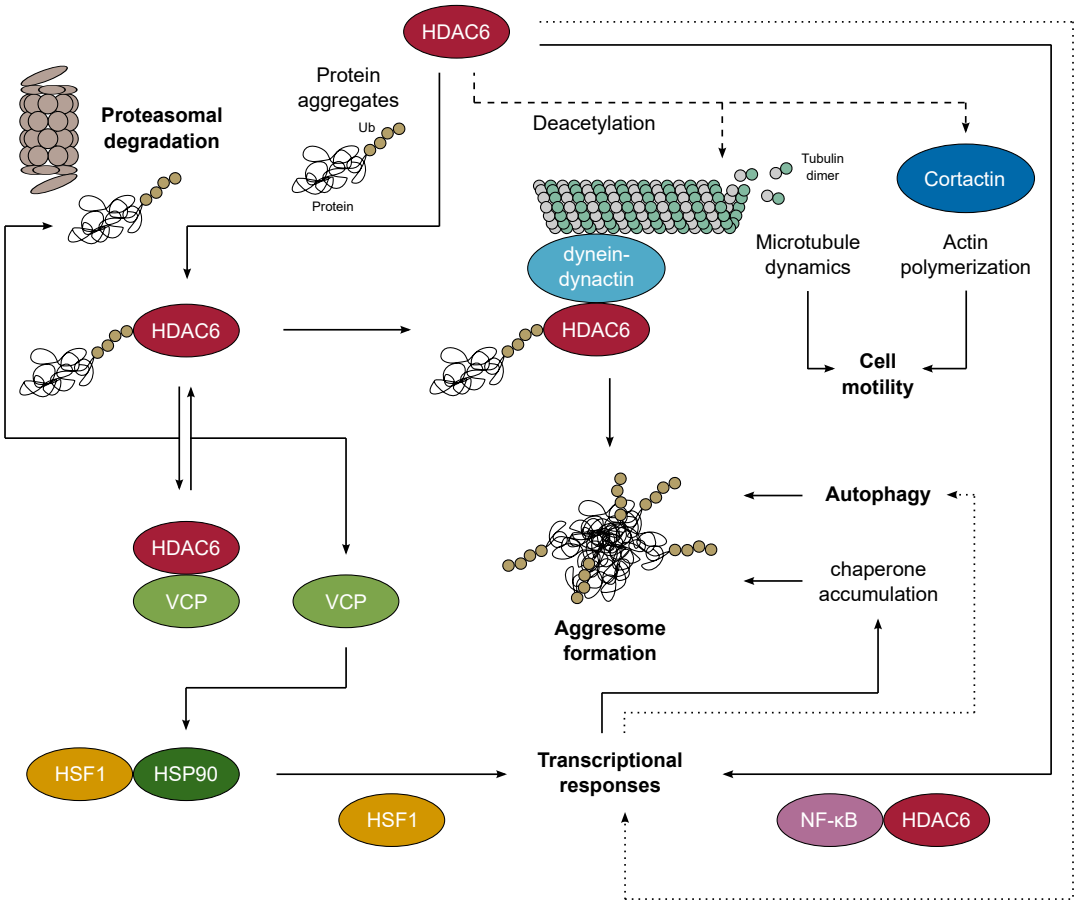

Figure 47: Schematic overview of several known and putative functions of HDAC6 in the regulation of cellular processes (bold script). Dashed lines indicate direct deacetylation of target proteins, whereas dotted lines represent activation by yet unknown mechanisms. For a detailed description refer to the text below. Ub: Ubiquitin.

influence binding and motility of the attached motor proteins.[262] A third regulatory influence of HDAC6 on misfolded protein processing might be indirectly mediated by the chaperone HSP90. While other functions of HSP90 are thought to be regulated by HDAC6 through direct deacetylation, in this pathway ubiquitin binding by HDAC6 leads to dissociation of the HDAC6-VCP complex, with VCP then being able to release heat shock transcription factor 1 (HSF1) from an inactive HSP90-HSF1 complex. HSF1 subsequently activates various HSP genes, leading to the cellular accumulation of chaperones.[263]

Presence of a variety of cytoskeletal and especially actin related proteins in the interactomes of the αTub-, CRTC- and PPIA-probes seems consistent with the putative role of HDAC6 in migrating cells. Through tubulin deacetylation HDAC6 is known to regulate the dynamics of microtubule stability at the leading edge of cells, thus increasing cell motility.[49] However, it might in addition be plausible that HDAC6-dependent regulation of the actin cytoskeleton is involved in this process, since HDAC6 was shown to deacetylate the protein cortactin (CTTN).[197] CTTN, which is also present in the interactome of the PPIA probe, if

deacetylated, binds to actin and promotes F-actin polymerization and branching. HDAC6 is also known to interact with the actin elongation factor mDia2.[264] The observed enrichment of additional proteins involved in both polymerization and depolymerization of F-actin, especially on the αTub-probe, further supports a role of HDAC6 in regulation of the actin cytoskeleton.[47,50]

Although primarily cytoplasmic, HDAC6 is also thought to elicit transcriptional responses under certain circumstances. By association with several transcription factors, e.g. Runx2, or transcriptional co-activators like SUMOylated p300, HDAC6 mediates a transcriptional repressor function of these proteins.[265,266] HDAC6 was also reported to induce a repressional function of the important transcription factor NF-κB by interaction with its p50 (NFKB1) and p65 (RELA) subunits.[267] Notably, while the p52 / p100 (NFKB2) and p65 (RelA) subunits of NF-κB were significantly enriched in the interactome of the PPIA-probe, the HSP90 sequence recruited both subunits (CHUK, IKBKB) of the IκB kinase (IKK) complex, which is involved in NF-κB activation. The IKK complex phosphorylates inhibitors of NF-κB (IκB), with phosphorylation being a signal for subsequent ubiquitinylation and thus targeting of the inhibitor to the proteasome.[199]

Despite plausible hints which link the interactome data of HDAC6 substrate peptides **P10**–**P17** to established as well as putative cellular functions of HDAC6, future experiments could lead to a more direct connection, e.g. by investigating the effects of HDAC6 knockdown on the interactomes or by incorporating an HDAC6-selective inhibitory moiety into the peptides instead of the broad-specificity AsuHd.

3.2.2.3 Effects of sequence context on catalysis

In order to examine the influence of sequence context on the velocity of HDAC6-catalyzed deacetylations of the substrate sites of αTub, CRTC, HSP90 and PPIA, an assay based on MALDI mass spectrometry was applied (Chapter 2.2.2.3).[175] Suitable substrates incorporating either acetylated or isotopically labeled free lysine were synthesized for all of the four sequences and an additional minimal control sequence, leading to peptides **P18**–**P27**. These peptides were then deacetylated by recombinant, full-length HDAC6 and substrate conversions could be quantified for each peptide in a direct manner due to the internal, isotopically labeled standard. The MALDI-based deacetylation assay therefore represented an ideal addition to the concept of high-throughput 96-well pulldowns, because it allowed fast measurement of reaction velocities without time-consuming HPLC analysis in a miniaturized format, requiring only minimal amounts of substrates and enzyme.

HDAC6 was able to deacetylate all of the five substrates, while displaying subtle differences in reaction velocity and thus substrate preference. The CRTC and PPIA sequences were deacetylated at a comparable rate, which may be attributed to residues of similar polarity at the ±1 and ±2 positions. Deacetylation of the minimal sequence context substrate was slightly faster and in a medium range. Surprisingly, while the HSP90 substrate was deacetylated fastest, reaction velocity was lowest for the αTub sequence. Taking this into account, it can be reasoned that preferred recruitment of HDAC6 to the αTub-probe might not be a result of direct enhancement of the enzyme-substrate interaction by the sequence, but of the sequence being less repulsive for HDAC6 than for other HDACs. In such a scenario

a slow reaction kinetics for HDAC6 would be plausible as long as deacetylation for other HDACs is even slower. Despite the fact that K40 of α-tubulin is a known substrate of HDAC6 and HSP90 was deacetylated with a high velocity, both sequences do not closely match the consensus sequence determined for HDAC6 substrates in this work (Figure 46) as well as in the related SPOT approach.[254] This may support the notion that substrate selectivity is not determined by HDAC6 alone, but may also be influenced and mediated by its interaction partners. These interacting proteins might be absent from recombinant forms of HDAC6, depending on the expression system and purification techniques used. However, the fact that the sequence context around K191 of HSP90 favored the HDAC6-catalyzed deacetylation is in line with the results from pulldown assays, where a strong recruitment to this sequence context in general was observed.

4 Conclusion and outlook

In this work, strategies for creating enzyme-specific peptide-based probes for histone deacetylases (HDACs) were developed. To this end, the influence of different zinc-binding functional groups and peptidic sequence contexts on the recruitment of individual HDACs and HDAC complexes was investigated.

In a first part, protected building blocks containing hydroxamate-, 2-aminopheylamide- and ketone-type inhibitory moieties were synthesized for incorporation into peptide-based probes as HDAC-trapping amino acids α-aminosuberic acid ω-hydroxamate (AsuHd), 2-amino-8-((2-aminophenyl)amino)-8-oxooctanoic acid (AsuApa) and 2-amino-8-oxodecanoic acid (Aoda) (Chapter 2.1). To this end, a common synthetic route was devised which relies on selective and simultaneous protection of the α-amino and -carboxy group of the respective amino acid precursor (Asu) with 9-BBN as oxazabololidinone (Chapter 2.1.1). This moiety is stable under a wide variety of conditions and allowed the selective modification of the amino acid side chain by introduction of either an *O*-trityl-protected hydroxamate (AsuHd), a Boc-protected 2-aminophenylamide (AsuApa) or an ethyl ketone moiety (Aoda). 9-BBN removal and subsequent Fmoc-protection furnished the final building blocks Fmoc-AsuHd(OTrt)-OH (**5**), Fmoc-AsuApa(Boc)-OH (**13**) and Fmoc-Aoda-OH (**5**). The first two building blocks have not been reported before and represent convenient tools for incorporation of hydoxamate and Apa moieties into synthetic peptides. Due to easily removable protecting groups, both building blocks are fully compatible with the requirements of automated, parallel SPPS necessary for generating large peptide libraries used in high-throughput assay approaches.

Incorporation of the AsuHd, AsuApa and Aoda building blocks into peptides with minimal sequence context yielded mini-AsuHd (**P2**), mini-AsuApa (**P3**) and mini-click-Aoda (**P7***) as HDAC affinity probes. While the probe design for the first two HDAC-trapping amino acids comprised a C-terminal cysteine residue for immobilization onto iodoacetyl-functionalized agarose beads, the Aoda moiety was immobilized by an on-resin azide-alkyne cycloaddition (click reaction). Pulldown assays with these probes and lysates from HeLa cells revealed distinct selectivity profiles for the recruitment of endogenous HDACs and HDAC complexes. While the AsuHd-containing probe **P2** could enrich all tested HDACs over a control peptide containing unmodified lysine instead of the HDAC-trapping amino acid, mini-AsuApa (**P3**) only enriched class I HDAC1, 2 and 3. Further analysis by MS-based proteomics revealed superior capability of mini-AsuApa (**P3**) to recruit the HDAC3 NCoR / SMRT complex (Chapter 2.1.2). Although a weaker HDAC binder when compared to hydroxamic acids, the Aoda-containing probe **P7*** was found to enrich class I HDAC1 more efficiently over the lysine control than class IIb HDAC6 (Chapter 2.1.3).

A second part of this work focused on the influence of peptide sequence contexts on HDAC recruitment by investigating the substrate selectivity of HDAC6 (Chapter 2.2). For this HDAC large sets of proteomic data are available, containing potentially regulated acetylation sites

that have to be further validated in biochemical assays. Motivated by the need for a high-throughput approach due to the high number of sites, a novel concept for HDAC pulldown assays based on the format of 96-well plates was developed (Chapter 2.2.1). In addition to an increased parallelization of handling achieved by using 96-well plates for all relevant steps during peptide synthesis, immobilization and pulldown, an optimized peptide probe design was key to the success of the approach. This design comprised AsuHd or the related ApmHd as central HDAC-trapping amino acids embedded into 14 residues of sequence context derived from potential HDAC6 substrate sites identified in two different proteomics experiments. The HDAC6 substrate probes further contained a C-terminal extension for protection against carboxypeptidases, a dansyl fluorophore for precise quantification, and an N-terminal thiol moiety for immobilization onto solid-support. Importantly, introduction of the thiol and fluorophore in the last step of the synthesis as the single building block Trt-Mpa-Lys(Dns)-OH (**22**) in combination with capping steps implemented after each synthesis cycle ensured that only full-length peptides contained the thiol for immobilization. Full-length probes could then be selectively captured from crude product mixtures with iodoacetyl-functionalized agarose, circumventing the need for time-consuming purification of peptides via preparative HPLC. Synthesis and cleavage protocols for these peptides using the building blocks Fmoc-AsuHd(OTrt)-OH (**5**) and Fmoc-ApmHd(OTrt)-OH (**10**) were optimized and side reactions that occurred during cleavage were analyzed in depth. Among these, reactions interfering with peptide immobilization and quantification could be addressed by using a DTT-modified version of the classical cleavage cocktail Reagent K, which resulted in greatly improved crude peptide purity.

Subsequent screening of 96 immobilized probe peptides for HDAC binding in large-scale pulldown experiments revealed that a majority of the chosen substrate sites was able to selectively enrich HDAC6 from cellular lysates on the AsuHd-containing probes when compared to the respective lysine controls. A minor fraction of sequences was not able to enrich HDAC6 over the lysine control and some sequences recruited both HDAC6 and HDAC1 in an unspecific manner. Together with a minimal sequence context probe as control, substrate sites of four promising candidates (TUBA1A, CRTC3, HSP90AA1, PPIA) showing selective enrichment of HDAC6 were chosen for further analysis (Chapter 2.2.2).

Probes were then re-synthesized with enantiomerically pure L-AsuHd using the design of established peptide-based HDAC affinity probes with a C-terminal cysteine residue for immobilization, furnishing mini- (**P2***), αTub- (**P11**), CRTC- (**P13**), HSP90- (**P15**) and PPIA-L-AsuHd (**P17**). The capability of these probes to recruit HDAC6 was again validated and pulldowns from cellular lysates were analyzed by MS-based proteomics in order to determine the interactome of each probe in relation to its lysine control. Identified interactors of the probe peptides and thereby potentially of HDAC6 included proteins associated with many important biological functions, such as histone modifying enzymes, cytoskeletal proteins, chaperones, ubiquitin-related proteins, transcription factors, signal transducers and cell cycle regulators. Each probe showed a distinct interaction profile and preference for functional categories of proteins, e.g. actin-related proteins for αTub, chaperones for HSP90, or ubiquitin-related proteins for PPIA. Finally, the ability of HDAC6 to catalyze the deacetylation of acetyllysine residues embedded in the four selected sequence contexts and the minimal sequence was tested *in vitro*. To this end, the peptides mini- (**P18**), αTub- (**P20**), CRTC- (**P22**), HSP90- (**P24**)

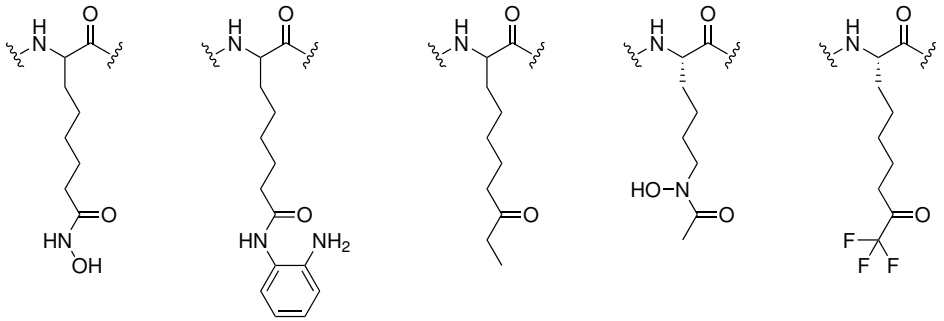

Figure 48: HDAC-trapping amino acids AsuHd (**38**), AsuApa (**32**), Aoda (**39**), *N*ε-acetyl-*N*ε-hydroxylysine (**40**) and Atona (**41**).

and PPIA-Lys(Ac) (**P26**) and corresponding isotopically labeled standards were synthesized and probed with recombinant human HDAC6 using a MALDI-MS-based kinetic assay. HDAC6 was able to deacetylate all of these substrates showing subtle differences in reaction velocities, with the HSP90 substrate being deacetylated fastest.

In summary, efficient tools and strategies could be developed that allow for fine-tuning the selectivity of peptide-based HDAC affinity probes, on the one hand through novel HDAC-trapping amino acids, and on the other hand through screening for peptide sequence contexts that mediate specific binding of HDACs. Although the current approach combining *in vitro* pulldown assays with MS-based interactomics and enzyme kinetics could increase confidence in a majority of investigated acetylation sites to be actually regulated by HDAC6, additional lines of experimentation are necessary and results should not be over-interpreted as direct relationships between HDAC6 and the potential substrates and binding partners. Besides using *in vitro* binding and activity assays, and "association-based" proteomics approaches, a high confidence HDAC substrate should ideally be validated by an additional cell-based or *in vivo* method.[39] With regard to potential HDAC interaction partners identified by MS-based interactomics, direct demonstration of the interaction by co-immunoprecipitation of the respective proteins from cellular lysates would be desirable.

Future work could focus on exploiting the obtained knowledge about HDAC substrate specificity to further improve the selectivity of peptide-based probes and inhibitors. This could be achieved by combining different HDAC-trapping amino acids and substrate site-derived sequence contexts, each with a distinct inherent selectivity, in a mix-and-match type of fashion. Besides AsuHd (**38**), AsuApa (**32**) and Aoda (**39**), which were used in this work, other promising HDAC-trapping amino acids are available, such as the retro hydroxamate *N*ε-acetyl-*N*ε-hydroxylysine (**40**) and the TFMK 2-amino-9,9,9-trifluoro-8-oxononanoic acid (Atona, **41**).[130,238] Yet unexplored potential remains in modifying the linker region of HDAC-trapping amino acids, which is an aliphatic carbon chain for all of the aforementioned compounds. For example, it appears plausible that selectivity of a certain compound can be steered towards HDAC6 by using an aromatic benzoyl moiety as linker. The potency of such an optimized peptide inhibitor could then be easily assessed with the MALDI-based HDAC deacetylation assay used in this work.

Although peptide-based HDAC affinity probes represent versatile tools for understanding HDAC function, so far, they are limited to *in vitro* applications. If HDAC-trapping amino acids could be used in a native cellular context *in vivo*, this could open new possibilities for studying HDAC complexes and the physiological processes in which they participate. To achieve this, HDAC-trapping amino acids could be genetically encoded with techniques such as amber suppression, in which the stop codon UAG ("amber") is reprogrammed and unnatural amino acids are introduced into target proteins by engineered tRNA synthetases.[268] This would allow to investigate HDAC-substrate interactions in a directed manner within living cells, and preliminary experiments with AsuHd have already been conducted.[269,270]

5 Materials and methods

5.1 Materials and general methods

All amino acid derivatives for solid-phase peptide synthesis and HBTU were purchased from *GL Biochem* (Shanghai, China), except Fmoc-D-Pro-OH and Fmoc-PEG_2-OH, which were bought from *Fluorochem* (Hadfield, UK), and Fmoc-PEG_3-OH, which was bought from *IRIS Biotech* (Marktredwitz, Germany). TentaGel HL RAM and TentaGel S RAM resins were obtained from *Rapp Polymere* (Tübingen, Germany).

All other chemicals were purchased from *Sigma Aldrich* (Steinheim, Germany), *Merck* (Darmstadt, Germany), *Carl Roth* (Karlsruhe, Germany), *TCI* (Eschborn, Germany), Bachem (Bubendorf, Switzerland) and *Carbolution* (St. Ingbert, Germany). Solvents were bought in addition from *J. T. Baker* (Deventer, Netherlands), *VWR* (Leuven, Belgium), *Fisher Scientific* (Loughborough, UK), *Biosolve* (Valkenswaard, Netherlands) and *Th. Geyer* (Renningen, Germany).

Fmoc-L-AsuHd(OTrt)-OH was synthesized as described in this work for the racemic building block **5** (Chapter 5.2.3) by *A. Kühn*.[269] Fmoc-Lys8(Boc)-OH was synthesized as reported.[175]

Manipulations that required air-free conditions were conducted using standard *Schlenk* techniques with argon or nitrogen as inert gas.[271] Reaction vessels were evacuated (~10^{-4} mbar) and filled with argon three times before usage. For filtration of solids frittet glass filters of pore size 3 or 4 were used.

5.2 Chemical methods

5.2.1 Analytical methods

5.2.1.1 TLC

Thin-layer chromatography (TLC) was performed on TLC silica gel foils with fluorescent indicator obtained from *Sigma-Aldrich*. Substances were visualized by illumination with UV light of 254 nm.

5.2.1.2 NMR spectroscopy

NMR spectra were recorded on a *Bruker* Advance III HD 300 XWB (Billercia, USA) or *Bruker* Advance III HDX 400 spectrometer. For the nuclei ^{1}H and ^{13}C chemical shifts δ in ppm are given relative to tetramethylsilane. For the assignment of ^{1}H resonances ^{1}H-^{1}H-COSY spectra were recorded. ^{13}C resonances were assigned on the basis of ^{13}C-DEPT-135, ^{1}H-^{13}C-HSQC and ^{1}H-^{13}C-HMBC experiments. ^{1}H spectra were referenced to the residual

proton signal of deuterated solvents (DMSO-d_5: δ/ppm = 2.50, $CDHCl_2$: δ/ppm = 5.32, MeCN-d_2: δ/ppm = 1.94, HDO: δ/ppm = 4.75), whereas ^{13}C spectra were referenced to the ^{13}C signal of the respective solvents (DMSO-d_6: δ/ppm = 39.5; CD_2Cl_2: δ/ppm = 54.0; MeCN-d_3: δ/ppm = 1.4, 118.7).

5.2.1.3 LC-MS

Compounds were characterized by liquid chromatography-mass spectrometry (LC-MS) using a *Shimadzu* LC-MS 2020 device (Kyoto, Japan) equipped with a Kinetex 2.6 µm C18 100 Å (100 × 2.1 mm) column (*Phenomenex*, Aschaffenburg, Germany). Samples were prepared with LC-MS solvents A (0.1 % formic acid in water) and B (80 % MeCN, 0.1 % formic acid in water) unless stated otherwise. The analytical gradient was 5–95 % B in 12.75 min or 40–99 % B in 12.00 min with a flow rate of 0.2 mL / min. Absorption was detected at 218 nm (oxazaborolidinone, amide / peptide bond) and 340 nm (dansyl group). The ESI-MS was operated in positive mode.

5.2.1.4 MALDI-MS

Matrix-assisted laser desorption / ionization (MALDI) mass spectrometry was performed on a *Bruker* Reflex IV MALDI-TOF device in reflection mode. α-Cyano-4-hydroxycinnamic acid (CHCA, 5 mg / mL in 50 % MeCN, 0.1 % TFA in water) or 2,5-dihydroxybenzoic acid (DHB, 20 mg / mL in 50 % MeCN, 0.1 % TFA in water) were used as matrices. Samples and matrix solutions were spotted in equal amounts onto a polished steel target. Spots were measured with at least 200 shots with laser intensity between 20 % and 50 %. Recorded mass spectra were baseline-corrected and smoothed with three runs of the Savitzky-Golay filter (window size 0.3 m/z) prior to peak analysis using mMass 5.5.0.[272]

5.2.2 Purification techniques

5.2.2.1 Preparative HPLC

HPLC purification was performed using a *Varian* ProStar 210 device equipped with a Reprosil 100 Å 5 µm C18 (250 × 20 mm) column (*Dr. Maisch*, Ammerbuch, Germany). Crude products were dissolved or emulsified in HPLC solvents A (0.1 % TFA in water) and B (80 % MeCN, 0.1 % TFA in water) prior to injection. The applied gradient was 5–95 % B in 40 min with a flow rate of 13 mL / min unless mentioned otherwise. Absorption was detected at 218 nm (oxazaborolidinone, amide / peptide bond). Collected fractions were analyzed by LC-MS and lyophilized.

5.2.2.2 Flash chromatography

Flash chromatography was performed with silica 60 M (0.04–0.063 mm particle size, *Macherey-Nagel*, Düren, Germany) and overpressure of 0.1–0.5 bar. Samples were loaded onto the column as solution in a small amount of the eluent. Fractions were analyzed by TLC and LC-MS and concentrated under reduced pressure.

5.2.3 Hydroxamic acid building block synthesis

5.2.3.1 Asu-BBN (2) and Apm-BBN (7)

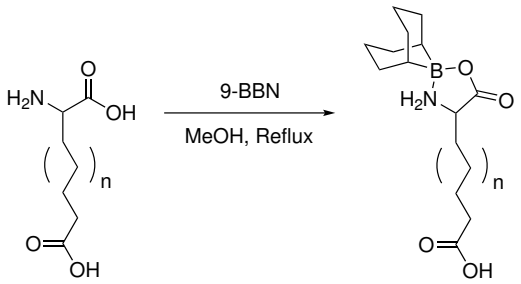

1 (n = 2)
6 (n = 1)

2 (n = 2)
7 (n = 1)

Asu-BBN (2)

Under argon atmosphere DL-α-aminosuberic acid (**1**) (1.89 g, 10 mmol, 1 eq) was suspended in anhydrous MeOH (60 mL) and heated at reflux. Subsequently, 9-BBN (0.5 M in THF, 22 mL, 11 mmol, 1.1 eq) was added dropwise, and heating was continued until gas evolution had ceased and the reaction mixture became a clear solution (approximately 2 h). The solvent was removed under reduced pressure and the colorless, viscous residue purified by preparative HPLC (Chapter 5.2.2.1), after which the desired product **2** was obtained as a white, powdery solid (2.81 g, 9.09 mmol, 91 %).

HPLC (5–95 % B in 12.75 min, 0.2 mL / min): $t_{ret.}$ = 11.58 min.

ESI-MS: $[M-9\text{-BBN}+H]^+$, m/z = 190.1 (calculated), 190.1 (found); $[M+H]^+$, m/z = 310.2 (calculated), 310.1 (found); $[M+Na]^+$, m/z = 332.2 (calculated), 332.2 (found); $[2\,M-9\text{-BBN}+H]^+$, m/z = 499.3 (calculated), 499.3 (found); $[2\,M+H]^+$, m/z = 619.4 (calculated), 619.3 (found); $[2\,M+Na]^+$, m/z = 641.4 (calculated), 641.5 (found).

^{1}H-NMR (400 MHz, DMSO-d$_6$): δ / ppm = 0.46 (s, 1 H, CH_{BBN}), 0.51 (s, 1 H, CH_{BBN}), 1.22–1.86 (m, 20 H, 6 CH_{2BBN}, 4 CH_{2Asu}), 2.21 (t, $^3J_{HH}$ = 7.3 Hz, 2 H, ζ-CH_2), 3.41–3.53 (m, 1 H, α-CH), 5.68–5.86 (m, 1 H, NH_2), 6.30–6.48 (m, 1 H, NH_2), 11.96 (br s, 1 H, CO_2H).

^{13}C{^{1}H}-NMR (101 MHz, DMSO-d$_6$): δ / ppm = 1.2, 22.3 (CH_{BBN}), 23.5 (CH_{BBN}), 23.9, 24.3 (ε-CH_2), 25.3, 28.2, 30.3, 30.7, 30.7, 31.2, 31.3, 33.5 (ζ-CH_2), 54.4 (α-CH), 173.7 (α-CO_2), 174.5 (ζ-CO_2).

Apm-BBN (7)

Apm-BBN (**7**) was synthesized as described for Asu-BBN (**2**), but using DL-α-aminopimelic acid (**6**) (1.41 g, 8.07 mmol, 1 eq), anhydrous MeOH (45 mL), and 9-BBN (0.5 M in THF, 18 mL, 8.9 mmol, 1.1 eq). The product **7** was obtained as a white, powdery solid (1.93 g, 6.53 mmol, 81 %).

HPLC (5–95 % B in 12.75 min, 0.2 mL / min): $t_{ret.}$ = 11.45 min.

ESI-MS: $[M-9\text{-BBN+H}]^+$, m/z = 176.1 (calculated), 176.1 (found); $[M+H]^+$, m/z = 296.2 (calculated), 296.0 (found); $[M+Na]^+$, m/z = 318.2 (calculated), 318.0 (found); $[2\,M-9\text{-BBN+H}]^+$, m/z = 471.3 (calculated), 471.2 (found); $[2\,M+H]^+$, m/z = 591.4 (calculated), 591.3 (found); $[2\,M+Na]^+$, m/z = 613.4 (calculated), 613.5 (found).

^{1}H-NMR (400 MHz, DMSO-d$_6$): δ / ppm = 0.46 (s, 1 H, CH_{BBN}), 0.51 (s, 1 H, CH_{BBN}), 1.33–1.84 (m, 18 H, 6 CH_{2BBN}, 3 CH_{2Apm}), 2.22 (t, $^3J_{HH}$ = 6.9 Hz, 2 H, ε-CH_2), 3.40–3.55 (m, 1 H, α-CH), 5.69–5.86 (m, 1 H, NH_2), 6.31–6.48 (m, 1 H, NH_2).

^{13}C{^{1}H}-NMR (101 MHz, DMSO-d$_6$): δ / ppm = 22.3 (CH_{BBN}), 23.4 (CH_{BBN}), 23.9, 24.2, 24.6 (δ-CH_2), 25.2, 30.2, 30.7, 31.2, 31.3, 33.6 (ε-CH_2), 54.4 (α-CH), 173.7 (α-CO_2), 174.4 (ε-CO_2).

5.2.3.2 AsuHd(OTrt)-BBN (3) and ApmHd(OTrt)-BBN (8)

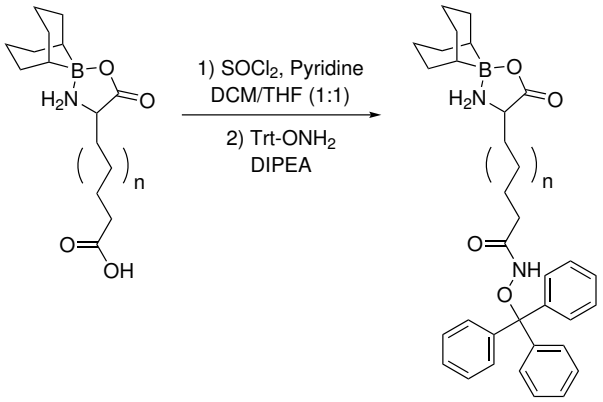

2 (n = 2)
7 (n = 1)

3 (n = 2)
8 (n = 1)

AsuHd(OTrt)-BBN (3)

Crude Asu-BBN (**2**) (corresponding to 5.00 mmol of **1**) was dissolved in anhydrous DCM / THF (1:1, 100 mL) under argon atmosphere. After addition of pyridine (0.41 mL, 5.00 mmol, 1 eq) and $SOCl_2$ (0.37 mL, 5.00 mmol, 1 eq) the reaction mixture was stirred at room temperature for 1 h. The mixture was cooled in an ice bath and a solution of Trt-ONH_2 (1.38 g, 5.00 mmol, 1 eq) and DIPEA (2.62 mL, 15.0 mmol, 3 eq) in anhydrous DCM / THF (1:1, 25 mL) was added dropwise. The mixture was brought to room temperature overnight while stirring, and then

concentrated under reduced pressure to yield the crude product **3**, which was used in the next step without further purification.

HPLC (40–99 % B in 12.00 min, 0.2 mL / min): $t_{ret.}$ = 15.48 min.

ESI-MS: $[M+Na]^+$, m/z = 589.3 (calculated), 589.5 (found).

ApmHd(OTrt)-BBN (8)

ApmHd(OTrt)-BBN (**8**) was synthesized as described for AsuHd(OTrt)-BBN (**3**), but using HPLC-purified Apm-BBN (**7**) (1.48 g, 5.00 mmol, 1 eq) in anhydrous DCM / THF (1:1, 100 mL), pyridine (0.41 mL, 5.00 mmol, 1 eq), and $SOCl_2$ (0.37 mL, 5.00 mmol, 1 eq). Trt-ONH_2 (1.38 g, 5.00 mmol, 1 eq) and DIPEA (2.62 mL, 15.0 mmol, 3 eq) were dissolved in anhydrous DCM / THF (1:1, 25 mL) and the crude product **8** was used in the next step without further purification.

HPLC (40–99 % B in 12.00 min, 0.2 mL / min): $t_{ret.}$ = 15.23 min.

ESI-MS: $[M+Na]^+$, m/z = 575.3 (calculated), 575.3 (found).

5.2.3.3 H-AsuHd(OTrt)-OH (4) and H-ApmHd(OTrt)-OH (9)

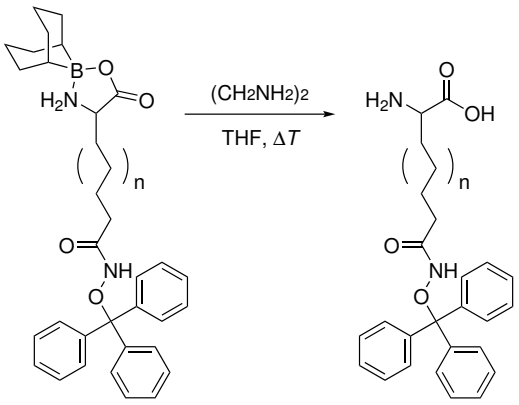

3 (n = 2)
8 (n = 1)

4 (n = 2)
9 (n = 1)

H-AsuHd(OTrt)-OH (4)

Crude AsuHd(OTrt)-BBN (**3**) (corresponding to 5.00 mmol of **1**) was dissolved in THF (50 mL), ethylenediamine (1.67 mL, 25.0 mmol, 5 eq) was added, and the mixture was heated for 1 min below the boiling point. The precipitate was collected by centrifugation and dissolved in MeCN / H_2O. The pH was adjusted to 4 with aqueous HCl and the crude product purified by preparative HPLC (Chapter 5.2.2.1). The fractions were neutralized with aqueous NaOH, lyophilized, and the desired product **4** was obtained as white, powdery solid (1.36 g, 3.04 mmol, 61 % with respect to **1**).

HPLC (40–99 % B in 12.00 min, 0.2 mL / min): $t_{ret.}$ = 7.21 min.

ESI-MS: [M−Trt+H]$^+$, m/z = 205.1 (calculated), 205.3 (found); [M+H]$^+$, m/z = 447.2 (calculated), 447.3 (found); [M+Na]$^+$, m/z = 469.2 (calculated), 469.3 (found); [2 M+H]$^+$, m/z = 893.4 (calculated), 893.7 (found); [2 M+Na]$^+$, m/z = 915.4 (calculated), 915.3 (found).

^{1}H-NMR (400 MHz, MeCN-d_3 / D_2O (3:1)): δ / ppm = 1.49–1.64 (m, 2 H, δ-CH_2), 1.68–1.85 (m, 4 H, γ / ε-CH_2), 1.98–2.19 (m, 2 H, β-CH_2), 2.27–2.42 (m, 2 H, ζ-CH_2), 3.74–3.91 (m, 1 H, α-CH), 7.76–8.06 (m, 15 H, CH_{Trt}).

^{13}C{^{1}H}-NMR (101 MHz, MeCN-d_3 / D_2O (3:1)): δ / ppm = 25.7 (γ / ε-CH_2), 25.7 (γ / ε-CH_2), 29.3 (δ-CH_2), 33.3 (ζ-CH_2), 33.5 (β-CH_2), 56.4 (α-CH_2), 93.8* (CPh_3), 119.1 (CH_{Trt}), 128.9 (CH_{Trt}), 130.0 (CH_{Trt}), 143.3 (CCH_{Trt}), 173.2* (ζ-CO), 178.6* (α-CO_2).

Values marked with an asterisk were determined from the respective ^{1}H-^{13}C-HMBC-NMR spectrum.

H-ApmHd(OTrt)-OH (9)

H-ApmHd(OTrt)-OH (**9**) was synthesized as described for H-AsuHd(OTrt)-OH (**4**), but using crude ApmHd(OTrt)-BBN (**8**) (corresponding to 5.00 mmol of **7**), THF (50 mL), and ethylenediamine (1.67 mL, 25.0 mmol, 5 eq), resulting in product **8** as white, powdery solid (1.61 g, 3.73 mmol, 75 % with respect to **7**).

HPLC (40–99 % B in 12.00 min, 0.2 mL / min): $t_{ret.}$ = 6.51 min.

ESI-MS: [M−Trt+H]$^+$, m/z = 291.1 (calculated), 191.5 (found); [M+H]$^+$, m/z = 433.2 (calculated), 433.1 (found); [M+Na]$^+$, m/z = 455.2 (calculated), 455.0 (found); [2 M+H]$^+$, m/z = 865.4 (calculated), 865.6 (found); [2 M+Na]$^+$, m/z = 887.4 (calculated), 887.1 (found).

^{1}H-NMR (400 MHz, MeCN-d_3 / D_2O (1:1)): δ / ppm = 1.38–1.52 (m, 2 H, γ-CH_2), 1.52–1.64 (m, 2 H, δ-CH_2), 1.83–2.02 (m, 2 H, β-CH_2), 2.19 (t, $^3J_{HH}$ = 7.6 Hz, 2 H, ε-CH_2), 3.69–3.76 (m, 1 H, α-CH), 7.43–7.97 (m, 15 H, CH_{Trt}).

^{13}C{^{1}H}-NMR (101 MHz, MeCN-d_3 / D_2O (1:1)): δ / ppm = 25.3 (γ-CH_2), 25.6 (δ-CH_2), 32.4 (β-CH_2), 33.0 (ε-CH_2), 56.0 (α-CH_2), 94.0 (CPh_3), 119.7 (CH_{Trt}), 128.9 (CH_{Trt}), 129.8 (CH_{Trt}), 142.8 (CCH_{Trt}), 173.2 (ε-CO), 177.7 (α-CO_2).

5.2.3.4 Fmoc-AsuHd(OTrt)-OH (5) and Fmoc-ApmHd(OTrt)-OH (10)

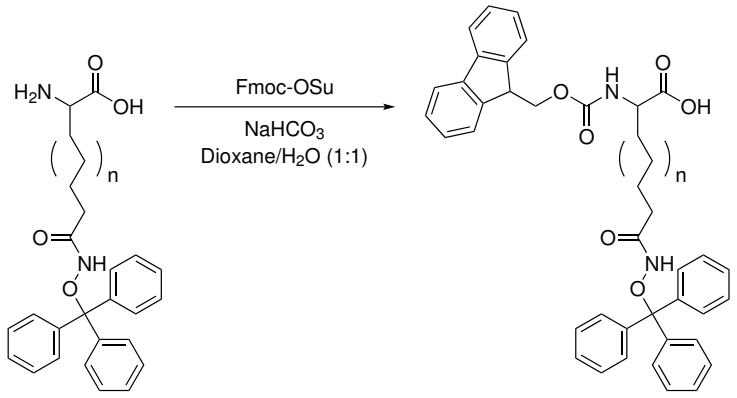

4 (n = 2)
9 (n = 1)

5 (n = 2)
10 (n = 1)

Fmoc-AsuHd(OTrt)-OH (5)

H-AsuHd(OTrt)-OH (**4**) (1.36 g, 3.04 mmol, 1 eq) and $NaHCO_3$ (0.74 g, 9.12 mmol, 3 eq) were dissolved in dioxane / H_2O (60 mL), and Fmoc-OSu (0.51 g, 1.52 mmol, 0.5 eq), dissolved in dioxane (6 mL), was added. The mixture was stirred for 1 h at room temperature and the reaction monitored via LC-MS. Further Fmoc-OSu, dissolved in dioxane, was added in portions of 0.1 eq (to prevent Fmoc-β-alanine formation by excess reagent) until full conversion was achieved. The reaction mixture was extracted with EtOAc (3×30 mL), the pooled organic phases dried over Na_2SO_4, and then concentrated under reduced pressure to yield the desired product **5** as colorless solid (1.61 g, 2.41 mmol, 79 %, 48 % with respect to **1**).

HPLC (40–99 % B in 12.00 min, 0.2 mL / min): $t_{ret.}$ = 15.23 min.

ESI-MS: $[M-Trt+H]^+$, m/z = 427.2 (calculated), 427.3 (found); $[M+H]^+$, m/z = 669.3 (calculated), 669.3 (found); $[M+Na]^+$, m/z = 691.3 (calculated), 691.4 (found); $[2\,M+Na]^+$, m/z = 1359.6 (calculated), 1359.9 (found).

Fmoc-ApmHd(OTrt)-OH (10)

Fmoc-ApmHd(OTrt)-OH (**10**) was synthesized as described for Fmoc-AsuHd(OTrt)-OH (**5**), but using H-ApmHd(OTrt)-OH (**9**) (1.61 g, 3.73 mmol, 1 eq), $NaHCO_3$ (0.78 g, 9.28 mmol, 2.5 eq), dioxane / H_2O (40 mL), and Fmoc-OSu (0.63 g, 1.86 mmol, 0.5 eq), dissolved in dioxane (4 mL). The desired product **10** was obtained as colorless solid (1.83 g, 2.80 mmol, 75 %, 56 % with respect to **6**).

HPLC (40–99 % B in 12.00 min, 0.2 mL / min): $t_{ret.}$ = 14.37 min.

ESI-MS: $[M+Na]^+$, m/z = 677.3 (calculated), 677.1 (found); $[2\,M+Na]^+$, m/z = 1331.5 (calculated), 1331.7 (found).

5.2.4 2-Aminophenylamide building block synthesis

5.2.4.1 AsuApa(Boc)-BBN (11)

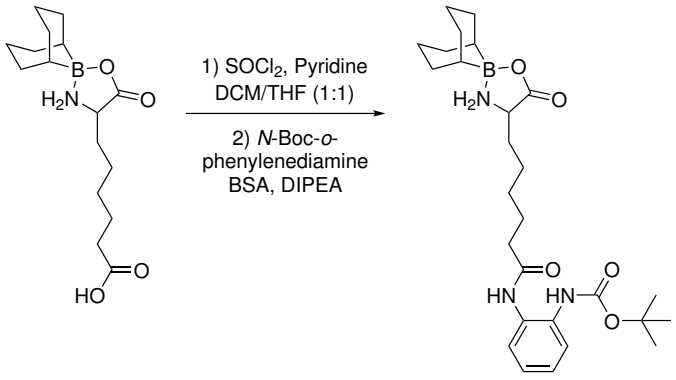

2 **11**

Asu-BBN (**2**) (1.55 g, 5.00 mmol, 1 eq) was dissolved in anhydrous DCM / THF (1:1, 100 mL) under nitrogen atmosphere. After addition of pyridine (0.40 mL, 5.00 mmol, 1 eq) and $SOCl_2$ (0.36 mL, 5.00 mmol, 1 eq) the reaction mixture was stirred at room temperature for 1 h, resulting in the acid chloride of **2**.

In parallel, *N*-Boc-*o*-phenylenediamine (1.08 g, 5.19 mmol, 1.03 eq) was dissolved in anhydrous DCM (20 mL) under nitrogen atmosphere, *N*,*O*-bis(trimethylsilyl)acetamide (2.43 mL, 10.0 mmol, 2 eq) was added, and the mixture was heated under reflux for 1 h. The mixture was cooled to room temperature, followed by addition of DIPEA (3.48 mL, 20.0 mmol, 4 eq).

This solution was added dropwise to the previously prepared acid chloride of **2**. The mixture was stirred overnight at room temperature and then concentrated under reduced pressure to yield crude product **11** as a reddish brown oil, which was used in the next step without further purification.

HPLC (40–99 % B in 12.00 min, 0.2 mL / min): $t_{ret.}$ = 13.41 min.

ESI-MS: $[M-9\text{-BBN+H}]^+$, m/z = 380.2 (calculated), 380.2 (found); $[M-\text{Boc+H}]^+$, m/z = 400.3 (calculated), 400.2 (found); $[M+H]^+$, m/z = 500.3 (calculated), 500.2 (found); $[M+Na]^+$, m/z = 522.3 (calculated), 522.2 (found); $[2\,M+Na]^+$, m/z = 1021.6 (calculated), 1021.5 (found).

5.2.4.2 H-AsuApa(Boc)-OH (12)

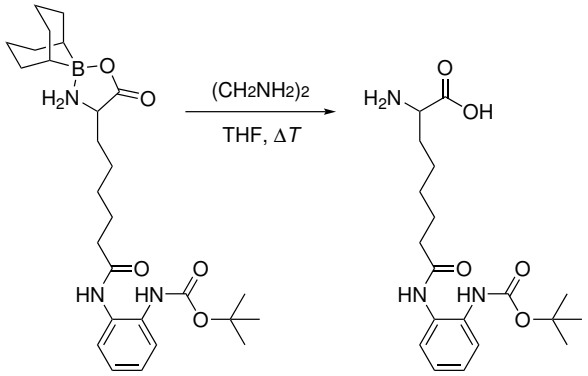

11 **12**

Crude AsuApa(Boc)-BBN (**11**) (corresponding to 5.00 mmol of **2**) was dissolved in THF (20 mL), ethylenediamine (3.34 g, 50.0 mmol, 10 eq) was added, and the mixture was heated for 1 min below the boiling point. Further ethylenediamine (3.34 g, 50.0 mmol, 10 eq) was added and the heating procedure was repeated. The solvent was removed under reduced pressure and the residue was dissolved in MeCN / H_2O. The pH was adjusted to 6 with TFA and the crude product was purified by preparative HPLC, resulting in **12**, which was obtained as a red powder (403 mg, 1.06 mmol, 21 % with respect to **2**).

HPLC (5–95 % B in 12.75 min, 0.2 mL / min): $t_{ret.}$ = 8.19 min.

ESI-MS: [M−Boc+H]$^+$, m/z = 280.2 (calculated), 280.2 (found); [M+H]$^+$, m/z = 380.2 (calculated), 380.0 (found); [M+Na]$^+$, m/z = 522.3 (calculated), 522.2 (found); [2 M+H]$^+$, m/z = 759.4 (calculated), 759.5 (found).

^{1}H-NMR (400 MHz, DMSO-d_6): δ / ppm = 1.28–1.40 (m, 4 H, 4/5-H), 1.45 (s, 9 H, 17- H), 1.54–1.66 (m, 2 H, 6-H), 1.71–1.85 (m, 2 H, 3-H), 2.35 (t, $^3J_{HH}$ = 7.3 Hz, 2 H, 7-H), 3.83–39.5 (m, 1 H, 2-H), 7.02–7.16 (m, 2 H, 11/12-H), 7.37–7.46 (m, 1 H, 10/13-H), 7.49–7.59 (m, 2 H, 10/13-H), 8.30 (s, 2 H, NH_2), 8.34 (s, 1 H, NH), 9.48 (s, 1 H, NH).

^{13}C{^{1}H}-NMR (101 MHz, DMSO-d_6): δ / ppm = 24.2 (C-4/5), 24.9 (C-6), 28.1 (C-17), 28.1 (C-4/5), 29.9 (C-3), 35.8 (C-7), 52.0 (C-2), 79.4 (C-16), 123.7 (C-10/13), 123.9 (C-11/12), 124.9 (C-10/13), 125.1 (C-11/12), 129.7 (C-9/14), 131.2 (C-9/14), 153.1 (C-15), 171.2 (C-1), 171.7 (C-8).

5.2.4.3 Fmoc-AsuApa(Boc)-OH (13)

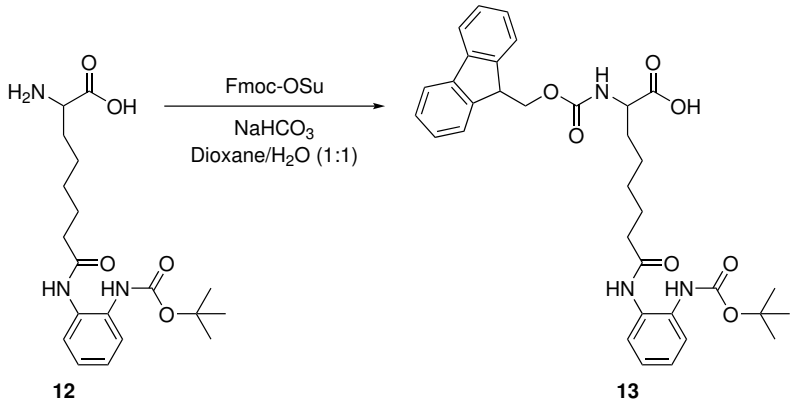

12 13

H-AsuApa(Boc)-OH (**12**) (403 mg, 1.06 mmol, 1 eq) and $NaHCO_3$ (267 mg, 3.18 mmol, 3 eq) were dissolved in dioxane / H_2O (1:1, 40 mL), and Fmoc-OSu (371 g, 1.10 mmol, 1.04 eq) was added. The reaction mixture was stirred for 3 h at room temperature, concentrated under reduced pressure, and lyophilized. The reddish crude product was purified by flash chromatography with silica gel as stationary and MeOH / DCM (1:19) as mobile phase. The desired product **13** was obtained as a colorless solid (375 mg, 0.62 mmol, 13 % with respect to **1**).

TLC: R_f = 0.27 (MeOH / DCM (1:19)).

HPLC (40–99 % B in 12.00 min, 0.2 mL / min): $t_{ret.}$ = 13.58 min.

ESI-MS: $[M-Boc+H]^+$, m/z = 502.2 (calculated), 502.1 (found); $[M+H]^+$, m/z = 602.3 (calculated), 602.3 (found); $[M+Na]^+$, m/z = 624.3 (calculated), 624.3 (found); $[2\,M+H]^+$, m/z = 1203.6 (calculated), 1203.9 (found); $[2\,M+Na]^+$, m/z = 1225.6 (calculated), 1225.6 (found).

^{1}H-NMR (400 MHz, CD_2Cl_2): δ / ppm = 1.28–1.45 (m, 4 H, 5/6-H), 1.45–1.57 (m, 9 H, 17-H), 1.57–1.77 (m, 4 H, 3/4-H), 1.77–1.92 (m, 1 H, 2-H), 2.34 (t, $^3J_{HH}$ = 7.2 Hz, 2 H, 7-H), 4.22 (t, $^3J_{HH}$ = 7.1 Hz, 1 H, 20-H), 4.39 (d, $^3J_{HH}$ = 6.7 Hz Hz, 2 H, 19-H), 7.05–7.22 (m, 2 H, 11/12-H), 7.25–7.34 (m, 2 H, 23-H), 7.34–7.50 (m, 4 H, 10/13/25-H), 7.50–7.67 (m, 2 H, 24-H), 7.77 (d, $^3J_{HH}$ = 7.5 Hz, 2 H, 22-H).

^{13}C{^{1}H}-NMR (101 MHz, CD_2Cl_2): δ / ppm = 25.4 (C-5/6), 25.8 (C-3/4), 28.6 (C-17), 29.0 (C-5/6), 32.5 (C-3/4), 37.2 (C-7), 47.7 (C-20), 67.6 (C-19), 81.6 (C-16), 120.5 (C-22), 125.0 (C-10/13), 125.5 (C-24), 120.6 (C-11/12), 126.1 (C-10/13), 126.9 (C-11/12), 127.6 (C-23), 128.3 (C-25), 130.3 (C-9/14), 131.7 (C-9/14), 141.8 (C-26), 144.3 (C-21), 155.0 (C-15), 156.9 (C-18), 173.9 (C-8), 175.9 (C-1).

5.2.5 Ketone building block synthesis

5.2.5.1 Asu(NMe-OMe)-BBN (14)

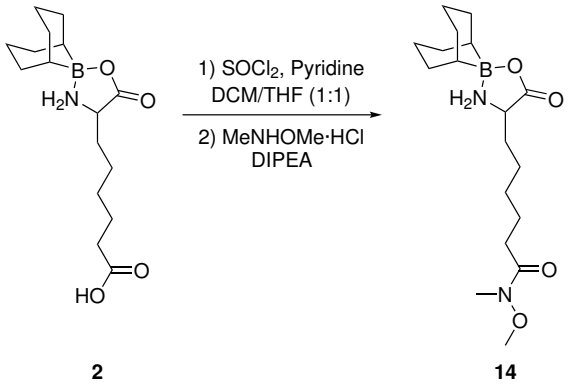

2 **14**

Asu-BBN (**2**) (1.55 g, 5.00 mmol, 1 eq) was dissolved in anhydrous DCM / THF (1:1, 100 mL) under nitrogen atmosphere. After addition of pyridine (0.40 mL, 5.00 mmol, 1 eq) and $SOCl_2$ (0.36 mL, 5.00 mmol, 1 eq) the reaction mixture was stirred at room temperature for 1 h. A solution of *N*,*O*-dimethylhydroxylamine hydrochloride (0.49 g, 5.00 mmol, 1 eq) and DIPEA (3.48 mL, 20.0 mmol, 4 eq) in anhydrous DCM / THF (1:1, 25 mL) was added dropwise to the reaction mixture. After stirring overnight the mixture was concentrated under reduced pressure, the residue dissolved in Et_2O (150 mL), and washed with aqueous HCl (1 M) and saturated $NaHCO_3$ solution. After drying over Na_2SO_4, the crude product **14** was obtained as light brown oil, which was used in the next step without further purification.

HPLC (40–99 % B in 12.00 min, 0.2 mL / min): $t_{ret.}$ = 9.80 min.

ESI-MS: $[M-9\text{-BBN+H}]^+$, m/z = 233.1 (calculated), 233.3 (found); $[M+H]^+$, m/z = 353.3 (calculated), 353.1 (found); $[M+Na]^+$, m/z = 375.2 (calculated), 375.3 (found); $[2\,M+H]^+$, m/z = 705.5 (calculated), 705.6 (found); $[2\,M+Na]^+$, m/z = 727.5 (calculated), 727.5 (found).

^{1}H-NMR (400 MHz, DMSO-d$_6$): δ / ppm = 0.46 (s, 1 H, CH_{BBN}), 0.51 (s, 1 H, CH_{BBN}), 1.23–1.82 (m, 20 H, 6 $CH_{2\,BBN}$, 4 $CH_{2\,Asu}$), 2.37 (t, $^3J_{HH}$ = 7.3 Hz, 2 H, ζ-CH_2), 3.08 (s, 3 H, NCH_3), 3.43–3.51 (m, 1 H, α-CH), 3.65 (s, 3 H, OCH_3), 5.71–5.82 (m, 1 H, NH_2), 6.35–6.45 (m, 1 H, NH_2).

^{13}C{^{1}H}-NMR (101 MHz, DMSO-d$_6$): δ / ppm = 12.4, 22.3 (CH_{BBN}), 23.4 (CH_{BBN}), 23.9, 24.2 (ε-CH_2), 25.3, 28.4, 30.3, 30.7, 30.7, 31.0 (ζ-CH2) 31.2, 31.3, 31.9 (NCH_3) 54.4 (α-CH), 61.0 (OCH_3) 173.7 (α-CO_2), 173.7 (ζ-CO).

5.2.5.2 H-Aoda-OH (15)

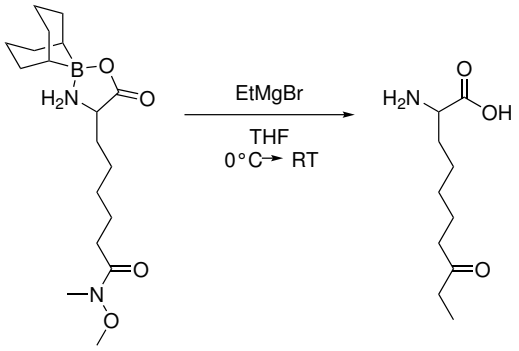

14 **15**

Under nitrogen atmosphere crude Asu(NMe-OMe)-BBN (**14**) (corresponding to 5 mmol of **2**) was dissolved in anhydrous THF (50 mL) and cooled in an ice bath. EtMgBr (1 M in THF, 5.0 mL, 5.0 mmol, 1 eq) was added and the solution was stirred for 2.5 h at ice bath temperature. The mixture was brought to room temperature, further EtMgBr (1 M in THF, 10.0 mL, 10.0 mmol, 2 eq) was added, and stirring was continued for 3 h. The reaction mixture was then slowly poured into an ice-cold solution of HCl (5 %) in EtOH (50 mL) under stirring. After concentration under reduced pressure, the residue was dissolved in H_2O (55 mL) and washed with EtOAc (3×25 mL). The aqueous phase was lyophilized and the crude product **15** was obtained as light brown solid, which was used in the next step without further purification.

HPLC (40–99 % B in 12.00 min, 0.2 mL / min): $t_{ret.}$ = 4.50 min.

ESI-MS: $[M+H]^+$, m/z = 202.1 (calculated), 202.4 (found).

5.2.5.3 Fmoc-Aoda-OH (16)

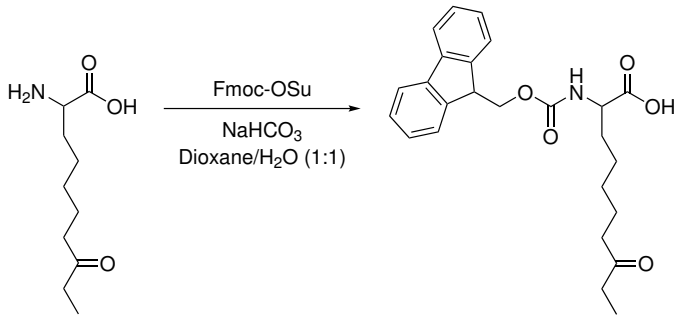

15 **16**

Crude H-Aoda-OH (corresponding to 2.00 mmol of **2**) was dissolved in dioxane / H_2O (20 mL), the pH was adjusted to 8 with aqueous $NaHCO_3$ (1 M), and Fmoc-OSu (0.34 g, 1.00 mmol,

0.5 eq), dissolved in dioxane (2 mL), was added. The mixture was stirred for 1 h at room temperature and the reaction monitored via LC-MS. Further Fmoc-OSu, dissolved in dioxane, was added in portions of 0.1 eq (to prevent Fmoc-β-alanine formation by excess reagent) until full conversion was achieved. The reaction mixture was acidified with aqueous HCl (2 M) and extracted with EtOAc (3×10 mL). The pooled organic phases were dried over Na_2SO_4 and then concentrated under reduced pressure.

The crude product was purified by flash chromatography with silica gel as stationary and hexane / EtOAc (1:19) as mobile phase, after which the desired product **16** was obtained as colorless oil (0.17 g, 0.41 mmol, 21 % with respect to **2**).

TLC: R_f = 0.35 (Hexane / EtOAc (1:19)).

HPLC (40–99 % B in 12.75 min, 0.2 mL / min): $t_{ret.}$ = 11.83 min.

ESI-MS: $[M+H]^+$, m/z = 424.2 (calculated), 424.5 (found); $[M+Na]^+$, m/z = 446.2 (calculated), 446.3 (found); $[2M+Na]^+$, m/z = 869.4 (calculated), 869.7 (found).

^{1}H-NMR (400 MHz, DMSO-d$_6$): δ / ppm = 2.76 (t, $^3J_{HH}$ = 7.3 Hz, 3 H, CH_{3Aoda}), 1.15–1.38 (m, 6 H, 3 CH_{2Aoda}), 1.38–1.51 (m, 2 H, CH_{2Aoda}), 1.51–1.75 (m, 2 H, CH_{2Aoda}), 2.39 (q, $^3J_{HH}$ = 7.2 Hz, 2 H, C$H_2$$CH_{3Aoda}$), 3.86–3.96 (m, 1 H, α-CH), 4.17–4.25 (m, 1 H, C$H$$CH_{2Fmoc}$), 4.25–4.32 (m, 2 H, CHCH_{2Fmoc}), 7.28–7.37 (m, 2 H, CH_{Fmoc}), 7.37–7.47 (m, 2 H, CH_{Fmoc}), 7.58–7.66 (m, 1 H, NH), 7.73 (d, $^3J_{HH}$ = 7.3 Hz, 2 H, CH_{Fmoc}), 7.89 (d, $^3J_{HH}$ = 7.6 Hz, 2 H, CH_{Fmoc}), 12.51 (br s, 1 H, CO_2H).

^{13}C{^{1}H}-NMR (101 MHz, DMSO-d$_6$): δ / ppm = 7.7 ($CH_2$$C$$H_{3Aoda}$), 23.0 ($CH_{2Aoda}$), 25.3 ($CH_{2Aoda}$), 28.1 ($CH_{2Aoda}$), 30.6 ($CH_{2Aoda}$), 34.9 ($C$$H_2$$CH_{3Aoda}$), 41.3 (ζ-$CH_2$), 46.7 ($CHCH_{2Fmoc}$), 53.7 (α-CH), 65.6 (CH$C$$H_{2Fmoc}$), 120.1 ($CH_{Fmoc}$), 125.3 ($CH_{Fmoc}$), 127.0 ($CH_{Fmoc}$), 127.6 ($CH_{Fmoc}$), 140.7 ($C_{qFmoc}$), 143.8 ($C_{qFmoc}$), 156.1 (CONH), 174.0 (COOH), 210.9 (CO$CH_2$$CH_{3Aoda}$).

5.2.6 Fluorophore building block synthesis

5.2.6.1 Lys-BBN (18)

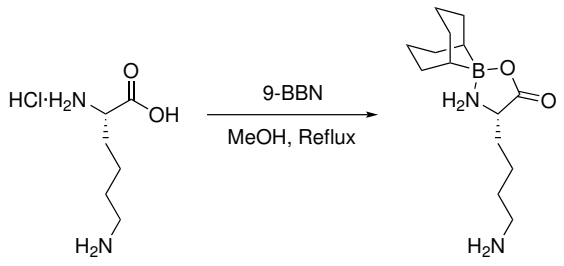

17 **18**

Under argon atmosphere H-Lys-OH · HCl (**17**) (1.83 g, 10 mmol, 1 eq) was suspended in anhydrous MeOH (60 mL) and heated at reflux. Subsequently, 9-BBN (0.5 M in THF, 22 mL, 11 mmol, 1.1 eq) was added dropwise, and heating was continued until gas evolution had

ceased and the reaction mixture became a clear solution (approximately 2 h). The solvent was removed under reduced pressure and the colorless, viscous residue purified by preparative HPLC (Chapter 5.2.2.1), after which the desired product **18** was obtained as mixture with the by-product from excess 9-BBN that could not be separated.

HPLC (5–95 % B in 12.75 min, 0.2 mL / min): $t_{ret.}$ = 7.86 min.

ESI-MS: [M−9-BBN+H]$^+$, m/z = 147.1 (calculated), 147.1 (found); [M+H]$^+$, m/z = 267.2 (calculated), 267.2 (found); [M+Na]$^+$, m/z = 289.2 (calculated), 289.2 (found); [2 M+H]$^+$, m/z = 533.4 (calculated), 533.3 (found); [2 M+Na]$^+$, m/z = 555.4 (calculated), 555.2 (found).

^{1}H-NMR (300 MHz, DMSO-d$_6$): δ / ppm = 0.46 (s, 1 H, CH_{BBN}), 0.51 (s, 1 H, CH_{BBN}), 1.16–1.92 (m, 18 H, 6 CH_{2BBN}, 3 CH_{2Lys}), 2.68–2.89 (m, 2 H, ε-CH_2), 3.41–3.59 (m, 1 H, α-CH), 5.69–5.96 (m, 1 H, NH_2), 6.35–6.64 (m, 1 H, NH_2), 7.87 (br s, 3 H, ε-NH_3^+).

^{13}C{^{1}H}-NMR (75 MHz, DMSO-d$_6$): δ / ppm = 22.4, 23.4 (CH_{BBN}), 23.5 (CH_{BBN}), 23.9, 24.3, 26.6, 29.7, 29.7, 30.7, 31.2, 31.3, 38.6 (ε-CH_2), 54.2 (α-CH), 173.7 (α-CO_2).

5.2.6.2 Lys(Dns)-BBN (19)

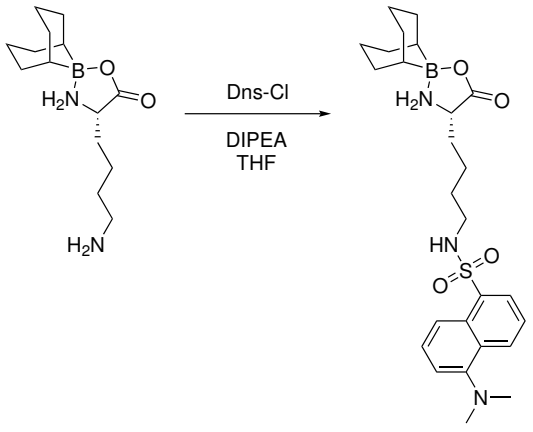

18 **19**

Crude Lys-BBN (**18**) (corresponding to 10.0 mmol of **17**) was dissolved in anhydrous THF (100 mL) and DIPEA (4.37 mL, 25.0 mmol, 2.5 eq) was added, followed by Dns-Cl (2.70 g, 10.0 mmol, 1 eq). The mixture was stirred overnight at room temperature and then concentrated under reduced pressure. The crude product **19** was used in the next step without further purification.

HPLC (40–99 % B in 12.00 min, 0.2 mL / min): $t_{ret.}$ = 13.41 min.

ESI-MS: [M−9-BBN+H]$^+$, m/z = 380.2 (calculated), 380.2 (found); [M+H]$^+$, m/z = 500.3 (calculated), 500.2 (found); [M+Na]$^+$, m/z = 522.3 (calculated), 522.2 (found); [2 M+H]$^+$, m/z = 999.5 (calculated), 999.4 (found); [2 M+Na]$^+$, m/z = 1021.5 (calculated), 1021.5 (found).

5.2.6.3 H-Lys(Dns)-OH (20)

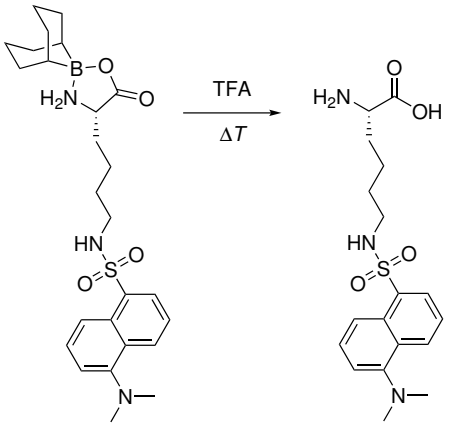

Crude Lys(Dns)-BBN (**19**) (corresponding to 10.0 mmol of **17**) was dissolved in TFA (50 mL) and stirred at 50 °C for 4 h. The reaction was monitored by LC-MS and further TFA was added until nearly full conversion was achieved. The mixture was concentrated under reduced pressure and the residue diluted with MeCN / H_2O, and lyophilized. The crude product **20** was used in the next step without further purification. A sample of **20** was purified by preparative HPLC (Chapter 5.2.2.1) to be used as a fluorescence standard (Chapter 5.3.5).

HPLC (40–99 % B in 12.00 min, 0.2 mL / min): $t_{ret.}$ = 5.24 min.

ESI-MS: $[M+2H]^{2+}$, m/z = 190.6 (calculated), 190.8 (found); $[M+H]^{+}$, m/z = 380.2 (calculated), 380.2 (found); $[2M+H]^{+}$, m/z = 759.3 (calculated), 759.3 (found).

^{1}H-NMR (400 MHz, DMSO-d$_6$): δ / ppm = 1.21–1.43 (m, 4 H, 4/5-H), 1.59–1.72 (m, 2 H, 3-H), 2.70–2.80(m, 2 H, 6-H), 2.83 (s, 6 H, CH_3), 3.76–3.85 (m, 1 H, 2-H), 7.23–7.30 (m, 1 H, 13-H), 7.55–7.67 (m, 2 H, 9/14-H), 7.90 (t, $^{3}J_{HH}$ = 5.7 Hz, 1 H, NH), 8.06–8.12 (m, 1 H, 8-H), 8.23 (br s, 3 H, NH_3^+), 8.28–8.34 (m, 1 H, 15-H), 8.43–8.49 (m, 1 H, 10-H).

^{13}C{^{1}H}-NMR (101 MHz, DMSO-d$_6$): δ / ppm = 21.5 (C-4/5), 28.7 (C-4/5), 29.5 (C-3), 42.1 (C-6), 45.1 (C-17), 51.8 (C-2), 115.2 (C-13), 119.2 (C-15), 123.6 (C-14), 127.8 (C-9), 128.2 (C-8), 129.1 (C-11/16), 129.1 (C-11/16), 129.3 (C-10), 136.0 (C-7), 151.2 (C-12), 171.0 (C-1).

5.2.6.4 Trt-Mpa-OSu (21)

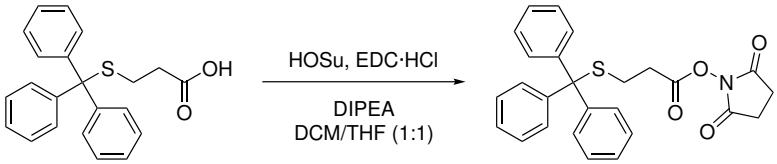

21

Under argon atmosphere Trt-Mpa-OH (1.74 g, 5.00 mmol, 1 eq), HOSu (1.15 g, 10.0 mmol, 2 eq) and EDC · HCl (1.15 g, 6.00 mmol, 1.2 eq) were suspended in anhydrous DCM / THF (1:1, 50 mL). DIPEA (2.62 g, 15.0 mmol, 3 eq) was added and the reaction mixture was stirred at room temperature overnight. The mixture was concentrated under reduced pressure and the residue was taken up in EtOAc, and washed with aqueous HCl (0.3 M, 3×). The organic phase was dried over Na_2SO_4 and the solvent removed *in vacuo* to yield the crude product **21** as white solid, which was used in the next step without further purification.

HPLC (40–99 % B in 12.00 min, 0.2 mL / min): $t_{ret.}$ = 15.29 min.

ESI-MS: $[M+Na]^+$, m/z = 468.1 (calculated), 468.1 (found); $[M+K]^+$, m/z = 484.1 (calculated), 484.0 (found).

5.2.6.5 Trt-Mpa-Lys(Dns)-OH (22)

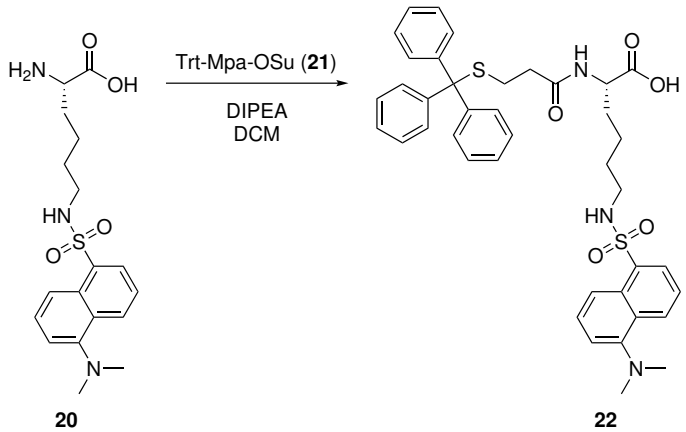

20 **22**

Crude H-Lys(Dns)-OH (**20**) (corresponding to 10.0 mmol of **17**) was dissolved in anhydrous DCM (50 mL). DIPEA (2.62 mL, 15.0 mmol, 3 eq) was added and the pH adjusted to 9 with additional DIPEA (approximately 9 eq). Trt-Mpa-OSu (**21**) (corresponding to 3.08 mmol, 0.34 eq of Trt-Mpa-OH), dissolved in DCM (20 mL), was added, and the reaction mixture was stirred overnight at room temperature. The solvent was removed under reduced pressure and the residue diluted with H_2O (100 mL). The pH was adjusted to 2-3 with saturated, aqueous $KHSO_4$ and the mixture extracted with Et_2O (3×50 mL) The pooled organic phases were dried over Na_2SO_4 and the solvent removed *in vacuo*.

The crude product was purified by flash chromatography with silica gel as stationary and MeOH / DCM (1:20) with formic acid (0.1 %) as mobile phase, after which the desired product **22** was obtained as yellow oil (1.79 g, 2.52 mmol, 82 % with respect to Trt-Mpa-OH).

TLC: R_f = 0.18 (MeOH / DCM (1:20), 0.1 % formic acid).

HPLC (40–99 % B in 12.00 min, 0.2 mL / min): $t_{ret.}$ = 15.07 min.

ESI-MS: $[M-Trt+H]^+$, m/z = 468.2 (calculated), 468.3 (found); $[M+H]^+$, m/z = 710.3 (calculated), 710.3 (found); $[M+Na]^+$, m/z = 732.3 (calculated), 732.2 (found); $[2\,M+H]^+$, m/z = 1419.5 (calculated), 1419.5 (found); $[2\,M+Na]^+$, m/z = 1441.5 (calculated), 1441.9 (found).

^{1}H-NMR (400 MHz, DMSO-d_6): δ / ppm = 1.09–1.80 (m, 8 H, 3/4/5/6-H), 2.15–2.25 (m, 4 H, 19/20-H), 2.68–2.76 (m, 2 H, 6-H), 2.81 (s, 6 H, 17-H), 3.97–4.06 (m, 1 H, 2-H), 7.17–7.26 (m, 4 H, 13/25-H), 7.26–7.34 (m, 12 H, 13/24-H), 7.54–7.63 (m, 2 H, 9/14-H), 7.87 (t, $^3J_{HH}$ = 5.7 Hz, 1 H, ε-NH), 7.97–8.03 (d, $^3J_{HH}$ = 7.8 Hz, 1 H, α-NH) 8.05–8.10 (m, 1 H, 8-H), 8.27–8.33 (m, 1 H, 15-H), 8.41–8.47 (m, 1 H, 10-H).

^{13}C{^{1}H}-NMR (101 MHz, DMSO-d_6): δ / ppm = 22.5 (C-4/5), 27.4 (C-19/20), 28.8 (C-4/5), 30.5 (C-3), 33.6 (C-19/20), 42.2 (C-6), 45.0 (C-17), 51.6 (C-2), 65.9 (C-21), 115.1 (C-13), 119.1 (C-15), 123.5 (C-14), 126.6 (C-25), 127.8 (C-9), 128.0 (C-23/24), 128.1 (C-8), 129.0 (C-23/24), 129.1 (C-11/16), 129.1 (C-11/16), 129.3 (C-10), 136.1 (C-7), 144.4 (C-22), 151.3 (C-12), 170.1 (C-18), 173.5 (C-1).

5.2.7 Solid-phase peptide synthesis

Peptides were synthesized via solid-phase peptide synthesis (SPPS) applying the Fmoc strategy with acid-labile side chain protecting groups. Standard amino acid side chains were protected as follows: Arg(Pbf), Asn(Trt), Asp(O*t*Bu), Cys(Trt), Gln(Trt), Glu(O*t*Bu), His(Trt), Lys(Boc), Ser(O*t*Bu), Thr(*t*Bu), Trp(Boc), Tyr(*t*Bu).

5.2.7.1 Manual peptide synthesis

Manual Synthesis was performed on a scale of 25 µmol on TentaGel HL RAM resin (capacity: 0.37 mmol / g) as solid support.

Coupling reactions of standard amino acid building blocks (4 eq) were performed with HBTU (3.6 eq) as activator and NMM (400 mM in DMF) as base for 1 h. Fmoc-PEG_3-OH (3 eq) was also coupled with HBTU (2.7 eq). Fmoc-AsuHd(OTrt)-OH (**5**) (2 eq), Fmoc-AsuApa(Boc)-OH (**13**) (2 eq) and Fmoc-Aoda-OH (**16**) (2 eq) were coupled using PyOxim (2 eq) as activator. The Fmoc group was deprotected with piperidine (20 % in DMF, 3×10 min). The resin was washed with DMF (3×), DCM (3×), DMF (3×) between each step.

Peptides were cleaved off the resin with a solution containing TFA, phenol, TIPS and water (7 mL, volume ratio 85:5:5:5) under agitation for 2 h. The resin was further shaken twice with the cleavage solution (1.5 mL) for 30 min. After concentration under reduced pressure cleaved peptides were precipitated in cold Et_2O (40 mL), centrifuged (4000 *g*, 10 min, –4 °C), dissolved in water / MeCN, and lyophilized. For Aoda-containing peptides the cleavage

cocktail consisted only of TFA and water (volume ratio 95:5) and precipitation in Et_2O was omitted. Peptides were purified by preparative HPLC (Chapter 5.2.2.1) and analyzed by LC-MS (Table 8).

Table 7: Sequences and LC-MS data of mini-probes **P1**–**P3** and precursors **P4**–**P7** of mini-click-probes **P5***–**P7***. Faz: *p*-Azidophenylalanine, Pra: Propargylclycine.

Peptide	Sequence	$t_{ret.}$/min	M (calculated)	M (found)
mini-Lys (**P1**)	Ac-G-Lys-G-PEG_3-C-NH_2	4.98	607.3	608.4
mini-AsuHd (**P2**)	Ac-G-AsuHd-G-PEG_3-C-NH_2	6.03	665.3	665.3
mini-AsuApa (**P3**)	Ac-G-AsuApa-G-PEG_3-C-NH_2	6.34	740.4	740.4
mini-C (**P4**)	Faz-Ahx-C-NH_2	8.17	421.2	421.1
mini-Lys-N (**P5**)	Ac-G-Lys-G-PEG_3-Pra-NH_2	6.06	599.3	599.3
mini-AsuHd-N (**P6**)	Ac-G-AsuHd-G-PEG_3-Pra-NH_2	6.74	657.3	657.3
mini-Aoda-N (**P7**)	Ac-G-Aoda-G-PEG_3-Pra-NH_2	8.64	654.4	654.6

5.2.7.2 Automated peptide synthesis

Automated synthesis was conducted on a *MultiSynTech* Syro I synthesizer (Witten, Germany). The scale was 25 µmol on TentaGel HL RAM resin (capacity: 0.37 mmol / g) as solid support.

Coupling reactions of the respective amino acids (3 eq) were performed by activation with DIC (3 eq) and oxyma (3 eq) in DMF for 40 min. Couplings were repeated once with HATU (3 eq) as activator and NMM (6 eq) as base in DMF for 30 min. Fmoc-L-AsuHd(OTrt)-OH (**5***) (2 eq) and Fmoc-Lys8(Boc)-OH (2 eq) were coupled manually with PyOxim (2 eq) and NMM (400 mM) in DMF for 1 h. Fmoc deprotection was performed by treating the resin twice with piperidine (40 % in DMF) for a total of 15 min. Between each step the resin was rinsed with DMF. N-terminal acetylation was performed with Ac_2O (5 %) and 2,6-lutidine (6 %) in DMF for 15 min.

Peptides were cleaved and purified as described for manual synthesis (Chapter 5.2.7.1). LC-MS data is summarized in (Table 8).

5.2.7.3 Automated 96-well peptide synthesis

Automated 96-well synthesis was conducted on an *Intavis* ResPep SL synthesizer (Cologne, Germany) in 96-well filter plates. The scale was 2 µmol on TentaGel S RAM resin (capacity: 0.23 mmol / g) as solid support. Stock solutions of Fmoc-AsuHd(OTrt)-OH (**5**) and Fmoc-ApmHd(OTrt)-OH (**10**) were prepared in NMP and adjusted to pH 7 with formic acid prior to use.

Coupling reactions of the respective amino acids (5.25 eq) were performed with HATU (5 eq) as activator and NMM (10 eq) as base in DMF twice for 20 min. Fmoc-AsuHd(OTrt)-OH (**5**) (2.2 eq), Fmoc-ApmHd(OTrt)-OH (**10**) (2.2 eq) and Trt-Mpa-Lys(Dns)-OH (**22**) (2.2 eq) were coupled with HATU (2 eq) and NMM (10 eq) in DMF twice for 20 min. After each cycle unreacted amino groups were capped by treatment with a solution of Ac_2O (5 %) and 2,6-lutidine (6 %) in DMF for 5 min. Fmoc deprotection was performed by treating the resin twice with piperidine (20 % in DMF) for a total of 15 min. Between each step the resin was rinsed with DMF.

Table 8: Sequences and LC-MS data of selected HDAC6 substrate peptides **P10**–**P17** and MALDI peptides **P18**–**P27**. p denotes D-Pro.

Peptide	Sequence	$t_{ret.}$/min	M (calc.)	M (found)
αTub-Lys (**P10**)	PDGQMPSD-Lys-TIGGGDDS-Ahx-C-NH_2	5.83	1890.8	1891.8
αTub-AsuHd (**P11**)	PDGQMPSD-L-AsuHd-TIGGGDDS-Ahx-C-NH_2	6.21	1948.8	1949.7
CRTC-Lys (**P12**)	PLHRRSGD-Lys-PGRQFDGS-Ahx-C-NH_2	5.10	2124.1	2125.0
CRTC-AsuHd (**P13**)	PLHRRSGD-L-AsuHd-PGRQFDGS-Ahx-C-NH_2	5.37	2182.1	2183.4
HSP90-Lys (**P14**)	GTKVILHL-Lys-EDQTEYLE-Ahx-C-NH_2	6.65	2230.2	2131.4
HSP90-AsuHd (**P15**)	GTKVILHL-L-AsuHd-EDQTEYLE-Ahx-C-NH_2	7.15	2288.2	2289.3
PPIA-Lys (**P16**)	VSFELFAD-Lys-VPKTAENF-Ahx-C-NH_2	7.72	2156.1	2157.4
PPIA-AsuHd (**P17**)	VSFELFAD-L-AsuHd-VPKTAENF-Ahx-C-NH_2	8.30	2214.1	2215.2
mini-Lys(Ac) (**P18**)	Ac-G-Lys(Ac)-G-$(PEG_2)_2$-p-NH_2	5.76	730.4	730.6
mini-Lys8 (**P19**)	Ac-G-Lys8-G-$(PEG_2)_2$-p-NH_2	5.02	696.4	696.5
αTub-Lys(Ac) (**P20**)	Ac-PDGQNlePSD-Lys(Ac)-TIGGGDDS-$(PEG_2)_2$-p-NH_2	7.20	2128.0	2129.2
αTub-Lys8 (**P21**)	Ac-PDGQNlePSD-Lys8-TIGGGDDS-$(PEG_2)_2$-p-NH_2	6.68	2094.0	2094.9
CRTC-Lys(Ac) (**P22**)	Ac-PLHRRSGD-Lys(Ac)-PGRQFDGS-$(PEG_2)_2$-p-NH_2	5.83	2379.2	2380.8
CRTC-Lys8 (**P23**)	Ac-PLHRRSGD-Lys8-PGRQFDGS-$(PEG_2)_2$-p-NH_2	5.40	2345.2	2346.6
HSP90-Lys(Ac) (**P24**)	Ac-GTKVILHL-Lys(Ac)-EDQTEYLE-$(PEG_2)_2$-p-NH_2	7.80	2485.3	2487.1
HSP90-Lys8 (**P25**)	Ac-GTKVILHL-Lys8-EDQTEYLE-$(PEG_2)_2$-p-NH_2	6.00	2451.3	2452.8
PPIA-Lys(Ac) (**P26**)	Ac-VSFELFAD-Lys(Ac)-VPKTAENF-$(PEG_2)_2$-p-NH_2	8.94	2411.2	2413.0
PPIA-Lys8 (**P27**)	Ac-VSFELFAD-Lys8-VPKTAENF-$(PEG_2)_2$-p-NH_2	8.34	2377.2	2378.7

Peptides were cleaved off the resin with a solution containing TFA, water, phenol, thioanisole, DTT and TIPS (81.5:5:5:5:2.5:1, 600 µL / well) for 3 h in total. This solution was added in portions of 200 µL and 3×100 µL to each well and the resin was incubated for 30 min after each addition, except the last one, after which it was incubated for 1.5 h. The resin was further rinsed with one additional portion of cleavage solution (100 µL / well) and the solution centrifuged into deep-well collection plates. Cleavage solutions were evaporated under ambient conditions in a fume hood overnight to a volume of approximately 200 µL / well. Cleaved peptides were precipitated in cold Et_2O (700 µL / well), centrifuged (2500 *g*, 20 min, –4 °C), and washed with additional Et_2O (2×500 µL / well). Peptides were then dissolved in water / MeCN (1:1, 500 µL / well), and lyophilized. All peptides were analyzed by LC-MS (Table 8).

Table 9: Sequences and LC-MS data of HDAC6 substrate peptides **6P1**–**6P96**. Mpa-Lys(Dns)-PEG_2- =R^1, R^2= -PEG_2-p-NH_2. p denotes D-Pro. Retention times of both diasteriomers are given where appropriate.

Number	Peptide	Sequence	$t_{ret.}$/min	M (calc.)	M (found)
6P1	mini-6-Lys	R^1-G-Lys-G-R^2	8.71	1095.5	1095.2
6P2	mini-6-ApmHd	R^1-G-ApmHd-G-R^2	8.43	1139.5	1139.5
6P3	mini-6-AsuHd	R^1-G-AsuHd-G-R^2	8.50	1153.5	1153.3
6P4	TP53-Lys	R^1-QSTSRHK-Lys-LMFKTEG-R^2	6.67	2612.3	2613.9
6P5	TP53-ApmHd	R^1-QSTSRHK-ApmHd-LMFKTEG-R^2	7.01	2656.3	2657.4
6P6	TP53-AsuHd	R^1-QSTSRHK-AsuHd-LMFKTEG-R^2	7.03	2670.3	2671.8
6P7	TUBA1A-Lys	R^1-DGQMPSD-Lys-TIGGGDD-R^2	8.09	2327.0	2327.6
6P8	TUBA1A-ApmHd	R^1-DGQMPSD-ApmHd-TIGGGDD-R^2	8.49	2371.0	2372.2
6P9	TUBA1A-AsuHd	R^1-DGQMPSD-AsuHd-TIGGGDD-R^2	8.53	2385.0	2385.6
6P10	CRTC3-Lys	R^1-LHRRSGD-Lys-PGRQFDG-R^2	6.77	2560.2	2561.6
6P11	CRTC3-ApmHd	R^1-LHRRSGD-ApmHd-PGRQFDG-R^2	7.22	2604.2	2605.2
6P12	CRTC3-AsuHd	R^1-LHRRSGD-AsuHd-PGRQFDG-R^2	7.38	2618.3	2619.7
6P13	ELOC-Lys	R^1-DGHEFIV-Lys-REHALTS-R^2	7.45	2573.2	2574.5
6P14	ELOC-ApmHd	R^1-DGHEFIV-ApmHd-REHALTS-R^2	7.90	2617.2	2618.3
6P15	ELOC-AsuHd	R^1-DGHEFIV-AsuHd-REHALTS-R^2	7.83	2631.3	2632.5
6P16	PKM-Lys	R^1-ETLKEMI-Lys-SGMNVAR-R^2	8.58	2541.3	2542.4

Number	Peptide	Sequence	$t_{ret.}$/min	M (calc.)	M (found)
6P17	PKM-ApmHd	R^1-ETLKEMI-ApmHd-SGMNVAR-R^2	8.77, 9.23	2585.2	2586.5
6P18	PKM-AsuHd	R^1-ETLKEMI-AsuHd-SGMNVAR-R^2	8.86, 9.31	2599.3	2600.4
6P19	GPI-Lys	R^1-ERMFNGE-Lys-INYTEGR-R^2	7.71	2678.2	2679.3
6P20	GPI-ApmHd	R^1-ERMFNGE-ApmHd-INYTEGR-R^2	8.22	2722.2	2723.5
6P21	GPI-AsuHd	R^1-ERMFNGE-AsuHd-INYTEGR-R^2	8.26	2736.2	2737.3
6P22	GAPDH-Lys	R^1-AHLQGGA-Lys-RVIISAP-R^2	7.51	2352.2	2352.9
6P23	GAPDH-ApmHd	R^1-AHLQGGA-ApmHd-RVIISAP-R^2	8.07	2396.2	2397.1
6P24	GAPDH-AsuHd	R^1-AHLQGGA-AsuHd-RVIISAP-R^2	8.03	2410.3	2411.2
6P25	HSP90AA1-Lys	R^1-TKVILHL-Lys-EDQTEYL-R^2	8.31	2664.4	2665.5
6P26	HSP90AA1-ApmHd	R^1-TKVILHL-ApmHd-EDQTEYL-R^2	8.65, 8.79	2708.3	2709.7
6P27	HSP90AA1-AsuHd	R^1-TKVILHL-AsuHd-EDQTEYL-R^2	8.71, 8.90	2722.4	2723.6
6P28	CANX-Lys	R^1-KTGIYEE-Lys-HAKRPDA-R^2	6.61	2577.3	2577.9
6P29	CANX-ApmHd	R^1-KTGIYEE-ApmHd-HAKRPDA-R^2	6.82	2621.3	2622.2
6P30	CANX-AsuHd	R^1-KTGIYEE-AsuHd-HAKRPDA-R^2	6.92	2635.3	2636.1
6P31	CCT5-Lys	R^1-LMGLEAL-Lys-SHIMAAK-R^2	8,93	2447.2	2448.4
6P32	CCT5-ApmHd	R^1-LMGLEAL-ApmHd-SHIMAAK-R^2	9.32, 9.85	2491.2	2492.4
6P33	CCT5-AsuHd	R^1-LMGLEAL-AsuHd-SHIMAAK-R^2	9.49, 10.03	2505.3	2507.1
6P34	CCT2-Lys	R^1-LGPKGMD-Lys-ILLSSGR-R^2	8.29	2406.3	2407.3
6P35	CCT2-ApmHd	R^1-LGPKGMD-ApmHd-ILLSSGR-R^2	8.75, 8.95	2450.2	2451.2
6P36	CCT2-AsuHd	R^1-LGPKGMD-AsuHd-ILLSSGR-R^2	8.82, 9.02	2464.3	2465.4
6P37	PPIA-6-Lys	R^1-SFELFAD-Lys-VPKTAEN-R^2	8.87	2530.2	2531.5
6P38	PPIA-6-ApmHd	R^1-SFELFAD-ApmHd-VPKTAEN-R^2	9.31, 9.44	2574.2	2575.1
6P39	PPIA-6-AsuHd	R^1-SFELFAD-AsuHd-VPKTAEN-R^2	9.35, 9.47	2588.2	2589.4
6P40	ENAH-Lys	R^1-RRRRIAE-Lys-GSTIETE-R^2	6.42	2636.4	2637.8
6P41	ENAH-ApmHd	R^1-RRRRIAE-ApmHd-GSTIETE-R^2	6.70	2680.3	2681.7
6P42	ENAH-AsuHd	R^1-RRRRIAE-AsuHd-GSTIETE-R^2	6.86	2694.4	2695.6
6P43	PRDX4-Lys	R^1-DHSLHLS-Lys-AKISKPA-R^2	6.76	2466.3	2467.3
6P44	PRDX4-ApmHd	R^1-DHSLHLS-ApmHd-AKISKPA-R^2	7.18	2510.3	2511.3
6P45	PRDX4-AsuHd	R^1-DHSLHLS-AsuHd-AKISKPA-R^2	7.19	2524.3	2525.2
6P46	CTTN87-Lys	R^1-ASHGYGG-Lys-FGVEQDR-R^2	7.36	2442.1	2443.0
6P47	CTTN87-ApmHd	R^1-ASHGYGG-ApmHd-FGVEQDR-R^2	7.90	2486.1	2486.8
6P48	CTTN87-AsuHd	R^1-ASHGYGG-AsuHd-FGVEQDR-R^2	7.98	2500.1	2501.0
6P49	CTTN124-Lys	R^1-SVRGFGG-Lys-FGVQMDR-R^2	8.01	2475.2	2476.2
6P50	CTTN124-ApmHd	R^1-SVRGFGG-ApmHd-FGVQMDR-R^2	8.55	2519.2	2520.3
6P51	CTTN124-AsuHd	R^1-SVRGFGG-AsuHd-FGVQMDR-R^2	8.54	2533.2	2534.3
6P52	KPNA6-Lys	R^1-ETMASPG-Lys-DNYRMKS-R^2	7.40	2549.1	2550.6
6P53	KPNA6-ApmHd	R^1-ETMASPG-ApmHd-DNYRMKS-R^2	7.84	2593.1	2594.2
6P54	KPNA6-AsuHd	R^1-ETMASPG-AsuHd-DNYRMKS-R^2	7.86	2607.2	2608.2
6P55	EIF4B-Lys	R^1-PEENPAS-Lys-FSSASKY-R^2	7.88	2476.1	2476.9
6P56	EIF4B-ApmHd	R^1-PEENPAS-ApmHd-FSSASKY-R^2	8.27, 8.43	2520.1	2521.0
6P57	EIF4B-AsuHd	R^1-PEENPAS-AsuHd-FSSASKY-R^2	8.33, 8.48	2534.1	2534.9
6P58	PEX5-Lys	R^1-AGHFTQD-Lys-ALRQEGL-R^2	7.65	2505.2	2505.7
6P59	PEX5-ApmHd	R^1-AGHFTQD-ApmHd-ALRQEGL-R^2	8.12	2549.2	2550.2
6P60	PEX5-AsuHd	R^1-AGHFTQD-AsuHd-ALRQEGL-R^2	8.15	2563.2	2564.1
6P61	AHNAK-Lys	R^1-SLEGPEG-Lys-LKGPKFK-R^2	7.34	2449.3	2450.1
6P62	AHNAK-ApmHd	R^1-SLEGPEG-ApmHd-LKGPKFK-R^2	7.84	2493.3	2494.4
6P63	AHNAK-AsuHd	R^1-SLEGPEG-AsuHd-LKGPKFK-R^2	7.86	2507.3	2508.4
6P64	RANBP2-Lys	R^1-NFSEKAS-Lys-FGNTEQG-R^2	7.82	2478.1	2478.8
6P65	RANBP2-ApmHd	R^1-NFSEKAS-ApmHd-FGNTEQG-R^2	8.36	2522.1	2523.0
6P66	H6-RANBP2-AsuHd	R^1-NFSEKAS-AsuHd-FGNTEQG-R^2	8.38	2536.1	2537.4
6P67	ZYX-Lys	R^1-KFTPVAS-Lys-FSPGAPG-R^2	8.25	2325.2	2326.0
6P68	ZYX-ApmHd	R^1-KFTPVAS-ApmHd-FSPGAPG-R^2	8.75	2369.1	2370.1
6P69	ZYX-AsuHd	R^1-KFTPVAS-AsuHd-FSPGAPG-R^2	8.76	2383.2	2384.4
6P70	PAK1-Lys	R^1-RSILPGD-Lys-TNKKKEK-R^2	6.70	2576.4	2577.4
6P71	PAK1-ApmHd	R^1-RSILPGD-ApmHd-TNKKKEK-R^2	6.91	2620.4	2621.6
6P72	PAK1-AsuHd	R^1-RSILPGD-AsuHd-TNKKKEK-R^2	7.02	2634.4	2635.5
6P73	NUP214-Lys	R^1-LQPAVAE-Lys-QGHQWKD-R^2	7.79	2569.3	2570.4
6P74	NUP214-ApmHd	R^1-LQPAVAE-ApmHd-QGHQWKD-R^2	8,20	2613.2	2614.4
6P75	NUP214-AsuHd	R^1-LQPAVAE-AsuHd-QGHQWKD-R^2	8,24	2627.3	2628.6

Number	Peptide	Sequence	$t_{ret.}$/min	M (calc.)	M (found)
6P76	TRIM25-Lys	R^1-PVPALPS-Lys-LPTFGAP-R^2	9.24	2326.2	2327.0
6P77	TRIM25-ApmHd	R^1-PVPALPS-ApmHd-LPTFGAP-R^2	9.78	2370.2	2371.1
6P78	TRIM25-AsuHd	R^1-PVPALPS-AsuHd-LPTFGAP-R^2	9.83	2384.2	2385.1
6P79	CREBBP-Lys	R^1-KNNKKTN-Lys-NKSSISR-R^2	5.69	2581.4	2582.0
6P80	CREBBP-ApmHd	R^1-KNNKKTN-ApmHd-NKSSISR-R^2	6.06	2625.3	2625.6
6P81	CREBBP-AsuHd	R^1-KNNKKTN-AsuHd-NKSSISR-R^2	6.07	2639.4	2639.8
6P82	MYH9-Lys	R^1-QEQGTHP-Lys-FQKPKQL-R^2	6.85	2628.3	2629.7
6P83	MYH9-ApmHd	R^1-QEQGTHP-ApmHd-FQKPKQL-R^2	7.20	2672.3	2673.7
6P84	MYH9-AsuHd	R^1-QEQGTHP-AsuHd-FQKPKQL-R^2	7.30	2686.3	2687.6
6P85	PPL-Lys	R^1-FRKRNKG-Lys-YSPTVQT-R^2	6.70	2644.4	2645.8
6P86	PPL-ApmHd	R^1-FRKRNKG-ApmHd-YSPTVQT-R^2	7.16	2688.4	2689.9
6P87	PPL-AsuHd	R^1-FRKRNKG-AsuHd-YSPTVQT-R^2	7.15	2702.4	2703.6
6P88	JADE3-Lys	R^1-SKIPNEH-Lys-KPAEVFR-R^2	6.83	2614.3	2615.6
6P89	JADE3-ApmHd	R^1-SKIPNEH-ApmHd-KPAEVFR-R^2	7.17	2658.3	2659.4
6P90	JADE3-AsuHd	R^1-SKIPNEH-AsuHd-KPAEVFR-R^2	7.19	2672.4	2637.4
6P91	RSF1-Lys	R^1-GGGVGRG-Lys-DISTITG-R^2	7.81	2209.1	2209.8
6P92	RSF1-ApmHd	R^1-GGGVGRG-ApmHd-DISTITG-R^2	8.26	2253.1	2254.0
6P93	RSF1-AsuHd	R^1-GGGVGRG-AsuHd-DISTITG-R^2	8.31	2267.1	2267.9
6P94	MATR3-Lys	R^1-VRVHLSQ-Lys-YKRIKKP-R^2	6.63	2714.5	2715.9
6P95	MATR3-ApmHd	R^1-VRVHLSQ-ApmHd-YKRIKKP-R^2	6.84	2758.5	2759.4
6P96	MATR3-AsuHd	R^1-VRVHLSQ-AsuHd-YKRIKKP-R^2	6.87	2772.5	2773.9

5.3 Biochemical methods

5.3.1 Cell culture

All reagents, buffers and media for cell culture were purchased from *Sigma-Aldrich*. HeLa S3 cells (DSMZ-No. ACC 161) were cultured in Dulbecco's Modified Eagle's Medium (DMEM, high glucose) supplemented with 10 % fetal calf serum (FCS) and 1 % penicillin-streptomycin at 37 °C in a humidified atmosphere with 5 % CO_2. Subcultivation was performed every 3-4 days by treating the cells with 0.05 % trypsin containing 0.2 g / L EDTA. Afterwards cells were reseeded in fresh medium.

5.3.2 Preparation of cell extracts

HeLa cell extracts were prepared according to the protocol of *Dignam et al.*[273] Prior to lysis, cells were grown for four days in cell culture dishes (165 cm^2).

The following buffers were used: Dignam buffer A (10 mM HEPES, 1.5 mM $MgCl_2$, 10 mM KCl, pH 7.9 at 4 °C), Dignam buffer B (300 mM HEPES, 30 mM $MgCl_2$, 1.4 M KCl, pH 7.9 at 4 °C), Dignam buffer C (20 mM HEPES, 1.5 mM $MgCl_2$, 420 mM NaCl, 25 % glycerol, pH 7.9 at 4 °C), Dignam buffer D (20 mM HEPES, 100 mM KCl, 20 % glycerol, pH 7.9 at 4 °C). Shortly before usage, AEBSF (0.5 mM), DTT (0.5 mM), $NaVO_3$ (1 mM) and NaF (2 mM) were added to Dignam buffer A, B and C, while Dignam Buffer D was only supplemented with AEBSF (0.25 mM).

The medium was removed from the cell culture dishes and cold PBS (10 mL) was added. The PBS was removed again, fresh PBS (10 mL) was added, and cells were harvested using a cell scraper. All following steps were performed at 4 °C.

The cell suspension was centrifuged (1000 *g*, 10 min), the supernatant was discarded and the approximate pellet volume V_P was determined. Cells were resuspended in PBS (5 V_P) and centrifuged (1000 *g*, 10 min). After removing the PBS, Dignam buffer A (5 V_P) was added, the suspension was incubated for 10 min on ice, and then centrifuged (1000 *g*, 10 min). The supernatant was discarded and the cell pellet resuspended in Dignam buffer A (2 V_P). The suspension was transfered to a glass douncer and homogenized with ten strokes (tight pestle). The homogenate was centrifuged (1000 *g*, 10 min), the supernatant transferred to a fresh tube and the pellet centrifuged again (25000 *g*, 20 min). The supernatant was combined with the previous one to yield the cytosolic fraction of the extract, and the overall volume V_{CE} was determined. The pellet was further treated to yield the nuclear fraction of the extract. Dignam buffer B (0.11 V_{CE}) was added to the cytosolic fraction and the solution was cleared by centrifugation (100000 *g*, 1 h) to yield the final cytosolic extract (CE).

The nuclear pellet was resuspended in Dignam buffer C (1 mL / 10^8 cells), transfered to a glass douncer, and homogenized with ten strokes (tight pestle). The homogenate was stirred on ice (30 min) and then centrifuged (25000 *g*, 30 min). The supernatant was transferred to a fresh tube to yield the nuclear extract (NE).

Cytosolic (CE) and nuclear (NE) extract were combined to represent the whole cell extract (WCE), and dialyzed (molecular weight cut-off 3.5 kDa) overnight against Dignam buffer D. The WCE was cleared by centrifugation (25000 *g*, 30 min) and stored at –80 °C until usage.

5.3.3 Protein determination

Protein concentrations of HeLa whole cell extracts were determined using a bicinchoninic acid (BCA) assay kit (Pierce BCA Protein-Assay, *Thermo Fisher Scientific*, Rockford, USA). In clear 96-well plates, samples (25 µL) of suitable dilutions of cell extract (1:30 to 1:90) or protein standard (BSA, 0–240 µg / mL) in water were mixed with BCA solution (200 µL, reagent A / B (50:1)) and incubated at room temperature for 1 h. Each sample was prepared in triplicate. Absorption was measured at 562 nm using an Infinite 200 PRO microplate reader (*Tecan*, Männedorf, Switzerland).

5.3.4 Peptide immobilization

5.3.4.1 SulfoLink immobilization

For immobilization on agarose beads 100 mM stock solutions of purified peptides were prepared in water and diluted to 1 mM with SulfoLink coupling buffer (50 mM Tris · HCl, 5 mM EDTA-Na, pH 8.5).

Per peptide 300 µL of SulfoLink Coupling Resin (*Thermo Fisher Scientific*) as a 50 % suspension were drained and washed with coupling buffer (5×800 µL). The 1 mM peptide solution was added (300 µL) and the resin was firstly shaken for 15 min and then incubated without agitation for 45 min at room temperature. After washing with coupling buffer (3×500 µL) blocking buffer (500 µL, 50 mM β-mercaptoethanol in coupling buffer) was added and the resin was shaken for 15 min and then incubated without agitation for 45 min at room temperature. Subsequently, the resin was washed with 1 M NaCl solution (6×1 mL), water (2×1 mL) and

MeCN / water (1:1, 4×1 mL). After draining, MeCN / water (1:1, 450 µL) was added to the dry beads to achieve a 25 % suspension from which aliquots of 40 µL (10 µL resin) were generated and stored at –20 °C until further usage.

5.3.4.2 On-resin click reaction

Immobilization of the mini-click peptides **P5***, **P6*** and **P7*** was achieved in a two-step process. Firstly, the C-terminal fragment **P4** was immobilized on SulfoLink Coupling Resin as described in Chapter 5.3.4.1. Then, the resin was washed with SulfoLink coupling buffer (3×1 mL, Chapter 5.3.4.1) omitting the EDTA. Solutions of the N-terminal fragments **P5**-**P7** (1 mM) were prepared with the same buffer, containing in addition $CuSO_4$ (3 mM), histidine (3 mM) and ascorbic acid (550 mM). The resin was shaken with these solutions (300 µL) for 1 h at room temperature, then the pH was adjusted to 7 with aqueous NaOH, and additional $CuSO_4$ was added to achieve a final concentration of 9 mM. The resin was further shaken overnight and then washed with water (3×1 mL) and MeCN / water (1:1, 3×1 mL). After draining, MeCN / water (1:1, 450 µL) was added to the dry beads to achieve a 25 % suspension from which aliquots of 40 µL (10 µL resin) were generated and stored at –20 °C until further usage.

5.3.5 96-well peptide immobilization

In order to immobilize peptides for the 96-well pulldown assay, stock solutions (approximately 10 mM) were prepared, by assuming 2 µmol of peptide per well and adding MeCN / water (1:1, 200 µL). Concentrations of all 96 peptides were then adjusted to the same value by referencing their fluorescence signal to the signal of purified amino acid building block H-Lys(Dns)-OH (**20**) as fluorescence standard.

Excitation and emission spectra of **20** were recorded to determine optimal excitation and emission wavelengths. Samples of **20** (20 µL) in MeCN coupling buffer (SulfoLink coupling buffer containing 50 % MeCN, Chapter 5.3.4) were prepared in black 96-well plates and filled up to 200 µL with MeCN coupling buffer for measurement. Fluorescence readout was performed using an Infinite 200 PRO microplate reader (*Tecan*) and excitation and emission wavelengths were varied in steps of 1 nm.

A calibration curve was then recorded using known concentrations of purified amino acid building block H-Lys(Dns)-OH (**20**). Samples of **20** (20 µL) in MeCN coupling buffer with concentrations ranging from 0 to 2 mM were prepared in clear 96-well plates, filled up to 200 µL with MeCN coupling buffer before measurement, and fluorescence was read out ($\lambda_{ex.}$ = 333 nm, bandwidth = 9 nm; $\lambda_{em.}$ = 568 nm, bandwidth = 20 nm). The data were fitted by linear regression to obtain the following equation:

$$c_{well} \,/\, \mathrm{mM} = \frac{I}{m} \quad ,$$

where c_{well} is the concentration of fluorophore in the well, I the measured fluorescence intensity, and m the slope of the regression line. Samples of the 96 peptide stock solutions

were prepared and measured in the same way, but additionally diluted 1:20 with MeCN coupling buffer.

Exact concentrations of peptide stock solutions were then determined from the equation above, taking into account the additional dilution, and factors F were calculated by dividing the assumed stock concentration $c_{\text{approx.}}$ by the exact concentration c_{exact}. For adjusting differences in peptide concentration the volumes V of stock solutions used for immobilization were multiplied by their individual F value according to

$$V_{\text{exact}} = V_{\text{approx.}} \cdot F = V_{\text{approx.}} \cdot \frac{c_{\text{approx.}}}{c_{\text{exact}}} = V_{\text{approx.}} \cdot \frac{c_{\text{approx.}}}{c_{\text{well}} \cdot 20} \quad .$$

Peptide stock solutions were then diluted to 1 mM with MeCN coupling buffer using the modified volumes V_{exact}.

Per peptide 200 µL SulfoLink Coupling Resin suspension (*Thermo Fisher Scientific*) were transferred to each well of a 96-deep-well filter plate (MultiScreen 96 well High Volume Filter Plate, hydrophilic PVDF (0.45 µM), *Merck Millipore*, Darmstadt, Germany), drained using a vacuum manifold (MultiScreen$_{\text{HTS}}$ Vacuum Manifold, *Merck Millipore*), and washed with MeCN coupling buffer (5×800 µL / well). 1 mM peptide solutions (200 µL / well) were added and the resin was firstly shaken for 15 min and then incubated without agitation for 45 min at room temperature. After washing with MeCN coupling buffer (3×500 µL / well) blocking buffer (500 µL / well, 50 mM β-mercaptoethanol in MeCN coupling buffer) was added and the resin was shaken for 15 min and then incubated without agitation for 45 min at room temperature. Subsequently, the resin was washed with 1 M NaCl solution (6×1 mL / well), water (2×1 mL / well) and MeCN / water (1:1, 4×1 mL / well). After draining, MeCN / water (1:1, 300 µL / well) was added to the dry beads to achieve a 25 % suspension from which aliquots of 40 µL (10 µL resin) were generated, transfered to 96-well filter plates (MultiScreen$_{\text{HTS}}$-HV, hydrophilic PVDF (0.45 µM), *Merck Millipore*), and stored at –20 °C until further usage.

5.3.6 Pulldown assay

One aliquot of resin-bound peptide probes was transferred to a micro centrifuge filter unit (Ultrafree-MC-HV, *Merck Milipore*, Darmstadt, Germany) and washed with pulldown buffer (20 mM HEPES, 100 mM KCl, 20 % glycerin, pH 7.9) (3×200 µL) by shaking at 550 rpm for 2 min at room temperature. Between each step the resin was drained by centrifugation at 5000 rpm for 2 min.

HeLa whole cell extract was diluted to 1 mg / mL with pulldown buffer and the resin was incubated with this solution (200 µL) by shaking at 550 rpm for 1 h at room temperature. After draining, the resin was rinsed with washing buffer (20 mM HEPES, 300 mM KCl, 20 % glycerin, pH 7.9) (6×500 µL) by shaking at 550 rpm for 2 min at room temperature and then dried by centrifugation.

Peptide-bound proteins were eluted by incubation with 3× SDS sample buffer (20 µL, 5× SDS sample buffer: 250 mM Tris · HCl, 10 % SDS, 30 % glycerol, 0.5 M DTT, 0.02 % bromphenol blue) for 10 min at 95 °C and 550 rpm, followed by centrifugation at 12000 rpm for 5 min. For comparison an input sample was generated by mixing HeLa whole cell extract solution (16 µL, 1 mg / mL) with 5× SDS sample buffer (4 µL) and heating for 10 min

at 95 °C. Samples were then loaded onto polyacrylamide gels for separation by SDS-PAGE (Chapter 5.3.8).

Pulldown assays of interactome analysis (Chapter 5.3.11) were performed as described above with three different batches of HeLa whole cell extract (1 mg / mL for mini-probes **P1**–**P3** (Chapter 2.1.2.4), 0.5 mg / mL for selected HDAC6 substrate peptides **P10**–**P17** and mini-probes **P1** and **P2*** (Chapter 2.2.2.2)), using SDS sample buffer without bromphenol blue. Input samples were generated by mixing 20 µL of cell extract solution (1 mg / mL for **P1**–**P3**, 0.5 mg / mL for **P10**–**P17** and **P1** and **P2***) with 30 µL 5× SDS sample buffer without bromophenol blue. Eluted proteins were stored at 4 °C until subjected to filter aided sample preparation (FASP, (Chapter 5.3.11.1)).

5.3.7 96-well pulldown assay

One 96-well filter plate (MultiScreen$_{HTS}$-HV, hydrophilic PVDF (0.45 µM), *Merck Millipore*) with resin-bound peptide probes was washed with pulldown buffer (Chapter 5.3.6) (3×200 µL / well) by shaking at 550 rpm for 2 min at room temperature (using an *Eppendorf* (Hamburg, Germany) Thermomixer comfort with exchange block MTP for 96-well plates). Between each step the resin was drained using a vacuum manifold (MultiScreen$_{HTS}$ Vacuum Manifold, *Merck Millipore*).

HeLa whole cell extract was diluted to 1 mg / mL (0.5 mg / mL for **6P4**–**6P6**) with pulldown buffer and the resin was incubated with this solution (200 µL / well) by shaking at 550 rpm for 1 h at room temperature. After draining, the resin was rinsed with washing buffer (Chapter 5.3.6) (6×200 µL / well) by shaking at 550 rpm for 2 min at room temperature and then drained.

Peptide-bound proteins were eluted by incubation with 3× SDS sample buffer (Chapter 5.3.6) (30 µL / well) for 20 min at 70 °C and 550 rpm, followed by centrifugation at 3000 rpm for 10 min into 96-well collection plates. For comparison input samples were generated by mixing HeLa whole cell extract solution (16 µL, 1 mg / mL) with 5× SDS sample buffer (4 µL) and heating for 20 min at 70 °C. Samples were then loaded onto polyacrylamide gels for separation by SDS-PAGE (Chapter 5.3.8).

5.3.8 SDS-PAGE

SDS-PAGE was performed using discontinuous 12 % polyacrylamide gels. Resolving gels consisted of 375 mM Tris (pH 8.8), 12 % acrylamide / bisacrylamide (37.5:1), 0.1 % SDS, 0.04 % APS and 0.05 % TEMED. Stacking gels were prepared similarly but containing 250 mM Tris (pH 6.8) and 4 % acrylamide/bisacrylamide (37.5:1). The electrode buffer contained 25 mM Tris, 192 mM glycine and 0.1 % SDS and the electrophoretic separation was carried out at 130 V for 90 min. The PageRuler Prestained Protein Ladder (*Thermo Fisher Scientific*) was used as marker for molecular weight.

5.3.9 Western blotting

For transferring the separated protein samples onto PVDF membranes (Amersham Hybond Low Fluorescence 0.2 µm, *GE Healthcare*, Freiburg, Germany) the membrane was successively incubated with MeOH (15 s), water (2 min) and blotting buffer (25 mM Tris, 192 mM glycine, 0.05 % SDS, 10 % MeOH) (15 min) under agitation at room temperature. After incubating the polyacrylamide gel in blotting buffer for 30 min at room temperature, western blotting was performed in a wet tank blotting system with a constant current of 25 mA or 30 mA at 4 °C over night.

Blocking free binding sites of the membrane was achieved by shaking with blocking buffer (5 % low fat powdered milk in TBS (20 mM Tris, 150 mM NaCl, pH 7.3)) for 30 min at room temperature.

After washing with TBST (20 mM Tris, 150 mM NaCl, 0.1 % Tween 20, pH 7.3) the membrane was cut at appropriate sites and incubated with the respective primary antibody solutions for 2 h at room temperature or at 4 °C over night. Primary antibody solutions were prepared with incubation buffer (2.5 % low fat powdered milk in TBST) using the antibodies and dilutions summarized in Table 10.

The membrane was washed with TBST (3×15 s, 3×2 min) and then incubated with the respective secondary antibody solutions for 1 h at room temperature. Secondary antibody solutions were prepared with incubation buffer using the antibodies and dilutions summarized in Table 10.

After washing with TBST (3×15 s, 3×2 min) the membrane was incubated for 1 min with equal amounts of both reagents included in the Pierce ECL Western Blotting Substrate kit (*Thermo Fisher Scientific*) and chemiluminescence was then detected using a ChemiDoc MP Imaging System (*Bio-Rad Laboratories*, Feldkirchen, Germany) with an exposure time of 1 min.

Table 10: Antibodies used for Western blotting.

Primary antibodies				
Antigen	Isotype	Dilution	Product number	Manufacturer
HDAC1 (10E2)	mouse monoclonal IgG_1	1:500	sc-81598	Santa Cruz Biotechnology
HDAC2 (C-19)	goat polyclonal IgG	1:500	sc-6296	Santa Cruz Biotechnology
HDAC3 (H-99)	rabbit polyclonal IgG	1:500	sc-11417	Santa Cruz Biotechnology
HDAC4 (N-18)	goat polyclonal IgG	1:250	sc-5245	Santa Cruz Biotechnology
HDAC4 (B-5)	mouse monoclonal IgG_{2b}	1:250	sc-365093	Santa Cruz Biotechnology
HDAC6 (H-300)	rabbit polyclonal IgG	1:500	sc-11420	Santa Cruz Biotechnology
HDAC6 (D-11)	mouse monoclonal IgG_{2a}	1:500	sc-28386	Santa Cruz Biotechnology
HDAC8 (H-145)	rabbit polyclonal IgG	1:250	sc-11405	Santa Cruz Biotechnology
HDAC10 (F-4)	mouse monoclonal IgG_1	1:250	sc-376121	Santa Cruz Biotechnology
Secondary antibodies				
Reactivity	Isotype	Dilution	Product number	Manufacturer
anti-mouse	recombinant IgG_κ binding protein-HRP	1:5000	sc-516102	Santa Cruz Biotechnology
anti-goat	donkey IgG-HRP	1:5000	sc-2020	Santa Cruz Biotechnology
anti-rabbit	goat IgG-HRP	1:5000	sc-20040	Santa Cruz Biotechnology
anti-rabbit	mouse IgG-HRP	1:5000	sc-2357	Santa Cruz Biotechnology

5.3.10 Image analysis

Signal intensities of chemiluminescent images were analyzed using the Image Lab 6.0 software from *Bio-Rad*. Relative intensities $I_{rel.}$, corresponding to the fraction of bound protein (in %) in relation to the total amount of protein m_{sample} (200 µg) used in the pulldown experiment, were calculated by referencing the intensities of the respective sample bands to the intensities of the input sample with a known amount of protein m_{input} (16 µg) according to

$$I_{rel.} = \frac{m_{input} \cdot I_{sample}}{m_{sample} \cdot I_{input}} \cdot 100\,\% \quad .$$

5.3.11 Interactome studies

5.3.11.1 Filter aided sample preparation (FASP)

Protein samples from inputs and pulldown assays were processed using the FASP method as described previously.[143] Urea buffer (8 M urea, 0.1 M TrisHCl, pH 8.5) (450 µL) was added to eluted proteins or the input and the samples were incubated at 95 °C for 5 min under agitation, and the mixtures were transferred to centrifuge filter units (Microcon YM-10, *Merck Millipore*). After centrifugation (13900 *g*, 20 min) the filtrate was discarded. The samples were washed with urea buffer (3×450 µL) and drained by centrifugation (13900 *g*, 20 min). Chloroacetamide (55 mM in urea buffer, 100 µL) was added, the samples were incubated in the dark for 20 min without shaking, and centrifuged (13900 *g*, 15 min). The samples were washed with urea buffer (3×100 µL) and drained by centrifugation (13900 *g*, 10 min). The collection tubes were replaced and the samples were subjected to enzymatic cleavage. To this end, 1 µg Lysyl endopeptidase (Lys-C, *Wako Chemicals*, Neuss, Germany) (0.5 µg / µL in 50 mM ammonium bicarbonate (ABC) buffer) in urea buffer (40 µL) was added and the samples were incubated at room temperature for 1 h while shaking. Additional Lys-C (1 µg) was added and the mixture was incubated over night at room temperature under agitation. The solution was diluted with ABC buffer (300 µL) and 0.2 µg trypsin (MS approved, *SERVA*, Heidelberg, Germany) (1 µg / µL in 1 mM HCl) were added. The samples were incubated at 37 °C for 3.5 h under agitation, followed by an additional trypsination step. After centrifugation (13900 *g*, 10 min), ABC buffer (50 µL) was added and the centrifugation step was repeated. The eluates were acidified with TFA to a final concentration of 1 % and desalted using C18-StageTips (pulldown samples) or SDB-StageTips (3 fractions, input samples) (Chapter 5.3.11.2).

5.3.11.2 StageTips

StageTip preparation

Prior to analysis by LC-MS/MS, peptide mixtures subjected to FASP (Chapter 5.3.11.1) were desalted and pre-fractionated by solid phase extraction. To do so, stop-and-go-extraction tips (StageTips)[274] were used, which were assembled from usual micro pipette tips and Empore solid phase extraction disks (*3M*, St. Paul, USA). With a blunt-ended syringe needle small disks were cut out of three layers of the respective sorbent material (Pulldown

samples: C18 (octadecyl-bonded silica), product number 2215; input samples: SDB (styrene-divenylbenzene copolymer), product number 2240) and placed into 200 µL pipette tips with a *Hamilton* syringe stamp by applying slight force until the position was fixed.

StageTip loading
Solvents used in loading and elution of StageTips were either LC-MS grade (MeCN, water, formic acid), HPLC grade (methanol), or peptide grade (TFA). StageTips were placed on top of 2 mL reaction tubes with a tip-to-reaction tube adapter (*Sonation*, Biberach, Germany).

SDB-StageTips were first equilibrated with MeCN (100 µL) and then rinsed with StageTip buffer 1 (30 % MeOH, 1 % TFA in water) (100 µL) and StageTip buffer 2 (0.2 % TFA in water) (100 µL). Between each step the StageTips were centrifuged (1300 *g*, 2 min). Input samples were loaded onto the SDB-StageTips in three portions by centrifugation (500 *g*, 1 min; 500 *g*, 3 min, 600 *g*, 3 min). The tips were then washed with StageTip buffer 2 (100 µL) and drained by centrifugation (1300 *g*, 2 min).

C18-StageTips were equilibrated with MeOH (60 µL) and then rinsed with StageTip buffer 3 (80 % MeCN, 0.5 % formic acid in water) (60 µL) and StageTip buffer 4 (0.5 % formic acid in water) (60 µL). Between each step the StageTips were centrifuged (1300 *g*, 2 min). Pulldown samples were loaded onto the C18-StageTips in three portions by centrifugation (500 *g*, 1 min; 600 *g*, 3 min, 800 *g*, 3 min). The tips were then washed with StageTip buffer 4 (2×100 µL) and drained by centrifugation (1300 *g*, 2 min).

StageTip elution
SDB-StageTips were placed on top of new 1.5 mL reaction tubes and peptides were eluted in three steps with increasing pH value and amount of organic solvent. The tubes were replaced for each step. Elution was first performed with StageTip buffer 5 (100 mM NH_4HCO_3, 40 % MeCN, 0.5 % formic acid in water) (20 µL), then with StageTip buffer 6 (150 mM NH_4HCO_3, 60 % MeCN, 0.5 % formic acid in water) (20 µL) and in the last step with StageTip buffer 7 (5 % NH_3, 80 % MeCN in water) (20 µL). Between each step the StageTips were centrifuged (500 *g*, 5 min). The fractions were diluted with water (20 µL) and lyophilized.

C18-StageTips were placed on top of new 1.5 mL reaction tubes and peptides were eluted with StageTip buffer 3 (2×20 µL) by centrifugation (500 *g*, 5 min).

5.3.11.3 Nano-LC-MS/MS

Peptides from pulldown assays or input samples were separated using an EASY-nLC1200 UHPLC system (*Thermo Fisher Scientific*) equipped with a 16 cm column, packed in-house with ReproSil-Pur C18-AQ 1.9 µm resin (*Dr. Maisch*). The column temperature was maintained at 50 °C, and the column was coupled to a Q Exactive HF mass spectrometer (*Thermo Fisher Scientific*) via a nano-electrospray source.

Total peptides (0.5 µg) were loaded onto the column and separated over a segmented linear gradient from 3-80 % buffer B (0.5 % formic acid in MeCN) in 120 min. The mass spectrometer was operated in data-dependent mode, survey scans were obtained in a mass range of 300-1759 m/z, at a resolution of 120000 at 200 m/z and an AGC target value of 3×106. The 12 most intense ions were selected with an isolation width of 1.2 m/z, fragmented in the HCD cell at a collision energy of 25 and the spectra recorded at a target

value of 5×104 and a resolution of 15000. Peptides with a charge of +1 or +6 and higher were excluded from fragmentation, the peptide match and exclude isotope features were enabled and selected precursors were dynamically excluded from repeated sampling for 30 s.

5.3.11.4 Data processing and quantification

Raw data were processed using the MaxQuant software package (Version 1.6.3.4, https://www.maxquant.org/)[275] and searched against the human reference proteome (UP000005640_9606, https://www.uniprot.org/) and an internal database containing standard contaminants. The search was performed with full trypsin specificity and a maximum of two missed cleavages and a protein false discovery rate of 1 %. Minimal peptide length was set to seven amino acids. Carbamidomethylation of cysteine residues was set as fixed, oxidation of methionine and N-terminal acetylation were set as variable modifications. All other search parameters were left at default. The MaxLFQ algorithm integral to MaxQuant was used for label-free quantification with match between runs enabled and the LFQ minimum ratio count was set to 1.[140] Input and pull-down samples were searched in two different parameter groups for separate LFQ normalization.

Downstream data analysis was carried out in the Perseus software package (Version 1.6.1.1, https://www.maxquant.org/). All hits for contaminants and reversed sequences were removed and the LFQ values $\log_2$ transformed. For interactomes of selected HDAC6 substrate peptides **P10**–**P17** missing LFQ values were imputed for each sequence context separately from normal distributions for proteins which were detected at least once on Lys-containing and at least once on AsuHd-containing probes and in at least three replicates in total on either Lys-containing or AsuHd-containing probes. Imputation was carried out for each column separately with a width of 0.5 and a down shift of 1.8. Statistical analysis was performed with the limma package[276] for R (Version 3.5.2, https://www.r-project.org/) using the $\log_2$ ratios from three independent biological replicates. Volcano plots were generated with *Microsoft Excel*, plotting p-values from limma analysis against the $\log_2$ ratio. Data for all experiments is provided in Supplementary tables S1–S8 on the attached storage medium.

5.3.12 MALDI-MS-based deacetylation assay

Reactions for the MALDI-MS-based deacetylation assay were performed with recombinant HDAC6 (100 nM, full length with C-terminal FLAG-tag, catalog # 50056, *BPS Bioscience*, San Diego, USA) and peptide substrates **P18**, **P20**, **P22**, **P24** or **P26** (100 µM) in HDAC buffer (100 mM HEPES, 8 mM KCl, 100 mM NaCl, pH 8.0) at 37 °C. At selected time points (0 to 25 min) samples (2 µL) were taken and mixed with stopping solution (8 µL, 6.25 µM trichostatin A, 0.1 % TFA in water). To this mixture a solution of the respective isotopic standard peptide **P19**, **P21**, **P23**, **P25** or **P27** (10 µL, 4 µM in HDAC buffer) was added and the sample was further diluted with 0.1 % TFA in water (80 µL). 1 µL of this solution was spotted onto a polished steel target, mixed with 1 µL of matrix solution (CHCA for **P20**–**P27**, DHB for **P18** / **P19**), and analyzed by MALDI-MS (Chapter 5.2.1.4). The amount of formed product was determined from the signal intensity of the monoisotopic $[M+H]^+$ (**P20**, **P22**, **P24**, **P26**) or $[M+Na]^+$ (**P18**) peak of the product in relation to the respective peak of the

isotopically labeled references **P19**, **P21**, **P23**, **P25** or **P27** according to

$$c_{\text{product}} = F \cdot c_{\text{standard}} \cdot \frac{I_{\text{product}}}{I_{\text{standard}}} \quad ,$$

with the respective concentrations c, signal intensities I, and a dilution factor F. Initial velocities of the deacetylation reaction were determined from three independent experiments.

6 References

[1] R. D. Kornberg, *Science* **1994**, *184*, 868–871.

[2] K. Luger, A. W. Mäder, R. K. Richmond, D. F. Sargent, T. J. Richmond, *Nature* **1997**, *389*, 251–260.

[3] G. Felsenfeld, M. Groudine, *Nature* **2003**, *421*, 448–453.

[4] W. Hennig, *Chromosoma* **1999**, *108*, 1–9.

[5] A. J. Bannister, T. Kouzarides, *Cell. Res.* **2011**, *21*, 381–395.

[6] K. Luger, T. J. Richmond, *Curr. Opin. Genet. Dev.* **1998**, *8*, 140–146.

[7] C. Zheng, J. J. Hayes, *Biopolymers* **2003**, *68*, 539–546.

[8] C. T. Walsh, S. Garneau-Tsodikova, G. J. Gatto, *Angew. Chem. Int. Ed.* **2005**, *44*, 7342–7372.

[9] S. B. Rothbart, B. D. Strahl, *Biochim. Biophys. Acta. Gene Regul. Mech.* **2014**, *1839*, 627–643.

[10] D. J. Clark, T. Kimurai, *J. Mol. Biol.* **1990**, *211*, 883–896.

[11] A. A. Kalashnikova, M. E. Porter-Goff, U. M. Muthurajan, K. Luger, J. C. Hansen, *J. R. Soc. Interface* **2013**, *10*, 20121022.

[12] D. Y. Lee, J. J. Hayes, D. Pruss, A. P. Wolffe, *Cell* **1993**, *72*, 73–84.

[13] X. Wang, J. J. Hayes, *Biochem. Cell Biol.* **2006**, *84*, 578–588.

[14] S. S. Chahal, H. R. Matthews, E. M. Bradbury, *Nature* **1980**, *287*, 76–79.

[15] D. Doenecke, D. Gallwitz, *Mol. Cell Biochem.* **1982**, *44*, 113–128.

[16] C. A. Davey, D. F. Sargent, K. Luger, A. W. Maeder, T. J. Richmond, *J. Mol. Biol.* **2002**, *319*, 1097–1113.

[17] B. D. Strahl, C. D. Allis, *Nature* **2000**, *403*, 41–45.

[18] S. D. Taverna, H. Li, A. J. Ruthenburg, C. D. Allis, D. J. Patel, *Nat. Struct. Mol. Biol.* **2007**, *14*, 1025–1040.

[19] A. H. Hassan, P. Prochasson, K. E. Neely, S. C. Galasinski, M. Chandy, M. J. Carrozza, J. L. Workman, *Cell* **2002**, *111*, 369–379.

[20] H. Huang, B. R. Sabari, B. A. Garcia, C. D. Allis, Y. Zhao, *Cell* **2014**, *159*, 458–458.e1.

[21] A. Izzo, R. Schneider, *Brief. Funct. Genomics* **2011**, *9*, 429–443.

[22] W. Fischle, B. S. Tseng, H. L. Dormann, B. M. Ueberheide, B. A. Garcia, J. Shabanowitz, D. F. Hunt, H. Funabiki, C. D. Allis, *Nature* **2005**, *438*, 1116–1122.

[23] J.-S. Lee, A. Shukla, J. Schneider, S. K. Swanson, M. P. Washburn, L. Florens, S. R. Bhaumik, A. Shilatifard, *Cell* **2007**, *131*, 1084–1096.

[24] M. Biel, V. Wascholowski, A. Giannis, *Angew. Chem. Int. Ed.* **2005**, *44*, 3186–3216.

[25] V. G. Allfrey, R. Faulkner, A. E. Mirsky, *Proc. Natl. Acad. Sci. USA* **1964**, *51*, 786–794.

[26] C. Choudhary, J. Kumar, F. Gnad, M. L. Nielsen, M. Rehman, T. C. Walther, J. V. Olsen, M. Mann, *Science* **2009**, *325*, 834–840.

[27] C. Choudhary, B. T. Weinert, Y. Nishida, E. Verdin, M. Mann, *Nature Rev. Mol. Cell Biol.* **2014**, *15*, 536–550.

[28] I. V. Gregoretti, Y. M. Lee, H. V. Goodson, *J. Mol. Biol.* **2004**, *338*, 17–31.

[29] E. Seto, M. Yoshida, *Cold Spring Harb. Perspect. Biol.* **2014**, *6*, a018713.

[30] A. J. de Ruijter, A. H. van Gennip, H. N. Caron, S. Kemp, A. B. van Kuilenburg, *Biochem. J.* **2003**, *370*, 737–749.

[31] E. Verdin, F. Dequiedt, H. G. Kasler, *Trends Genet.* **2003**, *19*, 286–293.

[32] X. J. Yang, E Seto, *Nat. Rev. Mol. Cell. Biol.* **2008**, *9*, 206–218.

[33] D. H. Kwon, Y. K. Kim, H Kook, *J. Korean Med. Sci.* **2017**, *32*, 1738–1748.

[34] S. C. Galasinski, K. A. Resing, J. A. Goodrich, N. G. Ahn, *J. Biol. Chem.* **2002**, *277*, 19618–19626.

[35] J. Luo, F. Su, D. Chen, A. Shiloh, W. Gu, *Nature* **2000**, *408*, 377–381.

[36] Y Takami, T Nakayama, *J. Biol. Chem.* **2000**, *275*, 16191–16201.

[37] M. A. Moser, A. Hagelkruys, C. Seiser, *Chromosoma* **2014**, *123*, 67–78.

[38] W.-M. Yang, S.-C. Tsai, Y.-D. Wen, G. Fejér, E. Seto, *J. Biol. Chem.* **2002**, *277*, 9447–9454.

[39] T. B. Toro, T. J. Watt, *FASEB J.* **2020**, *34*, 13140–13155.

[40] N. A. Wolfson, C. A. Pitcairn, C. A. Fierke, *Biopolymers* **2013**, *99*, 112–126.

[41] M.-E. Terret, R. Sherwood, S. Rahman, J. Qin, P. V. Jallepalli, *Nature* **2009**, *462*, 231–234.

[42] T. A. McKinsey, C. L. Zhang, E. N. Olson, *Mol. Cell. Biol.* **2001**, *21*, 6312–6321.

[43] S Hu, E. H. Cho, J. Y. Lee, *Diabetes Metab. J.* **2020**, *44*, 234–244.

[44] X. Zhou, P. A. Marks, R. A. Rifkind, V. M. Richon, *Proc. Natl. Acad. Sci. USA* **2001**, *98*, 10572–10577.

[45] W. Fischle, F. Dequiedt, M. J. Hendzel, M. G. Guenther, M. A. Lazar, W. Voelter, E. Verdin, *Mol. Cell* **2002**, *9*, 45–57.

[46] G. M. Hudson, P. J. Watson, L. Fairall, A. G. Jamieson, J. W. Schwabe, *J. Biol. Chem.* **2015**, *290*, 18237–18244.

[47] C. Boyault, K. Sadoul, M. Pabion, S. Khochbin, *Oncogene* **2007**, *26*, 5468–5476.

[48] Y. Hai, D. W. Christianson, *Nat. Chem. Biol.* **2016**, *12*, 741–747.

[49] C. Hubbert, A. Guardiola, R. Shao, Y. Kawaguchi, A. Ito, A. Nixon, M. Yoshida, X. F. Wang, T. P. Yao, *Nature* **2002**, *417*, 455–458.

[50] A. Valenzuela-Fernández, J. R. Cabrero, J. M. Serrador, F. Sánchez-Madrid, *Trends Cell Biol.* **2008**, *18*, 291–297.

[51] J. J. Kovacs, P. J. Murphy, S. Gaillard, X. Zhao, J.-T. Wu, C. V. Nicchitta, M. Yoshida, D. O. Toft, W. B. Pratt, T.-P. Yao, *Mol. Cell* **2005**, *18*, 601–607.

[52] P. J. Murphy, Y. Morishima, J. J. Kovacs, T.-P. Yao, W. B. Pratt, *J. Biol. Chem.* **2005**, *280*, 33792–33799.

[53] Y. Kawaguchi, J. J. Kovacs, A. McLaurin, J. M. Vance, A. Ito, T.-P. Yao, *Cell* **2003**, *115*, 727–738.

[54] C. Boyault, B. Gilquin, Y. Zhang, V. Rybin, E. Garman, W. Meyer-Klaucke, P. Matthias, C. W. Müller, S. Khochbin, *EMBO J.* **2006**, *25*, 3357–3366.

[55] D. D. Fischer, R. Cai, U. Bhatia, F. A. Asselbergs, C. Song, R. Terry, N. Trogani, R. Widmer, P. Atadja, D. Cohen, *J. Biol. Chem.* **2002**, *277*, 6656–6666.

[56] J. J. Tong, J. Liu, N. R. Bertos, X.-J. Yang, *Nucleic Acids Res.* **2002**, *30*, 1114–1123.

[57] A. R. Guardiola, T.-P. Yao, *J. Biol. Chem.* **2002**, *277*, 3350–3356.

[58] Y. Hai, S. A. Shinsky, N. J. Porter, D. W. Christianson, *Nat. Commun.* **2017**, *8*, 15368.

[59] P. Bheda, H. Jing, C. Wolberger, H. Lin, *Annu. Rev. Biochem.* **2016**, *85*, 405–429.

[60] A. Chalkiadaki, L. Guarente, *Nat. Rev. Cancer* **2015**, *15*, 608–624.

[61] B. J. North, E Verdin, *Genome Biol.* **2004**, *5*, 224.

[62] J. Du, Y. Zhou, X. Su, J. J. Yu, S. Khan, H. Jiang, J. Kim, J. Woo, J. H. Kim, B. H. Choi, B. He, W. Chen, S. Zhang, R. A. Cerione, J. Auwerx, Q. Hao, H. Lin, *Science* **2011**, *334*, 806–809.

[63] H. Jiang, S. Khan, Y. Wang, G. Charron, B. He, C. Sebastian, J. Du, R. Kim, E. Ge, R. Mostoslavsky, H. C. Hang, Q. Hao, H. Lin, *Nature* **2013**, *496*, 110–113.

[64] D. Wu, Y. Li, K. S. Zhu, H. Wang, W.-G. Zhu, *Front. Endocrinol.* **2018**, *9*, 652.

[65] L. Tong, J. M. Denu, *Biochim. Biophys. Acta Proteins Proteom.* **2010**, *1804*, 1617–1625.

[66] L. Gao, M. A. Cueto, F. Asselbergs, P. Atadja, *J. Biol. Chem.* **2002**, *277*, 25748–25755.

[67] Z. Kutil, Z. Novakova, M. Meleshin, J. Mikesova, M. Schutkowski, C. Barinka, *ACS Chem. Biol.* **2018**, *13*, 685–693.

[68] R. D. Kelly, S. M. Cowley, *Biochem. Soc. Trans.* **2013**, *41*, 741–749.

[69] D. E. Ayer, *Trends Cell. Biol.* **1999**, *9*, 193–198.

[70] Y. D. Wen, V. Perissi, L. M. Staszewski, W. M. Yang, A. Krones, C. K. Glass, M. G. Rosenfeld, E. Seto, *Proc. Natl. Acad. Sci.* **2000**, *97*, 7202–7207.

[71] C. J. Millard, P. J. Watson, L. Fairall, J. W. Schwabe, *Trends Pharmacol. Sci.* **2017**, *38*, 363–377.

[72] T Hayakawa, J Nakayama, *J. Biomed. Biotechnol.* **2011**, *2011*, 129383.

[73] K. M. Viiri, H. Korkeamäki, M. K. Kukkonen, L. K. Nieminen, K. Lindfors, P. Peterson, M. Mäki, H. Kainulainen, O. Lohi, *Nucleic Acids Res.* **2006**, *34*, 3288–3298.

[74] A. Kuzmichev, Y. Zhang, H. Erdjument-Bromage, P. Tempst, D. Reinberg, *Mol. Cell. Bio.* **2002**, *22*, 835–848.

[75] H. Hoffmeister, A. Fuchs, F. Erdel, S. Pinz, R. Gröbner-Ferreira, A. Bruckmann, R. Deutzmann, U. Schwartz, R. Maldonado, C. Huber, A.-S. Dendorfer, K. Rippe, G. Längst, *Nucleic Acids Res.* **2017**, *45*, 10534–10554.

[76] J. Oberoi, L. Fairall, P. J. Watson, J.-C. Yang, Z. Czimmerer, T. Kampmann, B. T. Goult, J. A. Greenwood, J. T. Gooch, B. C. Kallenberger, L. Nagy, D. Neuhaus, J. W. R. Schwabe, *Nat. Struct. Mol. Biol.* **2011**, *18*, 177–184.

[77] M. S. Finnin, J. R. Donigian, A. Cohen, V. M. Richon, R. A. Rifkind, P. A. Marks, R. Breslow, N. P. Pavletich, *Nature* **1999**, *401*, 188–193.

[78] B. W. Matthews, *Acc. Chem. Res.* **1988**, *21*, 333–340.

[79] D. W. Christianson, W. N. Lipscomb, *Acc. Chem. Res.* **1989**, *22*, 62–69.

[80] P. M. Lombardi, K. E. Cole, D. P. Dowling, D. W. Christianson, *Curr. Opin. Struct. Biol.* **2011**, *21*, 735–743.

[81] P. M. Lombardi, H. D. Angell, D. A. Whittington, E. F. Flynn, K. R. Rajashankar, D. W. Christianson, *Biochemistry* **2011**, *50*, 1808–1817.

[82] D. Riester, D. Wegener, C. Hildmann, A. Schwienhorst, *Biochem. Biophys. Res. Commun.* **2004**, *324*, 1116–1123.

[83] A. Lahm, C. Paolini, M. Pallaoro, M. C. Nardi, P. Jones, P. Neddermann, S. Sambucini, M. J. Bottomley, P. Lo Surdo, A. Carfí, U. Koch, R. De Francesco, C. Steinkühler, P. Gallinari, *Proc. Natl. Acad. Sci. USA* **2007**, *104*, 17335–17340.

[84] R. Johnstone, *Nat. Rev. Drug Discov.* **2002**, *1*, 287–289.

[85] S. Minucci, P. G. Pelicci, *Nat. Rev. Cancer* **2016**, *6*, 38–51.

[86] J. E. Bolden, M. J. Peart, R. W. Johnstone, *Nat. Rev. Drug Discov.* **2006**, *5*, 769–784.

[87] R. Chen, M. Zhang, Y. Zhou, W. Guo, M. Yi, Z. Zhang, Y. Ding, Y. Wang, *J. Exp. Clin. Cancer Res.* **2020**, *39*, 138.

[88] M. Jung, K. Hoffmann, G. Brosch, P. Loidl, *Bioorg. Med. Chem. Lett.* **1997**, *7*, 1655–1658.

[89] T. A. Miller, D. J. Witter, S. Belvedere, *J. Med. Chem.* **2003**, *46*, 5097–5116.

[90] J. Melesina, C. V. Simoben, L. Praetorius, E. F. Bülbül, D. Robaa, W. Sippl, *ChemMedChem* **2021**, *16*, 1336–1359.

[91] A. V. Bieliauskas, M. K. H. Pflum, *Chem. Soc. Rev.* **2008**, *37*, 1402–1413.

[92] C. J. Vickers, C. A. Olsen, L. J. Leman, M. R. Ghadiri, *ACS Med. Chem. Lett.* **2012**, *3*, 505–508.

[93] N. J. Porter, F. F. Wagner, D. W. Christianson, *Biochemistry* **2018**, *57*, 3916–3924.

[94] J. R. Somoza, R. J. Skene, B. A. Katz, C. Mol, J. D. Ho, A. J. Jennings, C. Luong, A. Arvai, J. J. Buggy, E. Chi, J. Tang, B. C. Sang, E. Verner, R. Wynands, E. M. Leahy, D. R. Dougan, G. Snell, M. Navre, M. W. Knuth, R. V. Swanson, D. E. McRee, L. W. Tari, *Structure* **2004**, *12*, 1325–1334.

[95] J. C. Bressi, A. J. Jennings, R. Skene, Y. Wu, R. Melkus, R. De Jong, S. O'Connel, C. E. Grimshaw, M. Navre, A. R. Gangloff, *Bioorg. Med. Chem. Lett.* **2010**, *20*, 3142–3145.

[96] D. C. Beshore, G. C. Adam, R. J. O. Barnard, C. Burlein, S. N. Gallicchio, M. K. Holloway, D. Krosky, W. Lemaire, R. W. Myers, S. Patel, M. A. Plotkin, D. A. Powell, V. Rada, C. D. Cox, P. J. Coleman, D. J. Klein, S. E. Wolkenberg, *ACS Med. Chem. Lett.* **2021**, *12*, 540–547.

[97] L. Sealy, R. Chalkley, *Cell* **1978**, *14*, 115–121.

[98] M. Gottlicher, S. Minucci, P. Zhu, O. H. Kramer, A. Schimpf, *EMBO J.* **2001**, *20*, 6969–6978.

[99] N. Tsuji, M. Kobayashi, K. Nagashima, Y. Wakisaka, K. Koizumi, *J. Antibiot.* **1976**, *29*, 1–6.

[100] M. Yoshida, M. Kijima, M. Akita, T. Beppu, *J. Antibiot.* **1990**, *265*, 17174–17179.

[101] S. J. Haggarty, K. M. Koeller, J. C. Wong, C. M. Grozinger, S. L. Schreiber, *Proc. Natl. Acad. Sci. USA* **2003**, *100*, 4389–4394.

[102] K. V. Butler, J. Kalin, C. Brochier, G. Vistoli, B. Langley, A. P. Kozikowski, *J. Am. Chem. Soc.* **2010**, *132*, 10842–10846.

[103] A. Saito, T. Yamashita, Y. Mariko, Y. Nosaka, K. Tsuchiya, T. Ando, T. Suzuki, T. Tsuruo, O. Nakanishi, *Proc. Natl. Acad. Sci. USA* **1999**, *96*, 4592–4597.

[104] T. Suzuki, T. Ando, K. Tsuchiya, N. Fukazawa, A. Saito, Y. Mariko, T. Yamashita, O. Nakanishi, *J. Med. Chem.* **1999**, *42*, 3001–3003.

[105] C. Xu, E. Soragni, C. J. Chou, D. Herman, H. L. Plasterer, J. R. Rusche, J. M. Gottesfeld, *Chem. Biol.* **2009**, *16*, 980–989.

[106] D. J. Witter, P. Harrington, K. J. Wilson, M. Chenard, J. C. Fleming, B. Haines, A. M. Kral, J. P. Secrist, T. A. Miller, *Bioorg. Med. Chem. Lett.* **2008**, *18*, 726–731.

[107] F. F. Wagner, M. Weïwer, S. Steinbacher, A. Schomburg, P. Reinemer, J. P. Gale, A. J. Campbell, S. L. Fisher, W.-N. Zhao, S. A. Reis, K. M. Hennig, M. Thomas, P. Müller, M. R. Jefson, D. M. Fass, S. J. Haggarty, Y.-L. Zhang, E. B. Holson, *Bioorg. Med. Chem.* **2016**, *24*, 4008–4015.

[108] S. B. Singh, D. L. Zink, J. D. Polishook, A. W. Dombrowski, S. J. Darkin-Rattray, S. D. M., M. A. Goetz, *Tetrahedron Lett.* **1996**, *37*, 8077–8080.

[109] S. B. Singh, D. L. Zink, J. M. Liesch, R. T. Mosley, A. W. Dombrowski, G. F. Bills, S. J. Darkin-Rattray, D. M. Schmatz, M. A. Goetz, *J. Org. Chem.* **2002**, *67*, 815–825.

[110] H. Itazaki, K. Nagashima, K. Sugita, H. Yoshida, Y. Kawamura, Y. Yasuda, K. Matsumoto, K. Ishii, N. Uotani, H. Nakai, *J. Antibiot.* **1990**, *43*, 1524–1532.

[111] J. D. Walton, *Phytochemistry* **2006**, *67*, 1406–1413.

[112] A. Closse, R. Huguenin, *Helv. Chim. Acta* **1974**, *57*, 533–545.

[113] J. Taunton, C. A. Hassig, S. L. Schreiber, *Science* **1996**, *272*, 408–411.

[114] H. Mori, Y. Urano, F. Abe, S. Furukawa, S. Furukawa, Y. Tsurumi, K. Sakamoto, M. Hashimoto, S. Takase, M. Hino, T. Fujii, *J. Antibiot.* **2003**, *56*, 72–79.

[115] H. Mori, Y. Urano, T. Kinoshita, S. Yoshimura, S. Takase, M. Hino, *J. Antibiot.* **2003**, *56*, 181–185.

[116] S. J. Darkin-Rattray, A. M. Gurnett, R. W. Myers, P. M. Dulski, T. M. Crumley, J. J. Allocco, C. Cannova, P. T. Meinke, S. L. Colletti, M. A. Bednarek, S. B. Singh, M. A. Goetz, A. W. Dombrowski, J. D. Polishook, D. M. Schmatz, *Proc. Natl. Acad. Sci. USA* **1996**, *93*, 13143–13147.

[117] R. Furumai, Y. Komatsu, N. Nishino, S. Khochbin, M. Yoshida, S. Horinouchi, *Proc. Natl. Acad. Sci. USA* **2001**, *98*, 87–92.

[118] N. J. Porter, D. W. Christianson, *ACS Chem. Biol.* **2017**, *12*, 2281–2286.

[119] M. D. M. Traoré, V. Zwick, C. A. Simões-Pires, A. Nurisso, M. Issa, M. Cuendet, M. Maynadier, S. Wein, H. Vial, H. Jamet, Y.-S. Wong, *ACS Omega* **2017**, *2*, 1550–1562.

[120] R. R. Frey, C. K. Wada, R. B. Garland, M. L. Curtin, M. R. Michaelides, J. Li, L. J. Pease, K. B. Glaser, P. A. Marcotte, J. J. Bouska, S. S. Murphy, S. K. Davidsen, *Bioorg. Med. Chem. Lett.* **2002**, *12*, 3443–3447.

[121] A. S. Madsen, H. M. E. Kristensen, G. Lanz, C. A. Olsen, *ChemMedChem* **2014**, *9*, 614–626.

[122] A. S. Madsen, C. A. Olsen, *Med. Chem. Commun.* **2016**, *7*, 464–470.

[123] H. Ueda, H. Nakajima, Y. Hori, T. Fujita, M. Nishimura, T. Goto, M. Okuhara, *J. Antibiot.* **1994**, *47*, 301–310.

[124] N. Shigematsu, H. Ueda, S. Takase, H. Tanaka, K. Yamamoto, T. Tada, *J. Antibiot.* **1994**, *47*, 311–314.

[125] K. Taori, V. J. Paul, H. Luesch, *J. Am. Chem. Soc.* **2008**, *130*, 1806–1807.

[126] A. Bowers, N. West, J. Taunton, S. L. Schreiber, J. E. Bradner, R. M. Williams, *J. Am. Chem. Soc.* **2008**, *130*, 11219–11222.

[127] Y. Nakao, S. Yoshida, S. Matsunaga, N. Shindoh, Y. Terada, K. Nagai, J. K. Yamashita, A. Ganesan, R. W. M. van Soest, N. Fusetani, *Angew. Chem. Int. Ed.* **2006**, *45*, 7553–7557.

[128] N. Maulucci, M. G. Chini, S. Di Micco, I. Izzo, E. Cafaro, A. Russo, P. Gallinari, C. Paolini, M. C. Nardi, A. Casapullo, R. Riccio, G. Bifulco, F. De Riccardis, *J. Am. Chem. Soc.* **2007**, *129*, 3007–3012.

[129] N. Nishino, D. Yoshikawa, L. A. Watanabe, T. Kato, B. Jose, Y. Komatsu, Y. Sumida, M. Yoshida, *Bioorg. Med. Chem. Lett.* **2004**, *14*, 2427–2431.

[130] J. Sindlinger, J. Bierlmeier, L.-C. Geiger, K. Kramer, I. Finkemeier, D. Schwarzer, *J. Pept. Sci.* **2016**, *22*, 352–359.

[131] O. N. Jensen, *Nature Rev. Mol. Cell Biol.* **2006**, *7*, 391–403.

[132] C. Choudhary, M. Mann, *Nature Rev. Mol. Cell Biol.* **2010**, *11*, 427–439.

[133] T. Köcher, G. Superti-Furga, *Nat. Methods* **2007**, *4*, 807–815.

[134] M. Vermeulen, N. C. Hubner, M. Mann, *Curr. Opin. Biotechnol.* **2008**, *19*, 331–337.

[135] M. Mann, *EMBO Mol. Med.* **2012**, *4*, 75–77.

[136] J. Sindlinger, Dissertation, Eberhard Karls Universität Tübingen, **2018**.

[137] M. Bantscheff, S. Lemeer, M. M. Savitski, B. Kuster, *Anal. Bioanal. Chem.* **2012**, *404*, 939–965.

[138] S. E. Ong, B. Blagoev, I. Kratchmarova, D. B. Kristensen, H. Steen, A. Pandey, M. Mann, *Mol. Cell Proteom.* **2002**, *1*, 376–386.

[139] P. J. Boersema, R. Raijmakers, S. Lemeer, S. Mohammed, A. J. R. Heck, *Nat. Protoc.* **2009**, *4*, 484–494.

[140] J. Cox, M. Y. Hein, C. A. Luber, I. Paron, N. Nagaraj, M. Mann, *Mol. Cell. Proteomics* **2014**, *13*, 2513–2526.

[141] M. Bantscheff, C. Hopf, M. M. Savitski, A. Dittmann, P. Grandi, A.-M. Michon, J. Schlegl, Y. Abraham, I. Becher, G. Bergamini, M. Boesche, M. Delling, B. Dümpelfeld, D. Eberhard, C. Huthmacher, T. Mathieson, D. Poeckel, V. Reader, K. Strunk, G. Sweetman, U. Kruse, G. Neubauer, N. G. Ramsden, G. Drewes, *Nat. Biotechnol.* **2011**, *29*, 255–265.

[142] A. Dose, J. Sindlinger, J. Bierlmeier, A. Bakirbas, K. Schulze-Osthoff, F. Einsele-Scholz, M. Hartl, F. Essmann, I. Finkemeier, D. Schwarzer, *Angew. Chem. Int. Ed.* **2016**, *55*, 1192 –1195.

[143] A. Dose, Dissertation, Eberhard Karls Universität Tübingen, **2015**.

[144] D. Schwarzer, *J. Pept. Sci.* **2010**, *16*, 530–537.

[145] C. Schölz, B. T. Weinert, S. A. Wagner, P. Beli, Y. Miyake, J. Qi, L. J. Jensen, W. Streicher, A. R. McCarthy, N. J. Westwood, S. Lain, J. Cox, P. Matthias, M. Mann, J. E. Bradner, C. Choudhary, *Nat. Biotechnol.* **2015**, *33*, 415–423.

[146] J. E. Bradner, N. West, M. L. Grachan, E. F. Greenberg, S. J. Haggarty, T. Warnow, R. Mazitschek, *Nat. Chem. Biol.* **2010**, *6*, 238–243.

[147] T. Liu, G. Kapustin, F. A. Etzkorn, *J. Med. Chem.* **2007**, *50*, 2003–2006.

[148] D. M. Wilson, L. N. Silverman, M. Bergauer, K. R. Keshari, *Tetrahedron Lett.* **2013**, *54*, 151–153.

[149] A. Mahindra, C. J. Millard, I. Black, L. J. Archibald, J. W. R. Schwabe, A. G. Jamieson, *Org. Lett.* **2019**, *21*, 3178–3182.

[150] C. Moreno-Yruela, M. Bæk, A.-E. Vrsanova, C. Schulte, H. M. Maric, C. A. Olsen, *Nat. Commun.* **2020**, *12*, 62.

[151] S. Hanessian, S. Bouzbouz, A. Boudon, C. G. Tucker, D. Peyroulan, *Bioorg. Med. Chem. Lett.* **1999**, *9*, 1691–1696.

[152] P. G. M. Wuts, *Greene's protective groups in organic synthesis*, 5th ed., John Wiley & Sons, Hoboken, NJ, **2014**.

[153] K. Lang, K. Nuetzel, F. Schubert, *Chem. Abstr.* **1963**, *58*, 1488a.

[154] H. C. Brown, A. K. J. Gupta, *Organomet. Chem.* **1988**, *34*, 73–81.

[155] W. H. Dent, R. W. Erickson, S. C. Fields, *Org. Lett.* **2002**, *4*, 1249–1251.

[156] J. P. E. Human, J. A. Mills, *Nature* **1946**, *158*, 877.

[157] G. H. L. Nefkens, B. Zwanenburg, *Tetrahedron* **1982**, *39*, 2995–2998.

[158] Y.-Q. Long, F.-D. T. Lung, P. P. Roller, *Bioorg. Med. Chem.* **2003**, *11*, 3929–3936.

[159] B. M. Syed, T. Gustafssona, J. Kihlberg, *Tetrahedron* **2004**, *60*, 5571–5575.

[160] T. Ankner, T. Norberg, J. Kihlberg, *Eur. J. Org. Chem.* **2015**, 3767–3770.

[161] T. Meisinger, Bachelor thesis, Eberhard Karls Universität Tübingen, **2018**.

[162] H. Hess-Stumpp, T. U. Bracker, D. Henderson, O. Politz, *Int. J. Biochem. Cell Biol.* **2007**, *39*, 1388–1405.

[163] J. Seidel, T. Meisinger, J. Sindlinger, P. Pieloch, I. Finkemeier, D. Schwarzer, *ChemBioChem* **2019**, *20*, 3001–3005.

[164] J. Bajgrowicz, A. El Hallaoui, R. Jacquier, C. Pigière, P. Viallefont, *Tethrahedron* **1985**, *41*, 1833–1843.

[165] L. Mou, G. Singh, *Tethrahedron Lett.* **2001**, *42*, 6603–6606.

[166] P. J. Murray, M. Kranz, M. Ladlow, S. Taylor, F. Berst, A. B. Holmes, K. N. Keavey, A. Jaxa-Chamiec, P. W. Seale, P. Stead, R. J. Upton, S. L. Croft, W. Clegg, M. R. J. Elsegood, *Bioorg. Med. Chem. Lett.* **2001**, *11*, 773–776.

[167] M. L. Linares, F. J. Agejas, J. R. Alajarín, J. J. Vaquero, J. Alvarez-Builla, *Synthesis* **2006**, *12*, 2069–2073.

[168] S. Nahm, S. M. Weinreb, *Tetrahedron Lett.* **1981**, *22*, 3815–3818.

[169] R. Huisgen, *Proc. Chem. Soc.* **1961**, 357–369.

[170] V. V. Rostovtsev, L. G. Green, V. V. Fokin, K. B. Sharpless, *Angew. Chem. Int. Ed.* **2002**, *41*, 2596–2599.

[171] P. Krapf, R. Richarz, E. A. Urusova, B. Neumaier, B. D. Zlatopolskiy, *Eur. J. Org. Chem.* **2016**, 430–433.

[172] A. Lodek, Bachelor thesis, Eberhard Karls Universität Tübingen, **2020**.

[173] R. Frank, *Tetrahedron* **1992**, *48*, 9217–9232.

[174] D. F. Winkler, K. Hilpert, O. Brandt, R. E. Hancock in *Peptide Microarrays: Methods and Protocols*, (Eds.: M. Cretich, M. Chiari), 6th ed., Humana Press (Springer), Totowa, NJ, **2009**, 157–174.

[175] J. O. Jost, A. Hanswillemenke, D. Schwarzer, *Mol. BioSyst.* **2015**, *11*, 1820–1823.

[176] G. Schnorrenberg, H. Gerhardt, *Tetrahedron* **1989**, *45*, 7759–7764.

[177] R. Pipkorn, C. Boenke, M. Gehrke, R. Hoffmann, *J. Peptide Res.* **2002**, *59*, 105–114.

[178] C. Saxinger, T. P. Conrads, D. J. Goldstein, T. D. Veenstra, *BMC Immunol.* **2005**, *6*, 1.

[179] J. K. Murray, S. H. Gellman, *J. Comb. Chem.* **2006**, *8*, 58–65.

[180] S. L. Pedersen, K. J. Jensen in *Peptide Synthesis and Applications*, (Eds.: K. J. Jensen, P. Tofteng Shelton, S. L. Pedersen), 2nd ed., Humana Press (Springer), Totowa, NJ, **2013**, 215–224.

[181] N. A. Solé, G. Barany, *J. Org. Chem.* **1992**, *57*, 5399–5403.

[182] D. S. King, C. G. Fields, G. B. Fields, *Int. J. Peptide Protein Res.* **1990**, *36*, 255–266.

[183] Y. Yang, *Side Reactions in Peptide Synthesis*, 1st ed., Academic Press, Oxford, **2015**.

[184] D. L. Coffen, *Chem. Commun.* **1967**, 1089.

[185] M. Yenjerla, A. Panopoulos, C. Reynaud, R. Fotedar, R. L. Margolis, *Cell Cycle* **2013**, *12*, 837–841.

[186] S. F. Bakhoum, S. L. Thompson, A. L. Manning, D. A. Compton, *Nat. Cell Biol.* **2009**, *11*, 27–35.

[187] D. J. Escobar, R. Desai, N. Ishiyama, S. S. Folmsbee, M. N. Novak, A. S. Flozak, R. L. Daugherty, R. Mo, D. Nanavati, R. Sarpal, D. Leckband, M. Ikura, U. Tepass, C. J. Gottardi, *J. Cell Sci.* **2015**, *128*, 1150–1165.

[188] H. Masuda, K. Tanaka, M. Takagi, K. Ohgami, T. Sakamaki, N. Shibata, K. Takahashi, *J. Biochem.* **1996**, *120*, 415–424.

[189] S. W. Bai, M. T. Herrera-Abreu, J. L. Rohn, V. Racine, V. Tajadura, N. Suryavanshi, S. Bechtel, S. Wiemann, B. Baum, A. J. Ridley, *BMC Biol.* **2011**, *9*, 54.

[190] N. Bhattacharya, S. Ghosh, D. Sept, J. A. Cooper, *J. Biol. Chem.* **2006**, *281*, 31021–31030.

[191] S. Yeoh, B. Pope, H. G. Mannherz, A. Weeds, *J. Mol. Biol.* **2002**, *315*, 911–925.

[192] J. Harbour, R. X. Luo, A. D. Santi, A. A. Postigo, D. C. Dean, *Cell* **1999**, *98*, 859–869.

[193] V. Lalioti, D. Pulido, I. V. Sandoval, *Cell Cycle* **2010**, *9*, 284–311.

[194] M. Jackman, C. Lindon, E. A. Nigg, J. Pines, *Nat.Cell Biol.* **2003**, *5*, 143–148.

[195] F. Li, D. Kozono, P. Deraska, T. Branigan, C. Dunn, X.-F. Zheng, K. Parmar, H. Nguyen, J. DeCaprio, G. I. Shapiro, D. Chowdhury, A. D. D'Andrea, *Mol. Cell* **2020**, *80*, 410–422.e6.

[196] A. S. Kumar, I. Naruszewicz, P. Wang, C. Leung-Hagesteijn, G. E. Hannigan, *Oncogene* **2004**, *23*, 3454–3461.

[197] X. Zhang, Z. Yuan, Y. Zhang, S. Yong, A. Salas-Burgos, J. Koomen, N. Olashaw, J. T. Parsons, X.-J. Yang, S. R. Dent, T.-P. Yao, W. S. Lane, E. Seto, *Mol. Cell* **2007**, *27*, 197–213.

[198] S. Ayloo, J. E. Lazarus, A. Dodda, M. Tokito, E. M. Ostap, E. L. F. Holzbaur, *Nat. Commun.* **2014**, *5*, 4807.

[199] J. Napetschnig, H. Wu, *Annu. Rev. Biophys.* **2013**, *42*, 443–468.

[200] Y. Shen, L. M. Hendershot, *Mol. Biol. Cell* **2005**, *16*, 40–50.

[201] S. Shao, M. C. Rodrigo-Brenni, M. H. Kivlen, R. S. Hegde, *Science* **2017**, *355*, 298–302.

[202] I. E. Vainberg, S. A. Lewis, H. Rommelaere, C. Ampe, J. Vandekerckhove, H. L. Klein, N. J. Cowan, *Cell* **1998**, *93*, 863–873.

[203] G. Tian, Y. Huang, H. Rommelaere, J. Vandekerckhove, C. Ampe, N. J. Cowan, *Cell* **1996**, *86*, 287–296.

[204] J. Akaishi, M. Onda, J. Okamoto, S. Miyamoto, M. Nagahama, K. Ito, A. Yoshida, K. Shimizu, *BMC Cancer* **2006**, *6*, 260.

[205] P. Oettgen, Y. Akbarali, J. Boltax, J. Best, C. Kunsch, T. A. Libermann, *Mol. Cell. Biol.* **1996**, *16*, 5091–5106.

[206] H. Kawata, K. Yamada, Z. Shou, T. Mizutani, T. Yazawa, M. Yoshino, T. Sekiguchi, T. Kajitani, K. Miyamoto, *Biochem. J.* **2003**, *373*, 747–757.

[207] L. Korutla, P. Wang, T. G. Jackson, S. A. Mackler, *Neurochem. Int.* **2009**, *54*, 245–252.

[208] G.-M. Li, *Cell Res.* **2008**, *18*, 85–98.

[209] A. Plotnikov, E. Zehorai, S. Procaccia, R. Seger, *Biochim. Biophys. Acta Mol. Cell Res.* **2011**, *1813*, 1619–1633.

[210] J. Wysocka, M. P. Myers, C. D. Laherty, R. N. Eisenman, W. Herr, *Genes Dev.* **2003**, *17*, 896–911.

[211] S.-M. Kim, J.-Y. Kim, N.-W. Choe, I.-H. Cho, J.-R. Kim, D.-W. Kim, J.-E. Seol, S. E. Lee, H. Kook, K.-I. Nam, H. Kook, Y.-Y. Bhak, S.-B. Seo, *Nucleic Acids Res.* **2010**, *38*, 6389–6403.

[212] Y. Zhao, M. C. Majid, J. M. Soll, J. R. Brickner, S. Dango, N. Mosammaparast, *EMBO J.* **2015**, *34*, 1687–1703.

[213] J. Yuan, K. Luo, L. Zhang, J. C. Cheville, Z. Lou, *Cell* **2010**, *140*, 384–396.

[214] B. J. Fenner, M. Scannell, J. H. Prehn, *Biochim. Biophys. Acta Proteins Proteom.* **2009**, *1794*, 1010–1016.

[215] Y.-B. Wang, B. Tan, R. Mu, Y. Chang, M. Wu, H.-Q. Tu, Y.-C. Zhang, S.-S. Guo, X.-H. Qin, T. Li, W.-H. Li, A.-L. Li, X.-M. Zhang, H.-Y. Li, *J. Biol. Chem.* **2015**, *290*, 10395–10405.

[216] S. Spaich, R. D. Will, S. Just, S. Spaich, C. Kuhn, D. Frank, I. M. Berger, S. Wiemann, B. Korn, M. Koegl, J. Backs, H. A. Katus, W. Rottbauer, N. Frey, *Circ. Res.* **2012**, *111*, 1504–1516.

[217] M. U. Gack, Y. C. Shin, C.-H. Joo, T. Urano, C. Liang, L. Sun, O. Takeuchi, S. Akira, Z. Chen, S. Inoue, J. U. Jung, *Nature* **2007**, *446*, 916–920.

[218] R. Cao, Y. ichi Tsukada, Y. Zhang, *Mol. Cell* **2005**, *20*, 845–854.

[219] J. Tang, P. N. Kao, H. R. Herschman, *J. Biol. Chem.* **2000**, *275*, 19866–19876.

[220] N. Mitin, K. L. Rossman, C. J. Der, *Curr. Biol.* **2005**, *15*, R563–R574.

[221] C. J. Millard, P. J. Watson, I. Celardo, Y. Gordiyenko, S. M. Cowley, C. V. Robinson, L. Fairall, J. W. Schwabe, *Mol. Cell* **2013**, *51*, 57–67.

[222] N. Portolano, P. J. Watson, L. Fairall, C. J. Millard, C. P. Milano, Y. Song, S. M. Cowley, J. W. Schwabe, *J. Vis. Exp.* **2014**, *92*, e51897.

[223] P. Gomez-Martinez, M. Dessolin, F. Guibé, F. Albericio, *J. Chem. Soc., Perkin Trans. 1* **1999**, 2871–2874.

[224] P. J. Watson, C. J. Millard, A. M. Riley, N. S. Robertson, L. C. Wright, H. Y. Godage, S. M. Cowley, A. G. Jamieson, B. V. L. Potter, J. W. R. Schwabe, *Nat. Commun.* **2016**, *7*, 11262.

[225] A. Dose, J. Sindlinger, Personal communication, Eberhard Karls Universität Tübingen, **2017**.

[226] J. Seidel, Master thesis, Eberhard Karls Universität Tübingen, **2017**.

[227] M. Obkircher, C. Stähelin, F. Dick, *J. Pept. Sci.* **2008**, *14*, 763–766.

[228] S. Kirchgässner, Dissertation, Eberhard Karls Universität Tübingen, **2021**.

[229] F. Hu, C. J. Chou, J. M. Gottesfeld, *Bioorg. Med. Chem. Lett.* **2009**, *19*, 3928–3931.

[230] D. R. Bolin, I.-I. Sytwu, F. Humiec, J. Meienhofer, *Int. J. Peptide Protein Res.* **1989**, *33*, 353–359.

[231] A. Claraz, *Synlett* **2013**, *24*, 657–658.

[232] K. Huber, G. Doyon, J. Plaks, E. Fyne, J. W. Mellors, N. Sluis-Cremer, *J. Biol. Chem.* **2011**, *286*, 22211–22218.

[233] W. Kuriyama, T. Kitahara, *Heterocycles* **2001**, *55*, 1–4.

[234] S. Kim, E.-Y. Kim, H. Ko, Y. H. Jung, *Synthesis* **2003**, 2194–2198.

[235] V. Castro, H. Rodríguez, F. Albericio, *ACS Comb. Sci.* **2016**, *18*, 1–14.

[236] D. W. Christianson, W. N. Lipscomb, *J. Am. Chem. Soc.* **1986**, *108*, 4998–5003.

[237] M. J. Bottomley, P. Lo Surdo, P. Di Giovine, A. Cirillo, R. Scarpelli, F. Ferrigno, P. Jones, P. Neddermann, R. De Francesco, C. Steinkühler, P. Gallinari, A. Carfí, *J. Biol. Chem.* **2008**, *283*, 26694–26704.

[238] C. Moreno-Yruela, C. A. Olsen, *Synthesis* **2018**, *50*, 4037–4046.

[239] H. M. Geysen, R. H. Meloen, S. J. Barteling, **1984**, *81*, 3998–4002.

[240] R. A. Houghten, *Proc. Natl. Acad. Sci. USA* **1985**, *82*, 5131–5135.

[241] Á. Furka, F. Sebestyén, M. Asgedom, G. Dibó, *Int. J. Peptide Protein Res.* **1991**, *37*, 487–493.

[242] F. Sebestyén, G. Dibó, A. Kovács, Á. Furkua, *Bioorg. Med. Chem. Lett.* **1993**, *3*, 413–418.

[243] K. S. Lam, S. E. Salmon, E. M. Hersh, V. J. Hruby, W. M. Kazmierski, R. J. Knapp, *Nature* **1991**, *354*, 82–84.

[244] S. P. Fodor, J. L. Read, M. C. Pirrung, L Stryer, A. T. Lu, D Solas, *Science* **1991**, *251*, 767–773.

[245] A. A. Weiser, M. Or-Guil, V. Tapia, A. Leichsenring, J. Schuchhardt, C. Frömmel, R. Volkmer-Engert, *Anal. Biochem.* **2005**, *342*, 300–311.

[246] R. Zitterbart, N. Berger, O. Reimann, G. T. Noble, S. Lüdtke, D. Sarma, O. Seitz, *Chem. Sci.* **2021**, *12*, 2389–2396.

[247] O. Reimann, O. Seitz, D. Sarma, R. Zitterbart, *J. Pep. Sci.* **2019**, *25*, e3136.

[248] D. E. Krieger, B. W. Erickson, R. B. Merrifield, *Proc. Natl. Acad. Sci. USA* **1976**, *73*, 3160–3164.

[249] A. Inglis, P. Edman, *Anal. Biochem.* **1970**, *37*, 73–80.

[250] G. Kim, S. J. Weiss, R. L. Levine, *Biochim. Biophys. Acta Gen. Subj.* **2014**, *1840*, 901–905.

[251] W. Beck, G. Jung, *Lett. Pept. Sci.* **1994**, *1*, 31–37.

[252] R. Subirós-Funosas, A. El-Faham, F. Albericio, *Tetrahedron* **2011**, *67*, 8595–8606.

[253] A. Karlström, A. Undén, *Tetrahedron Lett.* **1996**, *37*, 4243–4246.

[254] Z. Kutil, L. Skultetyova, D. Rauh, M. Meleshin, I. Snajdr, Z. Novakova, J. Mikesova, J. Pavlicek, M. Hadzima, P. Baranova, B. Havlinova, P. Majer, M. Schutkowski, C. Barinka, *FASEB J.* **2019**, *33*, 4035–4045.

[255] J. Seidel, C Klockenbusch, D. Schwarzer, *ChemBioChem* **2016**, *17*, 398–402.

[256] M. C. F. Thomsen, M. Nielsen, *Nucleic Acids Res.* **2012**, *40*, W281–W287.

[257] H. V. Goodson, E. M. Jonasson, *Cold Spring Harb. Perspect. Biol.* **2018**, *10*, a022608.

[258] K.-J. Oh, H.-S. Han, M.-J. Kim, S.-H. Koo, *BMB Rep.* **2013**, *46*, 567–574.

[259] P. Bali, M. Pranpat, J. Bradner, M. Balasis, W. Fiskus, F. Guo, K. Rocha, S. Kumaraswamy, S. Boyapalle, P. Atadja, E. Seto, K. Bhalla, *J. Biol. Chem.* **2005**, *280*, 26729–26734.

[260] P. Wang, J. Heitman, *Genome Biol.* **2005**, *6*, 226.

[261] A. Iwata, B. E. Riley, J. A. Johnston, R. R. Kopito, *J. Biol. Chem.* **2005**, *280*, 40282–40292.

[262] N. A. Reed, D. Cai, T. L. Blasius, G. T. Jih, E. Meyhofer, J. Gaertig, K. J. Verhey, *Curr. Biol.* **2006**, *16*, 2166–2172.

[263] P. Matthias, M. Yoshida, S. Khochbin, *Cell Cycle* **2008**, *7*, 7–10.

[264] O. Destaing, F. Saltel, B. Gilquin, A. Chabadel, S. Khochbin, S. Ory, P. Jurdic, *J. Cell Sci.* **2005**, *118*, 2901–2911.

[265] J. J. Westendorf, S. K. Zaidi, J. E. Cascino, R. Kahler, A. J. van Wijnen, J. B. Lian, M. Yoshida, G. S. Stein, X. Li, *Mol. Cell. Biol.* **2002**, *22*, 7982–7992.

[266] D. Girdwood, D. Bumpass, O. A. Vaughan, A. Thain, L. A. Anderson, A. W. Snowden, E. Garcia-Wilson, N. D. Perkins, R. T. Hay, *Mol. Cell* **2003**, *11*, 1043–1054.

[267] W. Zhang, B. C. Kone, *Am. J. Physiol. Renal. Physiol.* **2002**, *283*, F904–F911.

[268] J. Xie, P. G. Schultz, *Curr. Opin. Chem. Biol.* **2005**, *9*, 548–554.

[269] A. Kühn, Master thesis, Eberhard Karls Universität Tübingen, **2020**.

[270] S. Kirchgässner, Personal communication, Eberhard Karls Universität Tübingen, **2020**.

[271] D. F. Shriver, M. A. Drezdzon, *The Manipulation of Air-Sensitive Compounds*, 2nd ed., John Wiley & Sons, New York, **1986**.

[272] M. Strohalm, D. Kavan, P. Novák, M. Volný, V. Havlíček, *Anal. Chem.* **2010**, *82*, 4648–4651.

[273] J. D. Dignam, P. L. Martin, B. S. Shastry, R. G. Roeder, *Methods Enzymol.* **1983**, *101*, 582–598.

[274] J. Rappsilber, M. Mann, Y. Ishihama, *Nat. Protoc.* **2007**, *2*, 1896–1906.

[275] J. Cox, M. Mann, *Nat. Biotechnol.* **2008**, *26*, 1367–1372.

[276] M. E. Ritchie, B. Phipson, D. Wu, Y. Hu, C. W. Law, W. Shi, G. K. Smyth, *Nucleic Acids Res.* **2015**, *43*, e47.

7 Appendix: NMR spectra and LC-MS data

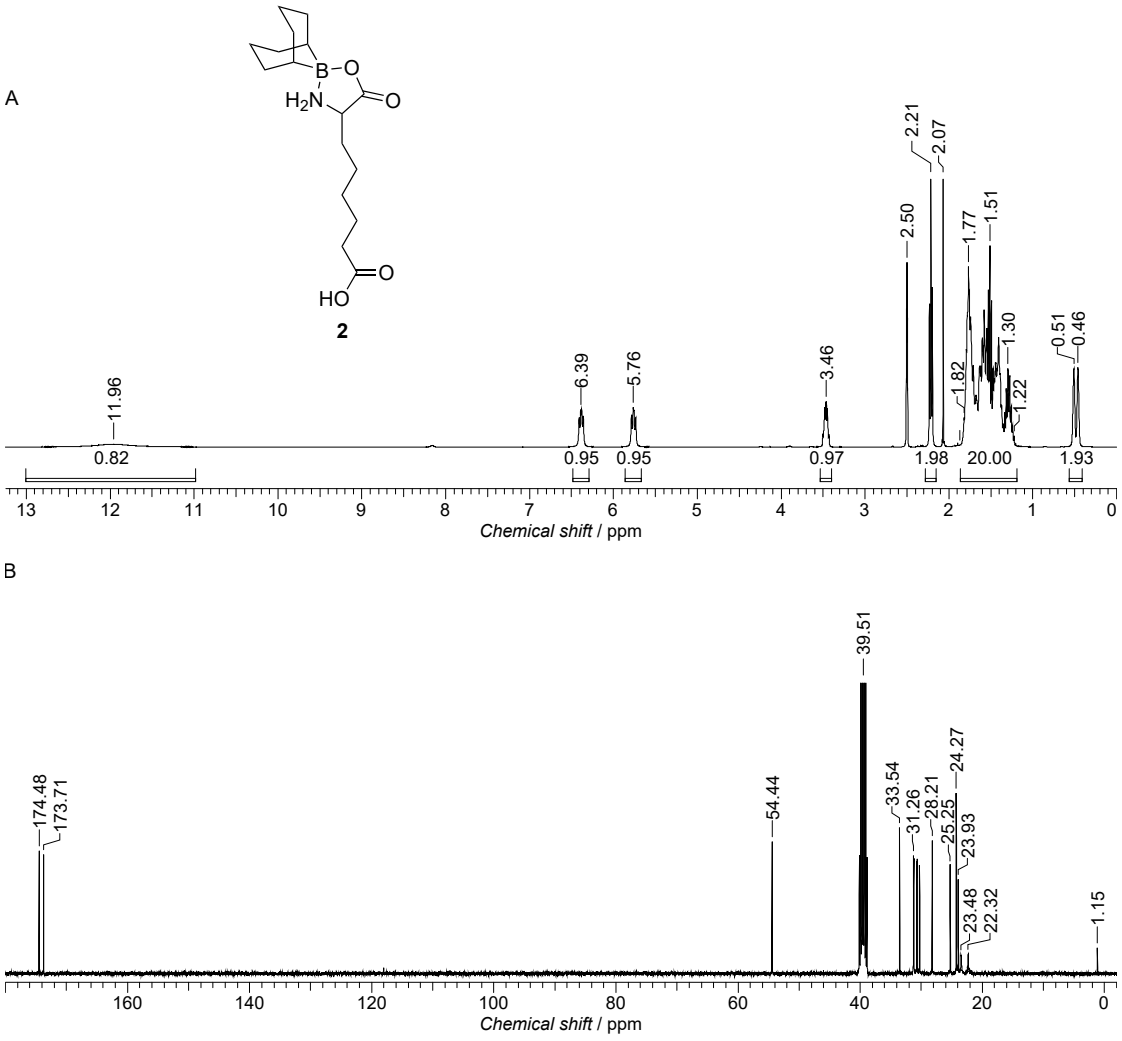

Figure 49: (A) ^{1}H-NMR spectrum (400 MHz, DMSO-d_6) and (B) ^{13}C-NMR spectrum (101 MHz, DMSO-d_6) of Asu-BBN (**2**).

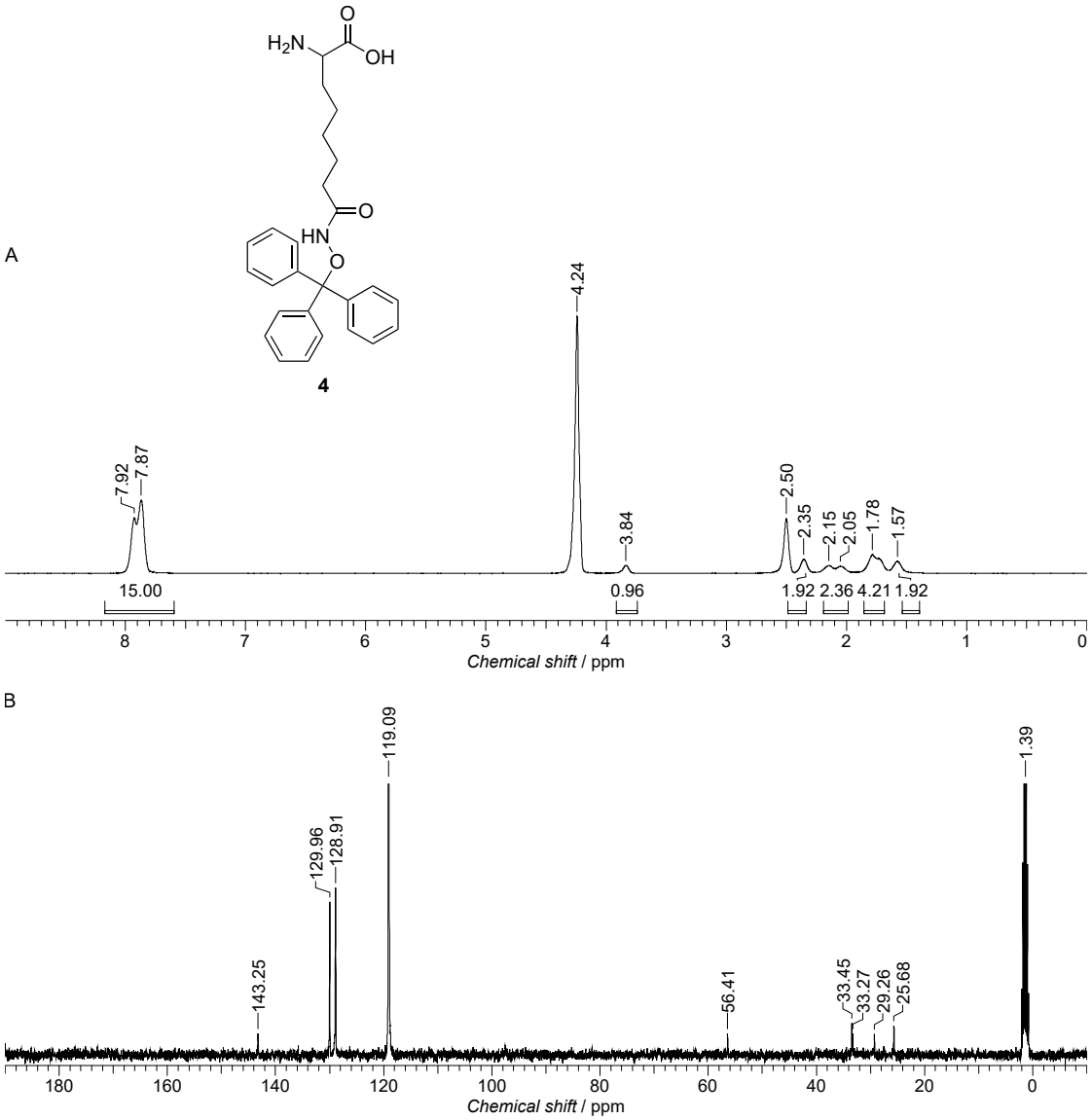

Figure 50: (A) ^{1}H-NMR spectrum (400 MHz, MeCN-d_3 / D_2O (1:1)) and (B) ^{13}C-NMR spectrum (101 MHz, MeCN-d_3 / D_2O (1:1)) of H-AsuHd(OTrt)-OH (**4**).

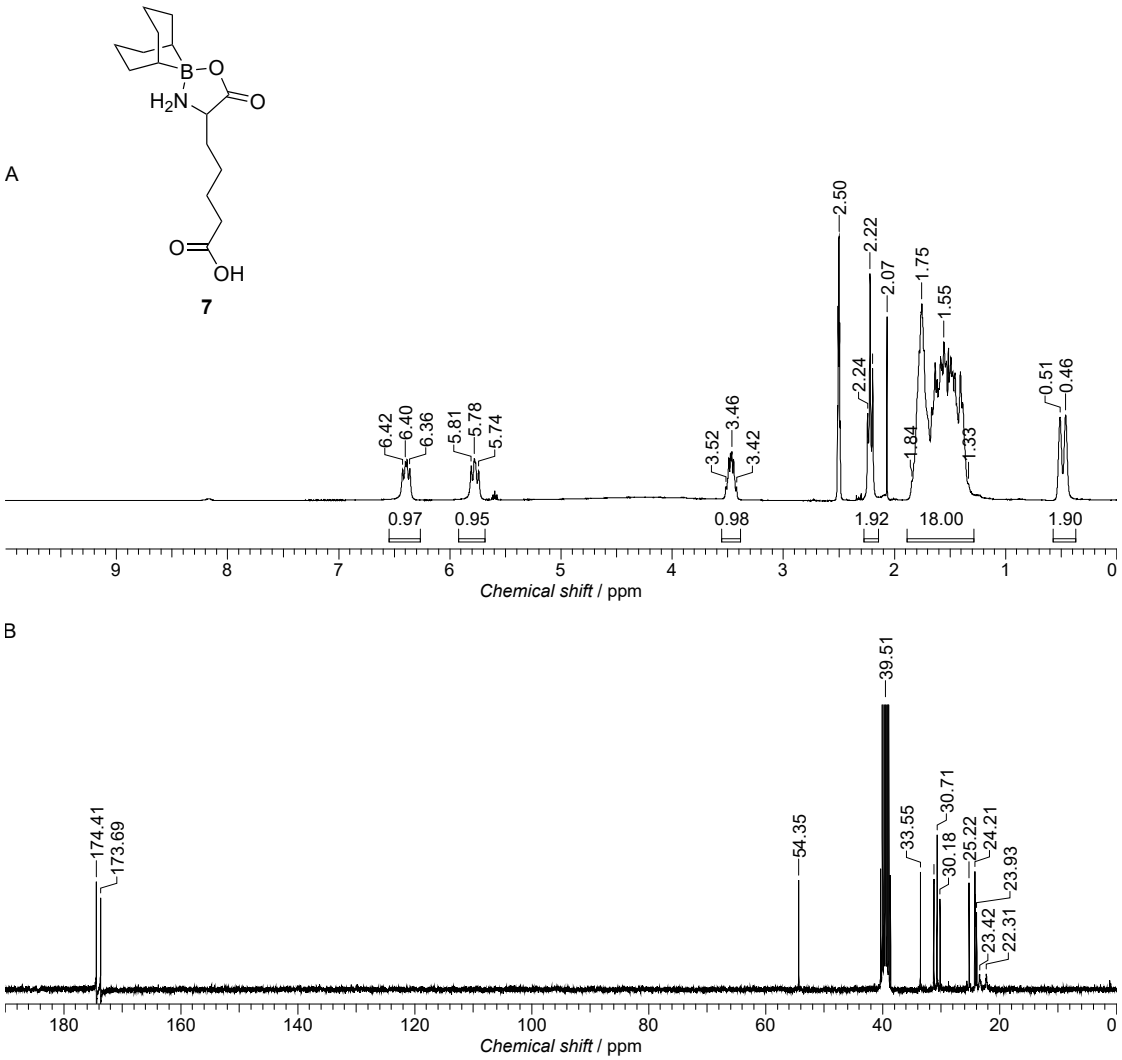

Figure 51: (A) ^{1}H-NMR spectrum (400 MHz, DMSO-d_6) and (B) ^{13}C-NMR spectrum (101 MHz, DMSO-d_6) of Apm-BBN (**7**).

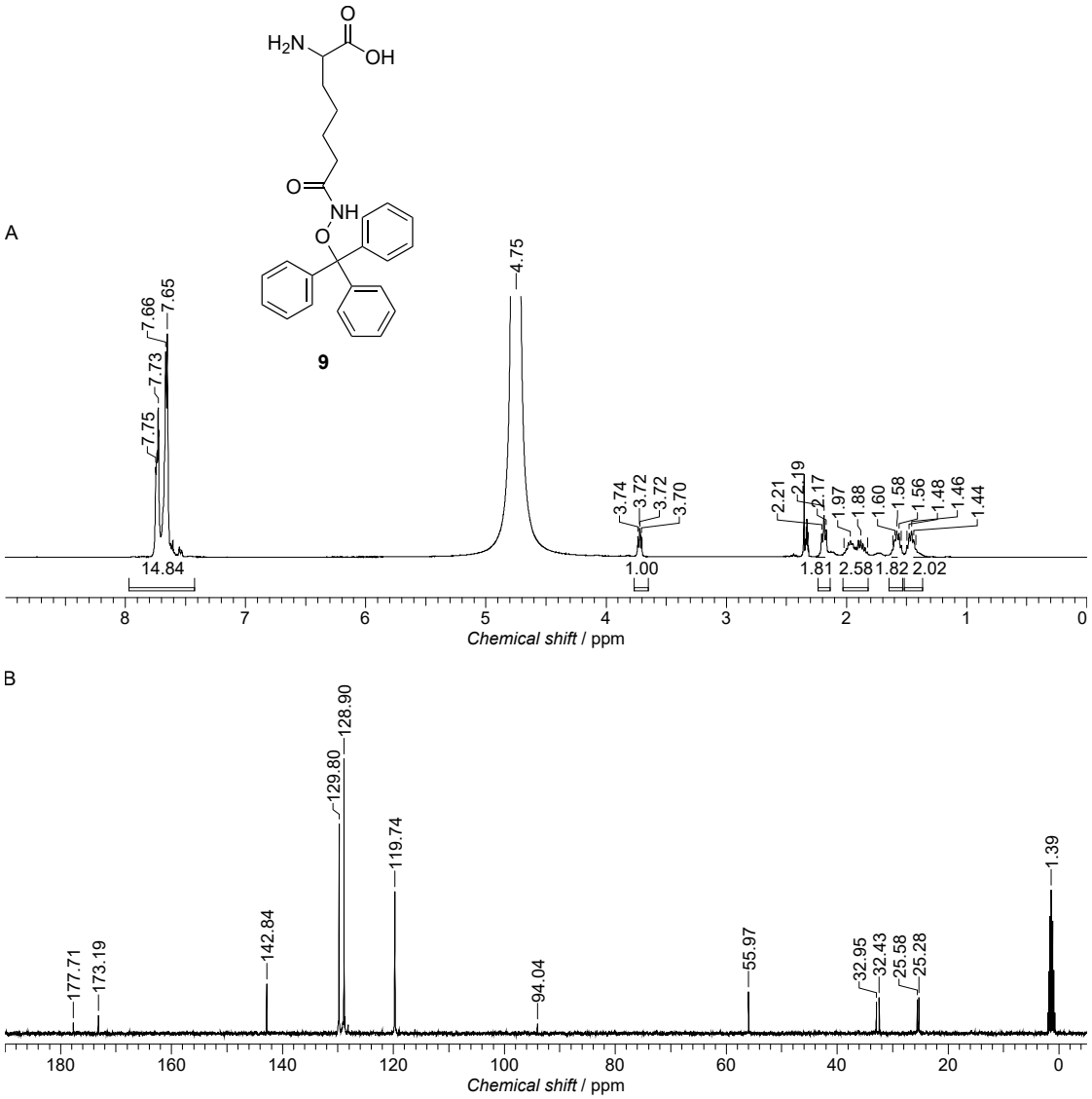

Figure 52: (A) ^{1}H-NMR spectrum (400 MHz, MeCN-d_3 / D_2O (3:1)) and (B) ^{13}C-NMR spectrum (101 MHz, MeCN-d_3 / D_2O (3:1)) of H-ApmHd(OTrt)-OH (**9**).

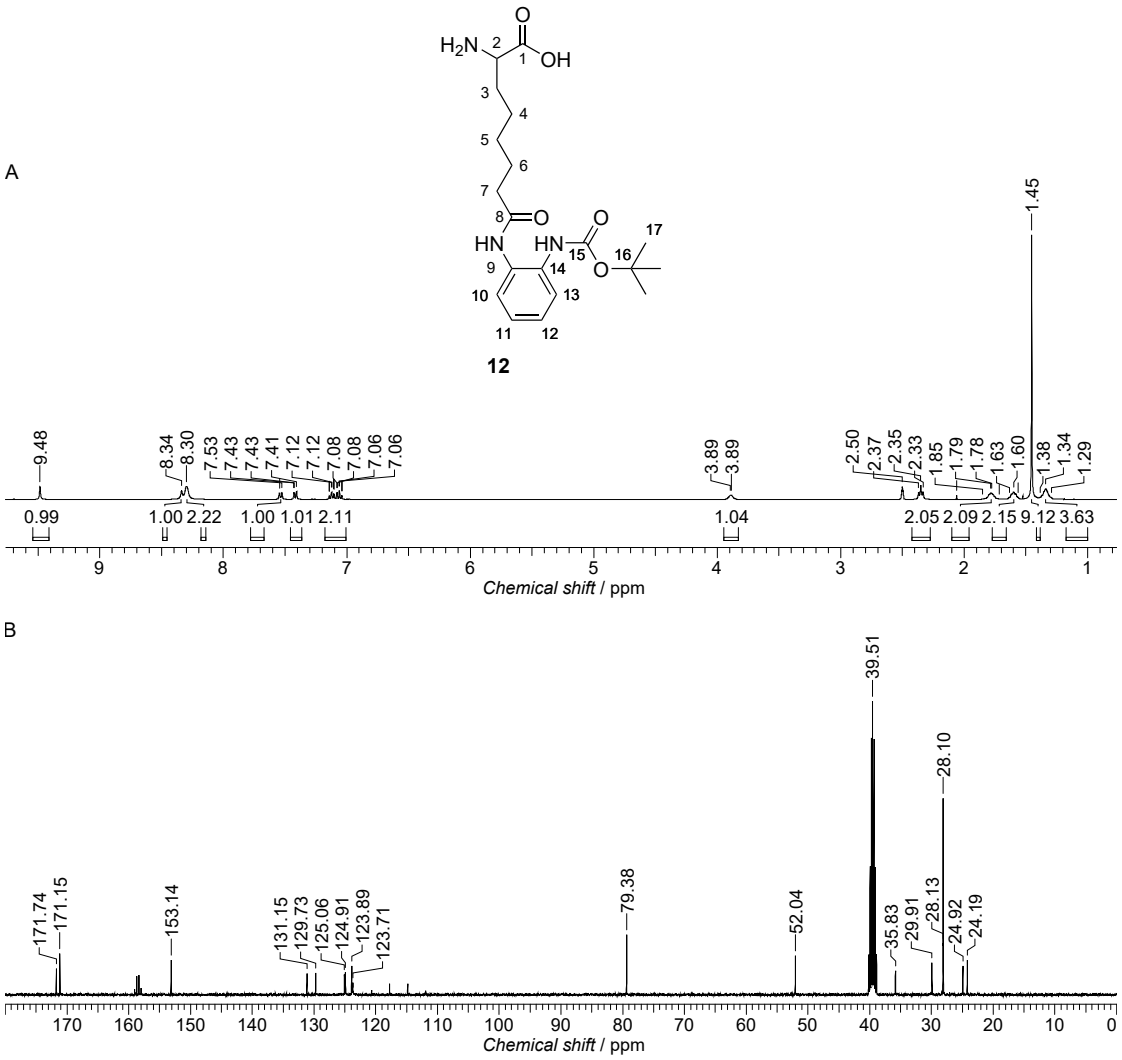

Figure 53: (A) ^{1}H-NMR spectrum (400 MHz, DMSO-d_6) and (B) ^{13}C-NMR spectrum (101 MHz, DMSO-d_6) of H-AsuApa(Boc)-OH (**12**).

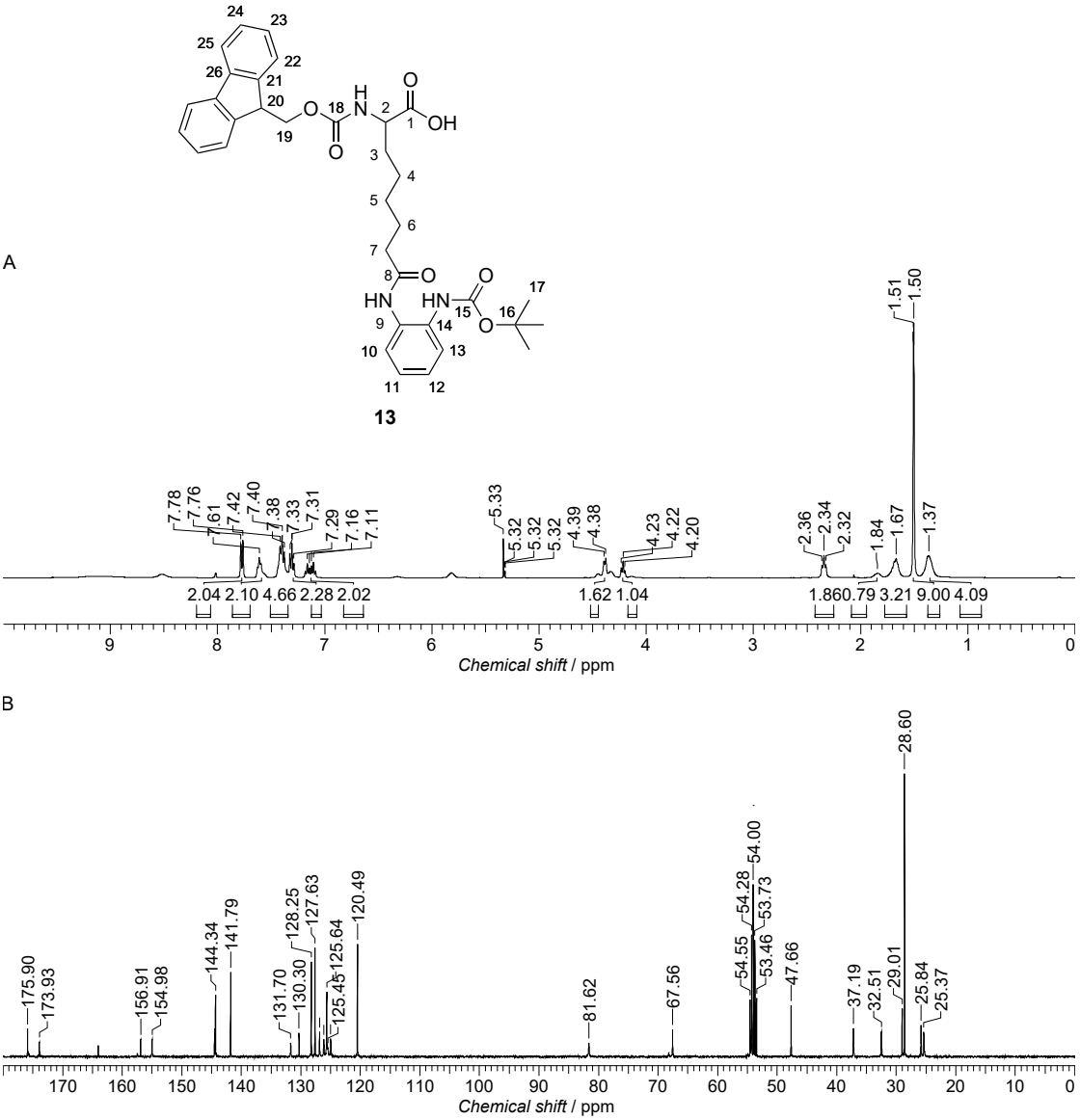

Figure 54: (A) ^{1}H-NMR spectrum (400 MHz, CD_2Cl_2) and (B) ^{13}C-NMR spectrum (101 MHz, CD_2Cl_2) of Fmoc-AsuApa(Boc)-OH (**13**).

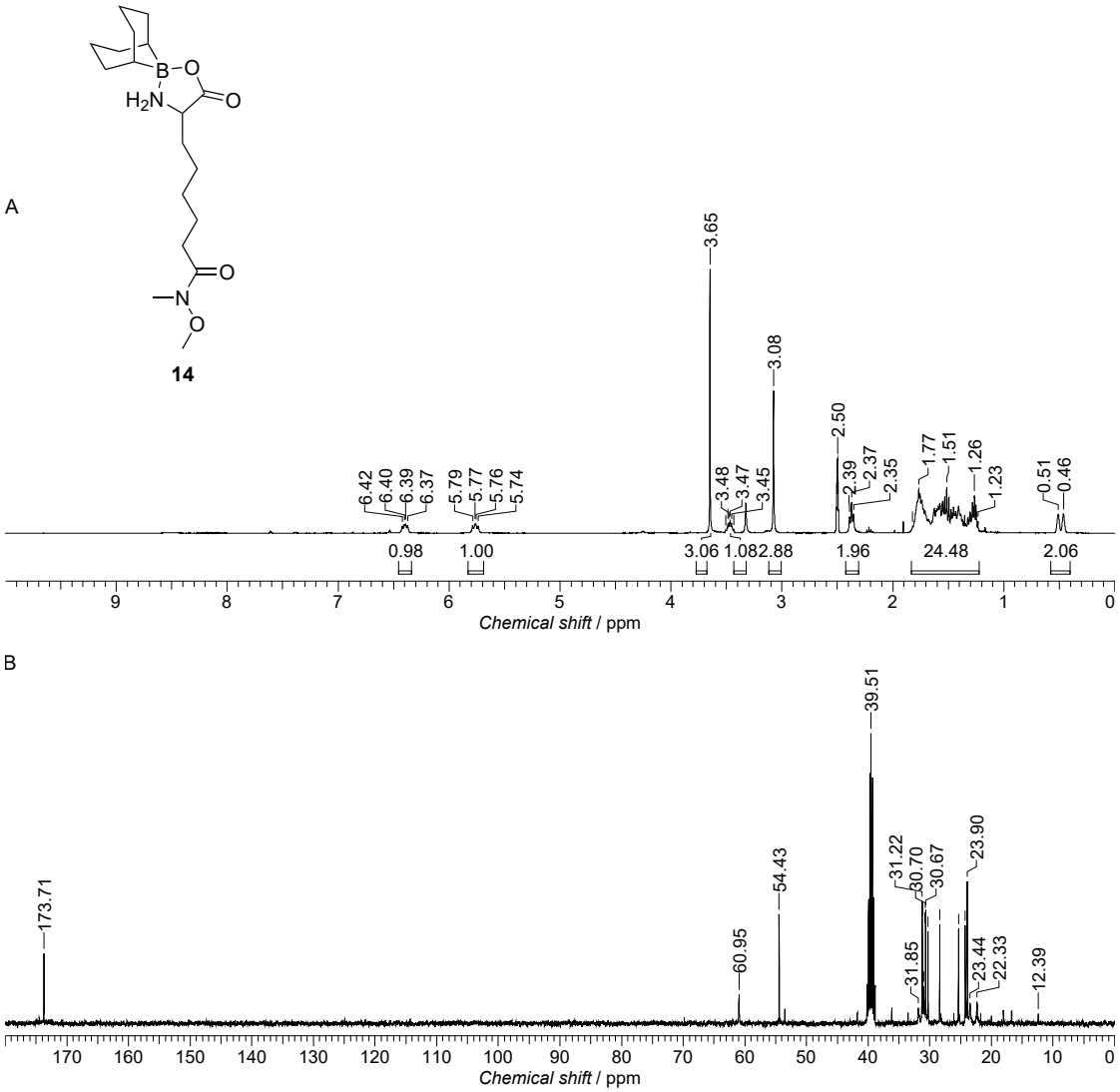

Figure 55: (A) ^{1}H-NMR spectrum (400 MHz, DMSO-d_6) and (B) ^{13}C-NMR spectrum (101 MHz, DMSO-d_6) of Asu(NMe-OMe)-BBN (**14**).

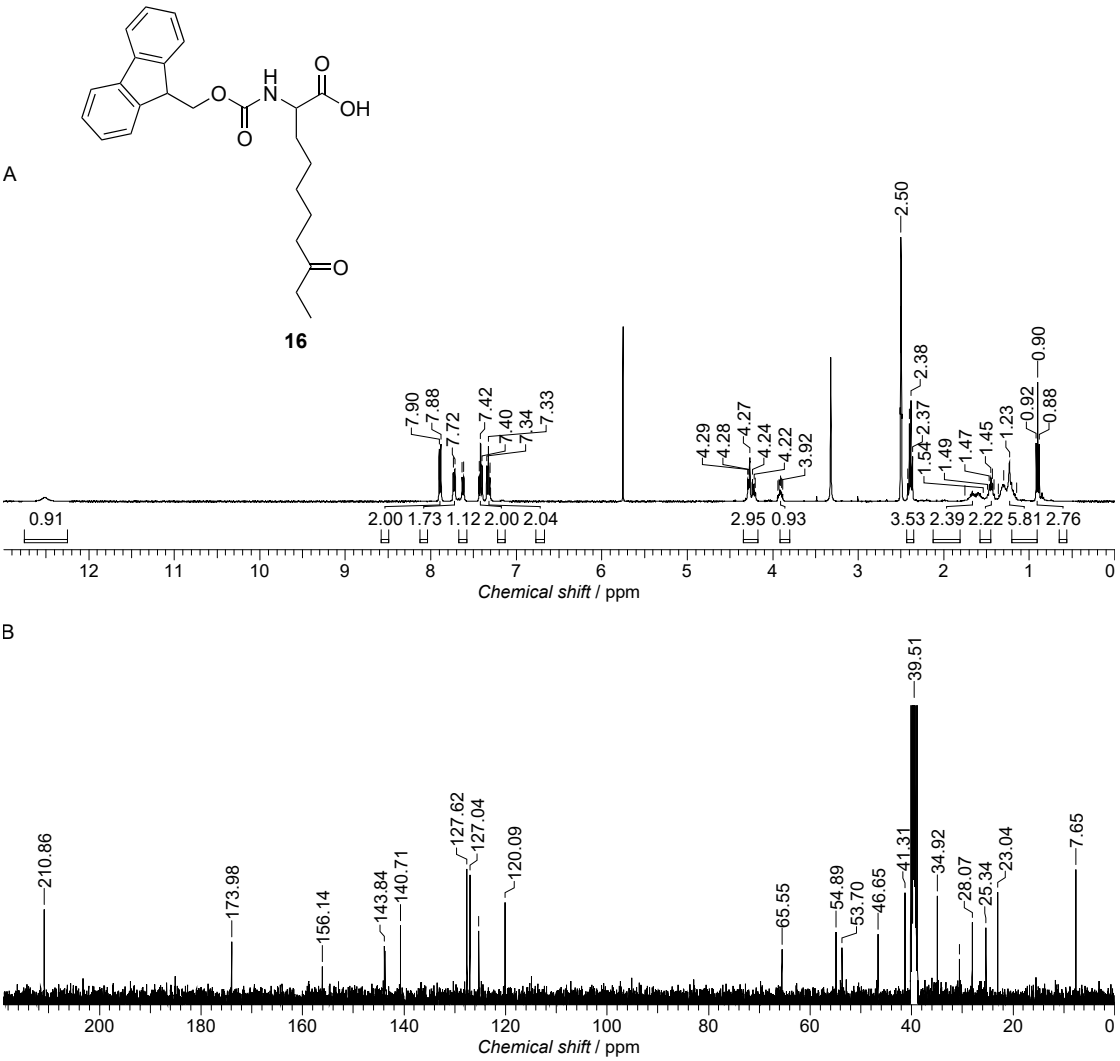

Figure 56: (A) ^{1}H-NMR spectrum (400 MHz, DMSO-d_6) and (B) ^{13}C-NMR spectrum (101 MHz, DMSO-d_6) of Fmoc-Aoda-OH (**16**).

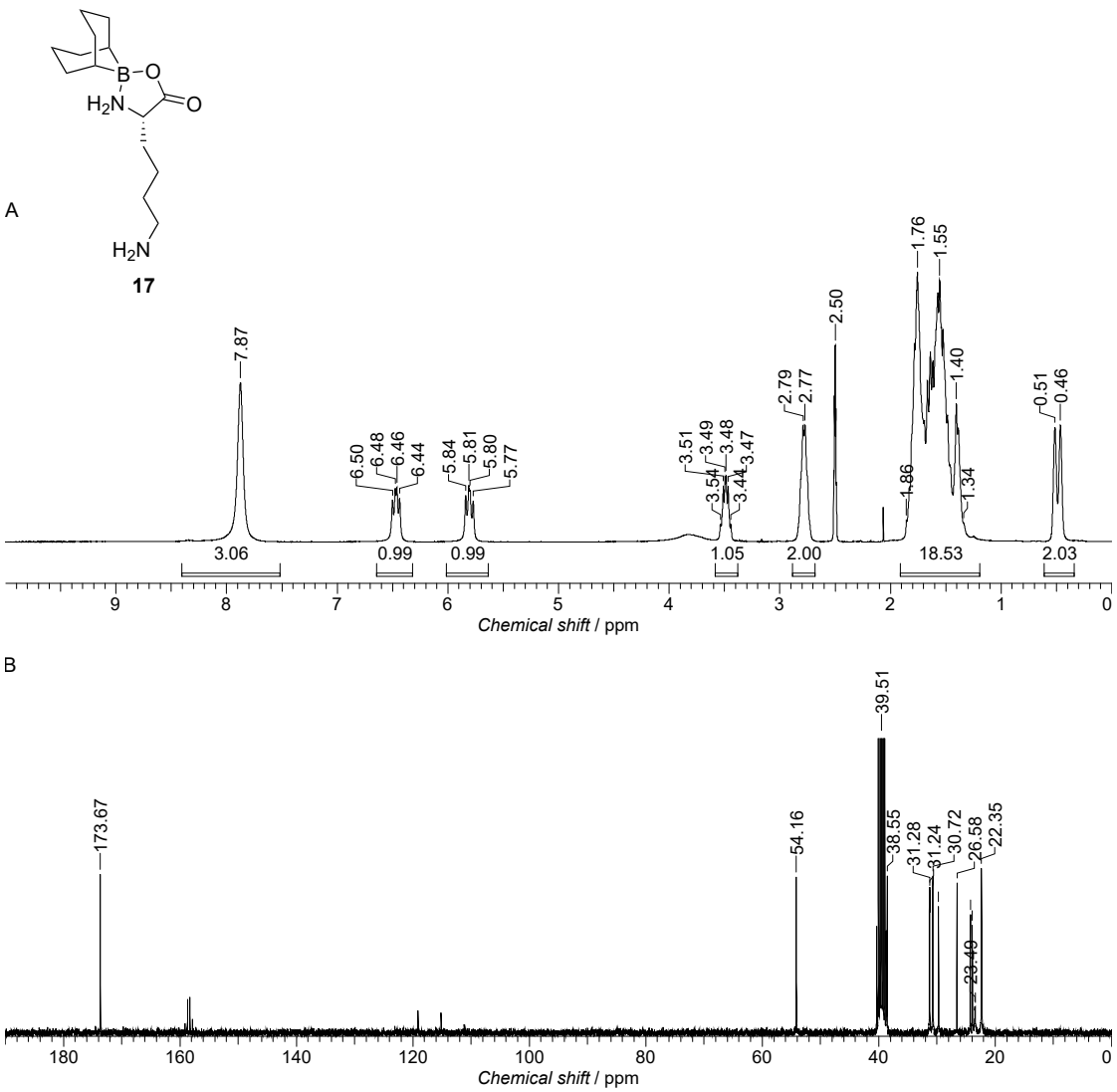

Figure 57: (A) ^{1}H-NMR spectrum (300 MHz, DMSO-d_6) and (B) ^{13}C-NMR spectrum (75 MHz, DMSO-d_6) of Lys-BBN (**17**).

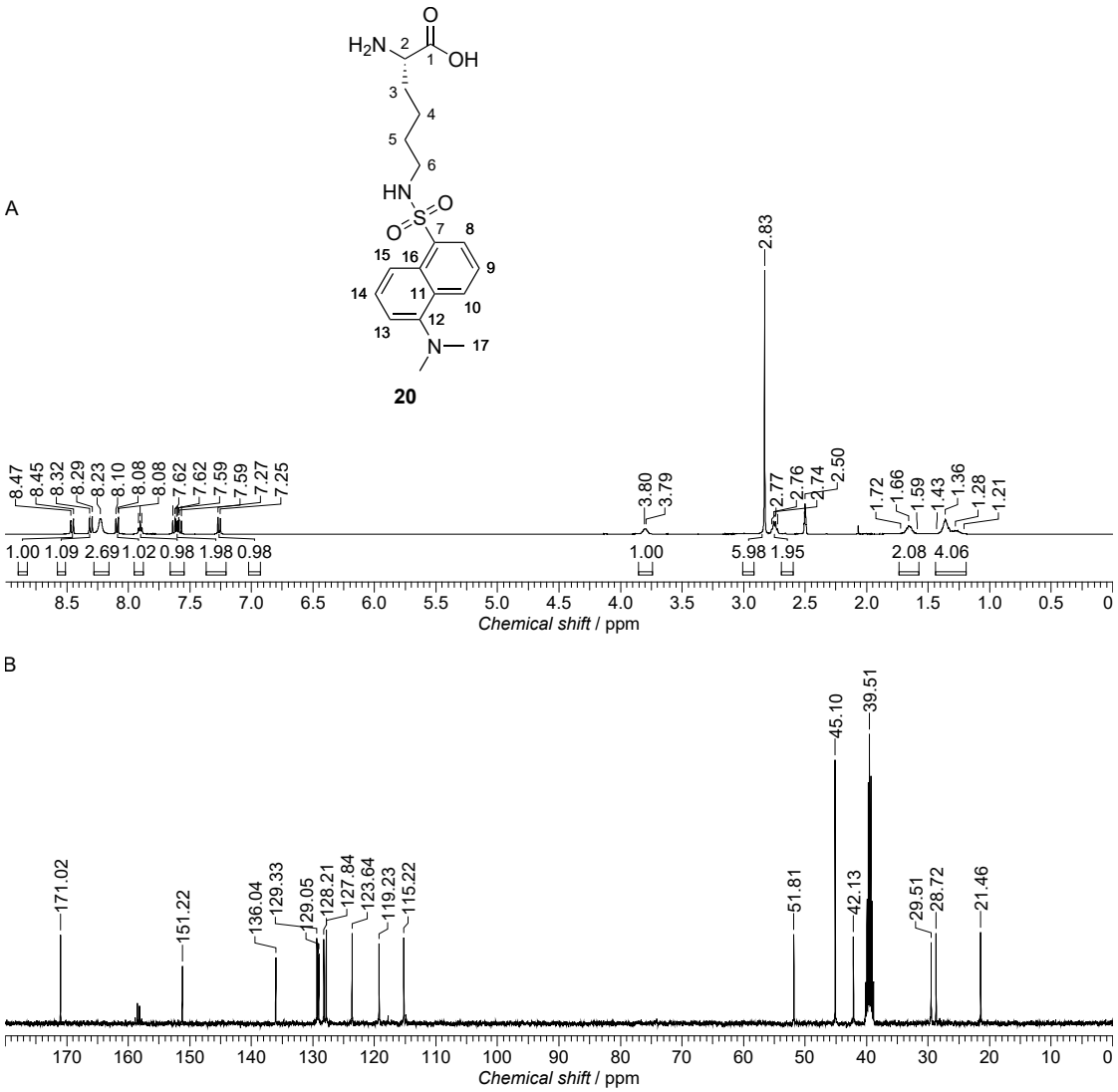

Figure 58: (A) ^{1}H-NMR spectrum (400 MHz, DMSO-d_6) and (B) ^{13}C-NMR spectrum (101 MHz, DMSO-d_6) of H-Lys(Dns)-OH (**20**).

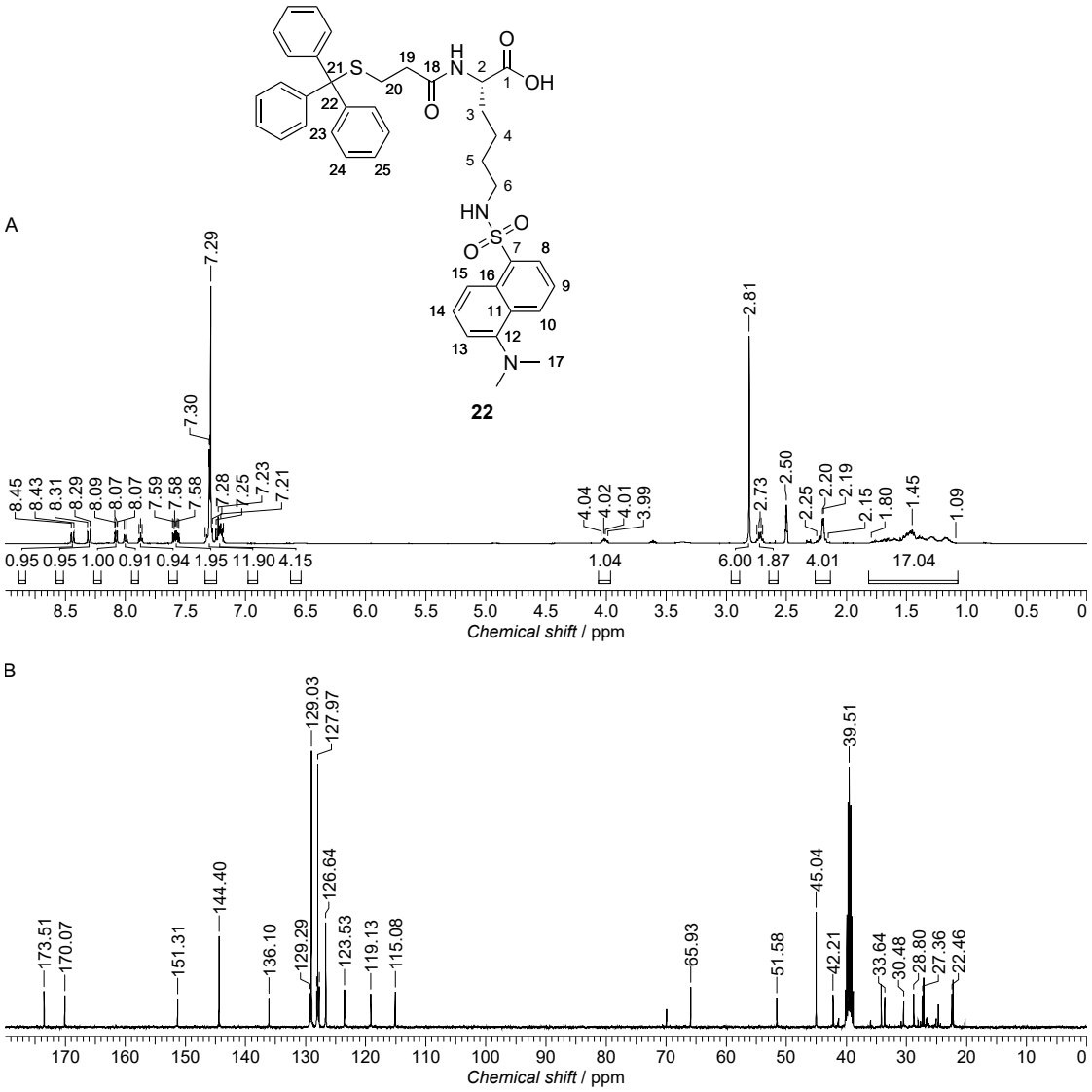

Figure 59: (A) ^{1}H-NMR spectrum (400 MHz, DMSO-d_6) and (B) ^{13}C-NMR spectrum (101 MHz, DMSO-d_6) of Trt-Mpa-Lys(Dns)-OH (**22**).

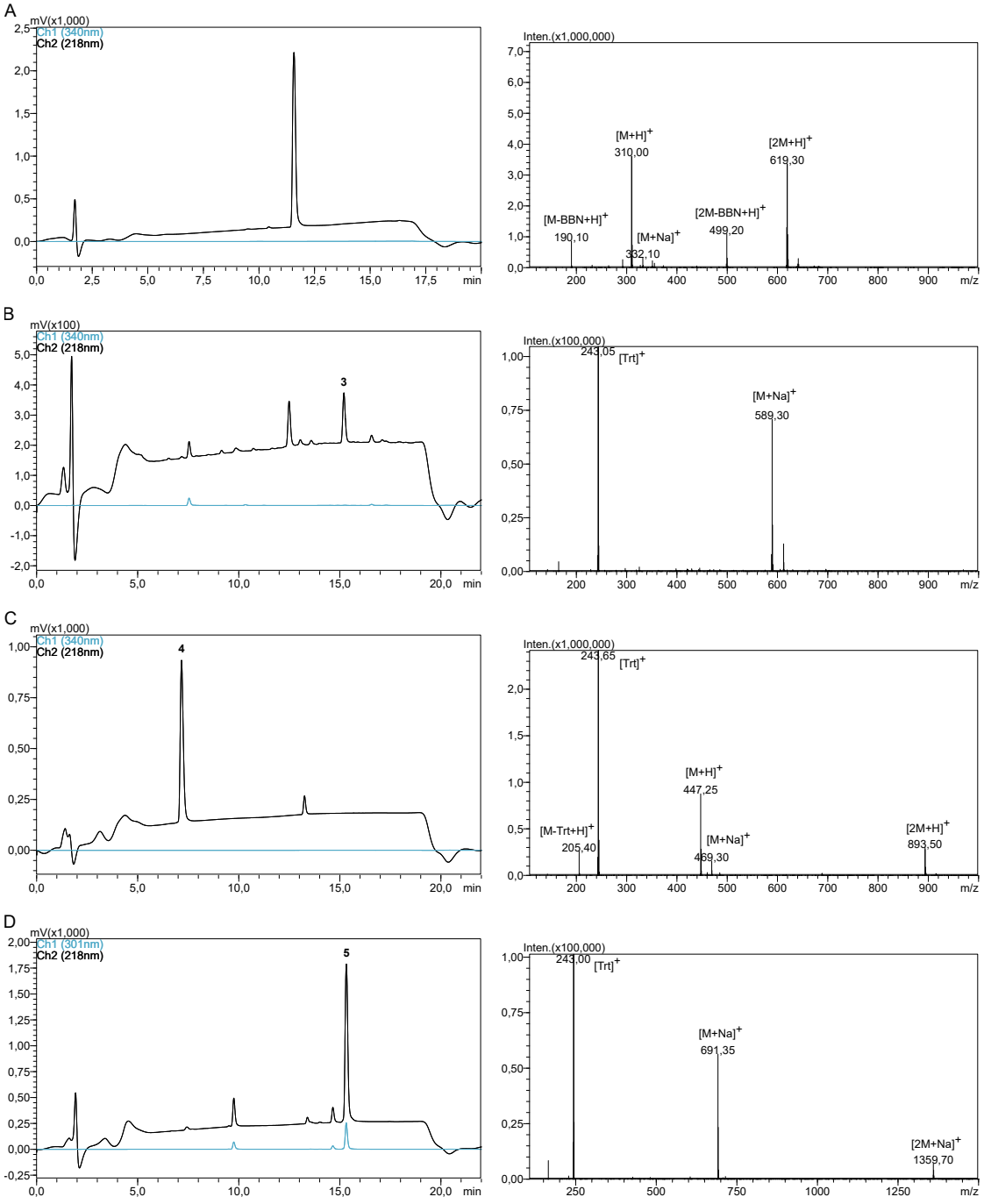

Figure 60: LC-MS analysis of (A) Asu-BBN (**2**), (B) AsuHd(OTrt)-BBN (**3**), (C) H-AsuHd(OTrt)-OH (**4**) and (D) Fmoc-AsuHd(OTrt)-OH (**5**).

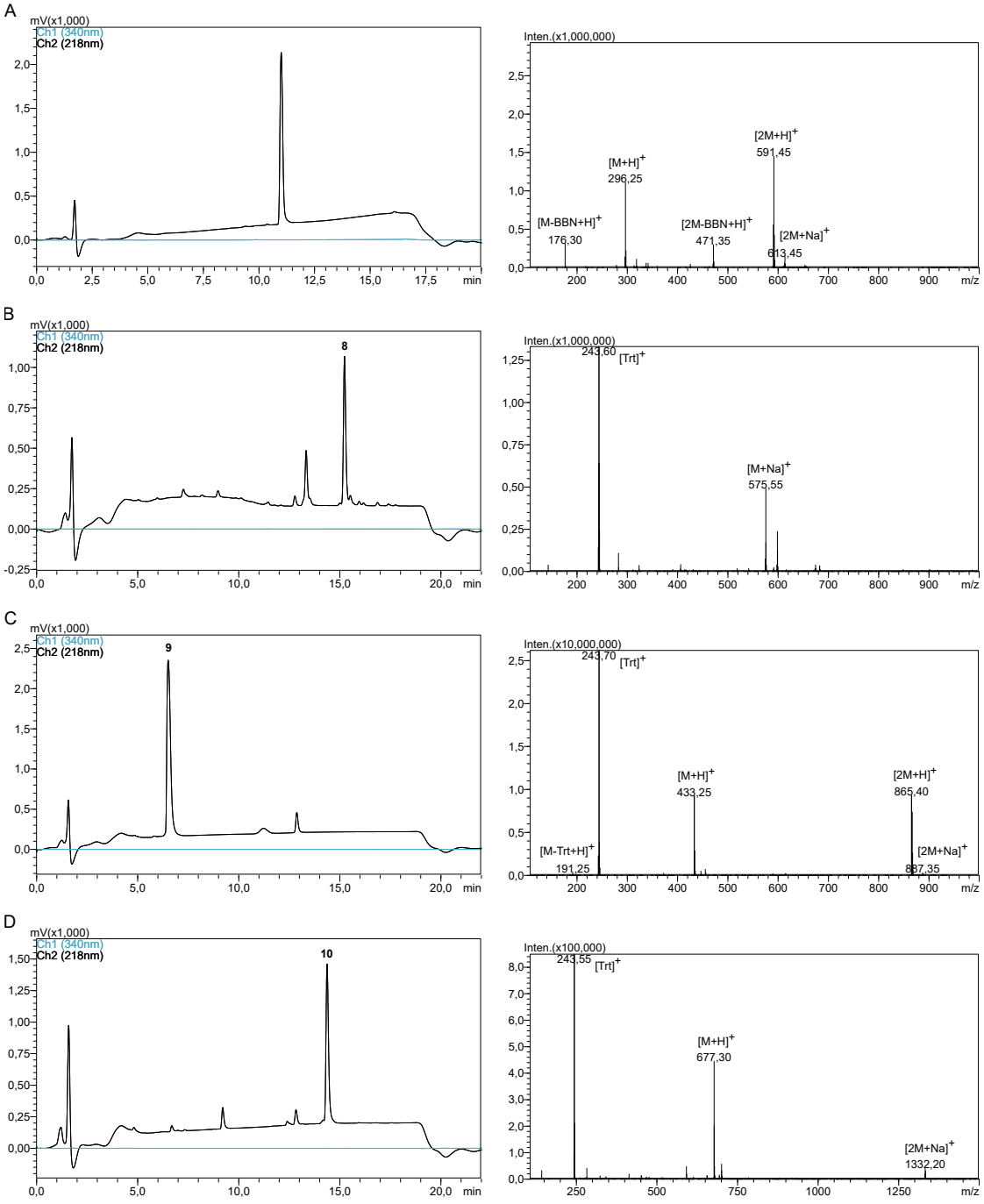

Figure 61: LC-MS analysis of (A) Apm-BBN (**7**), (B) ApmHd(OTrt)-BBN (**8**), (C) H-ApmHd(OTrt)-OH (**9**) and (D) Fmoc-ApmHd(OTrt)-OH (**10**).

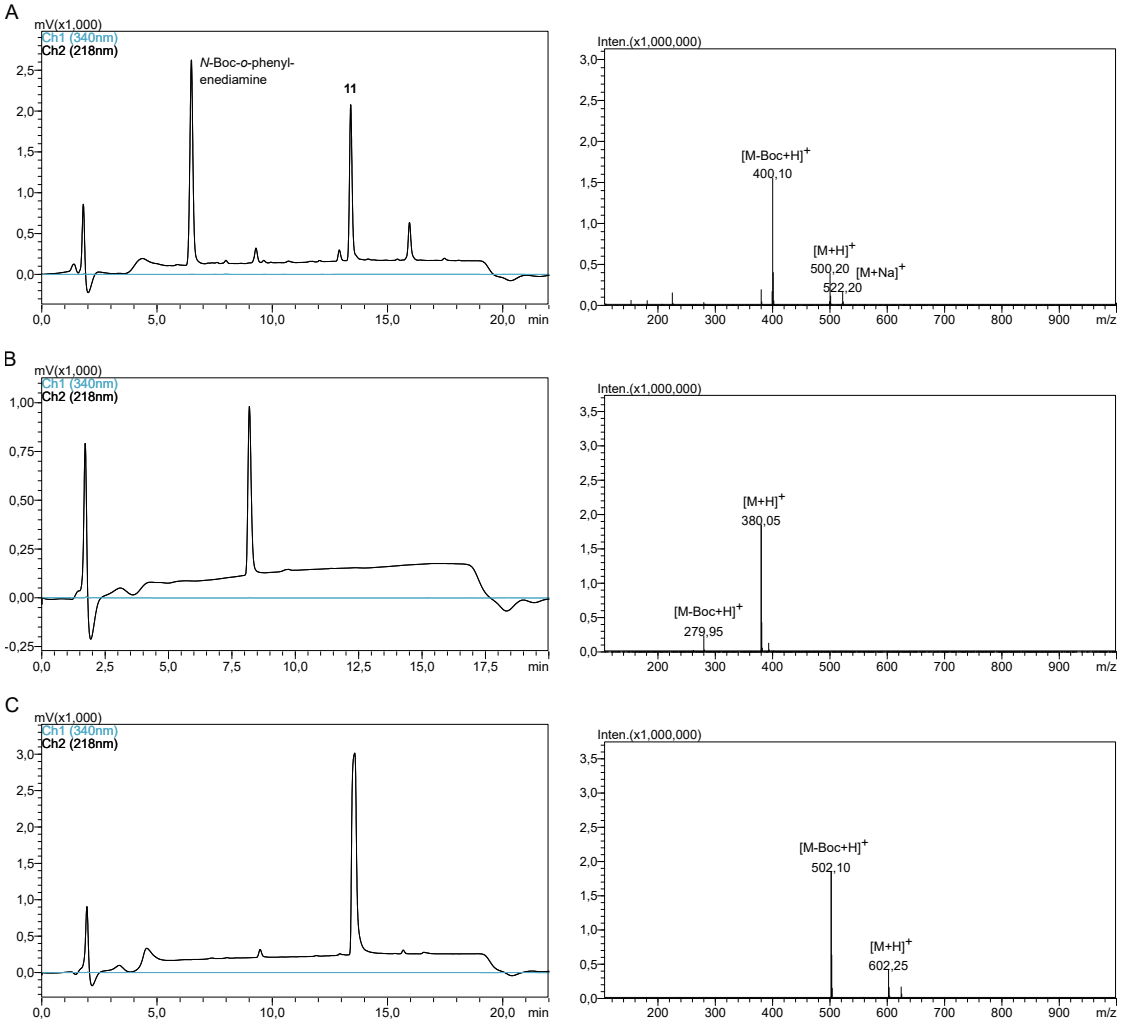

Figure 62: LC-MS analysis of (A) AsuApa(Boc)-BBN (**11**), (B) H-AsuApa(Boc)-OH (**12**) and (C) Fmoc-AsuApa(Boc)-OH (**13**).

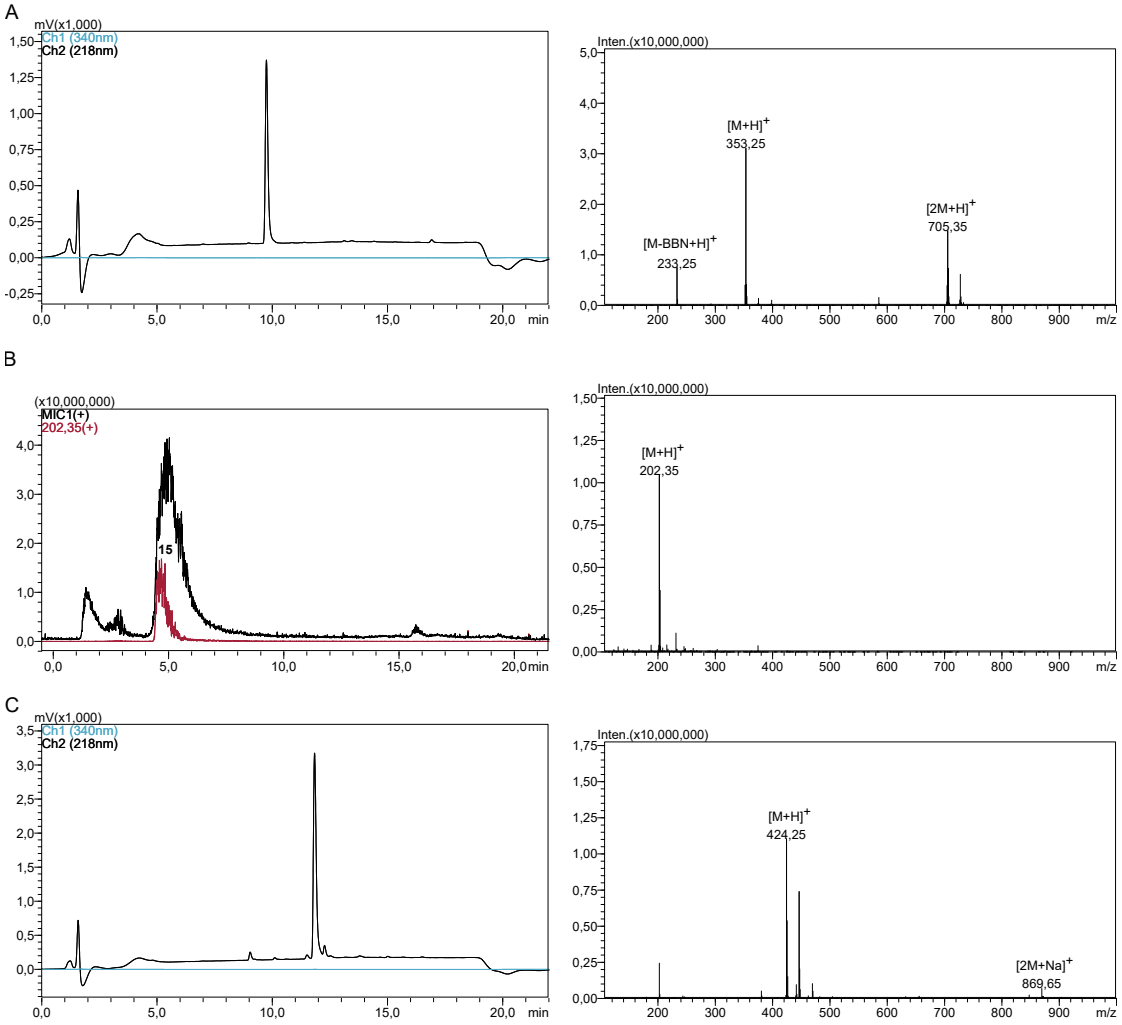

Figure 63: LC-MS analysis of (A) Asu(NMe-OMe)-BBN (**14**), (B) H-Aoda-OH (**15**) and (C) Fmoc-Aoda-OH (**16**). MIC: Multi ion count (m / z = 200–2000).

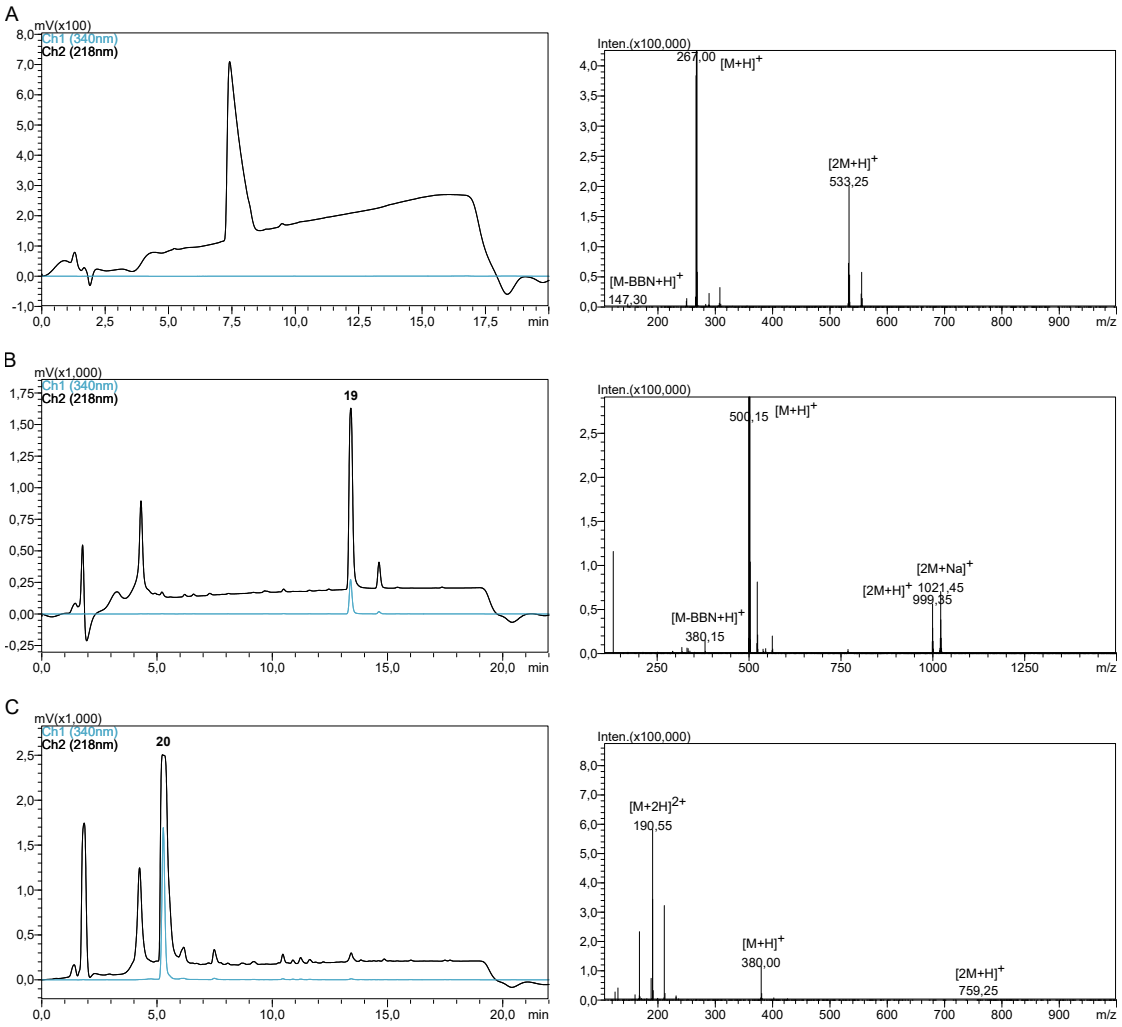

Figure 64: LC-MS analysis of (A) Lys-BBN (**18**), (B) Lys(Dns)-BBN (**19**) and (C) H-Lys(Dns)-OH (**20**).

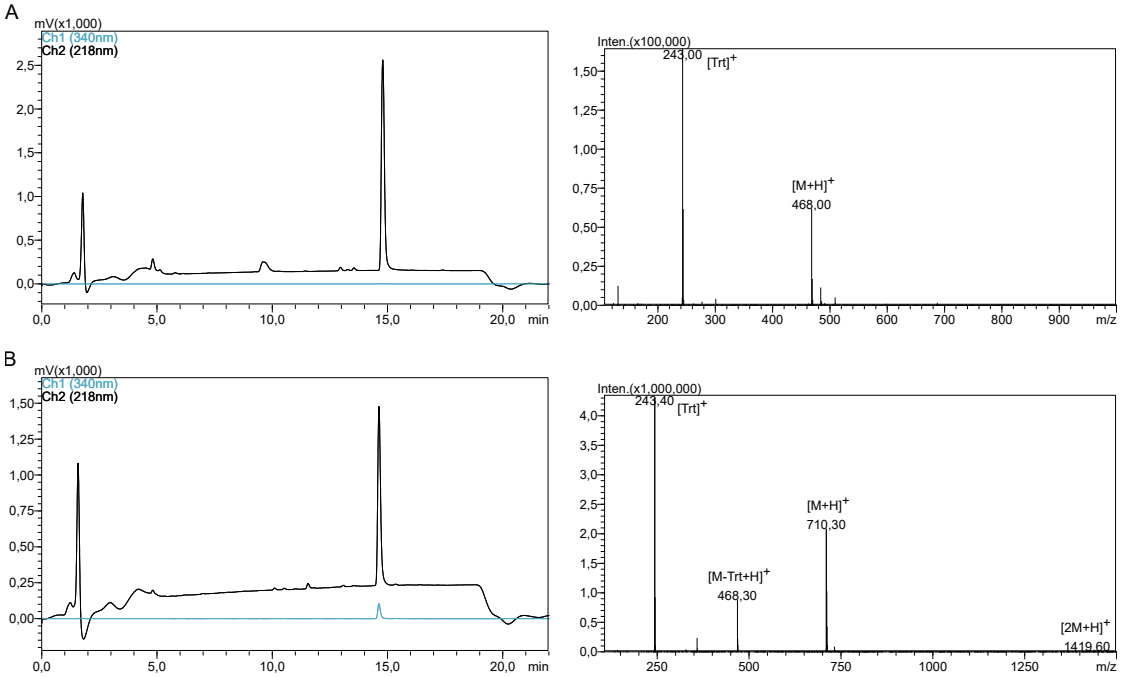

Figure 65: LC-MS analysis of (A) Trt-Mpa-OSu (**21**) and (B) Trt-Mpa-Lys(Dns)-OH (**22**).

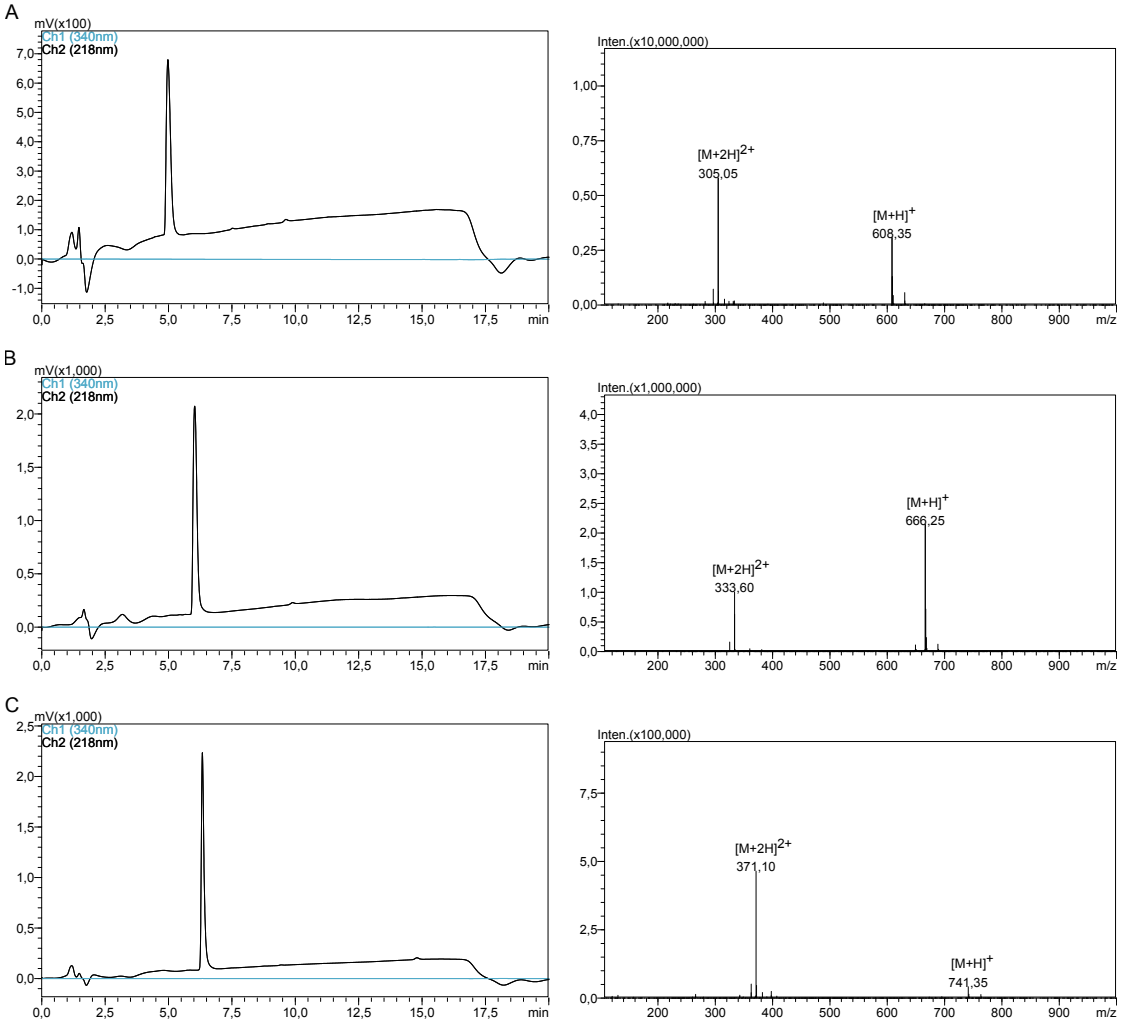

Figure 66: LC-MS analysis of mini-probes (A) mini-Lys (**P1**), (B) mini-AsuHd (**P2**) and (C) mini-AsuApa (**P3**).

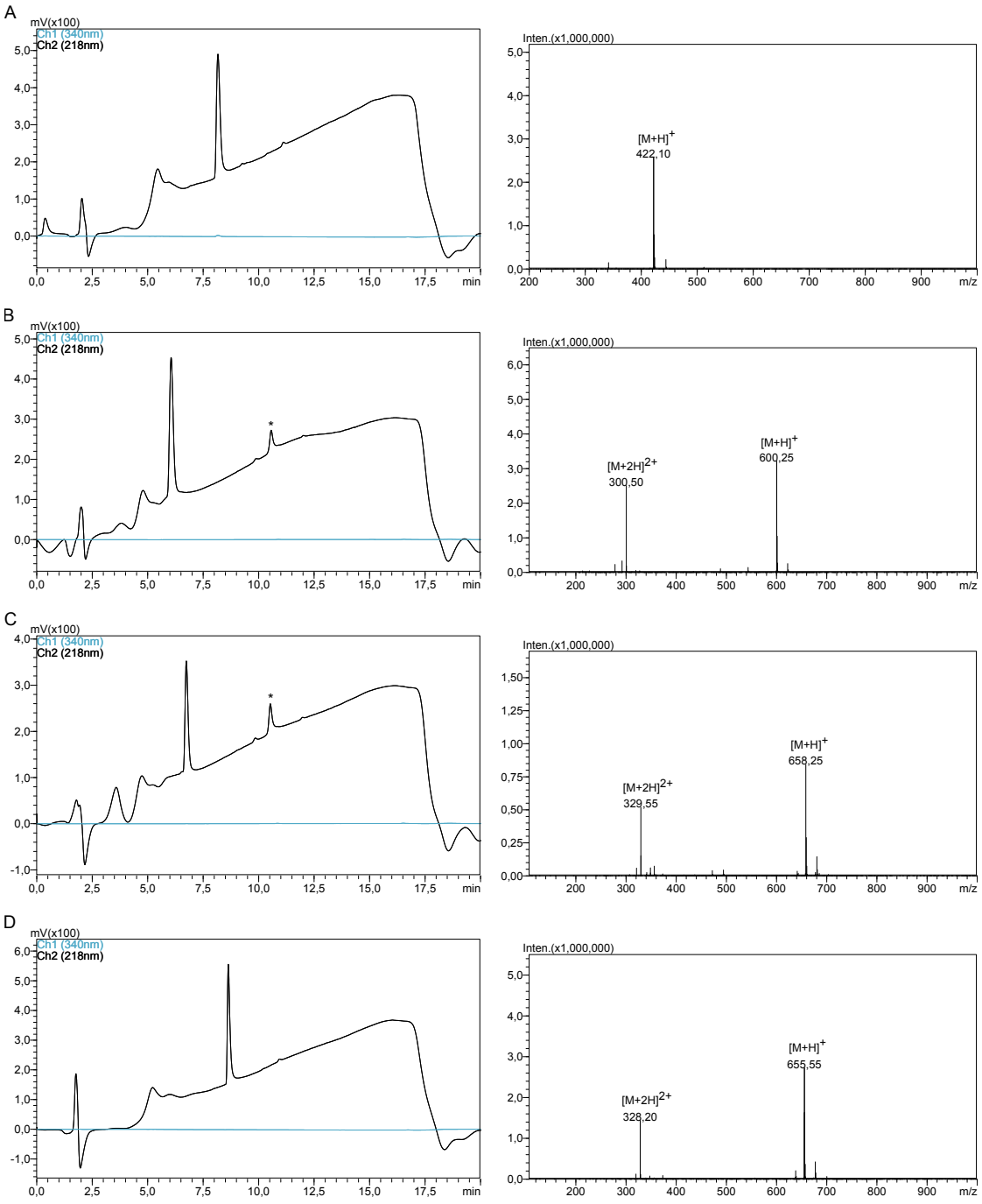

Figure 67: LC-MS analysis of precursors of mini-click-probes (A) mini-C (**P4**), (B) mini-Lys-N (**P5**), (C) mini-AsuHd-N (**P6**) and (D) mini-Aoda-N (**P7**). Peaks marked with an asterisk stem from impurities on the column.

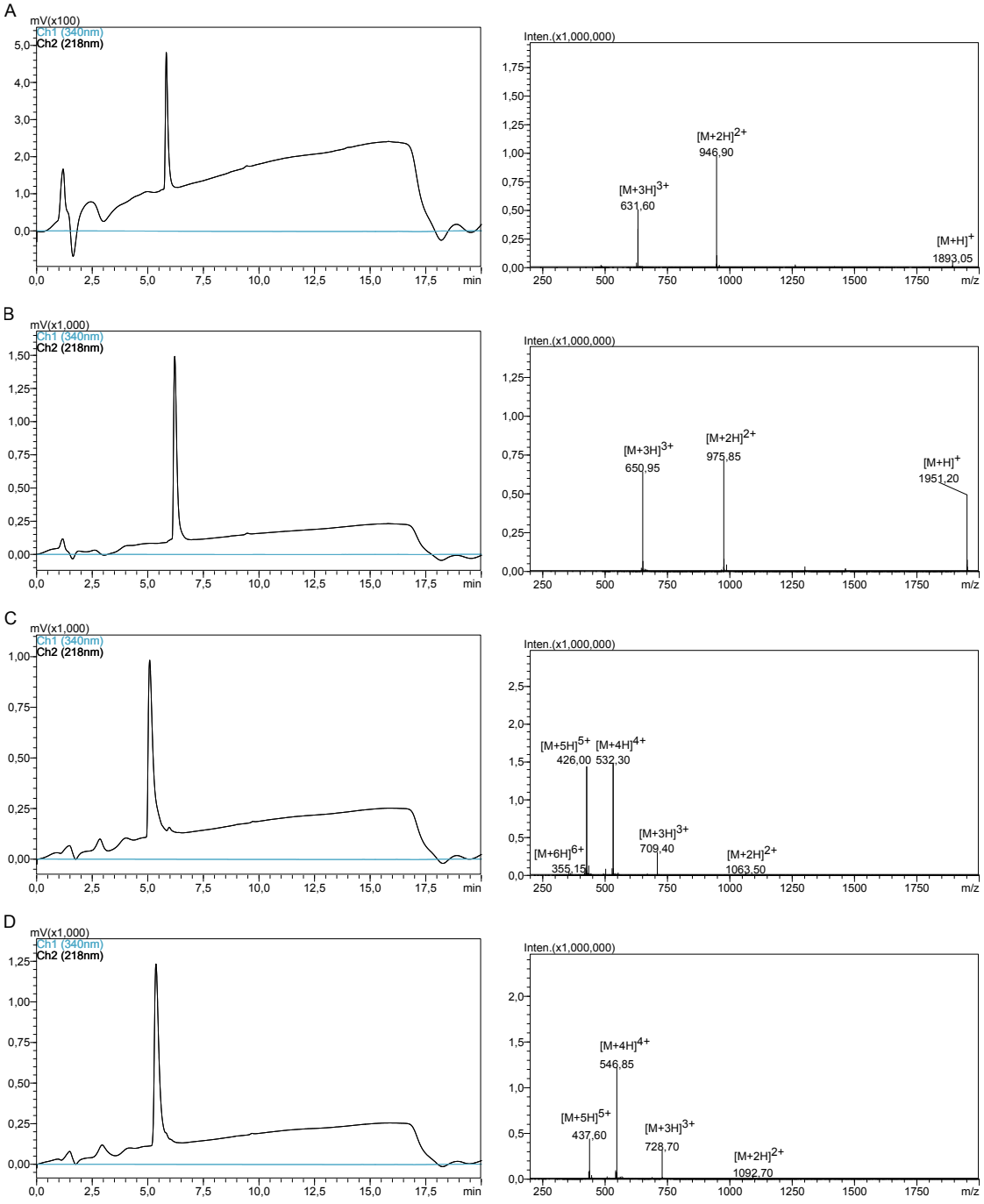

Figure 68: LC-MS analysis of selected HDAC6 substrate peptides (A) αTub-Lys (**P10**), (B) αTub-L-AsuHd (**P11**), (C) CRTC-Lys (**P12**) and (D) CRTC-L-AsuHd (**P13**).

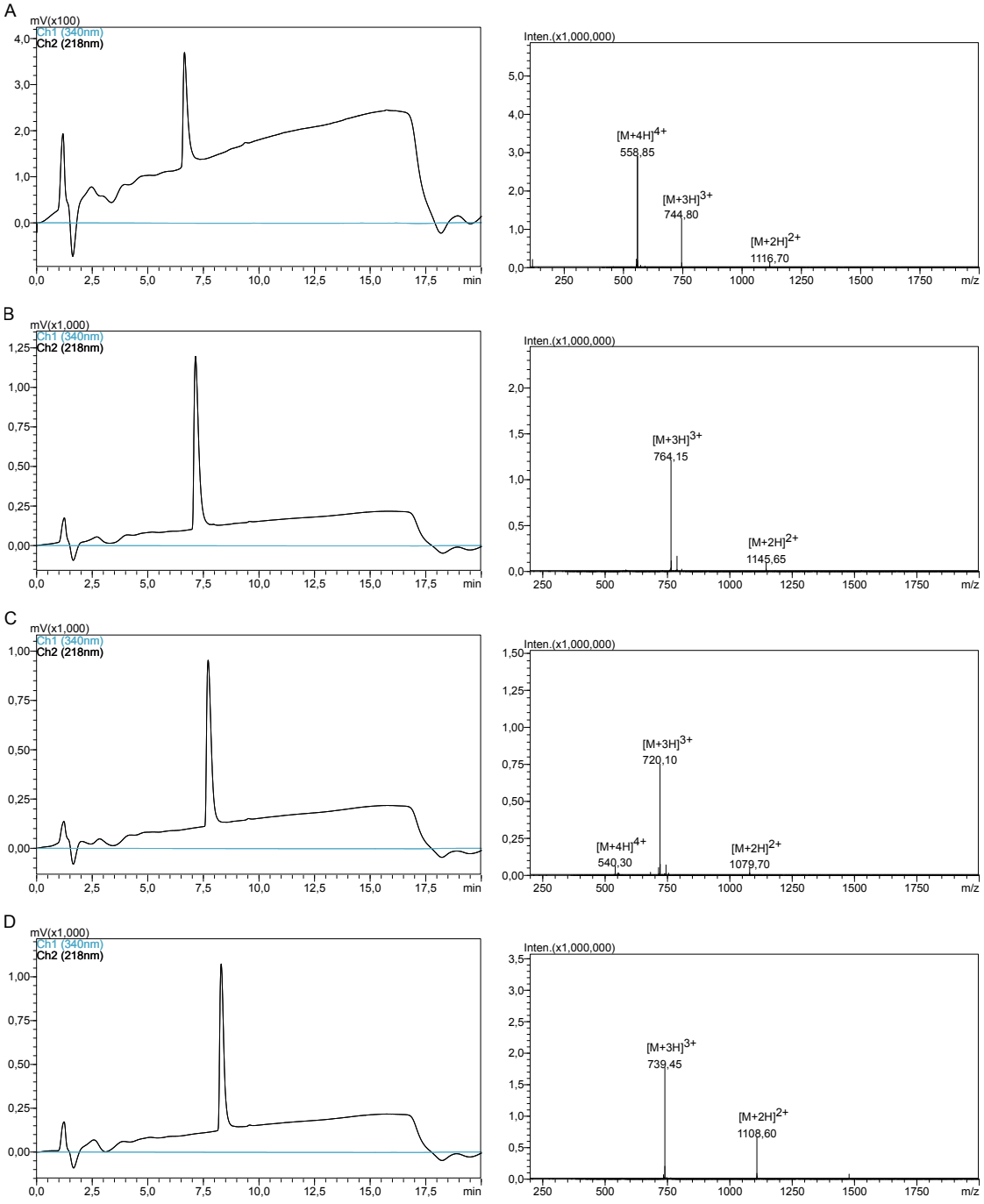

Figure 69: LC-MS analysis of selected HDAC6 substrate peptides (A) HSP90-Lys (**P14**), (B) HSP90-L-AsuHd (**P15**), (C) PPIA-Lys (**P16**) and (D) PPIA-L-AsuHd (**P17**).

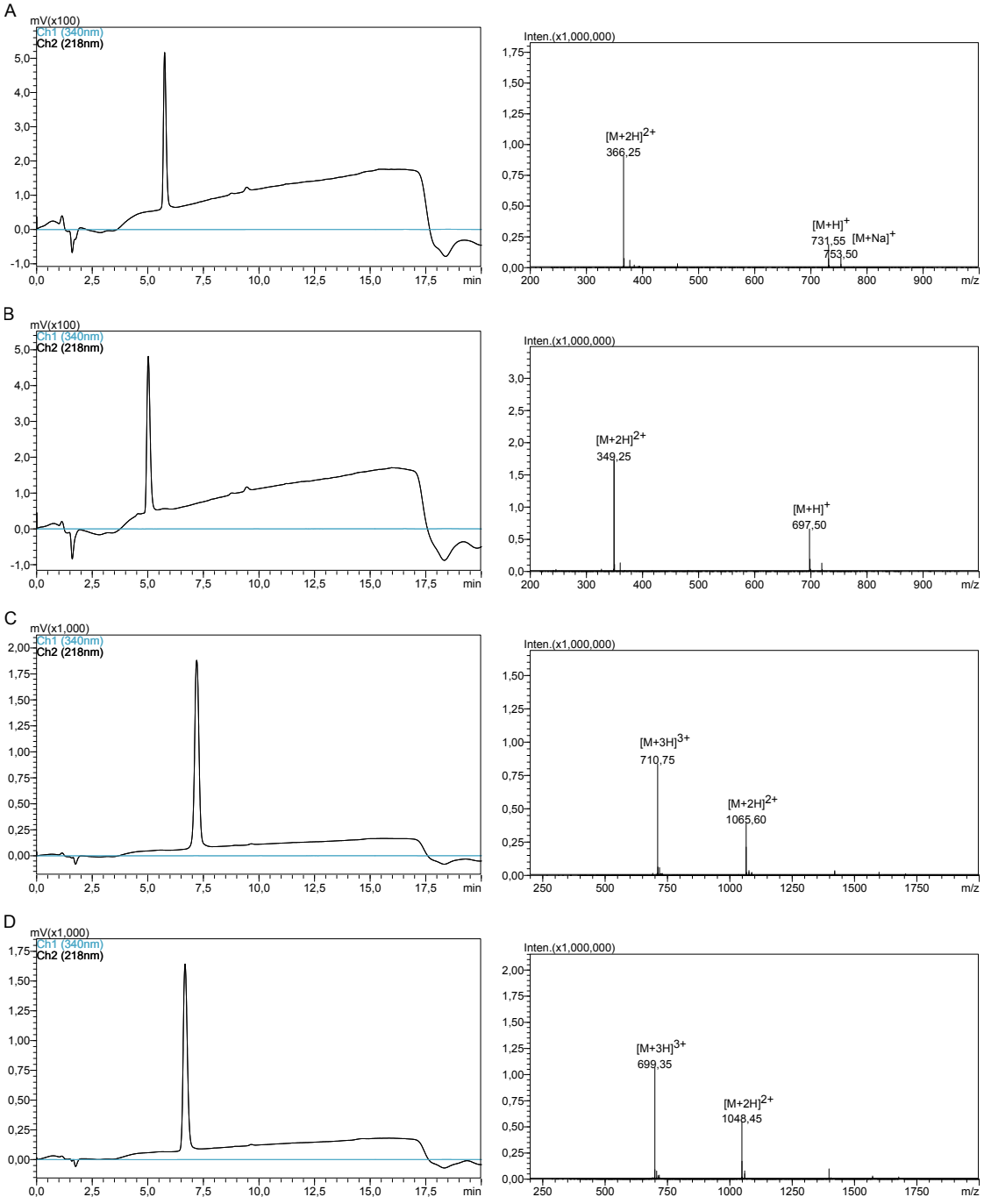

Figure 70: LC-MS analysis of substrate and isotopically labeled standard peptides for the MALDI-MS-based deacetylation assay: (A) mini-Lys(Ac) (**P18**), (B) mini-Lys8 (**P19**), (C) αTub-Lys(Ac) (**P20**) and (D) αTub-Lys8 (**P21**).

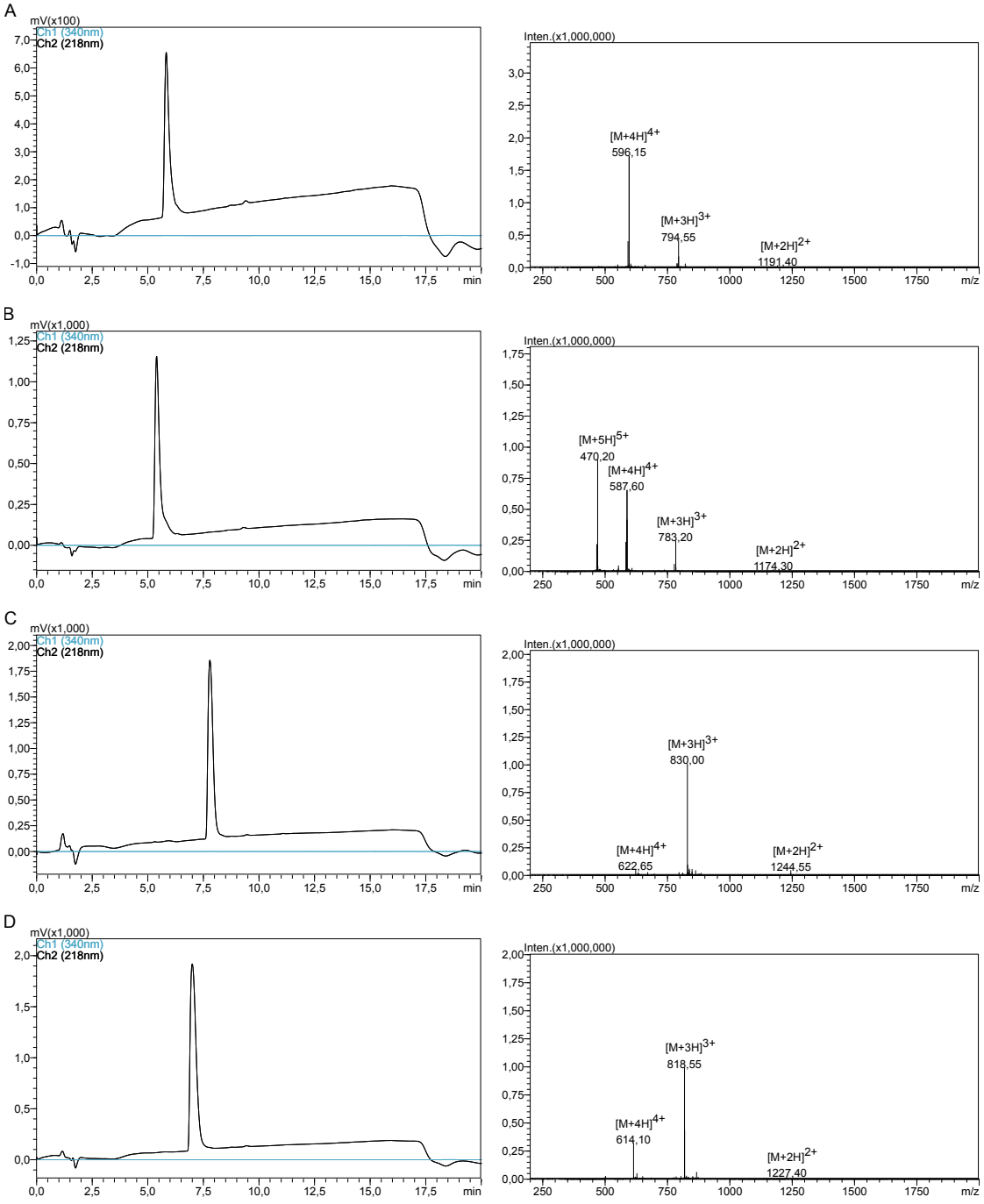

Figure 71: LC-MS analysis of substrate and isotopically labeled standard peptides for the MALDI-MS-based deacetylation assay: (A) CRTC-Lys(Ac) (**P22**), (B) CRTC-Lys8 (**P23**), (C) HSP90-Lys(Ac) (**P24**) and (D) HSP90-Lys8 (**P25**).

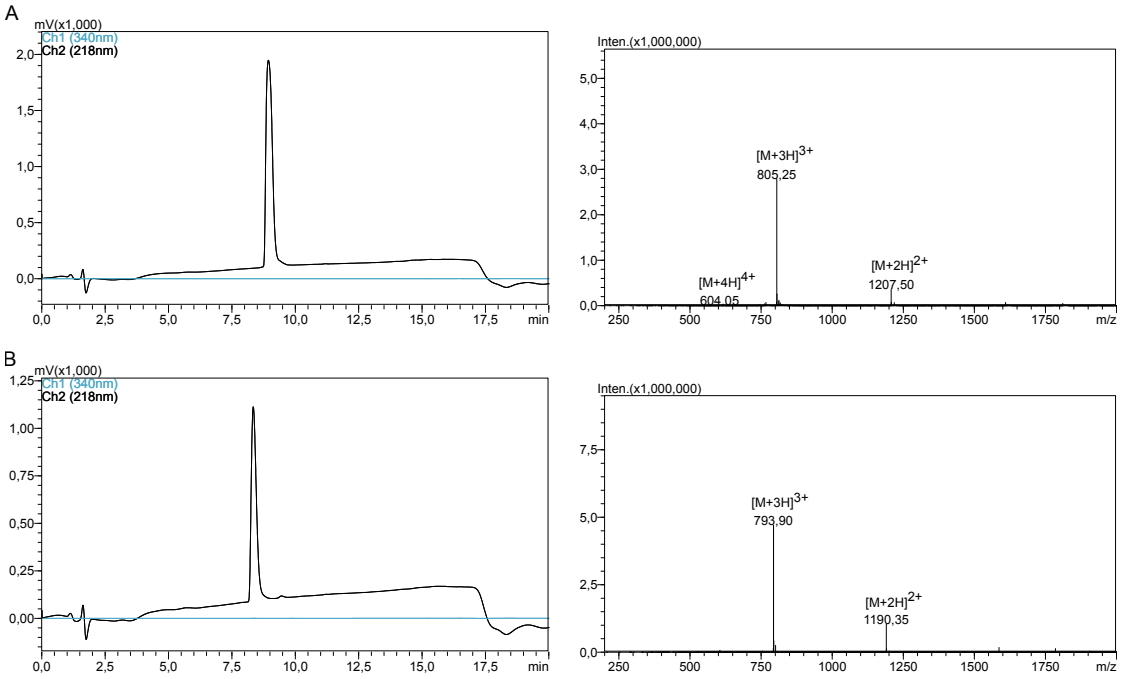

Figure 72: LC-MS analysis of substrate and isotopically labeled standard peptides for the MALDI-MS-based deacetylation assay: (A) PPIA-Lys(Ac) (**P26**) and (B) PPIA-Lys8 (**P27**).

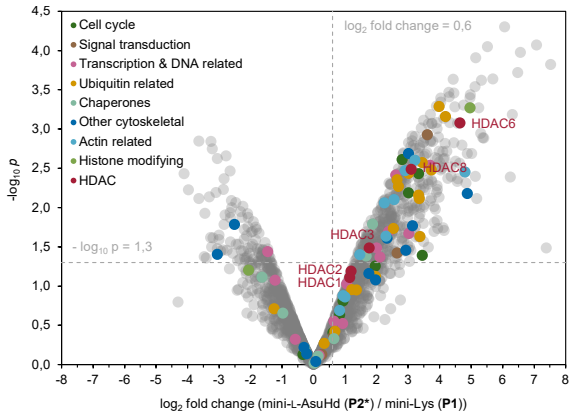

Figure 73: Volcano plot of proteomic pulldown experiments with mini-L-AsuHd (**P2***) versus mini-Lys (**P1**). Mean $\log_2$-fold enrichment ratios are plotted against the negative $\log_{10} p$ value of statistical analysis. Cut-off values indicating significantly enriched proteins were set at $p \leq 0.05$ ($-\log_{10} p > 1.3$) and $\log_2$-fold enrichment ≥ 0.6. Experiments were performed as biological triplicates using HeLa lysate (0.5 mg mL^{-1}, 100 µg total protein).